MIGMATITES OF HIGHER HIMALAYAN CRYSTALLINES: THEIR ROLE IN COLLISION TECTONICS

A THESIS

Submitted in partial fulfilment of the requirements for the award of the degree of

DOCTOR OF PHILOSOPHY

in

EARTH SCIENCES

by

TH. NIKUNJA BIHARI SINGHA

DEPARTMENT OF EARTH SCIENCES
INDIAN INSTITUTE OF TECHNOLOGY ROORKEE
ROORKEE-247 667 (INDIA)

APRIL, 2007

INDIAN INSTITUTE OF TECHNOLOGY ROORKEE
ROORKEE

CANDIDATE'S DECLARATION

I hereby certify that the work which is being presented in the thesis entitled **MIGMATITES OF HIGHER HIMALAYAN CRYSTALLINES: THEIR ROLE IN COLLISION TECTONICS** in partial fulfilment of the requirements for the award of the Degree of Doctor of Philosophy and submitted in the Department of Earth Sciences of the Indian Institute of Technology Roorkee, Roorkee is an authentic record of my own work carried out during a period from January 2004 to March 2007 under the supervision of **Dr. Sandeep Singh,** Associate Professor Department of Earth Sciences, Indian Institute of Technology Roorkee, Roorkee.

The matter presented in this thesis has not been submitted by me for the award of any other degree of this or any other institute.

(TH. NIKUNJA BIHARI SINGHA)

This is to certify that the above statement made by the candidate is correct to the best of our knowledge.

Date: 27th April 2007

Sandeep Singh
27th April 2007
(Dr. Sandeep Singh)
(Supervisor)
Associate Professor

The Ph.D. Viva-Voce examination of **Mr. Th. Nikunja Bihari Singha,** Research Scholar, has been held on 15th Oct. 2007

Sandeep Singh 15th Oct. 2007
Signature of Supervisor(s)

Signature of External Examiner

ABSTRACT

Himalaya is the youngest and evolving active mountain belt in the world displaying various geodynamic processes with the development of distinct tectonic units. This mountain belt extending laterally about 2500 km from west to east with 250-300 km width and providing an ample opportunity to study the exhumed rocks which have undergone deep burial, reactivation, remobilization, deformation, metamorphism and intrusion by the Tertiary Leucogranite due to the active collisional tectonics between Indian and Eurasian plate.

The Higher Himalayan Zone known as Higher Himalayan Crystallines (HHC), characterizes the northernmost exposed part of the Indian plate thrust southward over the Lesser Himalayan rocks along a major thrust called the Main Central Thrust (MCT) (also called Munsiari Thrust in Garhwal) with an estimated overthrusting of about 80-100 km. This MCT is about 2-5 km wide ductile shear zone and providing maximum crustal shortening of 250 km during collision, with reactivation afterward in different episodes. The northern boundary of the HHC is marked by the Trans Himadri Shear Zone (THSZ)/ Zanskar Shear Zone (ZSZ)/ Rohtang Shear Zone (RSZ)/ Martoli Fault (MF)/ Tethyan Thrust (TT)/ South Tibetan Detachment System (STDS) and its associated splays. The relationship among metamorphism, migmatisation, evolution of HHC and generation of leucogranite in the HHC with reference to the tectonic framework has been one of the major fields of interests in Himalayan geodynamics. Since the closure of the Indian and Eurasian plate about 57 Ma ago multiple phases of deformation, metamorphism, metamorphic fluid activation, compression, decompression, crustal loading and reloading has been

taking place. The occurrence of migmatite and leucogranite in this prevailing tectonic regime has left a good opportunity to evaluate the relationship between them and the Higher Himalayan Tertiary Leucogranite.

The HHC of Alaknanda and Dhauliganga valley is defined by the MCT in the South and Malari Fault in the north divides the rocks of the HHC into two major units as upper Vaikrita Group comprising Joshimath, Pandukeshwar and Badrinath Formations and basal Munsiari/Tapoban Formation. The rocks of the Vaikrita Group comprises greenschist facies to higher amphibolite facies rocks, which include mica-, garnet-, staurolite-, kyanite-, sillimanite-schists and gneisses, sillimanite-Kfs grade rock, migmatite and leucogranite with intermittent thin bands of calc-silicate, amphibolite and veins of pegmatite and quartz while the Munsiari Formation comprises predominantly of quartzite and metabasite with intercalations of phyllite and chlorite schist.

The pressure and temperature of the rocks from the two valleys have been attempted using THERMOCALC V-3.25 on the matrix (rim) and inclusion (core). Pressure temperature data and also garnet profiles clearly indicate a progressive P-T path experienced by the lower part of the Vaikrita Group where rim temperature varies from 520±90^{0}C to 708±40^{0}C with core and rim values consistently indicating increase in temperature from ~600 to ~700^{0}C and along with rim pressure increasing from ~7 to ~12 kbar. Towards north, pressure gradually reduces while temperature initially shows slight reduction in the central part of the thrust sheet followed by slight increase in the migmatite zone, where the temperature reaches to about 700^{0}C. The pressure on the other hand shows a total reduction of about 5-6 kbar from the Vaikrita Thrust to migmatite zone. The inclusion and matrix thermobarometry of the

migmatite zone shows an increase in temperature of about 30-50^{0}C from core to rim while pressure reduces to about 2 kbar from core to rim.

Trace elements and REE from 45 samples including metasediment, migmatite and leucosome and leucogranite clearly shows a similar pattern indicating the petrogenetic link among the rock types. The spider diagrams of the metasediment and the migmatite show similar pattern with negative anomalies of Ba, Nb, Sr, Zr and Ti; in addition to this Th and Y shows a slight positive anomaly. In the metasediments, Th is quite high as compared to U but gradually their pattern got reverse in migmatite and leucosome. The positive anomaly of Th and Y in the metasediment indicates the presence of accessory phases like monazite and apatite most of which retain in the restite during partial melting, therefore, shielding the elements from the melt and hence producing negative anomaly in the leucosome and leucogranite. The REE diagram of metasediment and migmatite shows a less fractionation in both LREE and HREE represented by a smooth pattern with slight positive Gd and Tm anomaly along with negative anomaly in Eu. The leucosome part on the other hand shows enriched pattern of HREE producing a slightly upward curve which can be attributed to the residual garnet in the leucosome. However, the concentrations of the REEs in the leucosome are largely reduced. The strong positive anomaly of Eu in leucosome indicates the accumulation of plagioclase in the leucosome which is one of the dominant mineral in leucosome samples. The heterogeneity in the REE in leucosome specially Sm, Nd and Eu are the clear indication of the disequilibrium melting or segregation. REE pattern of the leucosome can be attributed to metamorphic segregation, which differentiates minerals under subsolidus condition and can produce similar pattern with different concentration

level of the elements. The similar REE pattern and the field evidences of large numbers of small pods along main foliation clearly indicate partial melting under H_2O saturated condition as a suitable mechanism for the formation of migmatite and the generation of the leucogranite of Alaknanda and Dhauliganga valley.

Isotopic studies indicate muscovite ages of Vaikrita Group, for both the valleys range between 20 to 14 Ma with biotite ages varying between 13 and 7 Ma. However, majority of the muscovite give ages between 20 to 17 Ma and biotite giving between 13 to 10 Ma range. The lower ages are yielded by the pelitic sample sandwiched between the quartzite bands of Pandukeshwar Formation, the migmatite and adjacent to the Vaikrita Thrust (VT). However, the muscovite ages of the samples adjacent to the VT do not vary from those of the migmatite zone, while the biotite ages change largely, justifying the remobilization of the LILE due the ductile deformation at MCT zone. MCT zone samples yield muscovite age of 8.61 Ma while biotite ages are as low as 1.43 ± 0.01 Ma. Similarly, the Munsiari Formation yields biotite ages between 2.07-2.05 Ma. The age pattern, across the HHC, show a sharp break in the mica cooling ages across the VT, i.e., between the Vaikrita and the Munsiari Formation. ε_{Nd} and $^{87}Sr/^{86}Sr$ values have also been calculated at present day values, at 46 Ma value considering SHRIMP U-Pb age from Bhagirathi valley for re-homogenization age and at 500 Ma which has been considered by other workers as the time of re-homogenization. It is found that the calculated values at t=o and t=46 Ma, are more comparable with the range of the published data while the values calculated at t=500 Ma most of the samples resulted into positive values and their $^{87}Sr/^{86}Sr$ ratios are giving lesser values than the BABI (Basaltic Achondrite Best Initial). Therefore, for Vaikrita Group of HHC probably might have re-homogenized

post-dating 500 Ma, which has been widely used for the Himalayan rocks. It appears that the rocks of the HHC were re-homogenized comparatively in recent time. The values of $\varepsilon_{Nd}(46)$ and $^{87}Sr/^{86}Sr$ calculated at t=46 Ma gives clear separation of migmatite from mestasediment while the values at t=0 do not discriminate migmatite from metasediments. The average values of present day ε_{Nd} and $^{87}Sr/^{86}Sr$ gives about -16 and 0.901836 respectively while for Tethyan it is about -17 and 1.002341 and for Munsiari Formation the values are about -24 and 0.905278. Leucosome samples yield anomalous values of $\varepsilon_{Nd}(0)$ due to high Sm/Nd ratio and present day $^{87}Sr/^{86}Sr$ ratio gives very high values indicating a disequilibrium melting of the crustal rocks.

From the field observation and thin section study it reveals that the rocks of the Vaikrita Group and the Munsiari Formation experiences inverted metamorphism. The rim temperature and pressure of the lower Vaikrita Group increases from 520 ± 90^0C to 708 ± 40^0C and 6.8±2.0 to 11.4±1.1 kbar, while in the migmatite zone occurring at the northern upper part of the HHC shows clockwise P-T path. The substantial reduction in pressure of about 5-6 kbar (from Vaikrita Thrust to migmatite zone) and almost constant temperature (from Vaikrita Thrust to migmatite zone, with a small dip of temperature at the central part of the thrust sheet) along with the occurrence of small pods of melt along the foliation of the migmatite indicates near isothermal decompression causing partial melting of the metasediment and subsequent generation of leucogranite. The trace elements and REE for metasediment, migmatite and leucosome and leucogranite shows a very similar pattern indicating that source rock of the leucogranite could be from migmatite due to partial melting under H_2O saturated condition. The changing concentration in the

REE and few trace elements in the leucosome indicate the disequilibrium melting or segregation which is also supported by the highly anomalous values of Sm/Nd and $^{87}Sr/^{86}Sr$. Calculated cooling rate considering the average muscovite and biotite ages from the Vaikrita Group and the Munsiari Formation clearly indicate two distinct patterns. The samples of the Vaikrita Group give a gentle path indicating moderate exhumation rate between ~17 to ~11 Ma. Whereas, basal Munsiari Formation indicating a very fast cooling and exhumation rate.

Mineral assemblages, geochemical data and exhumation and/or cooling age history in addition to field character do indicate that migmatite leucosome and small volume of *insitu* tourmaline bearing leucogranite indicate cummulation rock from water-saturated melting of pelitic metasedimentary rocks. The formation of migmatite happened at around 46 Ma corresponding to peak metamorphic event due to collision tectonics of the Himalayan orogeny. At this time Sr-Nd isotopic ratio also got re-homogenized. The presence of feeder dykes for main tourmaline-bearing leucogranite indicate that the source for the main body could be migmatite which is also being supported by similarity in REE pattern of the main body could *insitu* tourmaline bearing leucogranite. The dyking occurred due to buoyancy or injection mechanism within the upper part of the HHC. After leucogranite formation, terrain exhumed separately with different exhumation rate, lower package being exhumed faster with overlying package as much slower rate. Within the upper package the central portion has exhumed at lesser rate as compared to the two flanks bounded by the Vaikrita Thrust in the south and the Malari Fault in the north.

ACKNOWLEDGEMENTS

First and foremost I convey my deep indebtness to my supersvisor Dr. Sandeep Singh, Associate Professor, Indian Institute of Technology, for his stipulated guidance, unwavering support and encouragement. This thesis could not have attained its present form, both in content and presentation, without his active interest, direction and guidance. His unmatched excellence in the subject, bountiful energy, and personal care has been the source of inspiration. He has devoted his invaluable time and took personal care in motivating me till the final printout of the thesis. His personal counselling and word of encouragement were cheering whenever I was in the period of plummation. His valuable advices and suggestions remains a source of inspiration.

I am also grateful to Prof. R. M. Manickavasagam, Retd. Head, Institute of Instrumentation Centre, IIT Roorkee for his valuable suggestions at various stages during geochemical analysis at IIC, IIT Roorkee. Provoking discussions and his inspiring presence helped me to ride over the problems and complete the analysis successfully. His helping and kindness nature remains a source of motivation.

My sincere thanks are due to Prof. A. K. Choudhuri, Head Institute Instrumentation Centre, IIT Roorkee for his valuable suggestions and guidance during my geochronological analysis at Instrumentation Centre, IIT Roorkee. Interesting discussions and instructive suggestions and for his scholarly advice helps immensely during the course of analysis.

I express my sincere thanks to Prof. A. K. Jain, Earth Sciences, IIT Roorkee for his valuable advice and suggestions during my research. His unambiguous instruction and fruitful discussions with him helped me a lot for this research.

I am greatly indebted to Dr. T. K. Ghosh, Instrument Instrumentation Centre, IIT Roorkee, for his sincere and active discussions during the EPMA analysis. It could not be possible to carry out the analysis without his copious help. I am greatful to Prof. H. Sinvhal and his team for helping in taking final printout.

Literature provided by Prof. Nigel Harris (UK), Prof. Jibamitra Ganguli (USA), Prof. Randall Parish (UK), Prof. Spear Frank (USA), Prof. Michael Brown (USA), Prof. Derek Vance (UK), Prof Allan Whittington (USA), Prof. DeCelles (USA) and Prof. An Yin (USA) is deeply acknowledged.

The non-teaching staffs of the Department of Earth Sciences are also gratefully acknowledged for their unstinted help in many ways.

I am thankful to my labmates Dr. Rajeev Kumar, Soumayjit and James for their loving support and coordination making a healthy working environment. I also appreciate my colleagues Dr. Balaji, Dr. Harrish, Dr. Vivesh, Dr. Ratnadeep, Narendra, Ajaey, Manish, Anshuman, Avnish, Mathur, Krishna, Srikishna, Deepak, Acharrya, Pati, Laxman and others for their loving support during my stay and lifting morals always high.

I owe my sincere thanks to, Kamalji, Rameshji, Handaji, Jawelji of IIC, for their helping hand during various stages of analysis at IIC. I am also thankful to Surender (TIMS, Lab) for his cheerful support at the TIMS lab and Bhimji (Earth Sciences) for his sincere effort during thin section preparation.

I am grateful to all those who have helped me directly or indirectly in the successful completion of this thesis.

Word fails to express to thank my parents and Tado. I would have never come so far without their rock solid support and unconditional love. I whole heartedly dedicate this work to them.

(TH. NIKUNJA BIHARI SINGHA)

CONTENTS

CHAPTER – 1

INTRODUCTION

1.1 BACKGROUND

Himalaya is the youngest and evolving active mountain belt in the world, displaying various geodynamic processes with the development of distinct tectonic units (Fig. 1.1; Le Fort, 1975; Honegger et al., 1982; Coward et al., 1982; Valdiya, 1989; Searle et al., 1993; Thakur, 1993; Hodges, 2000; Jain et al., 2002; Yin, 2006). This highest mountain chain has fourteen peaks, which are highest in the world extending laterally about 2500 km from Nanga Parbat (8126 m, $33^0$15' N & $74^0$36' E) in the west to Namche Barwa (7756 m, $29^0$37' N &$95^0$15' E) in the east having 250-300 km width. The geology of the orogenic belt has been summarized in recent syntheses (Hodges, 2000; Jain et al., 2002; Steck, 2003; Yin, 2006) after a long gap by work of Gansser (1964).

Since the inception of the profound theory of Plate Tectonics, evolution of Himalayas have been explained as the product of collision tectonics between the Indian and Eurasian plates which took place no latter than 57 Ma ago (Leech et al., 2005). However, the age of collision is poorly constrained ranging between ~65 to ~40 Ma. The most cited age is between 55 to 50 Ma. The discrepancy in age is resulted due the different approaches that have been employed for defining the continent-continent collision. On the basis of terrestrial faunas the age is 65 Ma (Jaeger, et al., 1989; Rage, et al., 1995). The similar age have been suggested on the basis of lithospheric plate reorganization in the Indian ocean (Courtillot, et al.,

1986) along with the basis of possible tectonic mélange emplaced along the Indian plate margin due to initial collision (Searle, 1983, 1987; Beck, et al., 1996). The palaeomagnetic data from the Indian oceanic floor also give an age of 65 Ma which record the direction and rate of plate motion (Klootwijt. et al., 1992). According to Dewey et al (1989) and Le Pichon et al. (1992), the initial collision started at about 45 Ma, which is incompatible with both the early foreland-basin stratigraphic record from Pakistan to Nepal, dominated by early Eocene detrital sediments from volcanic arc and ophiolites (Critelli and Garzanti, 1994; DeCelles et al. 1998; Najman and Garzanti, 2000). On the basis of sedimentologic constraints, Treolar and Coward (1991) and Rowley (1996), suggested that the first collision took place in the western syntaxis at around 55-50 Ma and then younging in age took place from the central to eastern part of the range between 50 to 45 Ma. Guillot, et al (2003), worked out the initiation age of collision to be ~55 Ma on the basis of stratigraphy, palaeomagnetism, geochronology and tectonophysics in the NW Himalaya. However, on the basis of age of UHP metamorphism and the possible geometry of subducting plate Leech et al., (2005, 2006, 2007) suggested that initial collision took place no latter than 57 Ma.

With continuous increase in lateral compression the folding and faulting of various nappes resulted in piling up of the continental crust over one another causing mass loading and crustal thickening of Indian plate to about 70 km (Le Fort, 1975; Molnar, 1988; Zhao et al.,1993).The crustal thickening and the southward propagation of thrust boundaries followed by subsequent reloading of masses or decompression due to the differential erosion of the rocks caused the exposure of deep seated rocks with maintaining a near isostatic balance. The

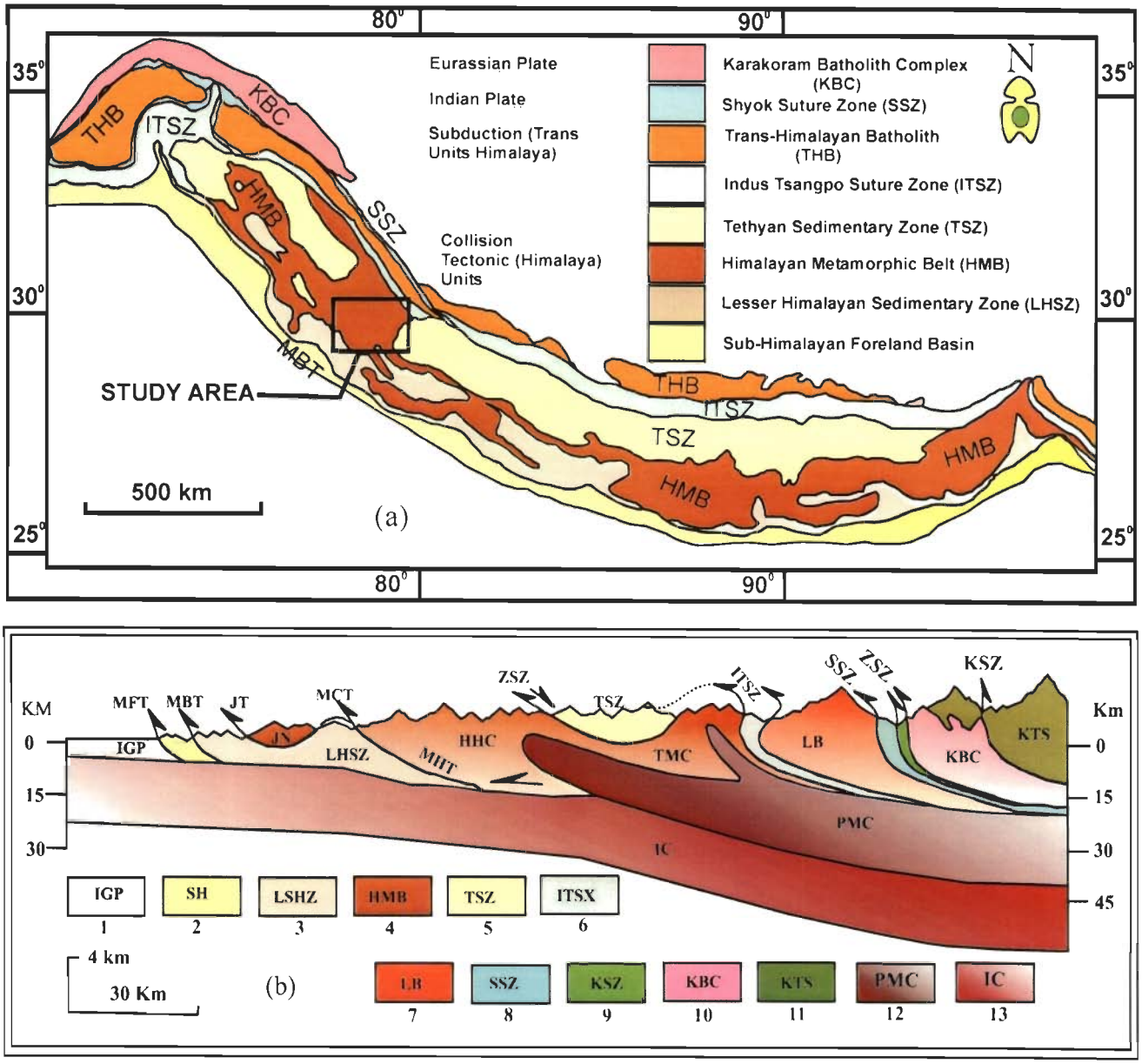

Figure1.1: (a) The Geological map of the Himalaya showing the main tectonic units demarcated by different thrusts (b) The simplified cross section of the Himalaya, where, 1= Indo-Gangetic Plain; 2= Sub-Himalaya; 3= Lesser Himalayan Sedimentary Zone; 4= Higher Metamorphic Belt; 5= Tethyan Sedimentary Zone; 6= Indus Tsangpo Sututre Zone; 7= Ladakh Batholith; 8= Shyok Suture Zone; 9=Karakoram Shear Zone; 10= Karakoram Batholith Complex; 11=Karakoram Tectonic; 12=Partial Molten Crust ; 13= Indian Crust.

collision between India and Eurasia has influenced not only the kinetics of lithospheric plates, but has also caused quantum changes in sedimentation, climate, oceanic circulation, and faunal distribution (e.g., Patriat and Achache, 1984; Jaeger et al., 1989; Harris, N., 1995; Rowley et al., 1996; Guillot et al., 2003 and Clift and Blusztajn, 2005).

The large scale loading, buckling and stripping off masses over other along with continuous subduction of the Indian plate under the Eurasian plate has caused about 2000 km of crustal shortening since the last ~40 Ma (Windley, 1988). However, the estimated values of this crustal shortening by different workers vary in a wide range possibly due to the consideration of different collision age, the negligence of the northern extension of the Indian plate below the Tibet and the different rate of convergence throughout the collision period. The paleomagnetic data indicate convergence of Indian Plate against Eurasian Plate to be about 2300 to 2150 km (Dewey et al., 1989 and Le Pichon et al., 1992) or 3000 Km (Molnar and Tapponnier, 1975; Replumaz and Tapponnier, 2003). However, various data on Himalayan shortening based on different data range from 1250±250 km (Achache et al., 1984; Besse et al., 1984; Powell et al., 1988; Dewey et al., 1989; Patzelt et al., 1996; Matte et al., 1997) to ~ 1100 km (Gulliot et al., 2003), ~900 km (Le Pichon et al., 1992) between ~700 km and 1500 km (Patzelt et al., 1996) to ~650 km (De Celles et al., 2002). However, shortening estimates within the various sectors of the Himalaya has also been constrained based on the balance cross-sectioning which varies from west to east. In Pakistan within Hazara Syntaxis it is about 470 km (Coward and Butler, 1985), within NW India it is between 480-591 km (Searle, 1986; Searle et al., 1997; Srivastava and Mitra, 1994), western Nepal between 485-669 km

(DeCelles et al., 2001; Murphy and Yin, 2003) and eastern Nepal between 318-419 km (Schelling and Arita, 1991; Schelling, 1992; Ratschabacher et al., 1994).

After collision tectonics, the crustal shortening has been accommodated along various southward propagating faults demarcating tectonostratigraphic zones (Fig. 1). These zones have been listed below:

1.2 OUTER HIMALAYAN ZONE

The Outer Himalaya zone is the southernmost zone of Himalaya bounded in the south by the Main Frontal Thrust (MFT) separating them from the Indo-Gangetic alluvial plain with a sharp topographic break (Nakata, 1972) and in the north by Main Boundary Thrust (MBT). This zone is characterized by Cenozoic sedimentary pile of about 9500 m mainly consisting of continental molassic sediments of Miocene to Upper Pleistocene age, derived from the erosion of the Himalaya. The outer-Himalayan belt extends along the southern flank of the Himalayan orogen and consists of numerous thrust slices beneath the MBT (Najman et al., 2000). The MBT was active during middle to late Miocene age (Meigs et al., 1995) or at least 10 Ma (Burbank et al., 1996), however, the MFT is still active during preset time (Najman, et al., 2006). However, the zone extends from Potwar Plateau to Jammu region in the west to Kumaon- Nepal in the east.

The rocks of the Outer Himalayan Zone or Foot Hills belt consist of sedimentaries of Subathu, Dagshai and Siwalik Formations (Gansser, 1964; Bhatia 1982). Subathu Formation contain marine sediments with marine fauna consisting shale and fine grained sandstone with calcareous bands, however, as one go into overlying Dagshai, Subathu and Siwaliks continental components are becoming more prominent. Dagshai is mainly a transitional facies consisting mudstone,

sandstone and few calcareous bands, however, Kasauli and Siwaliks are mainly alluvial facies.

$^{87}Sr/^{86}Sr$ isotopic data from Subathu Formation range between 0.710-0.715 for leached residue (Najman et al., 2000) and 0.710-0.721 for shaly sedimentaries (Dahl, 2006). However, underlying Kakra Formation show very high values of 0.793, 0.726, and 0.722 and overlying passage bed also indicate high Sr values of 0.731 (Dahl, 2006). On the contrary, Dagshai and Kasauli range between 0.755-0.775 for the leached samples (Najman et al., 2000) and 0.737-0.771 for the whole rock (Dey, 2006) indicating a strong affinity towards continental source. The data from upper Dharmshala sample show 0.775 on unleached sample and 0.785 on leached fraction (White et al., 2002). Paleosol carbonate samples from Upper Siwalik of Himachal Pradesh vary between 0.729 and 0.739 after selective leaching of the carbonates (Ghosh et al., 2004).

The $\epsilon_{Nd(0)}$ values for the Outer Himalayan Zone in the foreland basin of Himachal Pradesh consisting of Subathu, Dagshai and Kasauli Formation show two contrasting groups. The Subathu Formation yields $\epsilon_{Nd(0)}$ values of about -9 while the Dagshai and Kasouli Formation, the $\epsilon_{Nd(0)}$ values ranges between -12 to -18, characterizing the Indus Tsangpo Suture Zone and Tibetan sedimentary source for the former while the later group characterizes the dominant source area of Higher Himalayan Crystallines (Najman et al., 2000).

Siwalik sedimentary rocks (Neogene Foreland basin) from the Nepalese Himalaya along the Surai Khola and Karnali river sections give $\epsilon_{Nd(0)}$ values ranging between -14.2 to -19.2 (Huyghe et al., 2001) and the modern sediments of Karnali and Narayani rivers give $\epsilon_{Nd(0)}$ values ranging between -17.2 to -20.2 (Galy and

France-Lanord, 2001) which are very similar to that of Inner Lesser Himalayan values and also implying a very similar proportion of Lesser Himalyan sediments in the upper and middle members of the Siwalik Group of the area. The $\epsilon_{Nd(0)}$ decreases with the passage of time throughout the middle and upper members of the Siwalik Group due to the increasing proportion of the Outer Lesser Himalyan detritus.

1.3 LESSER HIMALAYAN ZONE

Lesser Himalayan Zone forms the low-lying hills between Sub Himalayan Zone in the south and Higher Himalayan Zone in the north. They expose (a) Lesser Himalayan Sedimentary Zone (LHSZ) and (b) southern most parts of the Higher Himalayan Crystallines (HHC). The Lesser Himalayan Sedimentary Zone (LHSZ) has been demarcated as Outer and Inner Lesser Himalayan Zone (Valdiya, 1995). The Inner Lesser Himalayan Sedimentary Zone (ILHSZ) forms low-grade non-fossiliferous Middle Proterozoic to Paleozoic metasediments, with mafic and felsic intrusions ranging in ages between 1900-1600 Ma (Miller et al., 2000). The rocks of Inner LHSZ are exposed within various window structures (e.g. Kisthwar, Kulu-Rampur, Garhwal-Deoban). However, the Outer Lesser Himalayan Sedimentary Zone (OLHSZ) is of Neoproterozoic to Cambrian age and even to Permian to Paleocene age in eastern Himalaya. They mainly contain Simla, Chandpur, Nagthat of Jaunsar along with Blaini, Krol and Tal Formation and their equivalents (Valdiya, 1995). They are exposed between MBT and Main Central Thrust (MCT). The maximum width of the Lesser Himalaya is exposed in the Kumaon and Garhwal region which is about 80 Km.

On the basis of isotopic composition of Nd, Ahmed et al. (2000) recognized the two subdivisions in the Lesser Himalaya in the Garhwal Himalayan metasedimentary rocks using ϵ_{Nd} value calculated at 500 Ma, the approximate age of most recent pre-Himalayan orogeny. The outer LHS gives $\epsilon_{Nd(500)}$ values ranging between -10 to -14 which is similar to that of HHC, indicated a Meso-Paleoproterozoic source. The values of $\epsilon_{Nd(500)}$ in the Inner zone range between -15 to -20 which implies a Late Archean or the earliest Proterozoic source (Richard, et al., 2005). Therefore, the isotopic break between Lesser Himalayan Sequence and the HHC is distinct in the NW India running from Sutlej to Alaknanda.

The isotopic composition of Nd and Sr has also been used to constrain important location of major thrusts and source of the rocks. The ϵ_{Nd} values of HHC/Tethys sediments normally give significantly lower negative values than from the Lesser Himalayan sediment. The previously documented $\epsilon_{Nd(0)}$ and $^{87}Sr/^{86}Sr$ values of Lesser Himalayan Sequences in central Nepal, India and Pakistan give $\epsilon_{Nd(0)}$ between -28 to -15 while the $^{87}Sr/^{86}Sr$ value are mostly greater than 0.8 (Parrish and Hodges, 1996; Ahmed, et al., 2000; France-Lanord, 1993; Najman et al.,2000; Robinson et al., 2001; Najman et al., 2006). The Sr isotopic composition of Vaikrita Group show partial reequilibration at 500 Ma, since the Rb-Sr isochron plot scatter around 500 Ma reference line (Ahmed et al., 2000; Richards et al., 2005), whereas the Munsiari Formation has not undergone Sr isotope homogenization since 1800 Ma (Ahmed et al., 2000), therefore it supports Nd isotope inference.

The detrital zircon ages of the Himalayan sedimentary formations give no significant distinction between the ages of source regions of the three Himalayan lithotectonic units viz, the Lesser Himalaya zone, the Tethyan Sedimentary zone and

the Higher Himalayan Crystalline (Myrow, 2003). However, Richards et al. (2005), found large zircon population of 1.13-0.81 Ga from the Vaikrita Group with a small population of 2.75-2.08 Ga., whilst in contrast, the rocks of the Jutogh Group and Rampur Formation of Inner Lesser Himalayan zone, zircon populations range between 2.26-1.87 Ga, which is similar to that of Parrish and Hodges (1996) and DeCelles et al. (2000).

Two distinct zircon population from the Vaikrita Group have characterized on Pb-Pb crystallization age versus ϵ_{DM}Hf plotting (a) one with ϵ_{Hf}(T) ranging between -2 to -10 mostly derived from Paleozoic sources of 2.1-1.7 Ga old and (b) the older one derived from Archean crust with model age of 3.4-2.6 Ga. (Richards et al., 2005).

1.4 HIGHER HIMALAYAN ZONE

This zone is the northernmost exposed part of the Indian plate overriding the Lesser Himalayan rocks with an estimated overthrusting of about 80-100 km. The northern boundary is marked by the Trans Himadri Shear Zone (THSZ)/ Zanskar Shear Zone (ZSZ)/ Rohtang Shear Zone (RSZ)/ Martoli Fault (MF)/ Tethyan Thrust (TT)/ South Tibetan Detachment System (STDS) and its associated splays (Jain et al., 2002 and references therein) and MCT in the south. The MCT was active about 22 Ma ago (Hubbard and Harrison, 1989; Hodges et al., 1996) and the latest movement took around 6 Ma ago (Harrison et al., 1997) while the extensional faulting of STDS took place between ~22 Ma and ~ 15 Ma (Searle, et al., 1999). The northern contact with the Tethyan sedimentary rocks have been described as conformable (Gansser, 1964; Windley, 1983), transitional (Stocklin, 1980) and tectonic (Burg et al., 1984). This zone comprises of 15-20 km thick crystalline slabs of inverted metamorphics ranging from green schist to upper amphibolite facies. This

zone has been one of the major attentions among the earth scientists because of its inverted metamorphism, polymetamorphism, multiple deformation and present day active collision tectonics. MCT is a very important single largest structure of the Indian plate (Kohn et al.,2001) having a zone of 2-5 km wide ductile shear which has provided the maximum crustal shortening of 250 km during collision (Hodges, 2000).

The orogenic evolution of Himalaya is divided into three main episodes (1) early or pre – Himalaya (Proto-Himalayan phase of Cretaceous-Early Eocene), (2) main Himalaya (Eo – Himalayan phase of Middle Eocene-Late Oligocene) and (3) post-Himalaya (Neo-Himalayan phase of Early Miocene-Present) (Le Fort, 1975; Searle, 1986; Burg et al., 1987; de Sigoyer et al., 2000; Hodges, 2000; Jain et al., 2002). The Pre-Himalayan phase is defined by the tectonometamorphic evolution prior to the India-Asia collision which is not recorded in the HHC (Guillot and Allamand, 2002). Eo-Himalayan phase is represented by corresponding M_1 metamorphic episode which is characterized by high-pressure granulitic to upper amphibolite facies condition preserved in all along the Himalayan belt. According to Guillot et al. (1999), the Eo-Himalayan metamorphism started at about 40 Ma with garnet growth and ended before 25 Ma. Neo-Himalayan phase of orogeny produces corresponding M_2 metamorphism preserved in the upper part of the HHC. The M_1 metamorphism (Eo-Himalayan) is described as the barrovian type metamorphism which affects the whole sequence of HHC while M_2 (Neo-Himalayan) metamorphism is describes as buchan type which affects the sillimanite zone leading to the production of migmatite and generation of leucogranite in the Higher HInalayan Crystallines (Hodges and Silverberg, 1988; Searle et al., 1999; Stephensen et al. 2000; Guillot and Allemand 2002).

The isotopic compositions for the Higher Himalayan Crystalline give -5 to -19 of ϵ_{Nd} (Parrish and Hodges, 1996; Whittington et al., 1999; Ahmed, et al., 2000; Najman et al., 2000; Robinson, et al., 2001; Najman et al., 2006) and 0.730 to 0.820 of $^{87}Sr/^{86}Sr$ while for the Higher Himalayan leucogranites, $^{87}Sr/^{86}Sr$ ranges from 0.715 to 0.805 (Najman, et al., 2000). There is no isotopic break between the HHC and the Tethyan Sedimentary Sequence.

After India-Eurassia collision, Himalaya witnessed exhumation as evident from crustal thickening, regional metamorphism and anatexis, rapid denudation of provenance and deposition within sedimentary basin with increased sedimentary influx (Jain et al., 2000). Initial exhumation appears to have started from the Trans Himalayan terrane, which has also been manifested in deposition of Outer Himalayan Zone of molassic sediments in Cenozoic foreland basin. This was followed by intense crustal shortening along south propagating faults and also resulted in deformation, metamorphism, anatexis, granite generation and exhumation of Higher Himalayan Zone (Jain and Anand, 1988; Jain et al., 2002 and references therein). The renewed early Miocene exhumation is also recorded from Trans Himalayan terrane, Siwalik sediments and Bengal Fan (Cerveny et al. 1988; Copeland and Harrison, 1990; Tandon 1991; Singh, 1999). This was followed by accelerated exhumation during Pliocene- Quaternary leading to formation of large scale domes and/ or windows which have been active either independently or in combination with major tectonic boundaries (Jain et al., 2000) or accelerated erosion causing the exhumation (Thiede et al., 2004 and references therein).

1.5 TETHYS HIMALAYAN ZONE

Tethys Himalaya zone lies on the northern edge of the Indian continental plate between the Indus Tsangpo Suture (ITSZ) and the Higher Himalaya Zone. They contain a complete stratigraphic sequence from Neo-Proterozoic to Eocene sediments. The Tethyan zone is also called Tibetan zone in the western Himalaya, which exposes in the north of Kumaon, Malla Johar, Spiti and Zanskar regions. This zone constitutes ~10 km thick pile of fossiliferous marine sedimentary rocks of Late Proterozoic to Eocene occurring in 50-80 Km wide Sedimentary Zone. To the north the zone is separated from Indus Tsangpo Suture Zone and to the south the sequence is separated from the HHC by Tethyan Thrust (TT) or Trans Himadri Fault (Valdiya, 1989). The recognition of major fault system along the southern boundary of the Tibetan or Tethyan zone was reported in the 80's by many workers (Burg et al., 1984; Burchfiel and Royden, 1985; Searle, et al., 1986; Herren, 1987).

According to Burchfield and Royden (1985) the extensional regime in the northern margin of the HHC took place simultaneously with the compressional regime in the southern margin of HHC. The Tethys Himalayan Sequence on the other hand has been affected by at least two generations of folding due to compressional tectonics (Thakur 1993). Since, the extensional regime is restricted to localized shear zones, the normal faulting has been described as the post-dated the south-directed overthrusting event (Thakur et al., 1990) of gravity-collapse related deformation (McElroy et al., 1990). Towards the western Himalaya the Tethys Himalayan range got widened where it decreases in the elevation and the folding of the Tibetan Himalaya got gentler and appeared to be more Jura-type as in the Spiti region (Gansser, 1964).

In the Kumaon region, Tethys Himalayan sequence is well exposed in the drainage basins of Goriganga, Dhauliganga, Darma and Kali rivers. The contact between the HHC and the sedimentary sequence of Tethys Himalaya in this region was described as gradual transition (Gansser, 1964; Valdiya and Gupta, 1972) or tectonic (Kumar et al., 1972; Shah and Sinha, 1974).

In Dhauliganga and Goriganga river sections, the contact is marked by a sharp contrast in metamorphic grade between the high grade, HHC and the weakly metamorphosed or unmetamorphosed sediments of the Tethyan Sedimentary Sequence. The mineral lineation of Martoli Formation is E-W (mean) while the HHC is NE (mean) which supports a tectonic contact. This tectonic contact is referred to as Dar-Martoli Fault (Kumar, et al., 1972) or Malari Fault (Shah and Sinha, 1974). In some places near the crest of the Himalaya the Lower Palaeozoic rocks of the Tibetan zone contains regional metamorphic assemblages of middle- to low-amphibolite facies conditions (Coleman, 1996; Hodges et al., 1996; Carosi et al., 1998). Usually these units are described as structural horses within the South Tibetan Fault system (Hodges, 2000).

The isotopic data from the Tethyan Sedimentary Sequence is very splash, the available data indicate ϵ_{Nd} values ranging from -6 to -20 (Parrish and Hodges, 1996; Ahmed, et al., 2000; Najman et al., 2000; Robinson, et al., 2001; Najman et al., 2006) while $^{87}Sr/^{86}Sr$ varies between 0.705 to 0.730 (Najman, et al., 2000).

1.6 TRANS HIMALAYAN ZONE

The Trans Himalaya zone lies in the north of the Tethys Himalaya Zone. Various lithotectonic units of this zone represent the junction between the Indian and Eurasian plates. The southern junction between the Indian and Eurasian plates is

defined by almost continuous suture zone, designated as Indus Tsangpo Suture Zone (ITSZ), comprising (a) ophiolite mélanges (e.g., Nidar Ophiolite, Shergol Ophioloite, Zildat Ophiolite, Shigaza Ophiolite etc.) representing Neo-Tethys oceanic crust of Upper Jurassic to Upper Cretaceous age, (b) volcanic arc of basalt, dacite, pillow lava and cherts and (c) the Indus molasses derived mainly from the adjoining eroded sequences (Gansser, 1964; Honegger et al., 1982; Thakur, 1993; Jain et al., 2002 and references therein).

To the north of ITSZ, calc-alkaline Trans-Himalayan Batholith occurs in almost entire length of the Himalaya which represents the Andean-type magmatism due to subduction of the Tethyan oceanic crust under the Eurasian plate (Kumar, 2005; Singh et al., in press). The batholith is variously called as the Kohistan (Auden, 1935; Wadia , 1937; Desio, 1977) and Ladakh batholith (Frank et al., 1977; Sharma 1982; Thakur, 1993) in the northwest, Kailas tonalite and Gangdese pluton in Tibet (Academica Sinica, 1980; Scharer et al., 1990) and Lohit batholith in Arunachal Pradesh (Thakur and Jain, 1975; Sharma et al., 1991; Jain et al., 2002). The northern boundary of the Ladakh batholith is demarcated by another suture zone called the Shyok Suture Zone (SSZ) or Main Karakoram Thrust (MKT) in Pakistan (Jain et al., 2002).

The isotopic compositions for Indus Tsangpo Suture Zone give mantle like ϵ_{Nd} value ranging between -7 to +13 and relatively low $^{87}Sr/^{86}Sr$ value <0.710 (Najman, et al., 2000).

1.7 SCOPE OF THE WORK

The relationship among metamorphism, migmatisation, geothermal, kinematics, and evolution of HHC and generation of leucogranite in the Higher

Himalayan Crystallines (HHC) with reference to the tectonic framework has been one of the major fields of interests in Himalayan geodynamics. Since the closure of the Indian and Eurasian plate about 57 Ma ago (Leech et al., 2005) multiple phases of deformation, metamorphism, metamorphic fluid activation, compression, decompression, crustal loading and reloading has been taking place. Out of these complex geological natures of the Himalayas, the earlier works has mostly been concentrated towards the metamorphism, thermal evolution and modeling of the inversion metamorphism of the HHC. The occurrence of migmatite and leucogranite within the prevailing tectonic regime in the HHC still left a good opportunity to conceive the relationship between them and the generation of the Himalayan Tertiary Leucogranite. In this regard, different approaches such as field data, petrology and petrography, geochemistry, geothermobarometry, thermochronolgy and geochronology using Rb-Sr and Sm-Nd systematics on separated minerals and whole rocks are considered for elucidating the role of migmatite in the collision tectonics vis a vis leucogranite generation while deformation or thrusting occurring as symbiotic or autocatalysis as a dynamic mechanism.

In the Eastern part of the Garhwal Himalaya unlike the Himalayas of Jammu and Kashmir, Himachal Pradesh, Western Garhwal and Nepal, very little geological informations are available in respect of metamorphism, migmatization and the generation of leucogranite. Keeping these in mind Alaknanda- Dhauliganga valleys in Eastern Garhwal Himalaya have been chosen as field area for this Ph. D. research.

1.8 AREA OF STUDY

The present study area of Ph D research program encompasses an area of about 4012 km^2 confined between longitudes $79^0$25' E and $79^0$55'E and latitudes $30^0$25'N and $30^0$50'N (Fig.1.2a,b,c) in the Chamoli district of Uttarakhand (Uttaranchal). Due to the rugged nature of the terrain, geological investigations of the area are concentrated mainly on the two Himalayan river valleys, the Alaknanda and the Dhauliganga. Good exposures of the HHC rocks are present in the Dhauliganga valley along the roadsides of Malari-Joshimath, which provides the systematic study of structure and petrology of the different rock units. Rock exposures of the Alaknanda are varied and discontinuous; however, it provides a good locality for migmatite-insitu melt generated leucogranite study. The ductile shear zone of MCT and VT (Vaikrita thrust) are exposed along the roadside of Joshimath-Helang road. However, substantially, there is not a workable exposure of HHC along the Govindghat-Hemkund and/or Valley of flower tracking route as well as along the Mana-Vasudhara track.

1.9 DRAINAGE

The Himalaya of the Garhwal region in Uttarakhand is largely drained by the Ganga and its tributaries, which includes Bhagirathi, Alaknanda, Dhauliganga, Pindar, Mandakini, Ramganga, Goriganga and Kali rivers (Fig.1.3). Bhagirathi is the name of the upper part of the river Ganga which rises in the great Himalayan range from the Gangotri glaciers near Gaumukh. The Bhagirathi basin is surrounded by high peaks generally above 6000 m, the highest peak being the Chaukhamba (7138 m). The Bhagirathi cuts across a gorge of the Great Himalayan Range in the north of Uttarkashi. Further south, it flows through the terraced valley of Dharasu and Tehri

and finally joins the river Akaknanda at Devprayag beyond which the river is known as the Ganga.The Alaknanda originate from the eastern slopes of the Chaukhamba peak (7138 m) fed by the twin glaciers of Bhagirathi Kharak and Sutopanth. Near Badrinath it flows past the glacially carved amphitheater. The Dhauliganga, flowing on the eastern side originate from Niti Pass (5069 m) and meets with Alaknanada just to the south of Joshimath. The Bhilangna river lies in between the Bhagirathi and Alaknanda and joins Bhagirathi at Tehri while Mandakini and Pindar joins Alakanada at Karanprayag and Rudrapratag espectively. The Nanda Devi region divides the upper drainage system, e.g., the west of which is the Alakanada flowing south-westerly while the eastern part includes the Ramganga, Goriganaga and Dhauliganga flowing south-easterly and joins Kali river in Kumaon.

1.10 METHODOLOGY

To achieve the objectives of the present work the following methods have been employed.

i. Geological mapping on 1:50,000 scale using second edition (1984) Survey of India toposheet Nos. 53 N/6, 53 N/10, 53 N/14 and 53 N/11.

ii. Detailed sampling of various rock types in different metamorphic grades and preparation of isograd map on the basis of mega and microscopic studies.

iii. Textural analysis of metapelites and psammites of the different units.

iv. Mineral paragenesis and determination of suitable mineral reaction.

v. Point analysis by Electron Probe Micro Analyzer (EPMA) for P-T estimation using suitable mineral assemblages and different geothermobarometric calibrations.

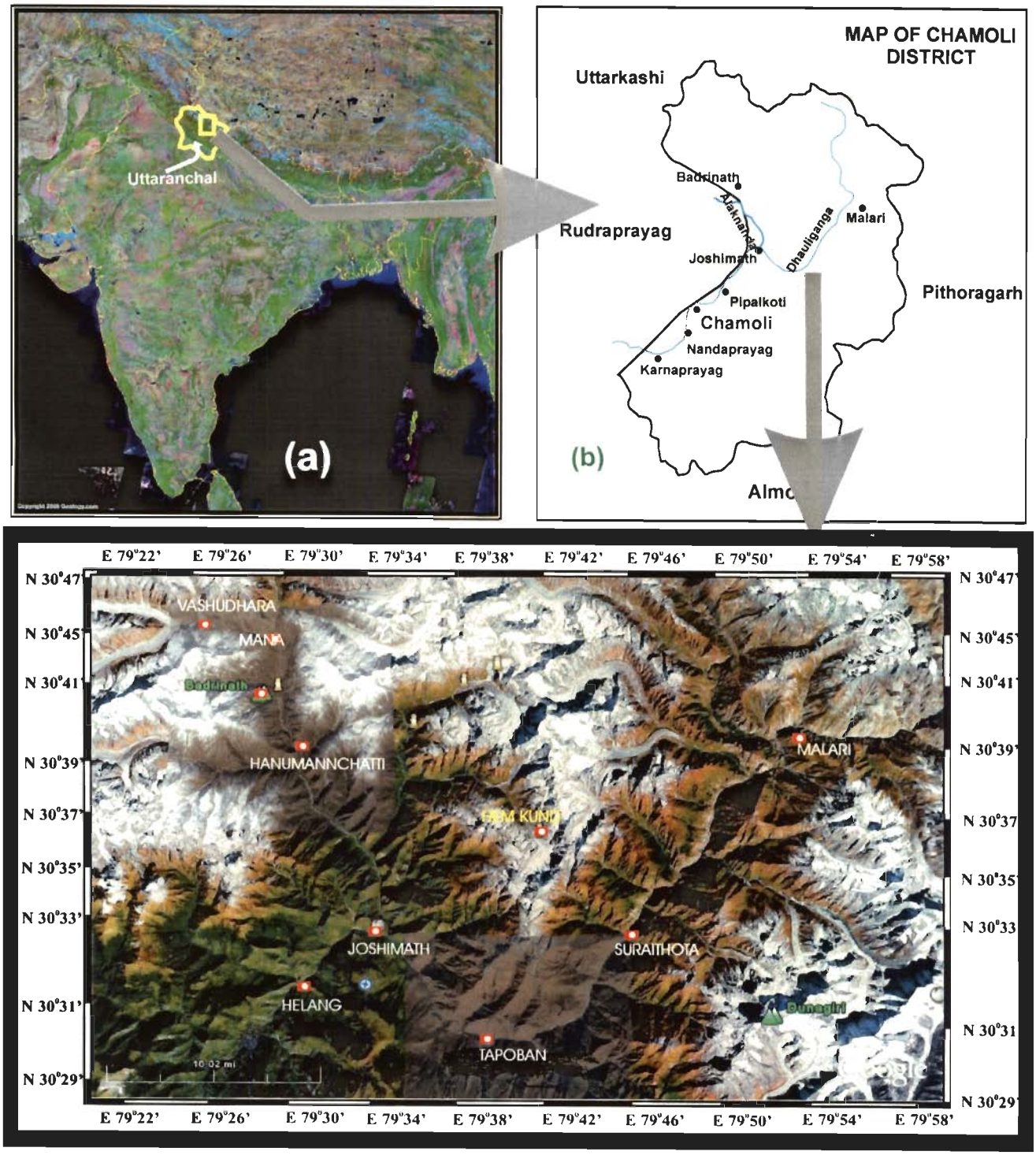

Figure 1.2: (a) The Google Earth image of India showing Uttaranchal state (b) map of Chamoli district in which the study area belongs to (c) Google Earth image of the study area with 1vertical exaggeration.

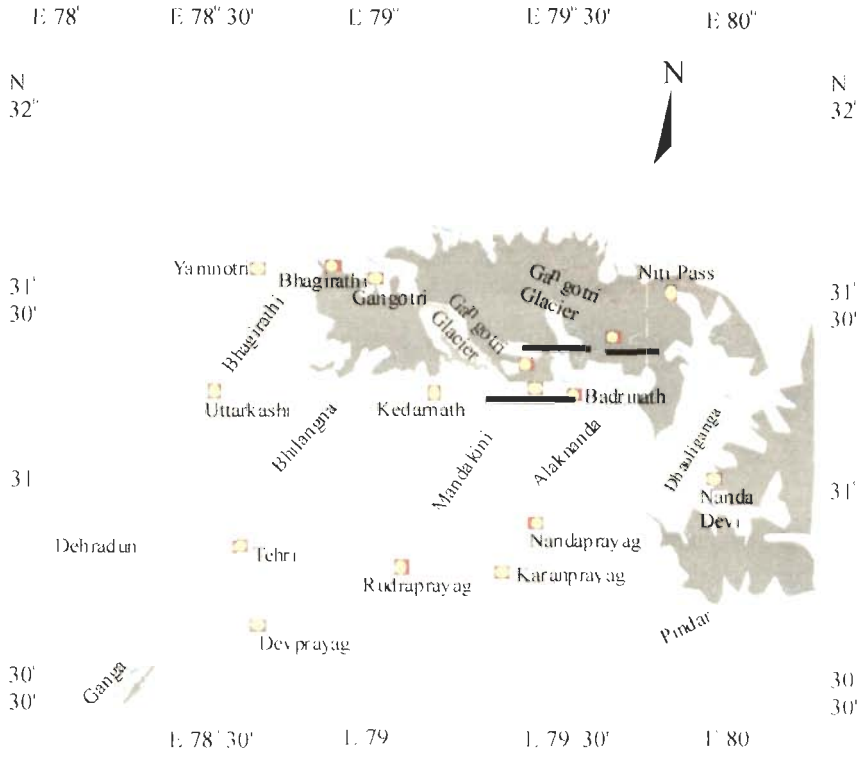

Figure 1.3: The drainage map of the study area and encompassing the downstream region. The red line marked the international border with China.

vi. Zoning in garnet

vii. Bulk geochemical analysis by ICP-MS

viii. Measurement of Rb-Sr and Sm-Nd isotopic ratios by Thermal Ionization Mass Spectrometer (TIMS), age calculation of wholerock-mineral pair for exhumation pattern.

ix. Nd-Sr plot for source rock characterization of the leucogranite and the metasediments.

CHAPTER - 2

GEOLOGICAL FRAMEWORK

2.1. INTRODUCTION

The geology of the Himalaya has always been equated with the tectonics of continent-continent collision developing intracontinental thrust zones separated by major tectonic boundaries. Out of these different tectonic units, the area of interest is confined to the Himalayan Metamorphic Belt (HMB) mainly on the Higher Himalaya along with some parts of the Lesser Himalaya. The HMB consists of Higher Himalayan Crystallines (HHC) having greenschist to granulite facies metamorphic rocks along with greenschist facies rocks of Lesser Himalaya. The HHC is exposed all along the Himalaya, about 2500 km in length with at least two breaks; one at Lahaul where it plunges underneath the Haimanta and second discontinuing in between Zozi La and Dras in Kashmir (Fig. 1.1a) and is known as Zanskar Crystalline (Thakur, 1993). The Higher Himalayan Crystallines (HHC) thrusts southward over Lesser Himalayan Proterozoic sedimentary zone, along the Main Central Thrust (MCT) and associated splays like Jutogh/ Munsiari/ Vaikrita Thrust (Auden, 1948; Berthelsen, 1952; Frank et al., 1977; Sharma 1977; Bhargava, 1980; Bhargava et al., 1991). The HHC has been variously called as the Central Crystalline Zone, Tibetan zone, and Higher Himalayan Crystalline (HHC) Belt etc. Southern part of this belt is thrust southward and exposed as metamorphic klippe within the Lesser Himalaya and is known as; the Salkhala Nappe in Kashmir having Paleo-Mesozoic sedimentary cover (Wadia, 1931), the Chamba Nappe and Chail Nappe in Himachal, the Garhwal Nappe having the Banali-Satengal-Landsdown klippe in Garhwal

(Auden, 1937), the Almora–Dudatoli Nappe in Garhwal-Kumaon (Gansser, 1964) and also incorporating the the Ramharh Nappe and Askote-Baijnath-Nandprayag Klippe (Valdiya, 1980), the Kathmandu Nappe in Nepal, the Daling Group in Sikkim, the Paro and Samchi sequence in Bhutan, and the Bomdila Group in Arunachal Pradesh (Kumar, 1997). The HHC forms the hanging wall of the Main Central Thrust (MCT) and incorporates pelite, psammite and quartzite sequences together with thin amphibolite and calc-silicate bands along with granitoids of various ages (Singh, 2001; Singh and Jain, 2003). It forms the remobilized basement, which is extensively deformed and metamorphosed under middle greenschist to almandine-amphibolite facies (Pilgrim and West, 1928; Berthelsen, 1951; Sharma, 1977; Bhargava, 1980) during main Himalayan phase and is uplifted to the highest elevation in the Himalaya. The HHC is overlain regionally by the Tethyan Sedimentary Zone along its northern margin with a distinct tectonic boundary Trans-Himadri Shear Zone (THSZ) or South Tibetan Detachment System (STDS) and its associated splays (Valdiya, 1989; Burchfiel et al., 1992). In parts of Kashmir, Himachal and Garhwal, it has been locally called as the Zanskar Shear Zone (Herren, 1987; Patel et al., 1993), Rohtang Shear Zone (Jain et al., 1999) and Trans-Himadri Thrust (Valdiya) or Martoli Fault, respectively.

The HHC is characterized by structures evolved in an intracontinental, about 15-20 km thick, ME-dipping ductile shear zone as a result of extreme crustal shortening within the Indian Plate (Brunel, 1986; Mattauer, 1986; Jain and Anand, 1988) and inverted metamorphism throughout the belt (Le Fort, 1975; Frank et al., 1977; Pecher, 1977, 1989; Hodges and Silverberg, 1988; Searle and Rex, 1989; Mohan et al., 1989; Jain and Manickavasagam, 1993). Inverted metamorphism is

characterizing both the Lesser and Higher Himalayan sequence (Heim and Gansser, 1939; LeFort, 1975; Pecher and LeFort, 1986), which is not of same age (Hodges, 2000). In the Garhwal section, the inverted metamorphic sequence of the Higher Himalayan Crystalline was noticed by the earlier workers like Medlicott (1864), Oldham (1883), Middlemiss (1887), Pilgrim and West (1928) and Auden (1937). However, the deformational and metamorphic evolution of the HHC along Dhauliganga and Alaknanda valley were worked out by Indo-Japanese exploration team (Maruo, 1979), Valdiya (1980), Virdi (1986), Roy and Valdiya (1988), Hodges and Silverberg (1988) and Gururajan and Choudhuri (1999).

2.2. GEOLOGY OF THE ALAKNANDA AND DHAULIGANGA VALLEYS

Heim & Gansser (1939) first studied in detail the HHC of Alaknanda valley and adjoining sections of eastern Garhwal and reported that the Higher Himalayan Crystallines (HHC) forms the crystalline succession of 7.8 km thick mica schist and gneiss along with 9.4 km thick quartzite and about 4 km thick para schist with calcsilicate layers. At later stage, Gairola (1975) and Gupta (1978) investigated the petrology of the crystalline rocks around Dhauliganga and Badrinath area. Valdiya (1978) classified the crystalline rocks of lower part of the HHC into the Munsiari/ Jutogh Formations and upper part as the Vaikrita Group, whereas, Virdi (1986) classified these rocks into Tapoban, Joshimath and Pandukeshwar Formations. Thakur (1993) proposed Badrinath Formation, a new lithostratigraphic unit in addition to the Virdi's classification.

The Higher Himalayan Crystallines (HHC) of the Dhauliganga valley comprises of Vaikrita Group of about 18 km thick and about 2 km thick metamorphic sequences of Munsiari Formation while in Alaknanda valley, the Vaikrita Group is

about 12 km thick (Fig. 2.1). The lithostratigraphic units of the HHC of Garhwal section have been described in detail by many workers (Valdiya, 1978, 1980; Yuji Maruo, 1979; Virdi 1986 and Thakur, 1993) and have been classified accordingly into Vaikrita Group and Munsiari or Tapoban Formation which covers most of the area while the overlying Tethys Sedimentary Sequence comprises of Martoli Formation of Haimanta Group in the north and the underlying Lesser Himalayan Sequence composed of Tejam Formation of Garhwal Group in the south. The lithostratigraphic succession along Alaknanda and Dhauliganga valleys is given in the table (Table: 2.1; see also Fig.2.1).

2.2.1 LESSER HIMALAYAN SEQUENCE (LHS)

The sedimentary belt occurring in the south of the MCT can be traced from the Simla area to the border of Nepal for about 350 km. The rock units of the LHS of the present study area comprise of sedimentary rocks of Garhwal Group which are weakly metamorphosed near the MCT. The rocks of this domain are mostly of calcareous in nature. The Garhwal group, comprising predominantly of quartzite and metabasic with intercalations of phyllite and chlorite schist is correlatable with the Berinag Formation.

2.2.2 HIGHER HIMALAYAN CRYSTALLINES (HHC)

The HHC along Alaknanda and Dhauliganga valleys is defined by the crystalline rocks of the Vaikrita Group, of greenschist facies to higher amphibolite facies which include mica-, garnet-, staurolite-, kyanite-, sillimanite-schists and gneisses, sillimanite-Kfs grade rock, migmatite and leucogranite with intermittent thin bands of calc-silicate, amphibolite and veins of pegmatite and quartz. The different

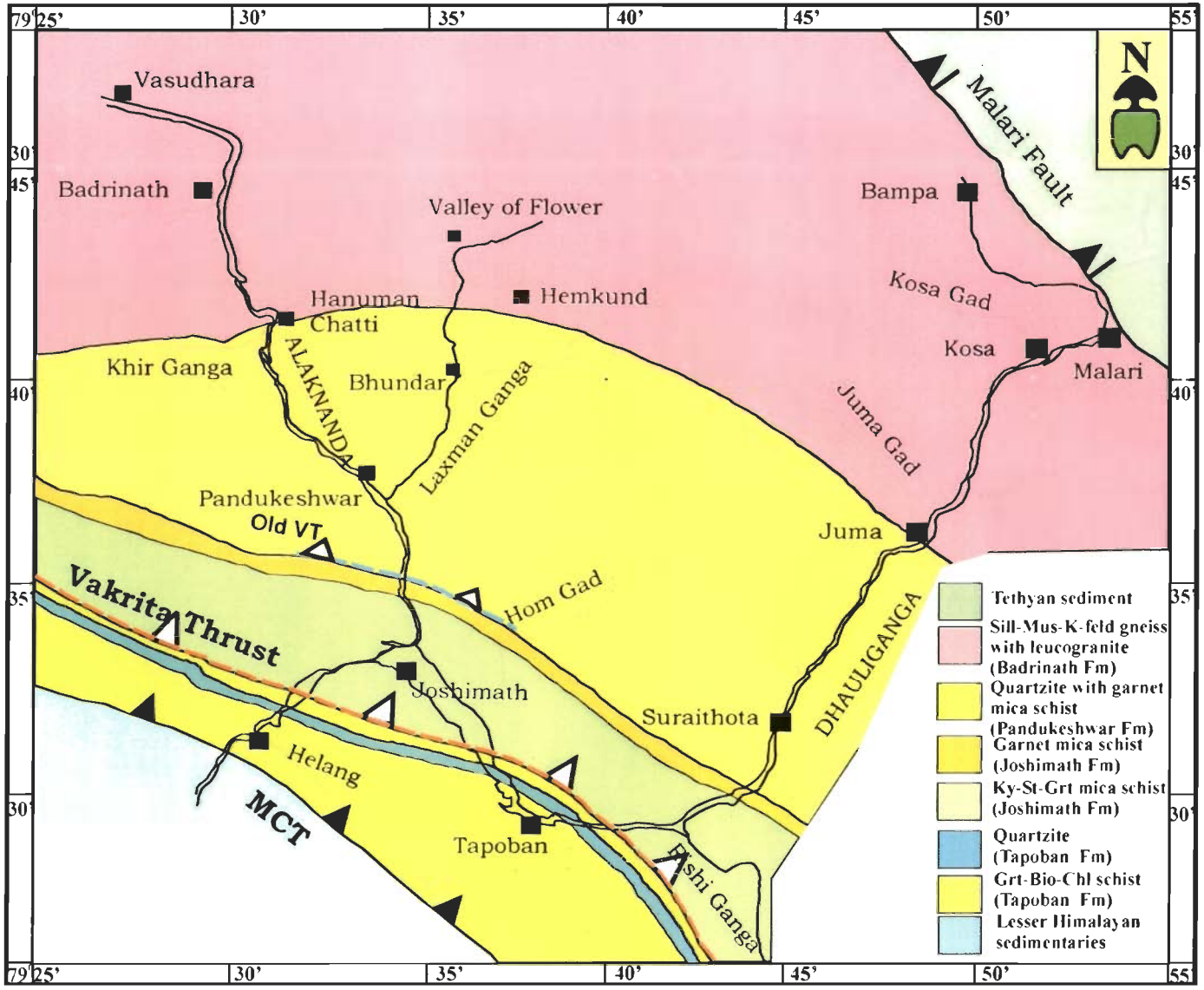

Figure 2.1: Geological amp of Alaknanda and Dhauliganga valley

rock types occurring in the different Formations of the Vaikrita Group area are given in the lithostratigraphic table (Table: 2.1).

2.2.2.1 Munsiari (Tapoban) Formation

Munsiari Formation consists of chlorite schist and sericite quartzite, mica schist, amphibolite, augen gneiss and garnet- mica schist which are dipping

Table 2.1: Tectonostratigraphy of the Central Crystallines in Alaknanda and Dhauliganga valleys (modified after Thakur, 1993)

Lithostratigraphic Unit	Lithology	Metamorphic Grade
Martoli Formation (= Haimanta)	Phyllite, quartzitic phyllite, quartzite and sandstone	Chlorite
- - - - - -	Malari Fault	- - - - -
Badrinath Formation	Garnet, sillimanite, muscovite and kyanite bearing sillimanite zone gneisses, mylonite, mica gneiss, migmatite, calc silicates, leucogranites, pegmatites and garnet amphibolite.	Sillimanite zone
Pandukeshwar Formation	Quartzite, quartz mica gneiss, amphibolite, mica-schist	Kyanite zone
Joshimath Formation	Garnet mica gneiss, garnet, and kyanite gneiss, mica gneiss, garnet amphibolite	Kyanite-zone
▲ ▲ ▲ ▲ ▲	VAIKRITA THRUST	▲ ▲ ▲ ▲ ▲
Munsiari/Tapoban Formation	Mica schist, amphibolite, augen gneiss, staurolite, garnet mica schist, chlorite schist, sericite quartzite	Staurolite zone Garnet and Biotite zone
▲ ▲ ▲ ▲ ▲	MCT / MUNSIARI THRUST	▲ ▲ ▲ ▲ ▲
Calc zone of Chamoli (= Tejam)	Limestone, shale, quartzite, chlorite and quartz-sericite schist	Chlorite zone

moderately towards north. About 2 km north of Helang, the gneisses alternating with bands of chlorite schist and quartzite become prominent while near the MCT thin amphibolite sills are present. The mica schist shows shearing affect with development of S-C fabric and crenulation cleavages.

Sericite quartzite and phyllite are frequently found to be intercalated with the mica schists over a wide zone. It is characterized by the light coloured silky appearance of the rock due to the presence of fine grained sericite sometimes interlaced with the quartzo-felspathic lenses resembling augen gneiss.

Chlorite and Mica schist are exposed near Helang where they are intercalated with thin bands of quartzite showing streaks of white mica. The mica schists and the quartzitic bands have a strong affinity to calcareous nature due to the presence of calcite in lenticles or strings. Sometimes thin bands of calc silicate rocks are intercalated the mica schists. Quartz and calcitic lenses are hosted in the country rocks showing the shearing effect. Mica schist shows folding and strong S-C fabric with the top-to-SSW sense of shearing.

Amphibolite is occurring at the lower part of the Munsiari unit in the form of sills which are characterized by medium grained dark green colour minerals of amphiboles mainly hornblende which are partially chloritized. Under microscope, the amphibolite shows abundant grains of epidote sprung into the foliation defined by the chlorite and amphibole where the amphibole porphyroclasts normally show oblique inclusion pattern of quartz. The microscopic study reveals that the amphibolite has undergone strong deformation as indicated by the microfoldings and fracturing of the hornblende porphyroblasts.

Garnet mica schist of the present study area is a thin band characterized by the presence of garnets in the matrix of biotite and muscovite occurring at about 6 km north of Helang. It is a dark colouerd medium grained rock composed of biotite, muscovite, garnet, plagioclase, quartz, ilmenite, zircon and apatite.

Augen gneiss is thin band of 15 m thick occurring near Tapoban which is characterized by small augens or lenses of quartz wrapped by the biotite flakes. It is medium grained and dark in appearance without any sign of alteration. The augens of about 1 cm size are nicely aligned along the foliation defined by the biotite flakes. The asymmetrical augens show shear directions top to southward which is underlain by garnet mica schist. The mineralogical composition of the rock consists of biotite, muscovite, albite, quartz, zircon and ilmenite.

Staurolite schist is occurring as very thin band just above the garnet mica schist. The rock is intercalated with thin bands of gannet gneiss. It is a light grey coloured fine grained and strongly foliated rock in which abundant numbers of garnets are present. The foliation of the rock is defined by chlorite and muscovite with fine streaks of quartz, ilmenite and tourmaline.

2.2.2.2 Joshimath Formation

Above Munsiari Formation, lies the Joshimath Formation as a apart of Vaikrita Group characterized by garnet-mica gneiss, staurolite-kyanite, kyanite gneiss, two mica gneiss and garnet amphibolite of staurolite-kyanite and kyanite grade. The boundary between the Munsiari Formation and Joshimath Formation has been designated as Vaikrita Thrust (VT) which is confined at the base of the kyanite grade and is located near Tapoban in Dhauliganga valley and near Joshimath in Alaknanda valley. The rocks of this Formation have a thickness of about 6 km.

Kyanite gneiss is occurring as thin band of about 30 meter exposing near the police check post at Joshimath and about 6 km east of Tapoban in the Dhauliganga valley. The rocks are fine- to medium-grained and well foliated with grey in colour. Large size kyanite blades are abundant in the rocks mostly in quartz rich domain within the rock. The kyanite-bearing gneisses near Tapoban is more of mylonitic in nature and are exposed near Joshimath, where discrete layers of quartz domains are dismembered into small augens or blobs arranged parallel to the foliation (Fig.2.2a). The mineral composition of the rock includes biotite, muscovite, plagioclase, kyanite, garnet, quartz, rutile, ilmenite, zircon and apatite.

Garnet mica gneiss is occurring in thin bands overlying the kyanite gneiss characterized by the foliated light colour fine to medium grained rocks which consists of garnet porphyroblasts in the matrix of quartz and mica. By volume the rock is quartz dominated with less than 20% mafic minerals including biotite, muscovite and garnet. The garnet porphyroblasts are normally containing quartz rich inclusions in haphazard manner and sometimes they show sieve texture.

Two-mica gneiss is quite similar with garnetiferous mica gneiss in appearance. The two rocks occur in alternative manner over a wide range. The only difference is being the absence of garnet in the two mica gneiss. In two mica gneiss mica abundance is more as compared to garnetiferous schist/gneiss. About 6 Km north of Joshimath, two-mica gneiss is more of politic in nature and developed S-C fabric and crenulation cleavage with discrete quartz layers deformed into sigmoid showing top-to-southwest (Fig. 2.2 b, c).

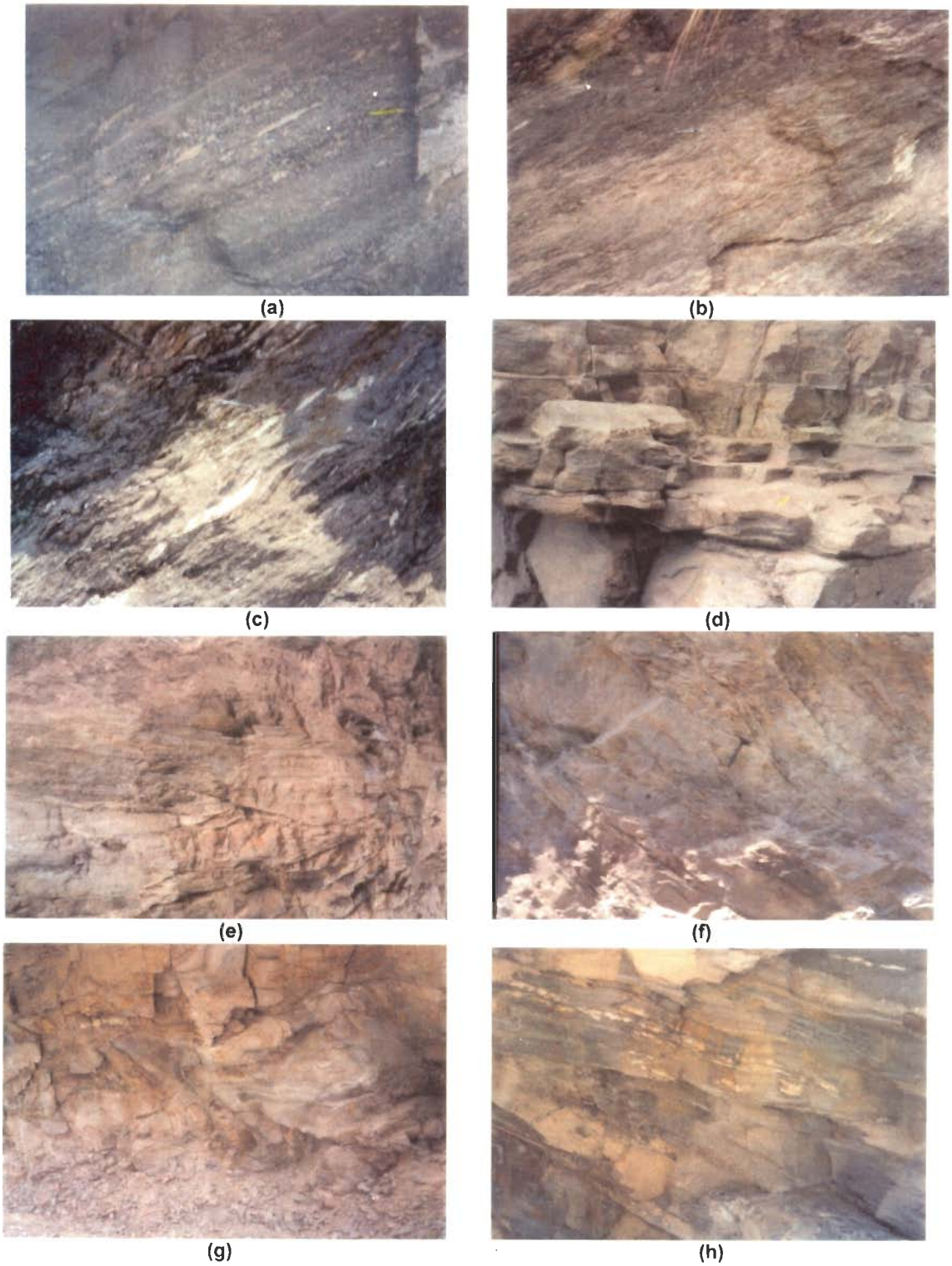

Figure 2.2: (a) kyanite bearing gneiss occurring near Tapoban showing mylonitic structure (b) & (c) S-C fabric and crenulation cleavage developed in mica gneiss (7 km north of Joshimath) (d) paleoripple marks in Pandukeshwar Quartzite, Hanuman Chatti (e) foliation boudin in quartzite, near Suraithota (f) fractures in quartzite producing sigmoidal, Suraithota (g) F_2 folding in quartzite near Juma (h) rootless intrfolial folds of quartz in quartzite near Juma.

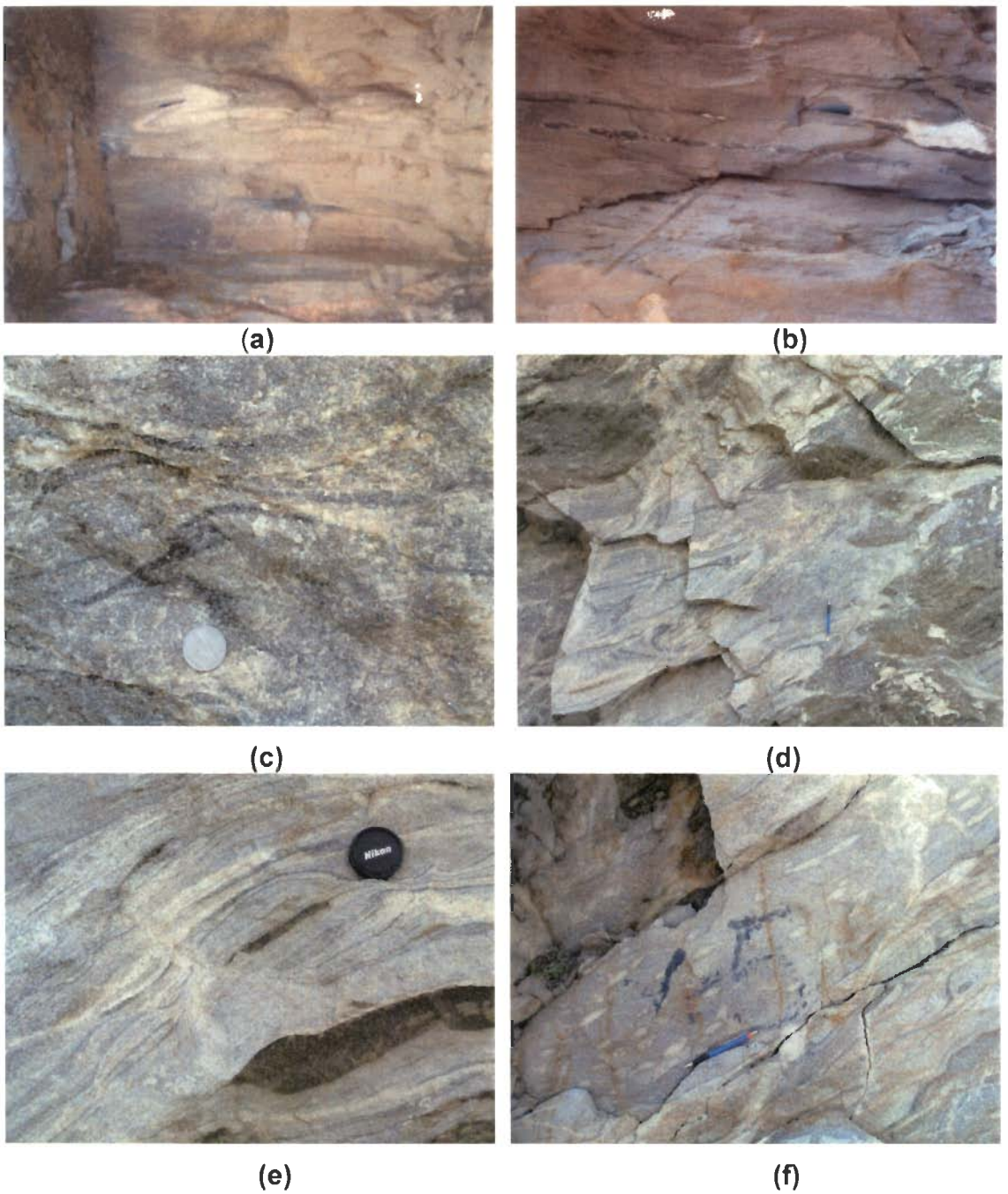

Figure 2.3: (a) Recumbent folding in quartzite, near Suraithota (b) lenticular body of amphibolite sandwiched in quartzite band (6 km north of Pandukeshwar) (c) sillimanite occurring in small lenses in sillimanite gneiss, Malari (d) deformed stromatic migmatite, Malari (e) leucosome occurring in pods in migmatite, Malari, (f) leucosome lenses occurring parallel to main foliation, Malari.

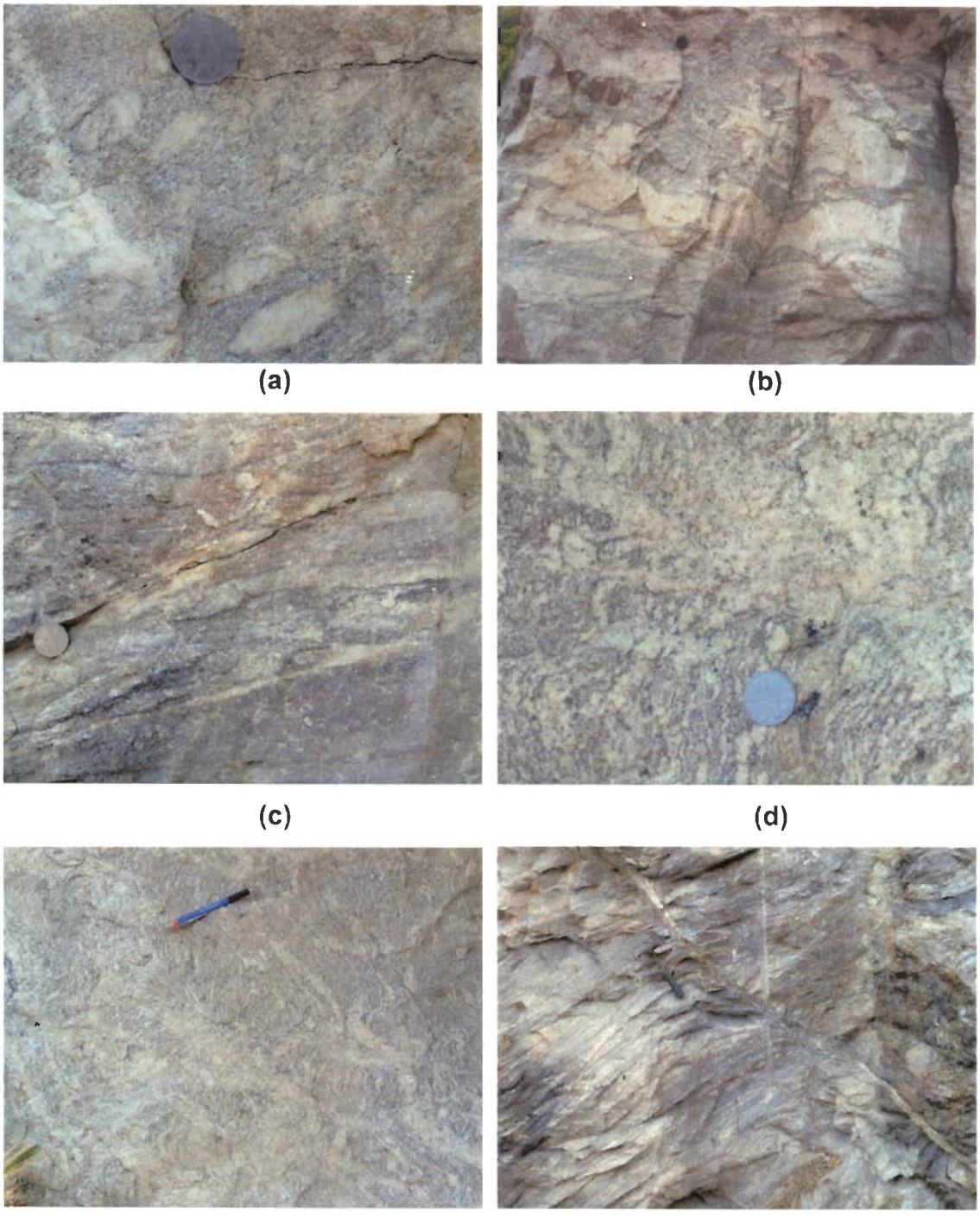

Figure 2.4: (a) leucosome in pods occurring along the foliation which is crosscut by another leucosome veinlet, Malari (b) migmatite with distinct bands of leucosome in which thin layers of garnet are present, Badrinath (c) thin sillimanite layers in the gneisses adjacent to migmatite zone, Malari (d) & (e) melts accumulating along the extensional fabric 2 Km north of Juma (f) normal faulting in migmatite, Malari.

(a)

(b)

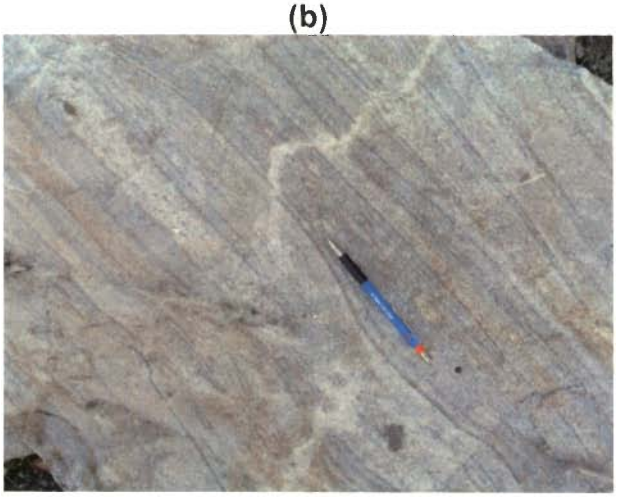

(c)

Figure 2.5: (a) mylonite with sigmoids of quartz, malaria (b) cross-cutting relationship between migmatite and leucogranite (c) small veins of leucogranite cross-cutting the migmatite layering, Malari.

Garnet amphibolite is not a major rock unit of the formation. It occurs as small lenticels along the foliation of the two-mica gneiss and garnetiferous gneiss. It is a medium to coarse grained rock with dark green in colour. The garnets of the rock range upto 3 cm in size.

2.2.2.3 Pandukeshwar Formation

The rocks of Pandukeshwar Formation are mainly consists of quartzite with few intercalations of thin bands of quartz mica gneiss and amphibolite. The rock units of this are described below:

Quartzite of this formation is also popularly known as Pandukeshwar Quartzite, is about 9 km thick band. The rock is characterized by very light gray colour psammatic bands intercalated with thin pelitic bands and composed of medium- to coarse-grain quartz, plagioclase, k-feldspar, quartz, biotite and muscovite. The compactness of the rock varies across the section with the mafic mineral content. At places the quartzite shows graded and cross-bedded structures (Fig. 2.2 d). The quartzite frequently shows foliation boudin structure (Fig. 2.2 e) and at few places intense fracturing produces sigmoidal bodies (Fig. 2.2 f). Near Juma on the western bank of Dhauliganga the quartzite shows large scale tightly folded structures of F_2 generation (Fig. 2.2 g). Rootless intrafolial folds shown by quartz are preserved in the quartzite in many locations (Fig. 2.h).

Quartz mica schist/gneiss is very frequently found sandwiched in between the psammitic bands and composed mainly of biotite and muscovite with quartz. It normally varies in thickness from few millimeters to about 3 m. It is light gray in colour with medium- to coarse-grain size. In few cases it appears greasy with coarse biotite porphyritic stacks abundantly occurring along the foliation. In most of the

cases the contact between the quartzite and the quartz mica gneiss is gradual. The rock unit also shows F_2 isoclinal recumbent fold (Fig. 2.3 a).

Amphibolite is sandwiched within the quartzite bands and contains large size garnets reaching sometimes about 3 cm in diameter. It is mostly occurring as lenticular bodies along the lithological layering (Fig. 2.3 b). Near Lambagar (about 6 km north of Pandukeshwar) in Alaknanda and Suraithota in Dhauliganga valley occurrence of garnet bearing amphibolites in the quartzite band is very frequent. It looks pale green in colour with medium to coarse grain minerals mainly of tremolite, hornblende, garnet, plagioclase, biotite, chlorite and quartz. The green colour tremolite shows aggregation of elongated needles. Thin layer of quartz of about 1 mm thick seems to envelop the amphibolite bodies in most of the cases.

2.2.2.4 Badrinath Formation

Badrinath Formation consists of garnet, sillimanite, muscovite and kyanite bearing sillimanite zone gneisses, mylonite, mica gneiss, migmatite, calc silicates, leucogranites, pegmatites and garnet amphibolite. The rock units present within this Formation are described below.

Kyanite gneiss is about 4 m thick band occurring about 3km north of Hanumann Chatti along the Alaknanda valley, which looks very similar to the kyanite gneiss occurring in the Dhauliganga valley about 6 km east of Tapoban. This gneiss appears to be richer in quartz content and is light grey in colour and mainly composed of coarse-grained minerals of biotite, muscovite, quartz, garnet and blades of kyanite. In this rock unit both rutile and ilmenite are absent, while Joshimath kyanite gneiss is richer in rutile and ilmenite. This kyanite band marks the boundary between Badrinath and Pandukeshwar Formation.

Mica gneiss is occurring in bands above the kyanite gneiss with varying thickness. The contact between two rock units is sharp, however, it gradually going into garnet gneiss. It is dark grey in colour with medium-grained biotite, muscovite, quartz and plagioclase.

Sillimanite schist is more prominent in the Dhauliganga valley, where it occurs as a thick band extending from Juma to Malari with intercalations of thin bands of mica gneiss and garnet-mica gneiss. In the Alaknanda valley, the sillimanite zone extends from Hanumann Chatti to Badrinath. The rock appears dark grey in colour with medium-sized minerals of prismatic sillimanite along with muscovite, biotite, plagioclase, garnet and quartz. Within the rock body sillimanite segregated into thin layers and sometimes in small lenses (Fig. 2.3 c).

Migmatite occurs in both the valleys near Badrinath in the Alaknanda and between Juma and Malari in the Dhauliganga valley. In the Dhauliganga valley, the zone is much wider with lesser generation of melt than that of the Alaknanda valley. The boundaries of migmatite zone are gradually transforming into psammitic gneiss on both side and are more prominently developed in the Dhauliganga valley. In both the valleys the migmatite is present as stromatic and diatexite type (Fig 2.3 d), with melt fraction ranging from 10% to around 40% with the lesser production of *in situ* melt probably due to presence of calc-silicate rocks. The presence of leucosome is more prominent in the Alaknanda valley migmatite, where it is segregated into bands, sometimes of about 40cm thick while such feature is absent in the Dhauliganga valley. Typically large numbers of small pods of leucosome (Fig. 2.3 e, f, 2.4 a) are present which occasionally deformed into ellipsoid and are observed in the Dhauliganga migmatite zone. It probably indicates the fossilized initial stage of *in*

situ melting. Thin layers of sillimanite alone or sillimanite and quartz veinlets are very prominent feature of the Dhauliganga migmatite leucosomes which is devoid of tourmaline and garnet (Fig. 2.4 b). On the contrary, leucosome of the Alaknanda valley contains thin segregated layers consists of garnet and tourmaline in the plagioclase rich groundmass (Fig 2.4 c). The appearance and composition is very similar to that of tourmaline bearing leucogranite from Higher Himalayan Leucogranite (HHL). At few places within the migmatite zone extensional fabric marks the conduit for *in situ* melt (Fig. 2.4 d, e). Towards north the migmatite zone shows normal faulting (Fig. 2.4 f).

Mylonite band is about 20 meter thick which is characterized by strongly crushed and mylonitised rock body occurring in the upward transition zone between the migmatite and the quartzo-feldspathic gneiss in the Dhauliganga valley about 500 meter south of Malari (Fig. 2.5 a). The rock appears green in colour with small augens of quartz of about 1-15 mm size embedded in fine-grained groundmass composed of chlorite, quartz and mica.

Leucogranite has been reported as small body of granite occurring near Malari Fault, upper contact with Tethyan Sedimentary Zone, at Malari. The body appeared to be greenish in colour due to presence of chlorite, on the contrary, large milky white tourmaline leucogranite boulders are present along the nearby nalas (Malari, Kosa, etc.) as well as regoliths in the vicinity of Malari. Small lenses, patches and feeder dykes hosted in psammite are found at about 200 meter south-east of the road, along the nala near the army camp (Fig. 2.5 b, c). This type of small bodies is also found to the north of Mana (3 Km north of Badrinath). It is found that such types

of bodies are result of partial melting of the metasediments of the sill-kfs grade occurring near the contact of the Tethyan Sedimentary Zone.

Pegmatite and Quartz vein are normally found as lenses, veins and dykes in the mica gneiss host. Pegmatite is characterized by large size minerals of feldspar, quartz, phlogopite and tourmaline. It is found in varying sizes ranging from 0.5-2 m size body. The body occurring at about 7 km north of Juma, the size of the tourmaline within the pegmatite goes upto 10 cm in length. The quartz veins are also present in mica gneiss ranging in size from 1 to 10 cm in width.

2.2.3 TETHYAN SEDIMENTARY SEQUENCE

The Tethyan sediments of the study area are mainly of phyllite, quartzitic-phyllite and green slate of Martoli Formation overlain by conglomerate and quartzites of Ralam Formation of the Haimanta Group. The rocks of the sequence have a gentler dip and show E-W mineral lineation.

2.3. TECTONIC BOUNDARIES

2.3.1 MAIN CENTRAL THRUST (MCT)

The MCT was first delineated by Heim & Gansser (1939) in the eastern Garhwal section which is located between the Berinag quartzite and/or Calc Zone of Tejam of Lesser Himalayan sedimentaries and the crystallines of Higher Himalaya. According to Valdiya (1980), the MCT of Heim and Gansser (1939) in the Garhwal Himalaya is designated as Munsiari Thrust (MT), along which, the crystalline thrust sheets have moved southward. The MCT is define by broad shear zone ranging from several hundred meters to several kilometers wide on either side of the thrust plane and not as a single plane. It appears to be developed in a tectonic mélange derived from both the Higher and Lesser Himalayan sequences collectively called as the

Main Central Thrust Zone (Pecher, 1978; Arita, 1983; Hubbard, 1989; Schelling and Arita, 1991; Macfarlane et al., 1992; Hodges et al., 1996; Vannay and Hodges, 1996; Vannay and Grasemann, 1998; Wyss et al., 1999; Stephenson et al., 2000). The nomenclature and the position of the MCT remain debatable. In Nepal Himalaya the MCT has been put at the base of the high grade kyanite-sillimanite rocks (Bordet, 1973; Hashimoto et al., 1973; Le Fort, 1975). However, the easterly extension of the Munsiari Thrust in Nepal is designated as the MCT-I (Arita, 1983).

2.3.2 VAIKRITA THRUST (VT)

The Vaikrita Thrust was first recognized by Valdiya in 1977, which marked the tectonic boundary between the high grade rocks of the Vaikrita Group and the underlying Munsiari Formation. In different sections of the Himalaya Vaikrita Thrust (VT) has been designated with different name and position. The easterly extension of the Vaikrita Thrust in Nepal is designated as the MCT-II (Arita, 1983). However, in the geological explanation of the present study area, the position and nomenclature of the MCT of Heim & Gansser (1939) and the Vaikrita Thrust of Valdiya (1977) is adopted for the tectonic boundaries. In the Alaknanda valley, the VT lies about 8 km north from the MCT (Munsiari Thrust). It is characterized by thin zone of intense shearing which marked the boundary between the Munsiari/ Tapoban Formation of Chlorite to amphibolite grade rocks and the upper amphibolite grade rocks of Vaikrita Group. In lithology there is no break across the contact or the boundary between these two rock Groups (Heim and Gansser, 1939; Gansser, 1964). However, the base of the Kyanite grade rocks near Joshimath has been considered as the boundary between the two rock Groups. The Munsiari or Tapoban Formation lying between the VT and Munsiari Thrust has been suggested as the imbricate zone

depicting a duplex structure with MCT as the floor thrust and VT as the roof thrust (Thakur, 1993).

2.3.3 MALARI FAULT (MF)

The northern boundary of HHC of the present study area is demarcated by Malari Fault (Shah and Sinha, 1974; Valdiya and Roy, 1988; Gururajan and Choudhuri 1999), which is also referred to as Dar-Martoli Fault (Kumar et al., 1972). This tectonic boundary has seldom defined as Malari Thrust (Virdi, 1986). The fault is demarcated by the sudden changes in the lithology of the high grade metamorphic rocks of the HHC to the weakly metamorphosed and sedimentary rocks of the Tethyan Himalayan Sedimentary Zone. The nature of this tectonic contact is characterized by the structural features of extensional tectonic present in the metasediments near the contact zone.

CHAPTER - 3

TECTONOMETAMORPHISM

3.1 INTRODUCTION

Collision tectonic within Himalaya led to large scale complex deformation and metamorphism mainly recorded in Higher Himalayan Crystallines (HHC). Careful study of the rocks in the field, petrographic studies, thin sections under microscope, for their structural history and textural relationship can shed light on the evolutionary history. This chapter is showing results of geological field investigations, structural-textural relationship with selected mineral chemistry and subsequent geothermobarometric estimations.

3.2 PREVIOUS STUDIES

Tectonometamorphic history of the Higher Himalayan Crystallines (HHC) of the different sections across the Himalaya has been published by many workers (Hodges and Silverberg, 1988; Staubli, 1989; Searle and Rex, 1989; Metcalfe, 1993; Guillot et al., 1999; Jain et al., 1999, Manickavasagam et al., 1999, Searle et al., 1999 and Stephensen et al., 2000 and others). In most of the cases, at least four main phases of deformation and three main stages of metamorphism have been worked out; which are (i) early pre-Himalayan metamorphism (ii) main-Himalayan metamorphism and (iii) post-Himalayan metamorphism. Metamorphism of first stage M_1 postulated as the pre-Himalayan stage related with the first deformation D_1 phase which have been superposed and largely obliterated by the later events of deformation and metamorphism, while the M_2 metamorphism has been correlated with D_2 deformation phase, which is the main Himalayan deformational phase

with D_2 deformation phase, which is the main Himalayan deformational phase resulting into formation of main foliatios and the M_3 metamorphism appears to be weak metamorphism developed during and post collisional D_3 deformation (Staubli, 1989; Pognante and Benna 1993; Searle and Rex 1989; Jain et al., 1999, 2002; Manickavasagam et al., 1999 and references therein). However, Searle et al. (1999) and Stephensen et al. (2000) have suggested two stages of metamorphism for HHC, in which M_1 is described as the barrovian type metamorphism (Eo-Himalayan) occurred in the lower parts going upto kyanite grade and the M_2 reaching upto sillimanite grade (Neo-Himalayan) associated with migmatite and leucogranite generation in the middle and higher structural levels. Along the Bhagirathi river section of western Garhwal, Metcalfe (1993) and Manickavasagam et al., (1999) have shown four stages of deformations. In Garhwal Himalaya, along Alaknanda and Dhauliganga sections two stages of metamorphism have suggested by Hodges and Silverberg (1988). They ascribed first stage M_1 metamorphism as the high pressure-temperature barrovian type metamorphism affecting the entire HHC, while, the M_2 has been described as the high temperature and low pressure buchan type metamorphism and are mainly exemplified by the upper section of the HHC. Using the rim thermobarometry and inclusion thermobarometry in garnet and modeling of garnet zoning, Hodges and Silverberg (1988) concluded that the peak M_1 condition took place at temperature greater than 623^0C and pressure greater than 9.6 Kbar while the M_2 event also took place at about the same temperature with that of M_1 with a substantial decrease in pressure to about 3.17 to 5.23 Kbar. They attributed the earlier event M_1 to a burial of about 36 km depth during the early stage of collision while the M_2 phase is related to thrust imbrication during uplift of the

Pognante and Benna (1993) have reported three stages of metamorphism along Everest section in eastern Nepal.

Deformation of HHC in Dhauliganga section have been studied by Gururajan and Choudhuri (1999) where they recognized two distinct deformation events D_1 and D_2 represented by S_1 and S_2 foliations. The second foliation S_2 is described as the regional penetrative feature which is parallel to Vaikrita Thrust (VT) and Main Central Thrust (MCT). According to them, these two stage foliations are more clearly observed in lower package of the Munsiari Formation than the overlying Vaikrita Group, where the two set foliations resembles S-C fabric. They correlated D_1 deformation with the formation of snowball garnet or garnet with spiral inclusions while D_2 deformation has been correlated with the foliation define by the matrix tail developed from the earlier S_1 foliation.

The timing of peak metamorphism has usually been constrained by dating of monazite, garnet and other mineral ages. In southeast Zanskar, monazites in the pelites from the base to top of the HHC have yielded 32 to 30 Ma by U-Pb method (Walker et al., 1999). U-Th-Pb dating on *insitu* monazite in garnet and matrix monazite from the Garhwal HHC yield 44-36 Ma and 34-25 Ma respectively (Foster et al., 2000). Garnet–whole-rock ages of Sm–Nd on kyanite grade rocks from Garhwal gives ~40 Ma (Prince et al. 1999), and Sm–Nd garnet core and rim ages from Zanskar Himalaya are calculated as 33 and 27 Ma (Vance & Harris 1999). *In situ* Sm-Nd analysis on single grain zoned garnet from Sikkim Himalayan migmatite gives rim and core ages 16.1±2.4 Ma and 23.0±2.6 Ma respectively (Harris et al., 2004) indicating that the peak temperature of the prograde metamorophism before decompression took place not later than 23 Ma while the near peak temperature for

decompression took place not later than 23 Ma while the near peak temperature for melting took place at around 16 Ma with a decompression rate of 2 mm yr^{-1}. The older age is predicted to be peak metamorphic condition for kyanite grade which coincides with the early movement of MCT as determined from monazite from the MCT zone in Sikkim (Catlos et al., 2003) and from the Bhutan transect (Daniel et al., 2003) while the younger age which lies within the uncertainties of U-Pb ages from kyanite migmatites above the MCT in Bhutan as 18-14 Ma (Daniel et al., 2003) and the age of monazite growth from the Lesser Himalayan Formation near the MCT in Sikkim as 15-14 Ma (Catlos et al., 2003). Based on Rb-Sr biotite and muscovite ages the age of the main M_1 metamorphism is considered to be older than 34 Ma, and took place during crustal thickening (Inger and Harris, 1992). In central Nepal along Kali-Gandaki valley, Ar-Ar hornblende suggest that the earlier prograde Eo-Himalayan metamorphism M_1 took place during the time of burial to a depth of about 35 Km at ~37 Ma (Vannay and Hodges, 1996). On the basis of these data it can be observed that the age of prograde metamorphism M_1 has been poorly constrained which might have taken place between 40 to 23 Ma. However, the timing of the M_2 event has been constrained by the dating on monazites by U-Pb technique from migmatite and leucogranite from various sections. The timing of crustal melting, the formation of migmatite and the generation of leucogranite from Zanskar Himalaya has been constrained by U-Pb dating on monazite from leucosome pods (Noble and Searle, 1995), which yielded 20.6 to 19.5 Ma and 20.8 ± 0.3 Ma that has been attributed to the age of peak metamorphism attained during M_2 metamorphism. In Sikkim Himalaya, Sm-Nd dating on garnet rim Harris et al., (2004) calculated 16.1±2.4 Ma and attributed to the peak metamorphism of the M_2 event. Based on Ar-

(Hubbard and Silverberg, 1989), the age of the M_2 metamorphism has been suggested to be between 20 and 17 Ma. Therefore, the age of M_2 event can be suggested to be between 20 to 16 Ma.

3.3 DEFORMATIONAL PATTERN

Traverses across the HHC and Lesser Himalayan Sedimentary Sequence from Malari and Badrinath to south of Helang (Fig. 3.1) four deformational phases were recognized depending on the basis of style, shape, orientation and structural relationships with each other.

3.3.2 FIRST DEFORMATIONAL PHASE (D_1):

The earliest structures of first deformation stage (D_1) are rare, however, oone can observe them at places along Malari-Helang and Badrinath-Joshimath sections. The lithological layering (S_0) has been deformed into tight isoclinal fold (F_1) of first generation having axial planar banding/ foliation S_1. The primary sedimentary structures in the quartzitic or psammitic bands are still preserved within the Pandukeshwar Formation in the form of current ripple marks at different localities in both the sections (Fig. 2.2d). This lithological layering or banding (S_0) are preserved mostly in medium and high grade rocks of the HHC and they are pronounced at the sharp contact between psammitic bands and pelititc bands consistently trending NW-SE and dipping moderately towards NE. The crests of the ripples trend $N310^0$ having up current sides dipped about 12^0 while the down current sides dip about 26^0. S_1 foliation, in these sections, is defined by the metamorphic segregation foliation of alternating quartzo-feldspathic and mica bands. The linear structures related with first stage deformation, appears to have been obliterated due to intense main deformational event.

first stage deformation, appears to have been obliterated due to intense main deformational event.

3.3.2 SECOND DEFORMATIONAL PHASE (D_2):

The second deformational phase is the most prominent and most pervasive deformational event in the Higher Himalayan Crystalline (HHC) rocks along Alaknanda and Dhauliganga valleys. This phase of deformation produced S_2 foliation which is parallel to earlier S_0 and S_1 foliations and forms the main composite foliation and can be termed as S_m the most prominent foliation of the ara. The S_2 foliation (2.2 g) is the axial planar foliation of F_2 fold. F_2 folds are mostly recline type in nature trending in NE with moderate angle, while the axial planar foliation (S_2), a ductile shear fabric, dipping at moderate angle striking NW-SE direction. It is persistently observed within both Munsiari Formation and Vaikrita Group along both the sections.

The rootless hinges of earlier folds are also present within the quartzitic layer (Fig. 2.2h). The main foliation S_m is a composite S-C planar fabric (cf. Berthe et al., 1979), where S-surfaces are progressively deflected and become subparallel to C-shear surfaces of high strain on millimeter scale (also, Patel, 1991; Singh, 1993; Jain and Manickavasagam, 1993; Patel et al., 1993). These S-C fabrics are associated with asymmetric individual folds along with asymmetric pressure shadows, all consistently showing top-to-southwest overthrust type ductile shearing along both the sections. The main lineation is the mineral lineation marked as the stretching lineation parallel to F_2 folds on S_2 foliation plunging towards NE in both the sections and they mark the tectonic transport direction of the zone (also Coward et al., 1982; Brunel, 1986; Jain and Anand

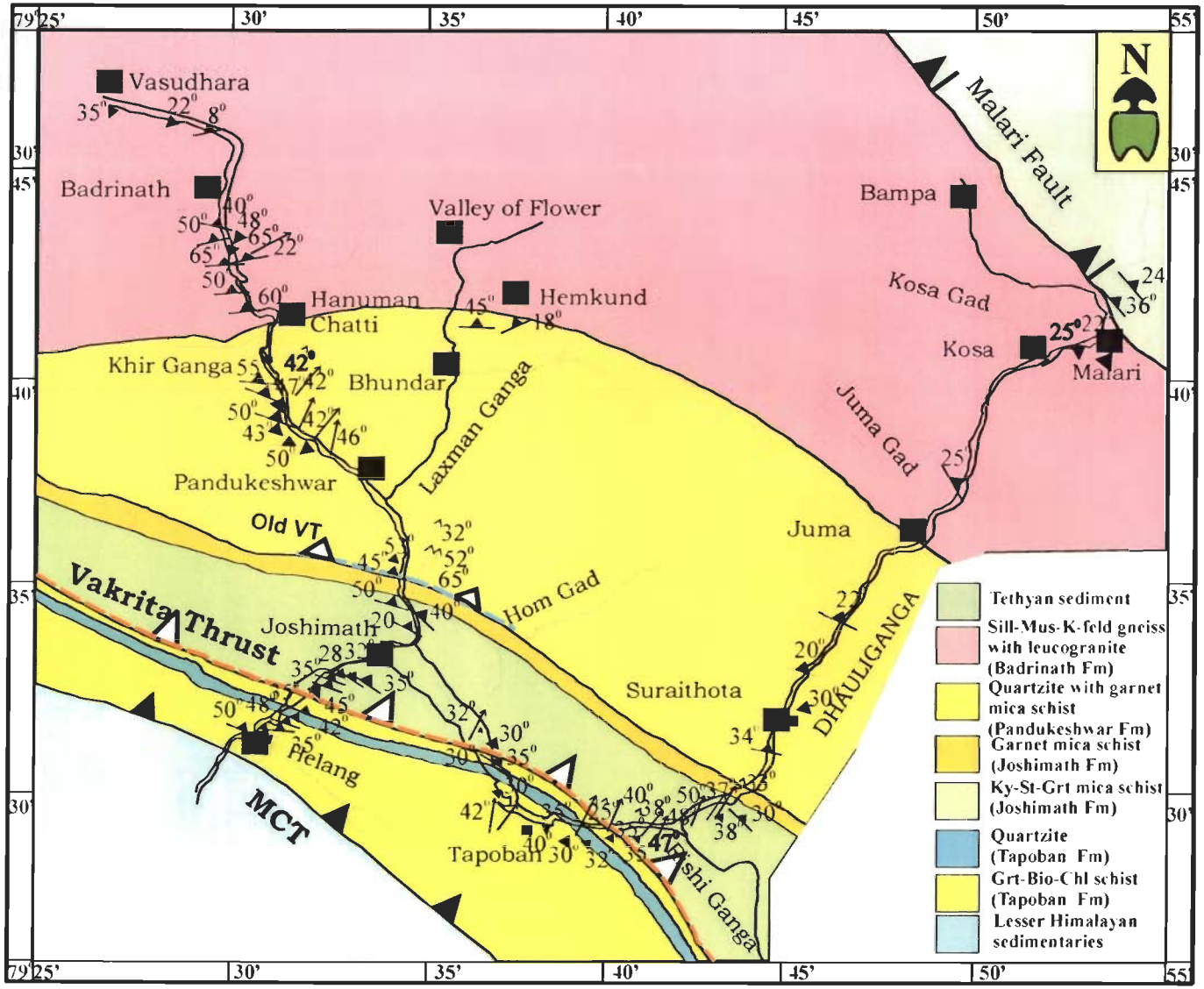

Figure 3.1: Structural map of Alaknanda and Dhauliganga valley showing trends of main foliations and lineations

1988; Epard et al., 1995). The mineral lineations are marked by preferred orientation of many prismatic and tabular minerals including kyanite, staurolite, sillimanite, biotite, muscovite and other prismatic crystals in all the lithologies. F_2 folds have type-3 hook shape interference pattern with F_1.

3.3.3 THIRD DEFORMATION STAGE (D_3):

The structures of D_3 deformation are superposed on all the earlier fabric and can be subdivided into two episodes of early D_{3a} and D_{3b} deformational phases. Earlier D_{3a} deformational event records close to isoclinal, recumbent to gently inclined F_{3a} fold with related (Fig. 2.2i) axial planar foliation S_{3a}. These F_{3a} folds are also prominent on other sections of Himalaya. Sometimes they mark most spectacular large kilometer-scale folds (e.g., Fozal Nala in Beas valley, Himachal Pradesh). The relationships with the earlier structures have not been observed. Along the F_{3a} folds earlier lineations have been modified, indicating that F_2 and F_{3a} folds are not coaxial in this area.

The late D_{3b} deformational phases is marked by open to close crenulation folds F_{3b} axial planar fabric. The L_2 lineations have also folded along F_{3b} hinge zone. The F_{3a} and F_{3b} folds are coaxial and at places indicate interference pattern type 3 (Ramsay, 1967).

3.3.5 FOURTH DEFORMATIONAL PHASE (D4)

Discrete shear zone with fault gauge development post dating F_{3b} folds are also observed along Dhauliganga valley near Tapoban. These appear to represent the late phase of brittle thrusting could be related with Vaikrita Thrust (VT). Kink bands, tension gashes have also been observed on the earlier main foliation and appear to have developed after the main thrusting events along these valleys.

3.4 METAMORPHIC PATTERN

The metamorphic pattern can be observed from the different rock types of Alaknanda and Dhauliganga valleys, mineralogical assemblages, relationship between the porphyroblasts and the matrix minerals, garnet morphology, their inclusion pattern, diffusion zoning and their P-T estimations from a large number of thin sections (around 150), collected from different locations between Helang to Badrinath and Malari (Fig. 3.2).

3.4.1 MUNSIARI FORMATION

For Munsiari Formation, samples were collected from the locations in the vicinity of Helang. The rocks are lying in the metamorphic mineral zones of chlorite-biotite and garnet occurring as inverted sequence. In most of the cases, chlorite is one of the dominant mineral and associated with calcite and aggregates of epidote in the basal part.

3.4.1.1 Chlorite-Biotite Zone

The typical mineral assemblage of the chlorite-biotite zone is Biotite-Muscovite-Chlorite-Epidote-Calcite-Quartz. The schists are mainly chlorite and phengite with subordinate muscovite and biotite occurring as patches along the periphery of the phengite and chlorite. Considering this textural relationship present among the rocks the reaction for the formation of biotite of this zone can be

Phengite + Chlorite → Biotite + Phengite-poor muscovite + Quartz + H_2O

---------- (3.1)

Nicely developed muscovite 'fish' have also been observed in the thin sections of the zone where muscovite is the dominant mineral occurring in the matrix

of quartz, muscovite and opaque, defining S and C-fabric (Fig. 3.3a, b). In epidote-chlorite schist abundant small grains of epidotes are matted in the chlorite-biotite defined foliation (Fig. 3.3c). In amphibolites of this formation, the schistosity is defined by hornblende and biotite with occasional segregation into thin layers. The mineral assemblage is: Hornblende-Biotite-Muscovite-Chlorite-Epidote-Quartz-Opaque.

Hornblende porphyroblasts show inclusions of muscovite and quartz in straight pattern which are embedded in fine matrix of hornblende, biotite and quartz (Fig. 3.3d). Fracturing along the inclusion in few grains might possibly develop during brittle shearing which might have enhanced inclusions or vice versa. On the other hand, the internal foliation S_1 is oblique to the external pervasive foliation S_2, this may be due to the rotation of the porphyroblast during late stage D_1 deformation.

3.4.1.2 Garnet zone

Garnets of this zone are occurring in the gneiss of thin band which got weakly mylonitized towards MCT. Under microscope, the garnet porphyroblast show S-type inclusion pattern of quartz in garnet with a distinct shadow zone.

The assemblage of the rock type is Garnet-Biotite-Muscovite-Plagioclase-Quartz-Chlorite-Opaque. The probable reaction for the garnet formation is

Muscovite+ Chlorite → Garnet+ Biotite+ Quartz+ H_2O

---------- (3.2)

3.4.1.3 Staurolite zone

Staurolite-garnet–schist occurs in a very thin band overlying the garnet zone in the higher structural level. Staurolites are occurring as syn- to post- kinamatic setup to S_2. Syn-kinematic staurolites are 1-3 in mm size and elongated in shape embedded in a chlorite rich matrix. The garnet of about 9 mm diameter size (Gt_1) is aligned with the crenulated internal foliation and contains staurolite as inclusion. Post kinematic staurolites are occurring as small ideoblasts in association with small subideoblastic garnets (Gt_2) in strongly foliated schist defined by chlorites and muscovite containing large garnet porphyroblasts with spiral inclusions of either quartz or ilmenite (Fig. 3.3e). Ilmenite is abundantly occurred as an altered product and primary stringent aligned along the foliation. The reaction forming the staurolite can be written as follows

Garnet + Muscovite + Chlorite → Staurolite + Biotite + Quartz + H_2O

---------- (3.3)

3.4.2 VAIKRITA GROUP

The rocks of Vaikrita Group exposed along the Alaknanda and Dhauliganga valleys are containing main;ly schists, gneisses and calc-silicates of kyanite-staurolite and sillimanite zone, along with migmatite, leucogranite, pegmatite and quartz veins. A thick quartzitic band known as Pandukeshwar Quartzite is occurring within the Vaikrita Group. It is generally poor in mica as compared to the quartzite of the Munsiari Formation. The quartzite of Pandukeshwar Formation is frequently intercalated with thin bands of mica schist, garnet-mica schist, psammitic schist and occasionally amphibolite and calc silicate bands.

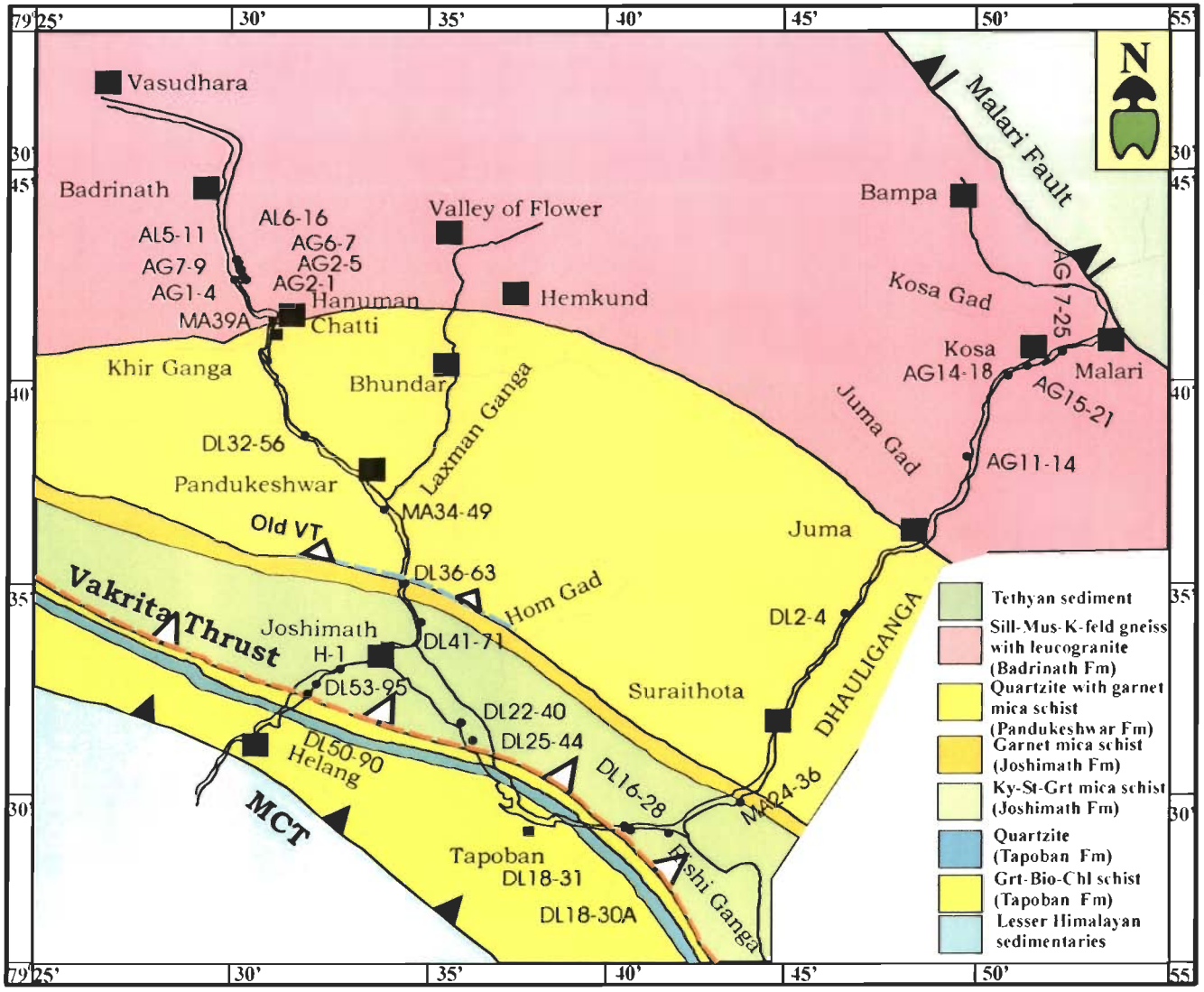

Figure 3.2: Sample location map along Alaknanda and Dhaulliganga valley for geothermobarometry

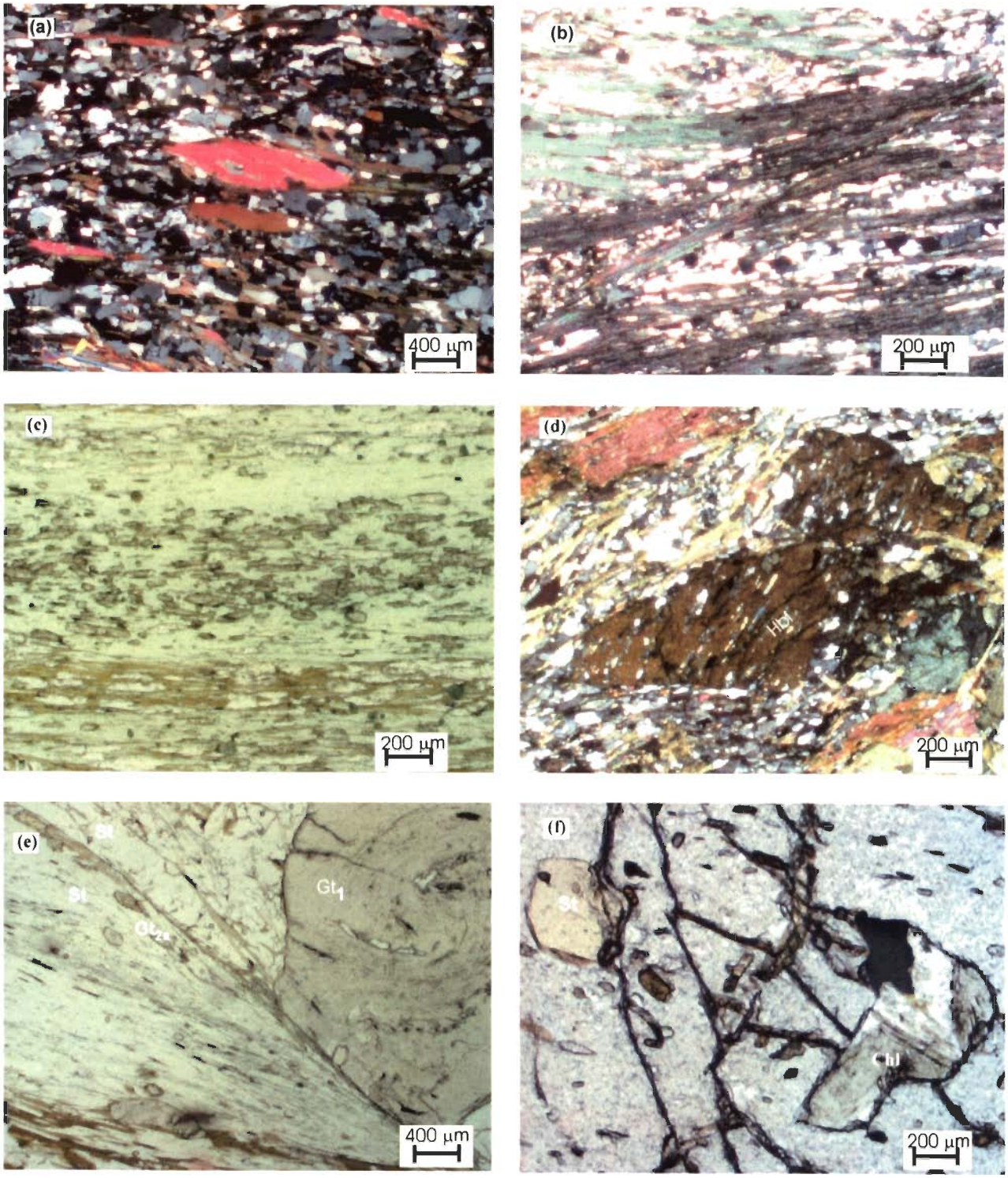

Figure: 3.3 (a) & (b) are the mica fish and S-C fabric developed in the mica schist of Munsiari Formation. (d) abundant small grains of epidote occurring along the foliation defined by biotite and chlorite in the Munsiari mica epidote schist (e) large syntectonic porphyroblast of hornblende occurring in the groundmass of foliation defined by biotite and quartz (f) two different stages of garnet Gt_1 and Gt_{2a} where Gt_1 is shown by large porphyroblast with spiral inclusion of quartz and ilmenite while Gt_2 is smaller in size and free from inclusion occurring along with staurolite in alignment parallel to the foliation & (e) garnet of third generation Gt_3 with presence of staurolite and chlorite inclusion.

3.4.2.1 Kyanite zone

Large porphyroblasts of kyanite are abundantly occurring in the schist and gneiss of this zone. Near Joshimath samples show occasional small garnets along with kyanite, muscovite, biotite, plagioclase, quartz and tourmaline, which indicate a progressive metamorphism. Garnets appears to be of two stages; one is pre-tectonic Gt_1 containing inclusions of quartz and ironoxide and other is post-tectonic Gt_2 occurring parallel to the foliation. Small patches of staurolite within large garnet of about 1 cm size clearly indicate a staurolite consuming reaction for the production of garnet (FiG. 3.3f). The assemblage is: Kyanite-Staurolite-Garnet-Muscovite-Biotite-Plagioclase-Calcite-Quartz-Tourmaline-Sphene-Zircon-Ironoxide.

The reaction for kyanite formation appears to be

Staurolite + Muscovite + Quartz → Kyanite + Biotite + H_2O

---------- (3.4)

At places, nucleation of sillimanite at the fringe of kyanite and plagioclase has also been observed which may be due to localized high temperature as a result of friction along the VT and the related faults (Fig. 3.4a). Therefore polymorphic transformation reaction of the Al_2SiO_5 is a clear evident.

Kyanite→Sillimanite ---------- (3.5)

3.4.2.2 Sillimanite zone

Both upper and lower sillimanite zone is present in the area. Sillimanite gneiss is occurring as discrete layers in the migmatite along with thin layer of prismatic crystals of millimeter size in the leucosome. Kyanite porphyroblasts are present along with the prismatic sillimanite in the schist while muscovite is present

only at lower structural level. At higher structural level muscovite is absent but K-feldspar starts appearing. In the lower sillimanite schist muscovite and biotites are fibrolitised with the generation of melt (Fig. 3.4b). The sillimanite forming reaction in lower sillimanite (+ muscovite) zone is given as

Muscovite + Biotite + Quartz + H_2O → Sillimanite (fibrolite) + melt

---------- (3.6)

and upper zone is characterized by the occurrence of k-feldspar with sillimanite which may be produced by the reaction as follows

Muscovite + Quartz → Sillimanite + K-feldspar + H_2O

---------- (3.7)

This muscovite consuming reaction seems to be valid in this case for the production of the sillimanite because muscovite is absent and k-feldspar is present. Amphibolite band occurring as a concordant body within the lower sillimanite zone contains large porphyroblasts of garnets of 4 to 20 mm diameter. The mineral assemblage is Garnet- Hornblende- Plagioclase- Biotite- Quartz- Ironoxide.

3.4.2.3. Pelitic migmatite

The pelitic migmatite contain both melanosome and leucosome layer and quartzo-feldspathic dykes. The melanosome of the migmatite contain sillimanite as thin ribbons with biotite and few garnets while the leucosome part is composed of mainly plagioclase (albitic) and quartz giving a modal composition of trondjhemite along with homogenized garnet, tourmaline prisms and relicts of sillimanite. Towards the core of the body, presence of myrmekitic replacement texture and perthite, mainly string types with wavy structures are abundant

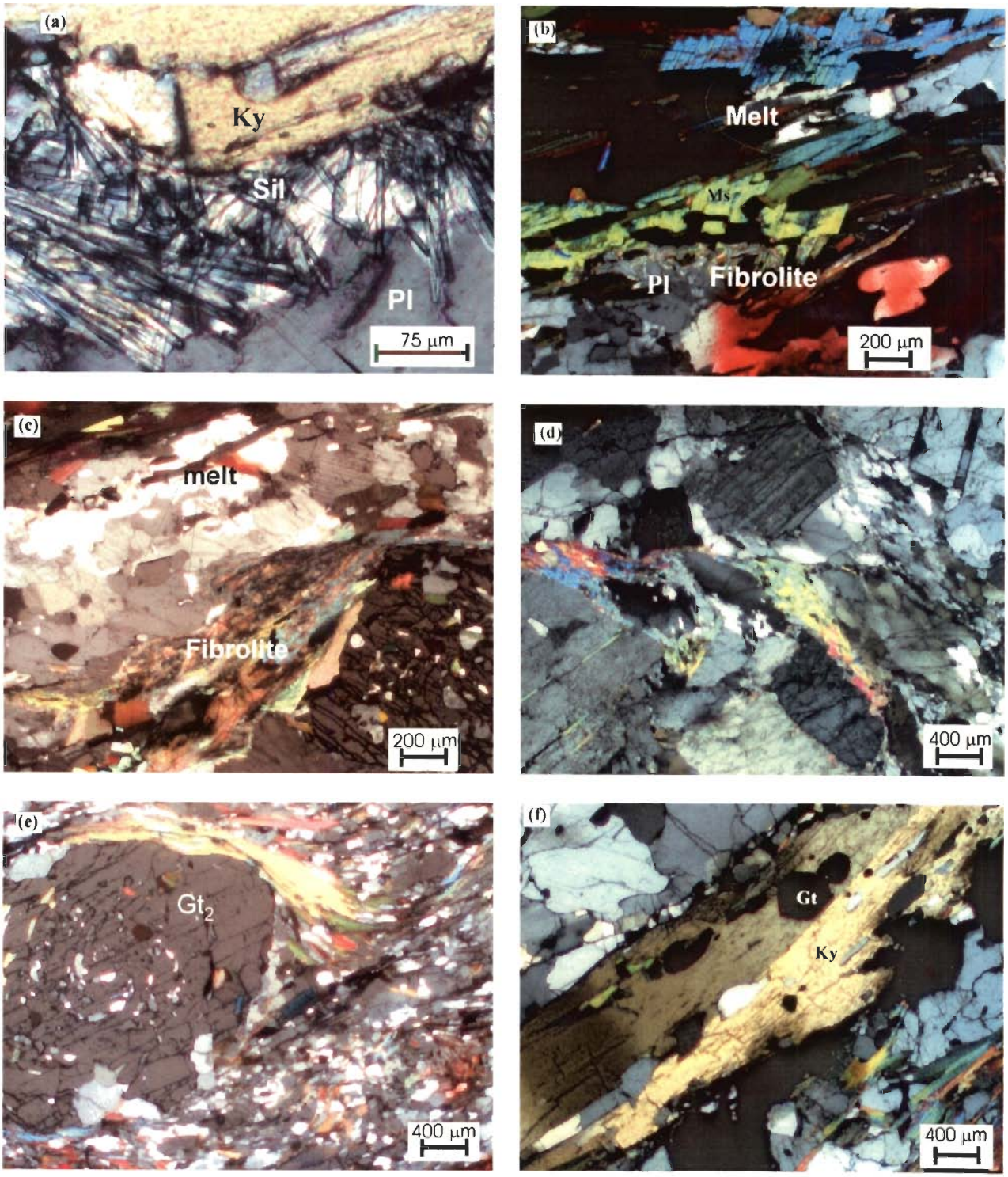

Figure 3.4 (a) Porphyroblasts of kyanite and plagioclase showing nucleation of sillimanite along their periphery (b) sillimanite nucleated in the form of fibrolite in the expense of muscovite also showing recrystallization of quartz along the grain boundaries (c) and (d) showing generation of melt at the expense of plagioclase and fibrolite at the expense of muscovite (e) garnet of second stage showing ó-type porphyroblast by curling the mica tail of S_2 (f) porphyroblast of kyanite blade showing simple twinning and also presence of euhedral garnet inclusion.

indicating that the rock approached anatexis or near melt condition. Within leucosome thin layers of skeleton and large garnets have also been observed, which might have consumed during partial melting. However, the mechanism that brings the heavier garnets afloat in the acidic melt layer is not investigated. Occurrence of sillimanite needles in the plagioclase and quartz indicates the incomplete reaction among the end members. In the melanosome the salvages of segregation and the initiation of migration of partial melts are prominent as characterized by the intercrystalline flow structures shown by fine grain aggregates of quartz, sillimanite and muscovite (Fig3.4c,d).

3.4.2.4 Leucogranite

Thin section study reveals that the leucogranite did not go any deformation and alterations after crystallization. The mineralogy of the rock type is very simple and mainly consists of plagioclase, k-feldspar, quartz and tourmaline with accessory minerals such as zircon and apatite.

3.5 MICROSTRUCTURES

3.5.1 PORPHYROBLASTS

From chlorite to sillimanite zone, a range of porphyroblasts have been observed (Table 3.1). All types of porphyroblast preserved some or the other inclusions of different minerals with intact internal foliation. Garnet is the only common porphyroblast that present in all the rock bodies from garnet to sillimanite zone and migmatite leucosome. The range of shape, size and their growth nature varies from rocks of one zone to the other (Table 3.1). The number of porphyroblast present in the rocks is highest in garnet to kyanite zone and the size

attained maximum to ~10 mm diameter in the staurolite-garnet schist. However, the garnets of the amphibolite and calc silicate bands exceed 20 mm in diameter.

In the garnet-mica schist of the Tapoban Formation garnet is highly abundant with a square centimeter area over the foliation surface it is about 3 to 5 in number having 0.5-2 mm diameter. The kyanite zone garnet on the other hand contains inclusions of quartz, chlorite, biotite, staurolite, ilmenite and sphene. In sillimanite and migmatite zone, garnets are generally of skeletal type, while, haphazard inclusions of biotite, muscovite, plagioclase, quartz and opaque.

Table 3.1: Inclusion Minerals with host minerals and the location of the samples

Porphyroblast		Inclusion minerals		Location
Garnet	Skele-ton	a) Tourmaline, biotite (with tourmaline inclusion), quartz (with inclusions of tourmaline and biotite) and chlorite.		Hanuman Chatti and Malari
Garnet	Hapha-zard	b) Core with plagioclase, biotite, muscovite, tourmaline, chlorite and quartz either as singly or group of two or more. In few cases the core is separated by a shell of biotite from the inclusion free rim.		Kosa, Juma and Pandukeshwar
Hornblende		Quartz and ironoxide		Hanuman Chatti
Plagioclase		Sillimanite and/or garnet (with haphazard inclusions of biotite, quartz and ironoxide).		Badrinath
Muscovite		Plagioclase and sillimanite		Badrinath
Garnet in Amphibolite		Quartz, plagioclase, chlorite, biotite, hornblende and ironoxide.		Hanuman Chatti
Garnet		Helicitic and spiral	Quartz, biotite and muscovite.	Suraithota
		Sieve	Quartz	
Microcline			Straight and oblique inclusions of biotite, garnet (with quartz inclusion) and chlorite.	Pandukeshwar
Kyanite		Staurolite, Garnet, biotite, muscovite, calcite, quartz, zircon and ironoxide.		Joshimath
Biotite		Sphene		
Garnet		Muscovite, sphene, quartz and chlorite		
Calcite		Staurolite (inclusion free).		
Plagioclase		Biotite and quartz		
Staurolite		Quartz and tourmaline		
Muscovite		Quartz		
Hornblende		Muscovite and quartz		Tapoban

3.5.2 PORPHYROBLAST-MATRIX RELATIONSHIP

Two generation of garnets have been observed and named as Gt_1 (syntectonic) and Gt_2 (post tectonic) present in the staurolite zone (Fig. 3.3e). Gt_1 is having diameter of average 2 mm showing spiral inclusion pattern with internal foliation (S_i /S_1) characterized by ilmenite and quartz while Gt_2 are smaller inclusion free in nature with average size of about 0.2 mm diameter occurring together with the staurolites along the main foliation S_2. The Gt_1 shows strain shadow by quartz aggregation at the opposite ends with sheared tails shown by mica along the main foliation S_2/S_m formed during main D_2 Himalayan deformation episode resembling **σ**-type porphyroblast (Fig. 3.4e), while Gt_2 garnet do not show any shadow zone. This small Gt_2 garnets also occurring as inclusions in kyanite (Fig. 3.4f) may be due rapid growth leading to the incomplete consumption of the earlier formed garnets Gt_1 or the rock has undergone high pressure brittle deformation followed by ductile stages, which might have occurred during the thrusting of VT as recorded from the mechanical breakdown of the earlier garnet Gt_1 and reorganized leading to rounded grain boundary floating in the ductile mantle, where some of them preserved the shearing effect by lying along foliation with occasional imbrications (Fig. 3.5a, b).

The second episode of mineral development may be classified into sub-stages as Gt_{2a} having inclusion free staurolite, aligning along the foliation S_2 indicating the first growth of staurolite St in the rock during the progressive metamorphism. The late stage generation of garnet porphyroblast Gt_{2b}, in terms of deformation–time, relationship is clearly defined by the inclusion of St in the garnet porphyroblast with a clear truncation in the matrix and elongation of staurolite in the internal

foliation within Gt_{2b} (Fig. 3.5c). The matrix or the host foliation S_2 is clearly demarcated by curve formation at the Gt_{2b} boundary. In the kyanite zone, the large garnets of about 12 mm diameter size show three set of cleavages with an abundant number of inclusions of various minerals. The identifiable mineral includes staurolite, biotite, muscovite, quartz, ilmenite and sphene. The boundary of which is marked by the curved matrix foliation S_{2b} (Fig. 3.5b). In the lower part of the Pandukeshwar Formation garnet porphyroblasts are of first generation Gt_1 characterized by **s**-shaped and oblique inclusion pattern S_i (Fig. 3.5e) defined normally by biotite, muscovite and quartz. The Gt_1 shows spiral inclusion.with rotation of the grains as evidenced from the thin sections as the axes of the garnet porphyroblasts which are not align in a plane (Fig. 3.5f), however, the detail kinetics of the rotation have not been attempted. Even then the systematic studies clearly indicate that the degree of rotation of porphyroblasts is decreases from south to north indicating decrease in shearing towards north. The garnets occurring in the adjacent overlying rocks bear core of haphazard inclusion of quartz inclusion and occasionally showing sieve structure (Fig. 3..6a, b), which can be recognized as Gt_2. These garnets are exemplified by the envelopment of garnet Gt_1 by growth shell of new generation garnet Gt_2, shown by clear partition of mica-quartz layer over the Gt_1 (Fig. 3.6c). The external foliation S_e which is also penetrative foliation parallel to S_2. In the leucosome of the migmatite, garnets are euhedral and shows minor inclusions of quartz can be assigned as Gt_3.

The study of mineral evolution and relation to metamorphism, inclusion mineral assemblages are represented in tabular form (Table 3.1). This table

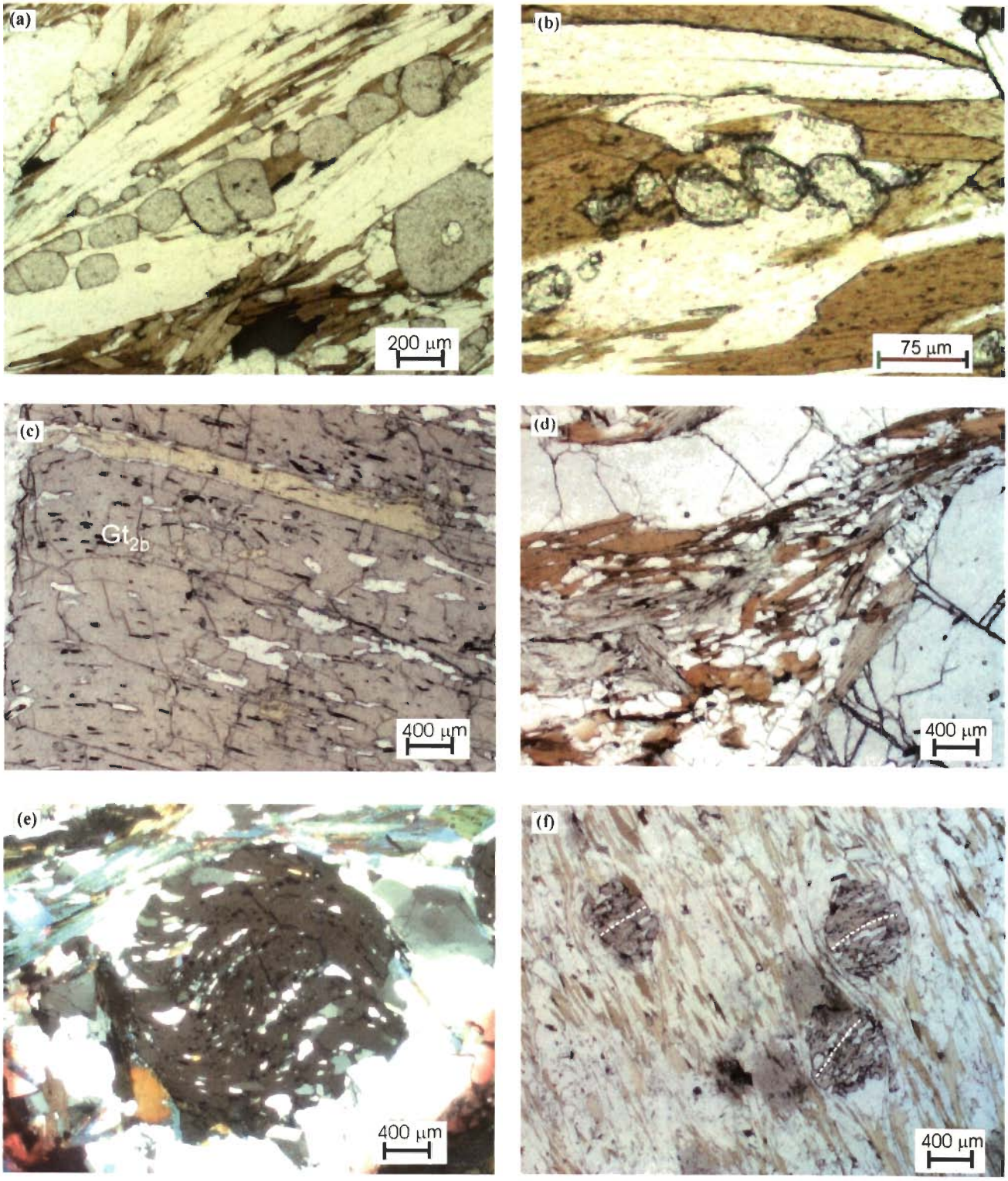

Figure 3.5 (a) small garnets of second stage occurring in alignment in the foliation (b) small rounded garnet showing grain imbrication structure (c) large garnet porphyroblast of late stage second generation and syntectctonic type Gt_{2b} showing inclusion of staurolite along the internal foliation (d) large garnet porphyroblast of third generation G_3showing shadow zone (e) second generation garnet porphyroblast with s-type internal inclusion (f) garnet porphyroblasts with oblique inclusions showing slightly rotational character.

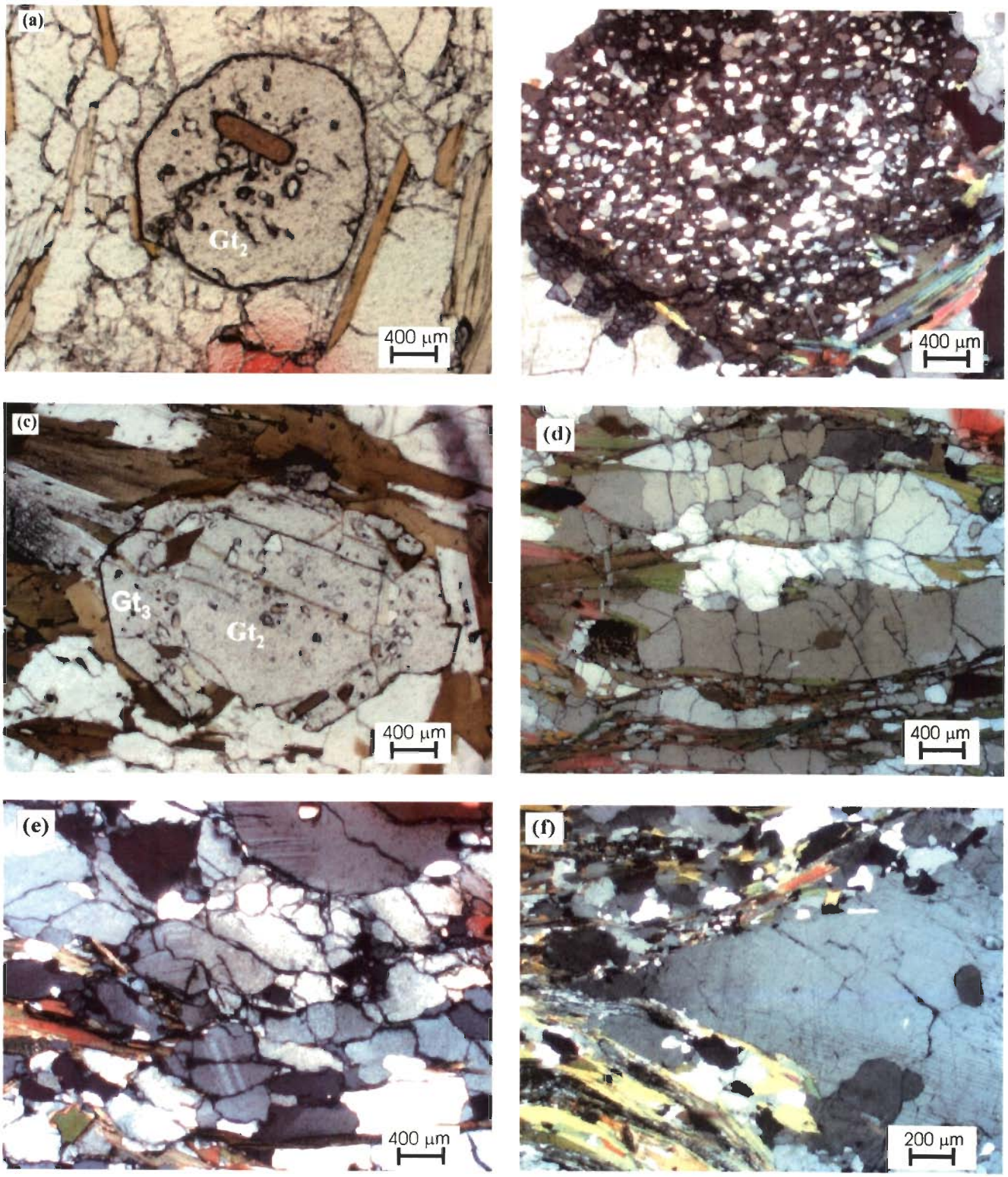

Figure 3.6 (a) second stage garnet showing haphazard inclusions of biotite and quartz (b) garnets of unknown stage showing sieve structure (c) nicely preserved garnet growth of third generation over second generation separated by thin shell of biotite and quartz in sillimanite zone (d) intragranular fracture developed in quartz-mica gneiss (e) extentional intragranular fracture shown by plagioclase in quartz-mica gneiss (f) core and mantle structure shown by deposition of aggregated mass of small quartz and mica at the periphery of large porphyroblast of plagioclase.

represents the inclusion mineral paragenesis in the host porphyroblast present in the different metamorphic zone with corresponding locations.

3.5.3 CATACLASIS OR PERMANENT LATTICE DISTORTION

The rocks occurring above the VT, specially the micaseous quartzite show cataclasis or permanent lattice distortion fabric by the intragranular extensional microfracture in plagioclase and quartz (Fig. 3.6d, e). Core and mantle structure have also been observed in the higher grade rocks e.g., near the migmatite zone (Fig. 3.6f).

3.5.4 DIFFUSIVE MASS TRANSFER

Diffusive mass transfer type of fabric is seen in the staurolite zone amphibolites where ribbons of quartz alternated with amphibole-mica rich layer undergone micro folding (Fig. 3.7a).

3.5.5 PERMANENT LATTICE DISTORTION WITHOUT FRACTURES OR INTRACRYSTALLINE PLASTICITY

Different microstructures are present in the quartzite of the Joshimath and Pandukeshwar Formation which are indicative of the permanent lattice distortion without fracture or intracrystalline plasticity. Undulosed extinction, subgrain and recrystallized grains of quartz, deformed twin lamellae in plagioclase, ribbon and grain shape fabric, kink band of mica, core and mantle structure of plagioclase have been recognized from the area (Fig. 3.7b, c, d).

3.5.6 SHEAR SENSE DEFORMATIONAL MICROSTRUCTURES

From the field observations it is evident that the rocks of the HHC in the Alaknanda and Dhauliganga valleys are consistently showing top-to-southwest sense of shearing, like other sections of the Himalayas. The ductile shearing is

present along the entire length of the Himalayan belt in the HHC and has also been considered to explain the main causes of inverted metamorphism from different sections of the Himalayas (e.g., Jain and Manickavasagam, 1993, Hubbard, 1996). The fabrics that characterize the shearing of the rocks of the two present sections are the microstructures preserved by them, for example, σ-type porphyroblasts, S-C` fabric, bookshelves structure, mica fish, asymmetric mineral microboudin and mineral imbrications (Fig. 3.3a, b, 3.4e, 3.7d).

3.6 MINERAL CHEMISTRY

To understand the variations in chemistry of the different minerals sensitive to pressure and temperature and to evaluate geothermobarometry different metamorphic zone mineral chemistry have been determined by Electron Probe Micro Analyzer (EPMA). The samples used for the EPMA analysis for pressure-temperature calculations and their mineral assemblages are shown in the Table 3.10. The detail data of the analyses are given in the (Appendix A) and the mole fraction data are given in the tables (Table 3.2 to 3.7).

3.6.1 ANALYTICAL PROCEDURE

With careful study of large number of thin sections of the different metamorphic zones, samples selected were unaltered and in mutual contact with each other. The samples were polished with alumina powder of 0.25 μm size at the thin section preparation laboratory in the Department of Earth Sciences, IIT Roorkee. Analyses were carried out with automated EPMA "JEOL JXA-8600M" housed at the Institute Instrumentation Centre, IIT Roorkee. Before putting the samples for analysis, thin layer of carbon coating of about 100 A^{o} thickness were made to provide conductivity to the samples. Analyses were performed at an

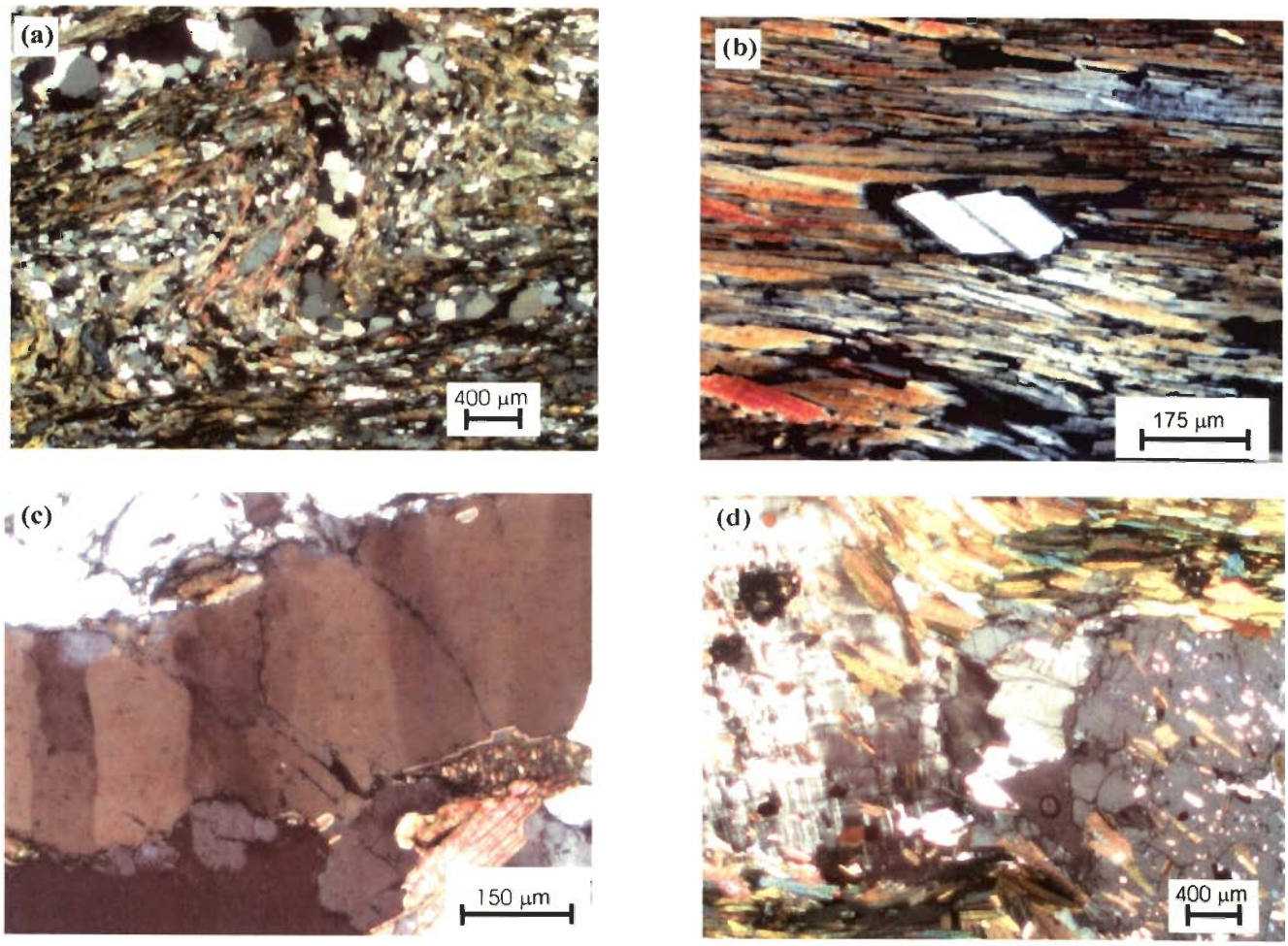

Figure 3.7 (a) micaceous layer sandwiching thin ribbons of quartz in amphibolite of Munsiari Formation showing microfolding (b) book shelve structure shown by plagioclase in mica schist (c) nicely developed deformation twinning in quartz in kyanite gneiss near Suaithota (d) large porphyroblasts of microcline showing boudin like structure and also showing internal foliation of biotite and quartz which is also parallel to the external foliation.

accelerating voltage of 15 kv and sample current of $2x10^{-8}$ ampere with a 1μm (for garnet and ilmenite) and 10μm (for Biotite, muscovite, chlorite and plagioclase) beam size. Three channel Wavelength Dispersive Spectrometers (WDS) attached with the instrument were used for quantitative analysis. During the analysis natural mineral standards (SPI, Standard, Canada) for different minerals such as almandine, pyrope, biotite, phlogopite, chlorite, albite, plagioclase, sanidine, diopside, etc. were used. Proper ZAF correction for atomic number effect, x-ray absorbtion, x-ray fluorescence, back scatter and ionization penetration loss were applied to the data using the software programme DEC LSI-11/23 and 11/73 associated with JEOL.

During the analysis special care has been taken in selecting the spots, as all the analysis, were made near the contacts within a range of about 2 μm rims. For biotite, muscovite and plagioclase; spots were selected either within 2 μm rim for those grains which are in mutual contact or the grains which are within a radial distance of about 200 μm, when they are not in mutual contact. For samples which do not contain muscovite (GASP), the garnet and plagioclase spots are considered at their mutual contacts, because, exchange of Ca between the two minerals is the main governing element for determination of geobarometry. For each of the minerals 3 to 7 points were analyzed to check the variation and only adjacent data points were considered for pressure and temperature calculations. The mole fractions of garnet, biotite, muscovite and plagioclase are listed in the Tables 3.2 to 3.7.

Table 3.2: Mole fraction data for Garnets of Alaknanda river section

Sample No.	GARNET				
	X_{Fe}	X_{Mg}	X_{Mn}	X_{Ca}	$\frac{Fe}{Fe+Mg}$
AL6-16-2-R	0.669	0.127	0.141	0.062	0.840
AL5-11-2-R	0.782	0.074	0.086	0.057	0.913
AG6-7-R	0.715	0.136	0.113	0.037	0.841
AG2-1R	0.671	0.088	0.033	0.207	0.884
AG2-5-R	0.658	0.104	0.196	0.042	0.863
MA39A-R	0.690	0.185	0.098	0.028	0.789
AG1-4-R	0.842	0.071	0.060	0.027	0.933
AG1-4-C	0.843	0.058	0.073	0.025	0.936
DL32-56-R	0.688	0.052	0.104	0.155	0.930
DL32-56-C	0.734	0.043	0.109	0.114	0.944
DL36-63-R	0.866	0.091	0.030	0.013	0.905
DL41-71-R	0.527	0.100	0.046	0.327	0.840
H-1-GT-R	0.645	0.150	0.039	0.165	0.812
H-1-GT-C	0.638	0.162	0.028	0.172	0.797
DL53-95-R	0.670	0.197	0.040	0.093	0.773
DL53-95-C	0.685	0.191	0.035	0.089	0.782
DL50-60R	0.803	0.120	0.015	0.062	0.870

Table3.3: Mole fraction data for Garnets of Dhauliganga river section

Sample No.	GARNET				
	X_{Fe}	X_{Mg}	X_{Mn}	X_{Ca}	$\frac{Fe}{Fe+Mg}$
AG17-25-R	0.766	0.068	0.137	0.029	0.918
AG17-25-C	0.760	0.073	0.142	0.025	0.912
AG15-21-R	0.749	0.070	0.102	0.079	0.915
AG15-21-C	0.747	0.067	0.126	0.060	0.918
AG14-18-C4-R	0.761	0.077	0.138	0.023	0.908
AG14-18-C4-C	0.748	0.089	0.133	0.029	0.893
AG14-18-C3-C	0.760	0.083	0.127	0.030	0.901
AG14-18-C1-C	0.753	0.086	0.135	0.026	0.897
AG11-14-R	0.777	0.081	0.124	0.018	0.905
AG11-14-C	0.796	0.088	0.096	0.020	0.900
DL2-4-R	0.822	0.068	0.036	0.075	0.924
MA23-36-R	0.666	0.278	0.016	0.040	0.705
DL16-28-R	0.708	0.160	0.045	0.086	0.816
DL18-31	0.704	0.244	0.026	0.026	0.743
DL25-44-R	0.554	0.107	0.021	0.317	0.838
DL25-44-CI	0.586	0.108	0.037	0.269	0.844
DL25-44-CII	0.557	0.107	0.028	0.308	0.839
DL25-44-CIII	0.591	0.111	0.037	0.262	0.842
DL25-44-CIV	0.580	0.108	0.033	0.278	0.842
DL25-44-CV	0.589	0.114	0.036	0.261	0.837
DL22-40-R	0.709	0.119	0.068	0.105	0.857
DL22-40-C	0.684	0.177	0.029	0.109	0.794
DL41-71-R	0.527	0.100	0.046	0.327	0.840
H-1-GT-R	0.645	0.150	0.039	0.165	0.812
H-1-GT2-C	0.638	0.162	0.028	0.172	0.797
DL53-95-R	0.677	0.199	0.032	0.092	0.773
DL53-95-C	0.685	0.191	0.035	0.089	0.782
DL50-60-R	0.803	0.120	0.015	0.062	0.870

Table3.4: Mole fraction data for Biotites of Alaknanda river section

Sample No.	BIOTITE				
	X_{Fe}	X_{Mg}	X_{Ti}	X_{Al}^{VI}	$\frac{Fe}{Fe+Mg}$
AL6-16-2-R	0.385	0.392	0.056	0.163	0.496
AL5-11-2-R	0.481	0.272	0.098	0.146	0.639
AG6-7-R	0.409	0.364	0.052	0.171	0.529
AG2-1-2-R	0.566	0.293	0.055	0.084	0.659
AG2-5-R	0.410	0.376	0.065	0.144	0.521
MA39A-R	0.332	0.474	0.030	0.162	0.412
AG1-4-R	0.591	0.220	0.096	0.092	0.729
AG1-4-C	0.586	0.241	0.060	0.111	0.709
DL32-56-R	0.598	0.226	0.055	0.114	0.726
DL32-56-C	0.629	0.176	0.052	0.133	0.781
DL36-63-R	0.529	0.302	0.030	0.138	0.636
DL41-71-R	0.407	0.408	0.037	0.143	0.500
H-1-GT-R	0.379	0.437	0.047	0.134	0.464
DL53-95-R	0.338	0.507	0.042	0.112	0.400
DL53-95-C	0.256	0.572	0.046	0.125	0.309
DL50-60-1R	0.390	0.436	0.025	0.148	0.472
DL50-60-2R	0.020	0.026	0.007	0.944	0.463

Table 3.5: Mole fraction data for Biotites of Dhauliganga river section

Sample No.	BIOTITE				
	X_{Fe}	X_{Mg}	X_{Ti}	X_{Al}^{vi}	$\frac{Fe}{Fe+Mg}$
AG17-25-R	0.563	0.215	0.083	0.135	0.724
AG17-25-R	0.532	0.253	0.075	0.137	0.677
AG15-21-R	0.547	0.258	0.049	0.141	0.679
AG15-21-C	0.550	0.242	0.078	0.127	0.695
AG14-18-C4-R	0.527	0.270	0.073	0.126	0.662
AG14-18-C4-C	0.485	0.324	0.067	0.121	0.600
AG14-18-C3-C	0.466	0.301	0.063	0.168	0.608
AG14-18-C1-C	0.475	0.285	0.064	0.160	0.625
AG11-14-R	0.504	0.305	0.038	0.148	0.623
AG11-14-C	0.474	0.342	0.054	0.126	0.581
DL2-4-R	0.566	0.238	0.053	0.143	0.704
MA23-36-R	0.308	0.486	0.024	0.181	0.388
DL16-28-R	0.375	0.438	0.040	0.147	0.461
DL18-31	0.274	0.558	0.022	0.145	0.329
DL25-44-R	0.376	0.450	0.039	0.132	0.456
DL25-44-CI	0.373	0.430	0.038	0.155	0.464
DL25-44-CII	0.342	0.477	0.057	0.123	0.418
DL25-44-CIII	0.339	0.483	0.058	0.118	0.412
DL25-44-CIV	0.332	0.492	0.055	0.120	0.403
DL25-44-V	0.331	0.482	0.049	0.136	0.407
DL22-40-R	0.420	0.398	0.060	0.121	0.514
DL22-40-C	0.290	0.508	0.051	0.150	0.363
DL41-71-R	0.407	0.408	0.037	0.143	0.500
H-1-GT-R	0.379	0.437	0.047	0.134	0.464
DL53-95-R	0.340	0.496	0.052	0.111	0.407
DL53-95-C	0.256	0.572	0.046	0.125	0.309
DL50-60-R	0.390	0.436	0.025	0.148	0.472

Table 3.6: Mole fraction data for Muscovites and Plagioclase of Alaknanda river section

Sample No.	Muscovite						Plagioclase
	X_{Fe}	X_{Mg}	X_{Ti}	X_{Al}^{vi}	X_{Ms}	X_{Pa}	X_{An}
AL6-16-2-R	0.025	0.008	0.026	0.939	0.714	0.062	0.237
AL5-11-2-R	0.026	0.023	0.036	0.911	0.630	0.060	0.160
AG6-7-R	---	---	---	---	---	---	0.220
AG2-1-2-R	---	---	---	---	---	---	0.428
AG2-5-R	0.030	0.031	0.018	0.918	0.637	0.068	0.244
MA39A-R	---	---	---	---	---	---	0.123
AG1-4-R	0.034	0.015	0.022	0.926	0.724	0.006	0.169
DL32-56-R	0.068	0.041	0.011	0.876	0.556	0.031	0.215
DL36-63-R	0.050	0.036	0.010	0.901	0.552	0.105	0.017
DL41-71-R	0.041	0.069	0.008	0.877	0.550	0.038	0.237
H-1-GT-R	0.040	0.058	0.022	0.876	0.535	0.052	0.257
DL53-95-R	0.027	0.043	0.027	0.900	0.547	0.101	0.167
DL53-95-C	0.064	0.062	0.009	0.860	0.390	0.153	--
DL50-60-R	---	---	---	---	---	---	---

Suffixes Ms=Muscovite , Pa = Paragonite and An= Anorthite

Table 3.7: Mole fraction data for Muscovites and Plagioclase of Dhauliganga river Section

Sample No.	Muscovite						Plagioclase
	X_{Fe}	X_{Mg}	X_{Ti}	X_{Al}^{vi}	X_{Ms}	X_{Pa}	X_{An}
AG17-25-R	0.035	0.022	0.026	0.912	0.679	0.011	0.145
AG15-21-R	0.042	0.022	0.012	0.921	0.709	0.010	0.249
AG15-21-C	0.041	0.017	0.022	0.916	0.675	0.029	0.132
AG14-18-R	0.036	0.028	0.019	0.914	0.627	0.070	0.214
AG14-18-C	0.032	0.031	0.023	0.910	0.610	0.074	0.214
AG11-14-R	0.026	0.027	0.012	0.932	0.753	0.000	0.097
DL2-4-R	0.036	0.024	0.022	0.915	0.691	0.006	0.192
MA23-36-2	0.019	0.033	0.014	0.932	0.576	0.176	0.168
DL16-28-R	0.033	0.046	0.028	0.889	0.516	0.102	0.193
DL25-44-R	0.044	0.073	0.011	0.869	0.525	0.042	0.396
DL22-40-R	0.043	0.051	0.027	0.875	0.498	0.083	0.205
DL41-71-R	0.041	0.069	0.008	0.877	0.550	0.038	0.237
H-1-GT2-R	0.040	0.058	0.022	0.876	0.535	0.052	0.257
DL53-95-R	0.027	0.043	0.027	0.900	0.547	0.101	0.167
DL53-95-C	0.064	0.062	0.009	0.860	0.390	0.153	--
DL50-602R	0.020	0.026	0.007	0.944	0.522	0.272	---

Suffixes Ms=Muscovite , Pa = Paragonite and An= Anorthite

3.6.1.1 Garnet

The quantitative point chemistry of the garnets of staurolite, kyanite and sillimanite grades of both the sections were used for calculating different end member concentrations and their variations in the different grades. It is evident that the garnets of both the sections are characterized by almandine-rich (Fe-garnet) composition with varying concentrations of pyrope (Mg garnet), spessartine (Mn-garnet), and grossular (Ca-garnet) (see Table 3.2, 3.3). The study of variation in these components of garnet from core to rim is restricted to the selected samples from staurolite, kyanite and sillimanite grade which is described in detail in section 3.8.

It is observed that the Fe/Fe+Mg in the garnet rim increases from staurolite grade to sillimanite grade indicating increase in temperature condition. In Alaknanda section the values increases from 0.802 in staurolite and 0.857 in kyanite to 0.867 in sillimanite grade (Fig. 3.8a & 3.9) while in Dhauliganga it increases from 0.802 in staurolite and 0.808 in kyanite to 0.909 in sillimanite grade (Fig. 3.8b & 3.10). Similarly, X_{Mn} also increases from staurolite to sillimanite grade. In Alaknanda section the values increases from 0.026 in staurolite and 0.062 in kyanite to 0.098 in sillimanite grade (Fig. 3.8a & 3.9) while in Dhauliganga it increases from 0.026 in staurolite and 0.035 in kyanite to 0.127 in sillimanite grade (Fig. 3.8b & 3.10). The values of X_{Mg} decreases from staurolite to sillimanite grade In Alaknanda section the values decreases from 0.177 in staurolite and 0.115 in kyanite to 0.108 in sillimanite grade (Fig. 3.8a & 3.9) while in Dhauliganga it decreases from 0.177 in staurolite and 0.161 in kyanite to 0.076 in sillimanite grade(Fig. 3.8b & 3.10). The value of X_{Ca} in both the section is highest in kyanite

grade while in sillimanite zone it decreases significantly in the Dhauliganga and in Alaknanda section the value is more than that of the staurolite grade signifying the different pressure condition in the sillimanite grade.

The nature of the variations of the mole fractions of garnet is shown in the (Fig. 3.8). In the staurolite grade, a good linear variation in X_{Mg} is seen in both the sections while poorly linear variations in X_{Fe}, and X_{Mn} is seen with non linear X_{Ca} (Fig. 3.9). The most interesting feature as depicted from the mole fraction plots is the clear discrimination of the sillimanite grade from the staurolite and kyanite grade for Dhauliganga section (Fig. 3.10). It is also apparent that the Dhauliganga section is more regular in the variations of all the parameters which may be due to its wider belt, possibly facilitating a better preservation of the evolution history of the minerals.

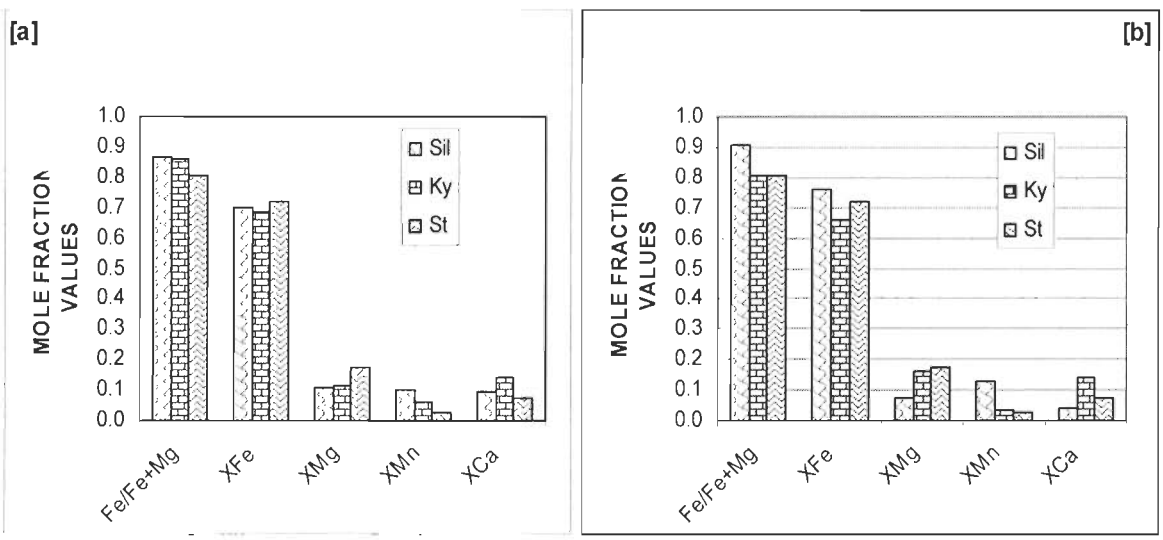

Figure 3.8: Variations in mole fractions in garnet of staurolite, kyanite and sillimanite grade of both the sections (a) Alaknanda section (b) Dhauliganga section

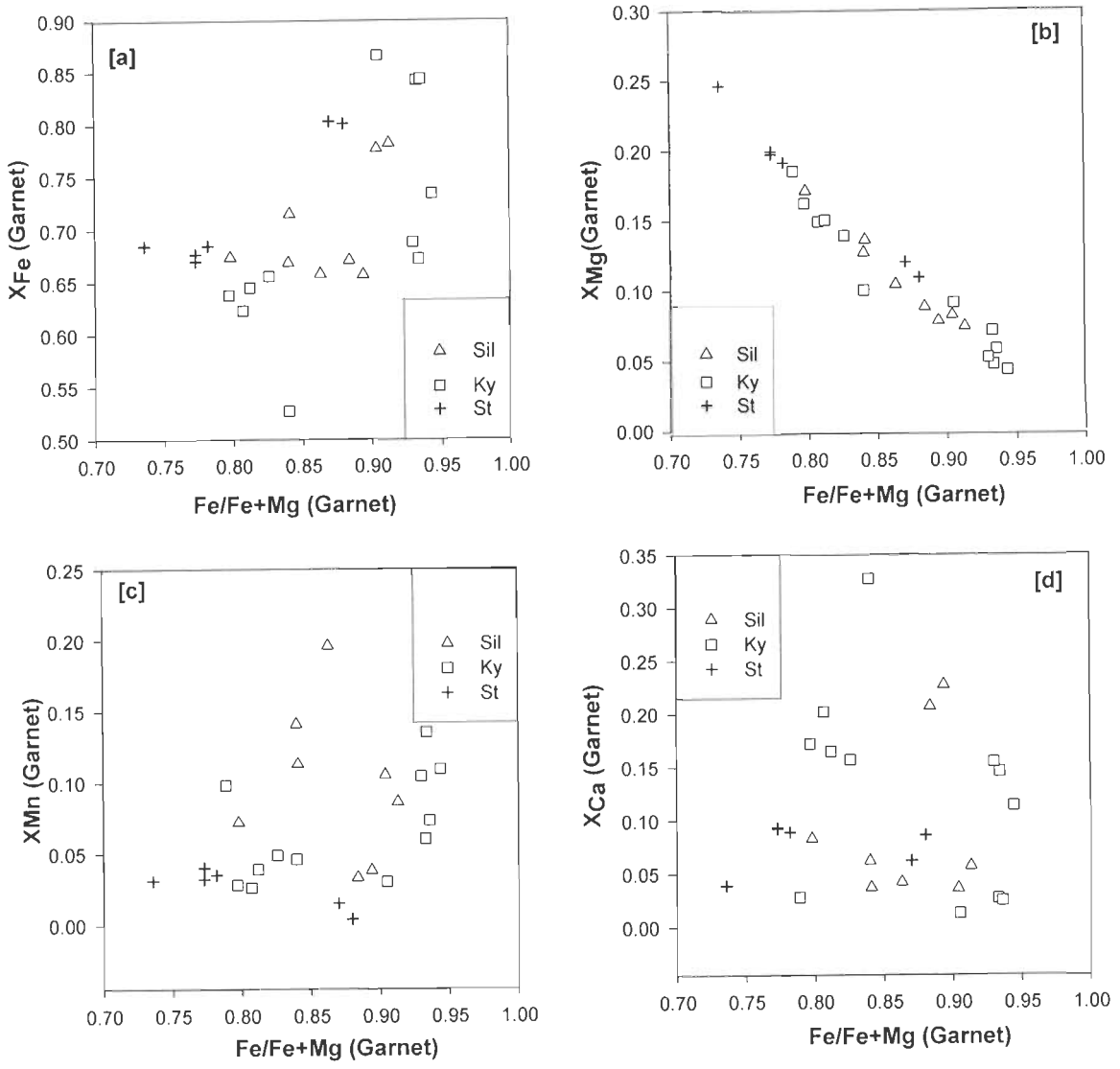

Fig 3.9: Mole fraction plotting of the garnets of different metamorphic zones of Alaknanda river section (a)-(d)

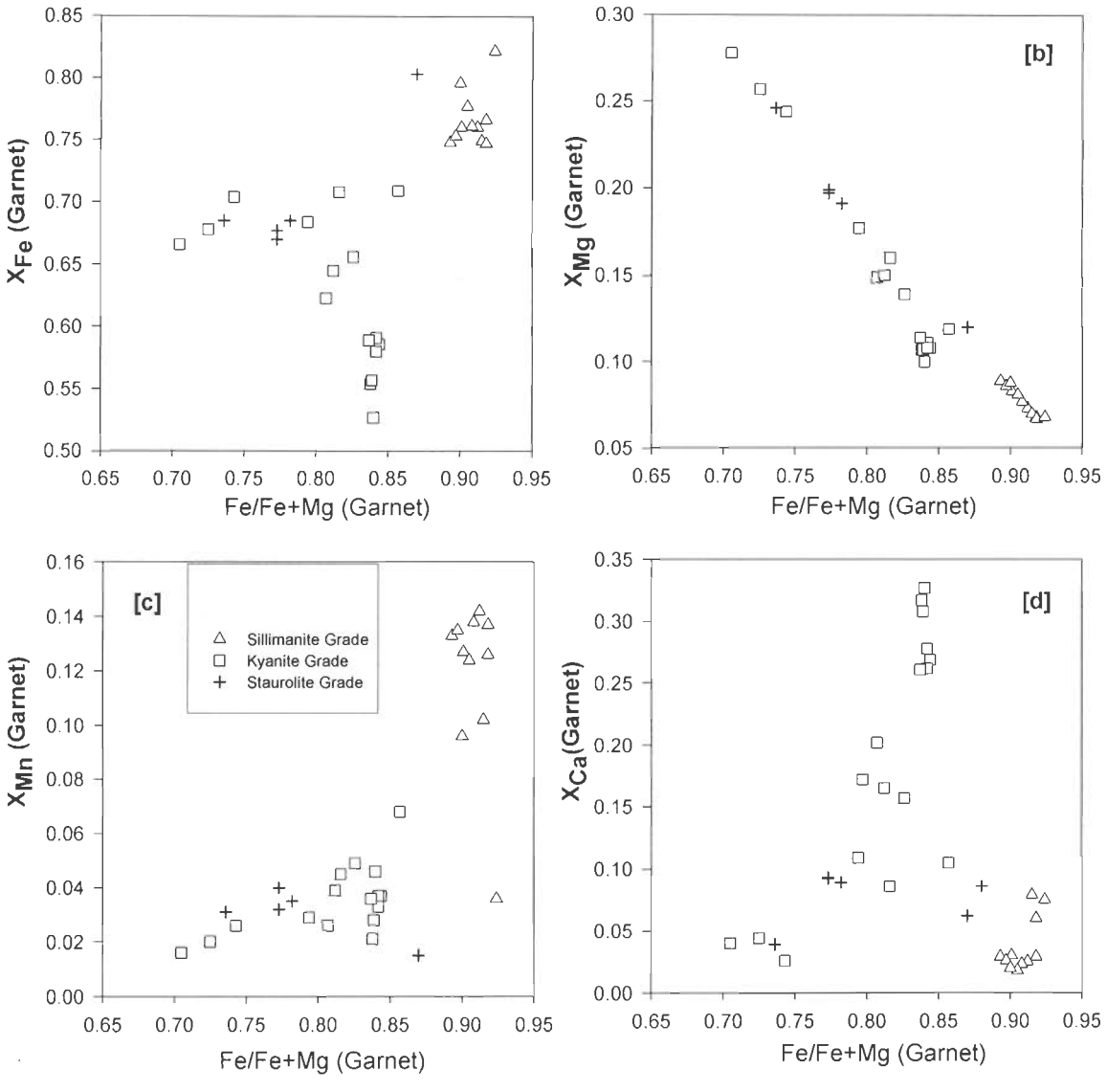

Fig 3.10: Mole fraction plotting of the garnets of different metamorphic zones of Dhauliganga river section (a)-(d), legend in (c) is similar to all.

3.6.1.2 *Biotite*

The average trend of Fe/Fe+Mg, X_{Fe}, X_{Mg}, X_{Al}^{VI} and X_{Ti} in biotite shows no regular pattern in the two sections (Fig. 3.11). The corresponding values are also varies substantially. However, the individual values when plotted, it reveals an increase in X_{Fe} while X_{Mg} decreases from staurolite to sillimanite grade in both the sections showing a very good linear pattern (Fig. 3.12 & 3.13). In both the sections, the exchange between Al↔Ti is clearly seen as the increased X_{Al}^{VI} value from staurolite to sillimanite grade is adjusted by the corresponding decrease in X_{Ti} (Fig. 3.12 & 3.16). It has been observed that the every parameter (mole fraction) is clearly discriminated for the sillimanite grade than from the staurolite and kyanite grade for Dhauliganga section (Fig. 3.12 & 3.13).

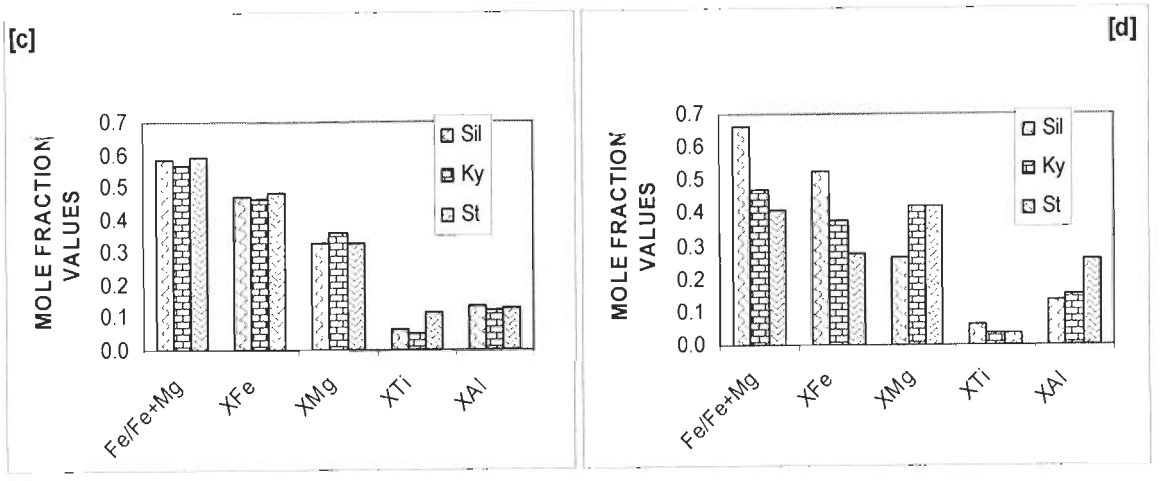

Figure 3.11: Variations in mole fractions in biotite of staurolite, kyanite and sillimanite grade of both the sections (c) Alaknanda section (d) Dhauliganga section

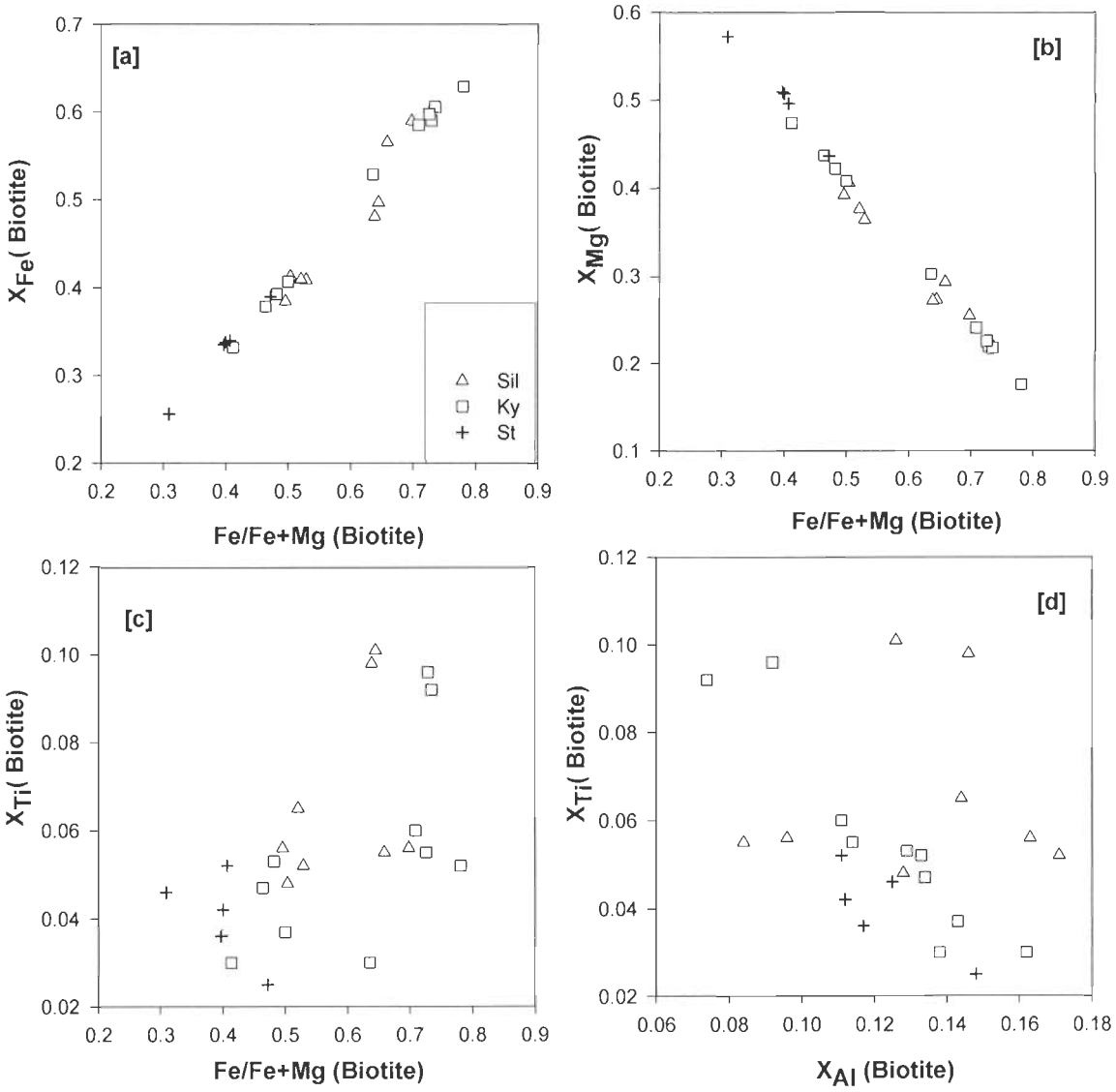

Fig 3.12: Mole fraction plotting of the biotites of different zones of Alaknanda River Section (a)-(d). Legend in (a) is similar to all.

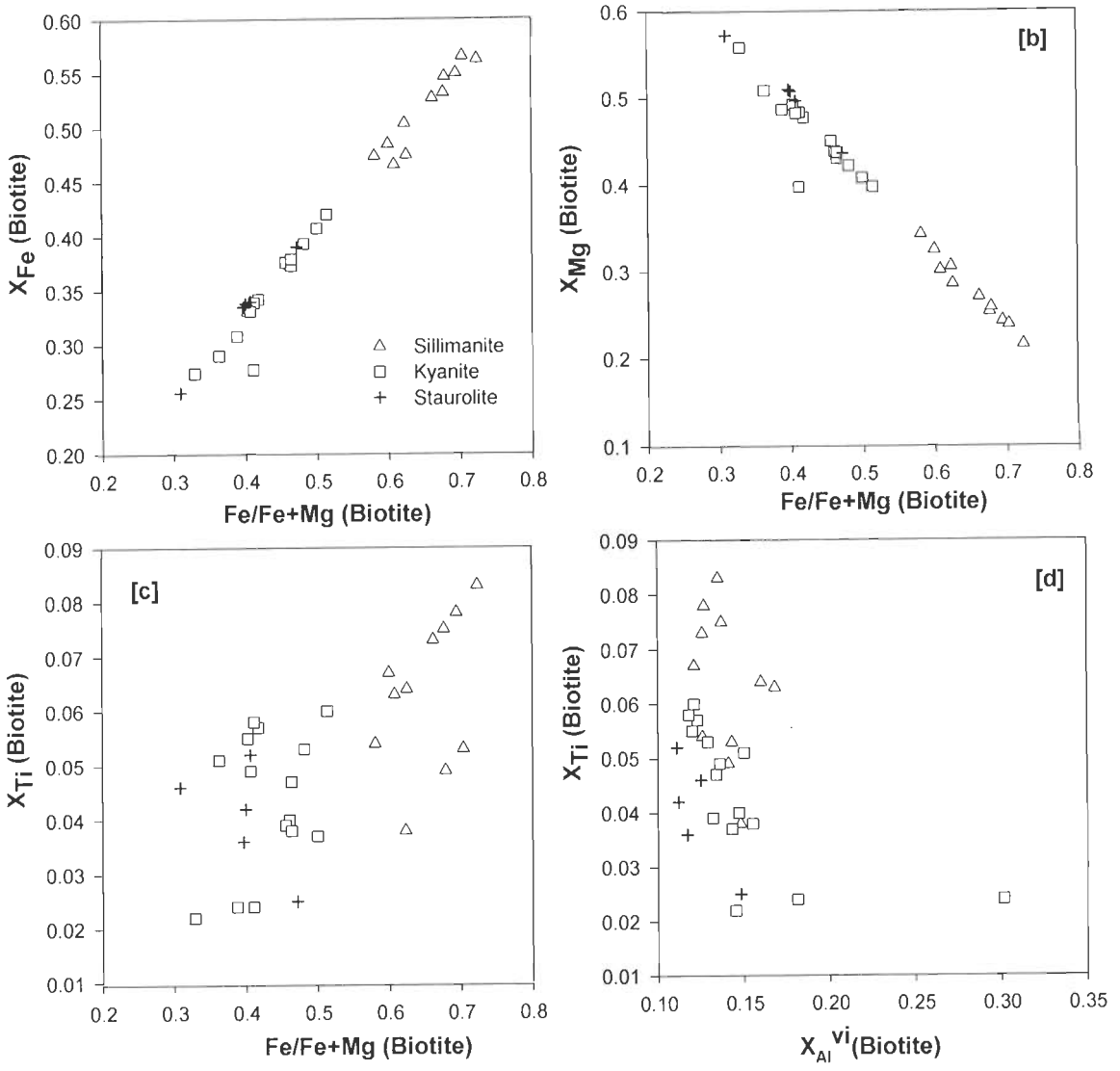

Fig 3.13: Mole fraction plotting of the biotite of different zones of Dhauliganga river section (a)-(d). Legend in (a) is similar to all.

3.6.1.3 *Muscovite*

In case of muscovite, the variations in X_{Fe}, X_{Mg}, X_{Ti}, X_{Al}^{VI}, $X_{Ms}$and X_{Pa} in the two sections show very similar pattern from staurolite to sillimanite grade (Fig. 3.14 see also Fig. 3.15 & 3.16). The values of X_{Al}^{VI} in the two sections vary within a very small range in all the grades. In kyanite grade it got slightly lowered to 0.88 but in the sillimanite and staurolite grade it remains almost constant at around 0.90 (Fig. 3.14). The values of X_{Ms} increases from staurolite to sillimanite grade in both the sections from 0.517 in staurolite and 0.536 in kyanite grade while in sillimanite grade the values are 0.640 in Alaknanda and 0.564 in Dhauliganga section. The values of X_{Pa} which is about 0.144 in staurolite grade in both the sections are higher than the other two grades. In kyanite grade the values got lowered to 0.052 in Alaknanda and 0.075 in Dhauliganga section.

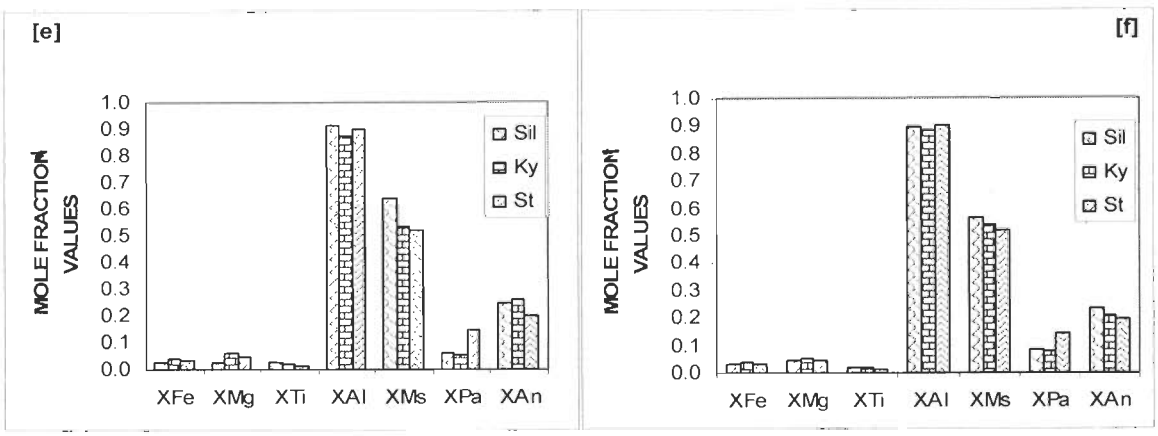

Fig 3.14: Different plots of average mole fractions of muscovite and plagioclase of staurolite, kyanite and sillimanite zones of both the sections (e) for Alaknanda and (f) for Dhauliganga sections.

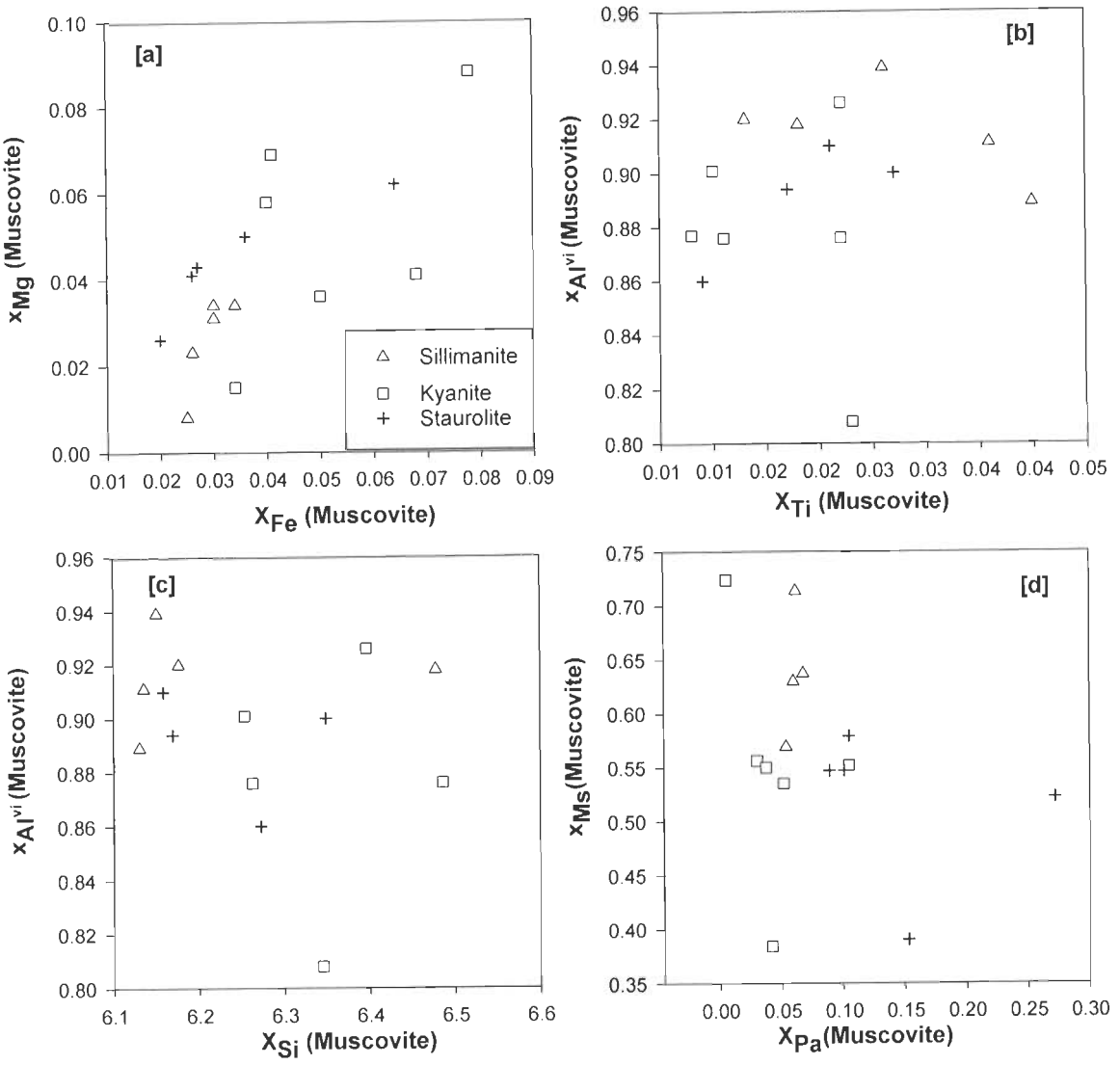

Fig 3.15: Mole fraction plotting of the muscovites of different zones of Alaknanda river section (a)-(d). Legend in (a) is similar to all.

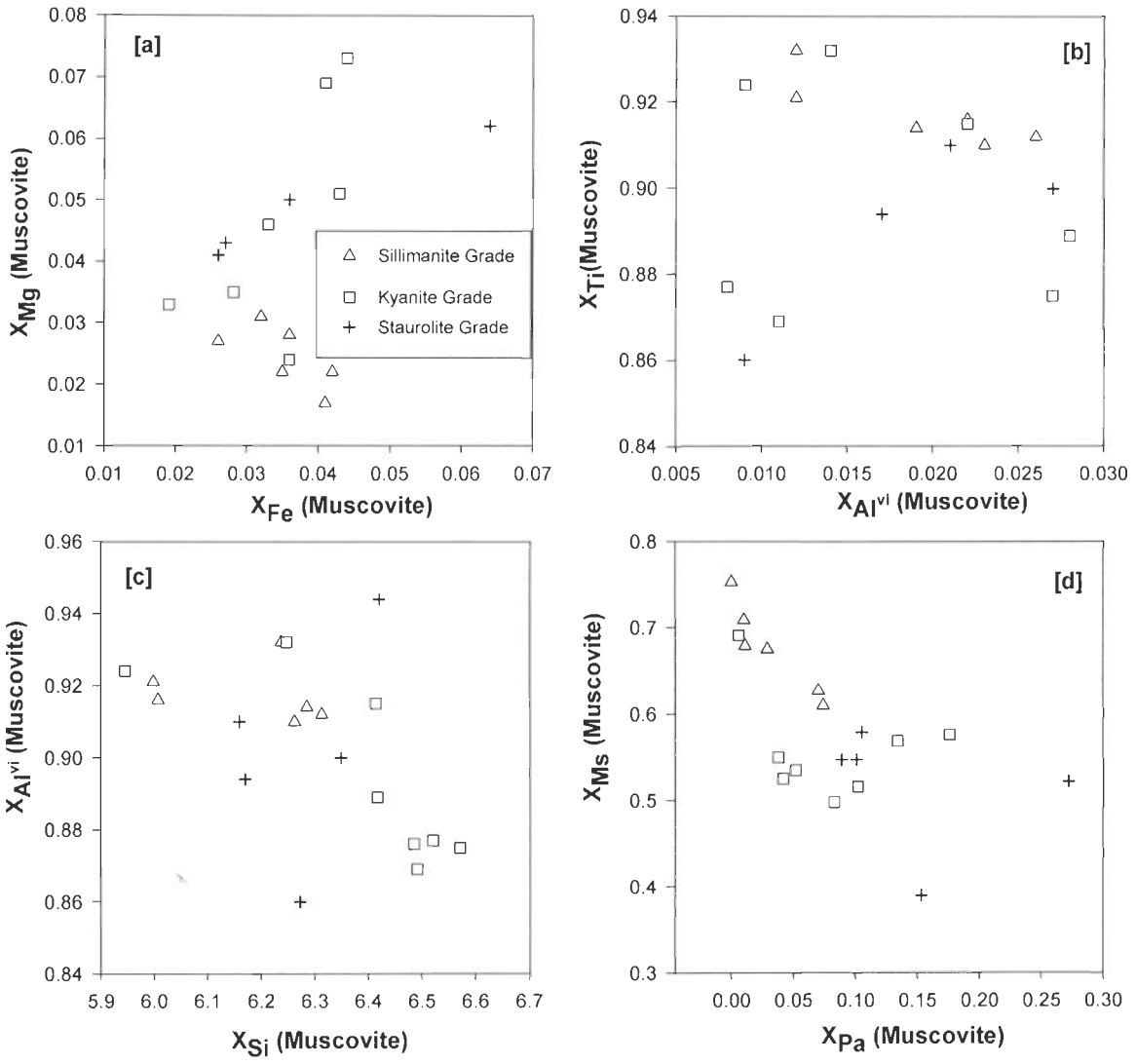

Fig 3.16: Mole fraction plotting of the muscovites of different zones of Dhauliganga river section (a)-(d). Legend in (a) is similar to all.

3.6.1.4 Plagioclase

In the Alaknanda section, the anorthite content (X_{An}) in the plagioclase ranging from 0.20 to 0.24 while in Dhauliganga section it varies between 0.20 to 0.23, except one sample, DL 25-44 which shows anorthite content of about 0.40 (X_{An}) (Table 3.6 & 3.7). The plot between the X_{An}(plagioclase) vs X_{Ca} (garnet) shows a good trend of variation in the two sections (Fig. 3.17). Clear correlation

between Fe/Fe+Mg of garnet and biotite has been observed in the samples indicating the interdependence of exchange of Fe and Mg with the temperature variations (Fig. 3.17).

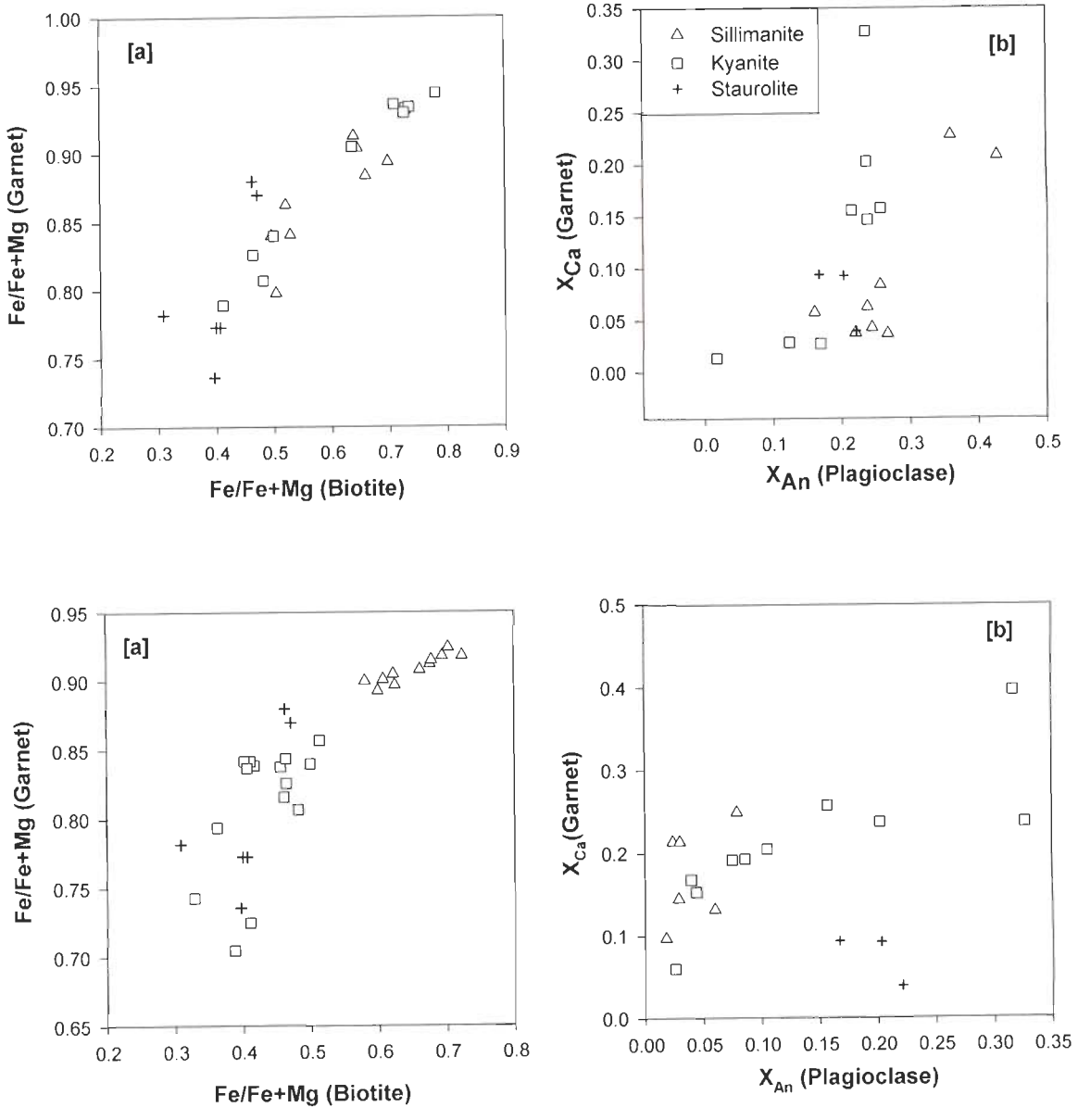

Fig 3.17: Plots of Fe/Fe+Mg (biotite) vs Fe/Fe+Mg (garnet) & X_{An} Plagioclase vs X_{Ca} (Garnet); (a)-(b) of Alaknanda section (c)-(d) of Dhauliganga sections. Legend in (b) is similar to all.

3.7 GEOTHERMOBAROMETRY

3.7.1 INTRODUCTION

The calculation of metamorphic condition of pressures and temperatures of equilibration using the temperature and pressure dependence of the equilibrium constant is described as geothermometry and geobarometry and collectively called geothermobarometry. It is one of the commonly employed tools in metamorphic petrology. In the earlier dates, studies were emphasized more on the appearance and disappearance of the index mineral and rock facies to characterize the metamorphic conditions. However, with the advent of the more and more improved instrumental techniques, the study of the mineral chemistry has been improved tremendously. Geothermometric and geobarometric techniques started being applied to the rocks whose mineral paragenesis and textural relationships were understood. Careful thin section studies have been done out before analysis to establish the mineral assemblages have attained equilibrium conditions, otherwise the result will give larger uncertainties or error in P, T values.

3.7.2 THERMODYNAMIC PRINCIPLES OF GEOTHERMOBAROMETRY

At equilibrium condition, the fundamental equation describing the formal thermodynamic relationship among pressure, temperature and mineral composition is given as:

$$\Delta G(P,T,X) = 0 = \Delta H_{(298,1)} + \int_{298}^{T} \Delta Cp \, dT + \int_{1}^{P} \Delta V \, dP - T\left[\Delta S_{(298,1)} + \int_{298}^{T} \frac{\Delta Cp}{T} \, dT \right] + RT\ln K_{eq} \qquad \text{----------(3.8)}$$

Where,

ΔG = Free energy (also called Gibb's free energy).

$\Delta H_{(298,1)}$ = Difference in enthalpy between the products and reactants of the reaction at 1 bar and temperature of 298 ^0K .

$\Delta S_{(298,1)}$ = Difference in entropy between the products and the reactants of the reaction at 1 bar and 298 ^0K

ΔV = Volume change from reactants to products

ΔC_p = Heat capacity of the reaction

K = Temperature in ^0K.

P = Pressure in bars

R = Gas constant (1.987 calories)

For reactions involving only solid phases as in most of the metamorphic reactions the value of ΔC_p can reasonably be assumed to be equal to zero, even though it is a strong function of T. Therefore, the reaction (3.8) can be written as:

$$0 = \Delta H_{(298,1)} + \Delta V (P-1) - T\Delta S_{(298,1)} + RT\ln K_{eq} \quad \text{----------(3.9)}$$

If mixing is ideal, then

$$RT\ln K_{eq} = RT\ln K_D \quad \text{----------(3.10)}$$

i.e., equilibrium constant is equal to distribution coefficient and if the mixing is non-idea, then

$$RT\ln K_{eq} = RT\ln K_D + RT\ln K_\gamma \quad \text{----------(3.11)}$$

Where, K_γ is activity coefficient. The numerical values can be calculated for both regular and non regular solution model using ionic solution model (e.g., Debye-Huckel theory) which modeled the ionic strength of solutions.

For geothermobarometry, equation (3.9) can be rearranged as

$$T = \frac{-\Delta H - (P-1)\Delta V}{R\ln K_D - \Delta S} \quad \text{----------(3.12)}$$

$$P = 1 + \frac{T(\Delta S - R\ln K_D) - \Delta H}{\Delta V} \qquad \text{----------(3.13)}$$

Where, P is in bars, T in ^{0}K, ΔH and ΔS in calories, ΔV in calories/bar and R = 1.987 calories (Spear, 1993).

3.7.3 APPLICATION OF GEOTHERMOBAROMETRY

A common approach for estimating pressure and /or temperature is to select an appropriate geothermometer and geobarometer available for the mineral assemblages of the rock occurring in equilibrium. It is also noteworthy to mention that for any given mineral assemblage there may be several reactions that can be write related to various subsets of minerals, and more such reactions may be calibrated as geothermometer and geobarometer. Therefore, several calibrations can be done in a single equilibrium and several equilibria as well. A range of pressure and/or temperature may yield from the possible equlibria and different calibrations from the same equilibrium. The metamorphic rocks of the present area of investigations, is composed of metapelite, metacalcareous, metabasite and quartzite. Across the whole section, metapelites dominate over the other rock types. Even in the quartzitic bands which are occurring as thick bands of about 4-9 km width, intercalations of thin bands of few millimeters to several feet thick metapelites are very common. This feature enables the systematic thermobarometric studies of the area. Since the metapelites of these two Himalayan sections of HHC ranges from chlorite to Sillimanite-K-feldspar grade metamorphism containing minerals such as garnet, plagioclase, biotite and/or muscovite and aluminosilicates in their assemblages providing a wide range of choice for geothermometers and geobarometers as numerous calibrations are available for these mineral compositions. In order to bring more appropriate

estimations, during selection of suitable and proper calibrations the above mentioned precautions were considered. The detail description of the geothermometer and geobarometer are described in the later sections.

Table 3.8: Mole Fractions considered for Geothermobarometry

Mineral	Mole Fractions		
Garnet	X_{Fe}	=	$\frac{Fe}{Fe+Mg+Mn+Ca}$
	X_{Mn}	=	$\frac{Mn}{Fe+Mg+Mn+Ca}$
	X_{Ca}	=	$\frac{Ca}{Fe+Mg+Mn+Ca}$
Biotite	X_{Fe}	=	$\frac{Fe}{Fe+Mg+Mn+Al^{vi}+Ti}$
	X_{Mg}	=	$\frac{Mg}{Fe+Mg+Mn+Al^{vi}+Ti}$
	X_{Al}^{vi}	=	$\frac{Al^{vi}}{Fe+Mg+Mn+Al^{vi}+Ti}$
	X_{Ti}	=	$\frac{Ti}{Fe+Mg+Mn+Al^{vi}+Ti}$
Muscovite	X_{Fe}	=	$\frac{Fe}{Fe+Mg+Mn+Al^{vi}+Ti}$
	X_{Mg}	=	$\frac{Mg}{Fe+Mg+Mn+Al^{vi}+Ti}$
	X_{Al}^{vi}	=	$\frac{Al^{vi}}{Fe+Mg+Mn+Al^{vi}+Ti}$
	X_{K}	=	$\frac{K}{K+Na+Ca}$
	X_{K}	=	$\frac{Na}{K+Na+Ca}$
	X_{Ms}	=	$X_K . (X_{Al^{vi}})^2$
	X_{Pa}	=	$X_{Na} . (X_{Al^{vi}})^2$
	where, Ms = Musccovite and Pa = Paragonite		
Plagioclase	X_{An}	=	$\frac{Ca}{K+Na+Ca}$
	where, An = Anorthite		

Table 3.9: Activity-Composition models of the minerals for Geothermobarometry

Garnet	$a_{Ca} = X_{Ca}.\exp\left\{\frac{(3300-1.5T)(X_{Mg}^2 + X_{fe}.X_{Mg} + X_{Mg}.X_{Mn})}{RT}\right\}$
	$a_{Fe} = X_{Fe}.\exp\left\{\frac{(1.5T-3300)(X_{Ca}.X_{Mg})}{RT}\right\}$
Biotite	$a_{Fe} = X_{Fe}$
Muscovite	$a_{Ms} = X_{Ms}.\exp\left\{\frac{X_{Pa}^2(W_{Ms} + 2W_{Ms}(W_{Pa} - W_{Ms}))}{RT}\right\}$
	Where, W indicates the Margule factor or parameter and
	$W_{Pa} = 2923.1 + 0.1590P(bar) + 0.1698T(^0K)$
	$W_{Ms} = 4650.1 + 0.1090P(bar) + 0.3954T(^0K)$
Plagioclase	$a_{An} = X_{An}.\exp\left(\frac{610.34}{T(^0K)}\right) - 0.3837$; Hodges and Crowley (1985)

3.7.4 UNCERTAINTIES IN GEOTHERMOBAROMETRY

It is evidenced that despite large numbers of geothermobarometric calibrations are available none of them are free from uncertainties (Spear, 1993; Thomas, 1998). The uncertainties in P-T estimation and the propagation of the errors or uncertainties stem out of a number of reasons.

I. Accuracy of experimental calibration of the exchange thermometer and geobarometer.

II. Error in the Δv of the reaction.

III. Crystal chemistry and physical parameters (e.g., Putin and Holland, 1986).

IV. Neglection of $^{+2}Fe/^{+3}Fe$ ratio in most of the minerals.

V. Analytical imprecision in microprobe analysis.

VI. Uncertainty of electron microprobe standard composition and correction factors.

VII. Cross correlations between errors in temperature estimates and error in pressure, because all thermobarometers are dependant to greater and lesser degrees on both P and T.

VIII. Uncertainties in a-X relationship or mineral activity models.

IX. Geological uncertainties arising from compositional heterogeneities in minerals.

Therefore, in general it is over-optimistic to expect the estimation of P-T for a mineral assemblage as the exact pressure and temperature at which the mineral assemblage was formed. The values give only a certain range of P-T in which a mineral assemblage was probably formed. Therefore, during geothermobarometric estimations, all these important factors were accordingly considered and tried to minimize the level of uncertainties.

The mineral compositions of the samples from Alaknanda and Dhauliganga sections ranging from garnet to sillimanite grade, amphibolite and migmatite are given in the Table 3.10., after careful study under microscope. Since last two to three decades, thermodynamic dataset for minerals have been enriched substantially. More experimental works on the different activity and solution models for different minerals have increased the knowledge for constraining P-T estimations. The more classic example of such thermodynamic dataset is the compilation of about 150 minerals (Berman 1988; Holland 1998). The output of long studies on mineral thermodynamics and development of new programme, THERMOCALC (Holland and Powell, 1998) on the basis of internally consistent thermodynamic dataset; the calculation of all the thermodynamics of rocks can easily be visualized. Since the THERMOCALC average pressure-temperature

calculations are based on internally consistent thermodynamic dataset, it provide only the average results of a numbers of thermodynamic equilibria of the end members of the minerals considered. The different independent end member reactions are internally consistent and were created in the programme (Table 3.11) assuming that all the end members are occurring in thermodynamic equilibrium condition. The activity compositions for all the phases are calculated using A-X programme (Holland and Powell, 2005) and the outputs along with the standard deviation were employed during the pressure –temperature calculations. The statistical check parameters of the calculations are also given in Table 3.13 & 3.14. The activity of H_2O plays a big role in estimation for average P-T, because, in anhydrous equilibria the average P-T yields larger uncertainties and if the activity of H_2O is not properly set in the hydrous equilibria It is seen that thermocalc results give commonly a larger range of uncertainty level, e.g., in case of temperature sometimes it may give more than 150^0C and pressure upto 2Kb or more. Geologically such a large deviation values of pressure and temperature itself may bring a significant change in the mineralogical and the composition of the rocks. However, the uncertainties derived in average pressure temperature corresponds to the overall accuracy of the estimations and its accuracy is 5-10 times greater than the precision of the results (Worley and Powell, 2000). As a rule for estimating the pressure and temperature of the samples, the analyzed point data were thoroughly checked their stoichiometry before adopting whole calculations of therobarometry for the present investigations. For tackling the larger uncertainties during the calculation, hat matrix was

Table 3.10: Mineral assemblages of the selected samples from the Alaknanda and Dhauliganga Valleys

Sample	Sil	Ky	St	Grt	Bt	Ms	Pl	Kfs	Qtz	Rt	Spn	Ap	Ilm	Tur	Chl	Hbl	Ep	Cal	Zrn	Gr
ALAKNANDA SECTION(VAKRITA GROUP)																				
AL 6-16	√	-	-	√	√	√	√	√	√	-	-	√	√	-	-	-	-	-	√	-
AL 5-11	√	-	-	√	√	√	√	√	√	-	-	√	√	-	-	-	-	-	√	-
AG 6-7	√	-	-	√	√	√	-	√	√	-	-	-	√	-	-	-	-	-	√	-
AG 2-5	√	-	-	√	√	√	-	√	√	-	-	-	√	-	-	-	-	-	√	-
AG 1-4	-	-	-	√	√	√	√	-	√	-	-	-	-	-	√	-	-	-	√	-
AG 2-1	-	-	-	√	√	-	√	-	√	-	-	-	√	-	√	√	-	√	-	-
MA39A	-	√	-	√	√	-	√	-	√	-	-	-	√	-	-	-	-	-	-	-
DL 32-56	-	-	-	√	√	√	√	√	√	-	-	-	-	-	-	-	√	-	-	-
DL 36-63	-	-	-	√	√	√	√	-	√	-	-	-	-	-	√	-	-	-	-	-
DL 41-71	-	-	-	√	√	√	√	√	√	-	-	-	-	-	-	-	-	-	-	√
H-1	-	√	-	√	√	√	√	√	√	√	-	√	√	-	-	-	-	-	√	-
ALAKNANDA SECTION(MUNSIARI FORMATION)																				
DL 53-95	-	-	√	√	√	√	√	√	√	√	-	-	√	-	-	-	-	-	-	-
DL 50-90	-	-	√	√	√	-	√	√	√	√	-	-	-	√	√	-	-	-	-	√
DHAULIGANGA SECTION(VAIKRITA GROUP)																				
AG 17-25	√	-	-	√	√	√	√	-	√	-	-	√	√	-	-	-	-	-	-	-
AG 15-21	√	-	-	√	√	√	√	√	√	-	-	-	√	√	-	√	-	-	√	-
AG 14-18	√	-	-	√	√	√	√	√	√	-	-	-	-	-	-	-	-	-	-	-
AG 11-14	√	-	-	√	√	√	√	√	√	-	-	-	√	-	-	-	-	-	√	-
DL2-4	-	-	-	√	√	√	√	-	√	-	-	-	√	-	-	-	-	-	-	-
MA 23-35	-	√	√	√	√	√	√	-	√	√	-	√	√	-	-	-	-	-	√	-
DL 16-28	-	-	-	√	√	√	√	√	√	-	-	-	-	-	-	-	-	-	-	-
DL 22-40	-	-	-	√	√	√	√	√	√	-	-	-	√	-	-	-	√	-	-	-
DL 25-44	-	√	-	√	√	√	√	√	√	-	√	-	√	√	-	-	√	-	√	-
DL18-30A	-	√	-	√	√	√	-	√	√	-	-	-	√	√	-	-	√	√	-	-
DL 18-31	√	√	√	√	√	-	√	√	√	-	-	-	-	√	-	-	-	-	√	-
H-1	-	√	-	√	√	√	√	√	√	√	-	√	√	-	-	-	-	-	√	-
DHAULIGANGA SECTION(MUNSIARI FORMATION)																				
DL 53-95	-	-	√	√	√	√	√	√	√	√	-	-	√	-	-	-	-	-	-	-
DL 50-90	-	-	√	√	√	-	√	√	√	√	-	-	-	√	√	-	-	-	-	√

Table 3.11: The end member equilibrium reactions employed during average P-T calculations (THERMOCALC) of the rocks from the Alaknanda and Dhauliganga river sections

Independent end member reactions used during average PT calculation in THERMOCALC V-3.25	
1) gr + q + 2sill = 3an	22) 3tr + 6parg + 18an = 4py + 8gr + 6ts + 3gl
2) pa + 3an = gr + ab + H2O + 3sill	23) py + 2gr + 3east + 6q = 3phl + 6an
3) 3east + 6q = py + phl + 2mu	24) 3east + 3tr + 3parg + 9ab = 2py + 4gr + 3phl + 6gl
4) 7phl + 12sill = 5py + 3east + 4mu	25) 8py + 12ann + 6parg + 18an = 8gr + 12alm + 12east + 3tr + 3gl
5) phl + east + 6q = py + 2cel	26) py + 3east + 4q = 3phl + 4ky
6) ann + q + 2sill = alm + mu	27) alm + 3east + 4q = 2phl + ann + 4ky
7) 2phl + 3an = py + gr + east + cel	28) east + cel + 3an = py + gr + 2mu
8) ann + 3an = gr + alm + mu	29) 3east + 3an + 6q = 2py + gr + 3mu
9) py + 2pa + 3cel = 3east + 2ab + 9q + 2H2O	30) 2py + 3gr + 3mu + 4pa = 3east + 9an + 4ab + 4H2O
10) gr + 2pa + 3q = 3an + 2ab + 2H2O	31) py + ann = alm + phl
11) 11phl + 12sill = 5py + 7east + 4cel	32) 2phl + pa + san + 6q = py + 3cel + ab
12) 3cel = phl + 2san + 3q + 2H2O	33) 3phl + 4ky = py + 3east + 4q
13) alm + 3east + 6q = 2py + ann + 2mu	34) 2phl + ann + 4ky = alm + 3east + 4q
14) 2phl + pa + san + 6q = py + 3cel + ab	35) gr + q + 2ky = 3an
15) phl + 3an = py + gr + mu	36) pa + 3an = gr + ab + H2O + 3ky
16) py + 2gr + 3east + 6q = 3phl + 6an	37) 3east + 7q + 2ky = 2py + 3mu
17) 2gr + 3alm + 3east + 6q = 2py + 3ann + 6an	38) py + 3cel + 2ky = 3east + 11q
18) ann + east + 6q = alm + 2cel	39) 3phl + 7q + 2sill = 2py + 3cel
19) 2py + 4gr + 3ts + 12q = 3tr + 12an	
20) 6tr + 21an = 10py + 11gr + 27q + 6H2O	
21) 6fact + 21an = 11gr + 10alm + 27q + 6H2O	

checked and accordingly the influential end members were diagnosed. In the present estimations, the activity of the water was assumed as unity ($aH_2O=1$). In the pressure-temperature table (Table 3.13 & 3.14) the overall uncertainties at 1σ confidence level, correlation between the uncertainties on P and T and the significant fit to measure the scatter in residuals of the enthalpies and activities normalized by their uncertainties are given.

Table3.13: P-T estimation of the samples from the Alaknanda section using THERMOCALC-3.25

SAMPLE NO.	TEMPERATURE (^{0}C)	PRESSURE (kb)	a (H_2O)	CORRELATION	FIT (>95%)	INDEPENDENT END MEMBER REACTIONS (Table 3.12)
AL6-16-2-R	670±28	7.6±1.2	1.0	0.897	0.47	(1), (3) ,(4), (6), (10),(11)
AL5-11-2-R	646±31	6.3±1.1	1.0	0.751	0.57	(3), (5) ,(8), (10), (15)
AG6-7-R	622±134	5.4±2.0	abs	0.792	0.12	(1), (16), (17)
AG2-1-R	663±56	6.7±1.3	1.0	0.620	0.92	(19), (20), (21), (22), (23), (24), (25)
AG2-5-R	687±38	5.5±1.2	1.0	0.732	0.93	(3), (8), (10), (15)
AG1-4-R	659±159	5.3±1.9	abs	0.792	0.67	(3), (5), (8), (15)
AG1-4-C	563	At 8.0	abs	-	-	(31)
MA39A-R	664±139	7.2±2.5	abs	0.871	1.04	(1), (33), (34)
DL32-56-R	653±28	8.6±1.0	1.0	0.727	0.70	(3), (5), (8), (9),(15)
DL32-56-C	659	At 6.0	abs	-	-	(31)
DL36-63-R	653±28	9.0±1.0	1.0	0.731	0.60	(3), (5), (8), (10), (15)
DL41-71-R	699±156	11.9±2. 6	abs	0.912	1.49	(3), (5), (8), (15)
H-1-GT2-R	708±41	11.9±1.4	1.0	0.823	1.30	(3), (5), (8), (9), (15)
H-1-GT2-C	610	At 7.5	abs	-	-	(31)
DL53-95-R	676±30	9.9±1.1	1.0	0.759	0.50	(3), (5), (8), (9) ,(15)
DL53-95-C	589	At 8.5	abs	-	-	(31)
VAIKRITA THRUST (VT)						
DL50-60-R	520±94	6.8±2.0	1.0	0.334	0.97	(3), (5), (18)

Abs=the phase is absent in the considered equilibrium reaction

Table3.14: P-T estimation of the samples from Dhauliganga section using THERMOCALC 3.25

SAMPLE NO.	TEMPERATURE (^{0}C)	PRESSURE (kb)	a (H_2O)	CORRELATION	FIT (>95%)	INDEPENDENT END MEMBER REACTIONS (Table 3.12)
MALARI FAULT						
AG17-25-R	694±164	5±1.6	abs	0.730	0.80	(1), (3), (5), (8) (39)
AG17-25-C	605	At 8.0	abs	---	---	(31)
AG15-21-R	704±66	6.2±4.9	1.0	0.831	1.78	(3), (5), (12), (13), (14)
AG15-21-C	654±28	7.9±1.2	1.0	0.695	0.24	(2), (5), (8), (10), (15)
AG14-18-R	646±37	5.2±1.5	1.0	0.728	1.15	(3), (5), (8), (10), (15)
AG14-18-C	619±132	7.5±2.2	1.0	0.351	0.88	(5), (18), (30)
AG11-14-R	663±56	6.7±1.3	1.0	0.620	0.92	(3), (5), (8), (15)
AG11-14-C	539	At 8.0	abs	---	---	(31)
DL2-4-R	629±149	7.3±2.1	abs	0.899	0.25	(3), (8), (15)
VAIKRITA THRUST						
MA23-36R	671±43	9.7±2.2	1.0	0.758	1.96	(3), (5), (8), (35), (36), (38)
DL16-28-R	614±25	8.0±1.0	1.0	0.731	0.58	(3), (5), (8), (10), (15)
DL18-31	653±28	9.0±1.0	1.0	0.731	0.60	(26), (27), (35)
DL25-44-R	708±40	11.4±1.1	0.6	0.877	0.79	(3), (5), (8), (9), (28)
DL25-44-CI	683	At 8.0	abs	---	---	(31)
DL25-44-CII	675	At8.0	abs	---	---	(31)
DL25-44-CIII	615	At 6.0	abs	---	---	(31)
DL25-44-CIV	607	At 6.0	abs	---	---	(31)
DL25-44-CV	602	At 6.0	abs	---	---	(31)
DL22-40-R	638±136	8.7±2.0	abs	0.898	0.70	(3), (8), (15)
DL22-40-C	550	At 6.0	abs	---	---	(31)
DL41-71-R	699±156	11.9±2. 6	abs	0.912	1.49	(3), (5), (8), (15)
H-1-GT2-R	701±32	10.7±1.1	1.0	0.808	0.99	(3), (8), (15), (19), (30)
H-1-GT2-C	610	At 7.5	abs			(31)
DL53-95-R	676±30	9.9±1.1	1.0	0.759	0.50	(3), (5), (8), (9) ,(15)
DL53-95-C	589	At 8.5	abs	-	-	(31)
DL50-60-R	520±94	6.8±2.0	1.0	0.334	0.97	(3), (5), (18)

Abs=the phase is absent in the considered equilibrium reaction

3.8 ZONING PROFILE IN GARNET

Porphyroblasts of garnet have been commonly employed for the study of zoning pattern since it commonly occurs in most of the metamorphic grades ranging from green schist to granulite facies, where the rate of diffusion is substantially sluggish invariably retaining the records up to a higher pressure temperature conditions. The line profiles of the selected elements such as Fe, Mg, Ca and Mn can give the idea about the diffusion pattern vis a vis the growth of the pressure temperature path as well as metamorphic history of the rocks according to their shape and pattern. The change is taken through the processes of diffusion of elements, which is driven by chemical potential gradients generated by the changing pressure temperature conditions. It has been observed that manganese diffusion in garnet is faster than Fe and Mg diffusion probably because, the 8- fold site in garnet is relatively larger which suits Mn as compared to Fe and Mg because of its size (Spear 1993).

With increasing pressure and temperature, normal zoning in garnet may develops due to continuous or discontinuous fractionation processes during the growth of garnet which is observed mostly up to staurolite-kyanite grade rocks (Tracy, 1982; Spear, 1988) normally showing bell-shaped pattern of Mn and/or Ca with an enrichment of Fe and Mg towards the rim. In sillimanite grade, growth pattern is modified by intracrystalline volume diffusion (Tracy, 1982). The magnitude of diffusion also depends upon distribution of minerals and grain size e.g., in rocks with a relatively uniform distribution of minerals and grain size, diffusion take only short distances while in rocks with highly heterogeneous

the smallest garnet DL50-90-C5-SML2 of about 0.2 mm diameter shows the Mg zoning similar to the big garnet (Gt_1), while Ca, Mn and Fe show similar pattern to the intermediate size garnet Gt_2 (DL50-90-C5-SML1). The relaxation in diffusion indicates that the growth zoning has partially been modified due to elevated temperature or may be due to reaction partitioning to other minerals such as biotite (Trzcienski, 1977). The reversal in zoning at the periphery of the grain may either be due to the post-metamorphic growth and/or the breakdown of Mn-rich chlorite (Kretz, 1973).

The zoning in garnets of kyanite grade from the two sections of HHC at different structural level show different pattern. Sample No. MA23-36 of this grade from near the VT about 7Km south of Suraithota consists of large size garnets. Two grains of the same sample have been analyzed of which one >1 cm and the other about 3.8 mm diameter (Fig. 3.19a, b). The former one shows almost flat pattern of Mn and Ca with a slight reversal zoning of all the four elements at the periphery of about 0.2 mm rim indicating relaxation in temperature and pressure. The characteristic change in the zoning of this garnet Gt_2 from the garnet Gt_1 is the increase in Fe towards the core which is reverse of the earlier pattern. The reversal zoning at the rim may be due to the decrease in temperature of the rock or retrogression. The sample, MA 39A from the kyanite gneiss, occurring at the contact of the sillimanite grade near Hanumann Chatti show characteristic change in zoning pattern (Fig. 3.20a) as compared to the earlier sample MA23-36 (Fig. 3.19a, b) of same grade occurring near Suraithota. The zoning pattern of the sample was checked in garnet of about 2.9 mm diameter size which reveals that

distribution of minerals, such as one containing sparse, isolated porphyroblasts, diffusion covers a greater scale to maintain equilibrium.

Grain size dependant for diffusional re-equilibration in garnet is significant e.g., temperature < 600^0C or staurolite grade (staurolite starts nucleation at ~577^0C, Spear et al., 1991); grains of about 2 mm or greater radii are unlikely to modified their zoning pattern (Spear et al., 1991). However, at higher temperatures ranging between 600^0C to 650^0C or above, significant modification in zoning pattern has not been observed in the grains of about 1 cm radii (Florence and Spear 1989; Spear et al., 1989; Spear et al., 1991).

Keeping all these factors in mind, the evaluation of both growth and diffusional zoning in garnets of pelitic rocks, were made from staurolite to sillimanite grade garnet grains mainly of syntectonic (garnet, Gt_1) and post tectonic (garnet, Gt_2) origin. In general, garnet G_1 shows zoning, whereas garnet Gt_2 is mostly homogeneous in composition. Therefore, garnet Gt_1 zoning is used to decipher the effects of temperature in particular and mineral assemblages on the growth and diffusional processes.

Normal zoning is seen in sample DL50-90(-C3-Big) of staurolite grade where the syntectonic garnet Gt_1 of about 3.8 mm diameter size showing spiral inclusion pattern (Fig. 3.18a) occurring in association with about 0.2-0.7 mm diameter size post tectonic garnet Gt_2, DL50-90(-C5-SML 1& 2; Fig. 3.18b & c). The former shows bell-shaped zoning pattern of Mn and Ca with increase in Fe and Mg towards the rim while the later garnet type shows minor reversal in Mn and considerable Mg reverse zoning with a sudden decrease in Ca, Mg and Fe near the grain periphery (DL50-90-C5-SML1, about 0.7 mm diameter). However,

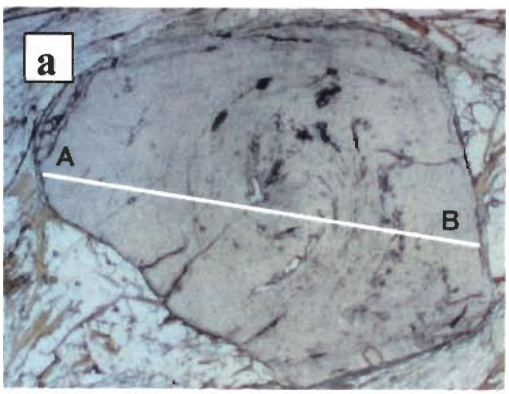

DL50-90-C3-BIG

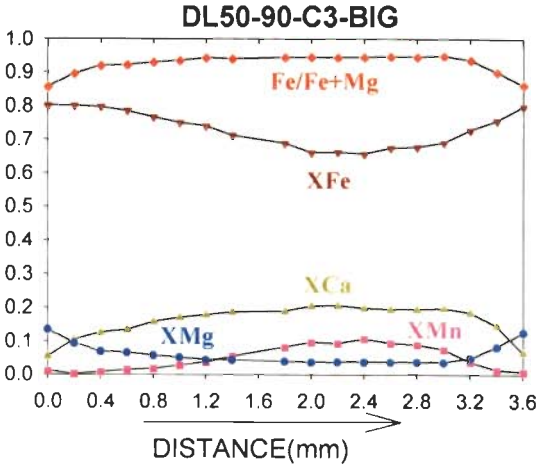

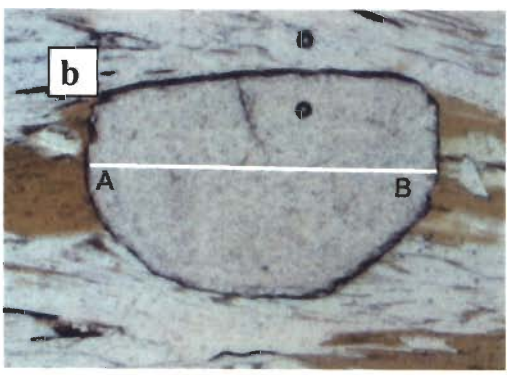

DL50-90-C5-SML1

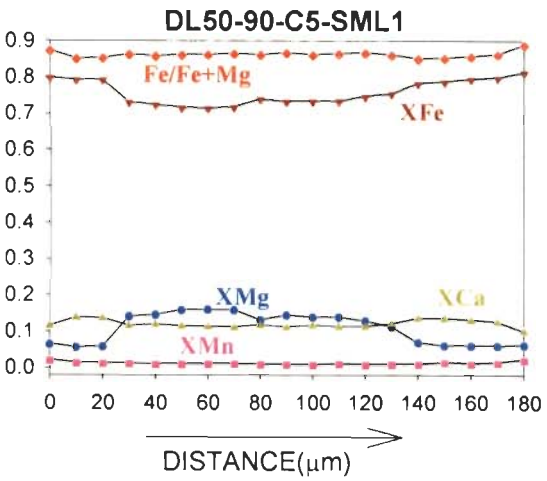

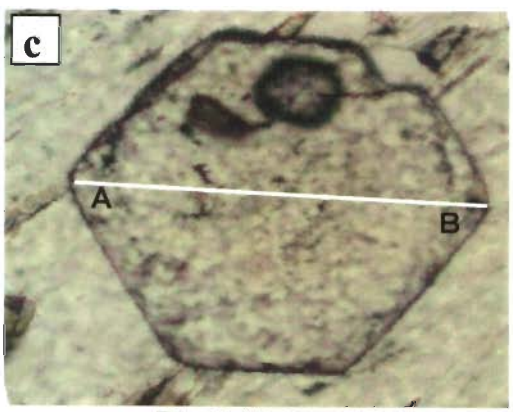

DL50-90-C5-SML2

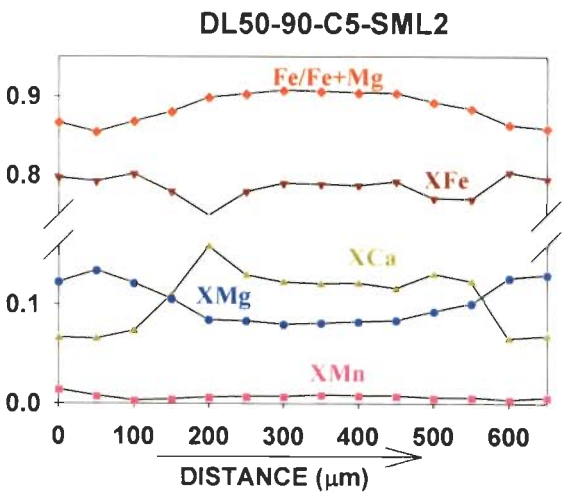

Figure 3.18: The line profile of garnets from Munsiari Formation (a), (b) and (c) are the garnets of the staurolite grade of different sizes where (a) is syntectonic and (b) and (c) are post tectonic. In all the profiles Y-axis represents the values of mole fraction of the garnet which are written in the corresponding profiles.

MA23-36-C1

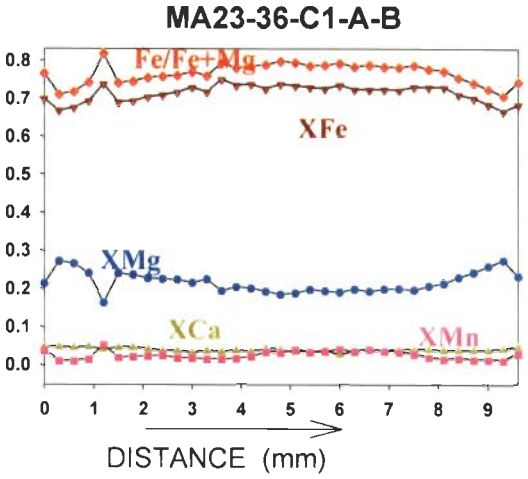

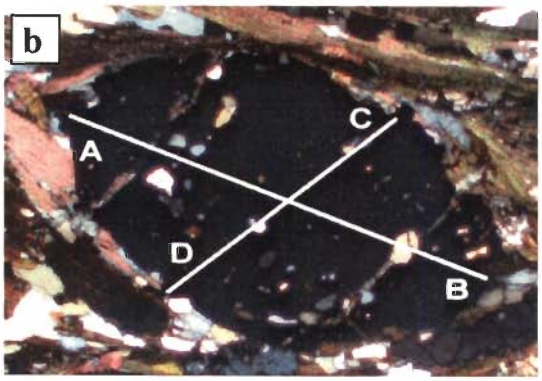

MA23-35-C2

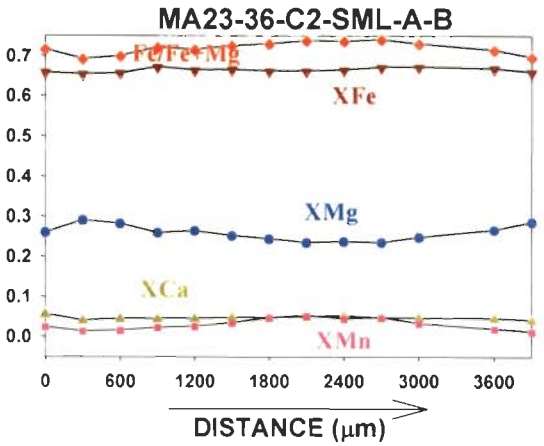

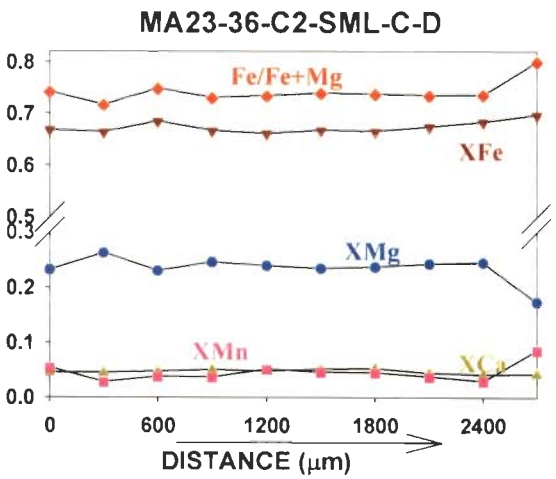

Figure 3.19: The profile of garnets from rim to core to rim from kyanite grade rocks occurring near Vaikrita Thrust with corresponding photomicrographs showing also the line long. which the analyses were done. Y-axis values are mole fractions and they are noted on the corresponding lines.

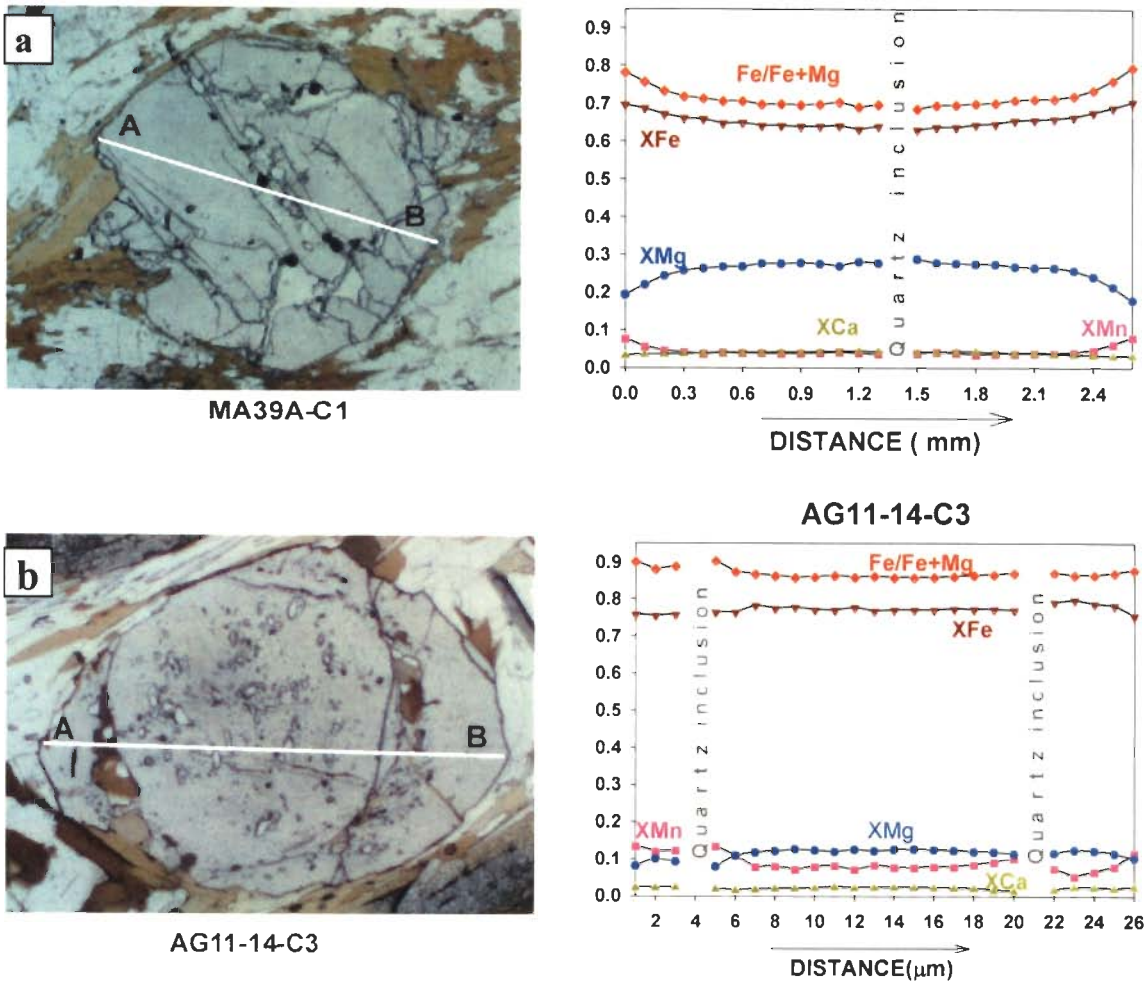

Figure 3.20 : The chemical profile of garnets from rim to core to rim from (a) Kyanite and (b) sillimanite grade rocks with corresponding photomicrographs showing also the line long which the analyses were done. Y-axis values are mole fractions and they are noted on the corresponding curves.

the zoning of Fe and Mg are totally reversed as compared to the earlier garnet of kyanite grade while Ca remains almost flat and Mn get slightly increased towards the rim. The later sample indicates a lower pressure and temperature as compared to the earlier sample (Table 3.13 & 3.14).

The zoning in garnet of the sillimanite grade, AG 11-14, of about 2.8 mm diameter has undergone two stage growth separated by a shell of biotite and quartz (Fig. 3.20b) reveal an almost similar zoning pattern to that of MA 39A of kyanite grade. However, zoning is flatter than the earlier sample (MA 39A) with a slight reversal of Fe at the edge. The temperature and pressure conditions of the two samples are quite similar (Table 3.13).

The reversal at the rim as seen in most of the samples appears to be due to the resorption of garnet edge during retrograde process. It is also noteworthy to mention that zoning is controlled by the type of exchange reaction and condition of metamorphism at which garnet has grown, e.g., grossular content in almandine garnet might be controlled by the presence of calcium-bearing phases like plagioclase, epidote, calcite, etc. in the assemblage. Normally plagioclase gets consumed and it becomes more albitic as the garnet grows, however, the consumption or growth of garnet is also depends upon the ratio of the amount of muscovite to plagioclase (Spear et al., 1991). Therefore, the mineral association in the rock plays a big role in the diffusion zoning.

The temperature changes during the growth of the garnets may be seen in the Fe/Fe+Mg pattern of all the samples because the ratio is probably the best indicator of temperature (Spear et al., 1991) in most pelitic rock (NCMnKFMASH). It is evident that the staurolite and kyanite grade garnets were formed in

increasing temperature conditions as the pattern of the ratio decreases towards the rim. However, sample MA39A (kyanite grade) occurring at the contact of the sillimanite grade shows increase in the ratio, indicating the effect of decreasing temperature by the rock (see Table 3.13). In the higher grades, higher Mg and lower Mn in the core correspond to the high temperature. MA39A and AG11-14 garnet indicate that yhey might have developed due to post growth diffusion since under amphibolite to granulite facies condition, where diffusion in garnet is significantly faster relative to growth (Jiang and Lasaga, 1989).The increase in Fe/Fe+Mg at the garnet edge indicates decreasing temperature (cooling) and readjustment in composition during post-growth diffusion, which is marked by the increase in Mn towards the rim and without much change in Ca (MA23-36-C2-SMLC-D, Fig. 3.19b). Increase in Mg can also be correlated with the growth of biotite where the later release Mg during its growth keeping the Fe and Mn almost unchanged in garnet (e.g., Tracy et al., 1976). The size of the garnet and biotite occurring at mutual contact also affects the mass balance of Fe and Mg between the diffusing phases (Spear 1993).

3.9 RESULTS AND DISCUSSION

It is very clearly seen that the preservation of diffusion pattern in garnet porphyroblast have been influenced by the size because in all the samples the smaller grains show more flatter pattern than the larger ones. All the grains bereft of their sizes and grade of metamorphism show outer rim retrogression pattern which indicates post tectonic or post main metamorphism M_2 episode and can be assigned to small scale retrograde metamorphism M_3. The zoning pattern of the garnets of different grade clearly gives the idea of the relative change in the

pressure and temperature of the rocks. The garnet porphyroblast of the staurolite grade contains Gt_1, larger size with spiral inclusion and Gt_2 of small size with free from inclusion. The Gt_1 gives the earlier part of the pressure temperature history of the rock which indicating an early progressive metamorphism as evident from gradual increase in pressure and temperature from core to rim (X_{Ca} and Fe/Fe+Mg). The profile of the X_{Mn} showing bell-shape is the marker of the changing pressure and temperature, because they can easily diffuse in the higher pressure and temperature condition. Moreover, the smallest garnet Gt_2 show flat pattern because of its smaller size and due to this the zoning got homogenized with the changing pressure and temperature. The quantitative change in the pressure and temperature was not possible to find out as the porphyroblasts of this grade do not contain inclusions of suitable assemblages. However, the changing pattern of the Fe/Fe+Mg and X_{Ca} clearly gives an idea of progressive metamorphism. The rim temperature of the garnet Gt_1 gives 520±90^{0}C and pressure 6.8±2.0 Kbar while the core of the garnet Gt_2 of the sample from about 1km meter above this gives 589^{0}C at 8.5 Kbar with the rim of 698±90^{0}C and 10.3±1.1 kbar. The upper part of the kyanite gneiss (MA 23-36) near Suraithota overlying the staurolite zone gives rim temperature of 708±41^{0}C and 11.9±1.4 Kbar of pressure while its core gives temperature of about 610^{0}C at 7.5 Kbar giving an increment of about 100^{0}C and about 4.5 Kbar from core to rim. On the contrary, the uppermost part of Joshimath Formation which is lying just below the Pandukeshwar quartzite gives slightly lower rim temperature of 675±43^{0}C and pressure of about 11.5±1.3.

The rocks of Pandukeshwar and Badrinath Formation on the other hand show an almost constant temperature with decrease in pressure from 7.3±2.1 Kbar to 5±1.6Kbar towards the northern part at migmatite zone. The pressure and temperature change as shown by different samples is supported by the core (inclusion) & rim thermobarometry of the samples AG 14-18 and AG15-21. In these two samples the reduction of pressure is about 2 Kbar from core to rim while the corresponding increase in temperature is about 50^{0}C. The pressure-, temperature versus structural distance from the MCT is shown in the Figure 3.21. The figures clearly show that both pressure and temperature in both the sections increases toward the north in the lower part of the Vaikrita Group then it maintains an almost stable temperature followed by an slight increase in temperature with subsequent reduction in pressure. This thermobarometric information suggests the decompression of the overloading crustal slabs due to the surface erosion or extensional tectonic operating in the northern boundary of the HHC. It is also clear that the temperature of the rocks nearby Vaikrita Thrust (VT) and the temperature of the migmatite zone are almost same, however, reduction in pressure of about 5 kbar from Vaikrita Thrust to Migmatite zone indicating near-isothermal decompression. However at the central portion of the Vaikrita Group of HHC indicates a slight reduction in temperature and pressure than those of the rocks nearby VT.

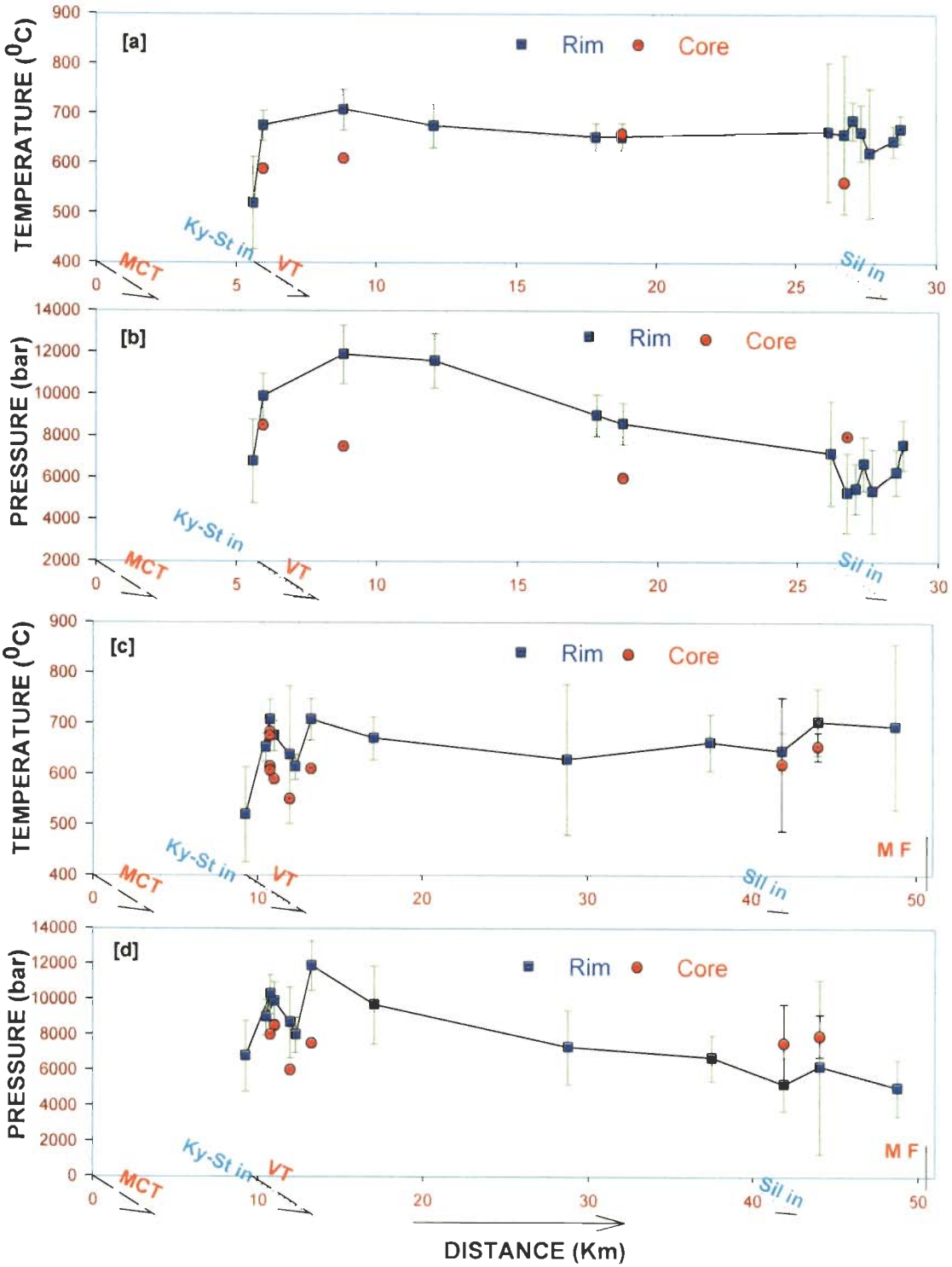

Figure 3.21: Pressure vs.distance and Temperature vs.distance plots; (a) & (b) for Alaknanda section while (c) & (d) for Dhauliganga section using THERMOCALC data.

CHAPTER - 4

GEOCHEMISTRY

4.1. INTRODUCTION

The chemical compositions of metamorphic rocks are governed by number of factors. The most important factor is the composition of the source rock from which the rock has derived. In case of sediment changing into metasediments a number of steps/stages normally occur to reach the final condition and the chemical composition can be affected in a number of ways: (a) Active fluids; an important factor other than pressure-temperature condition which can transport the dissolved ions in substantial quantity. The process of transportation is enhanced by tectonic activity within the terrane e.g., the development of weak zones like faulting, folding and ductile stage deformations. (b) Diffusion Processes; in the high grade metamorphic rocks diffusion processes in solid state can alter the composition of the rock even if the rock does not contain fluid. (c) Solubility ranges of minerals; at the elevated pressure-temperature condition the mineralogical assemblage changes due to different stability range of different minerals and hence the composition of the rocks can be affected.

REEs and trace elemental analysis can help in understanding a number of problems due to their normal mobile and immobile character and chemical similarities, particularly the REEs as they always occur in association rather than isolation. The pattern of change in concentration of the elements, anomalies and their discrimination in different environment are the indicators which can define the rocks petrogenesis. Partial melting, disequilibrium melting and segregation from

the parent body can be understood with the help of REE and trace elemental behaviour. In the present study, the geochemical behaviour of the rocks are considered to understand the relationship among the metasediments of the Higher Himalayan Crystallines and the coexisting migmatite and leucogranite and their source rock characterization.

4.2 TRACE ELEMENTS

Large number of elements in a rock constituting less than 0.1 wt % (1000 ppm) of total rock volume even though sometimes they form their own minerals are called trace elements. Trace elements in a rock body can be affected by the processes of hydrothermal alteration and metamorphism due to mobility of the elements. During metamorphism the mineral composition of a rock changes with increasing pressure and temperature and the active fluid present in the system also affected the trace elements in the rock. Therefore, the elements preferring to remain in melt i.e., incompatible elements, are classified as Low Field Strength Element (LFSE; charge/ size is <2.0) comprising of Cs, Sr, K, Rb, Ba are relatively mobile, they are also called as Large Ion Lithofile Elements (LILE), whereas, the High Field Strength Elements (HFSE; charge/ size is >2.0) consisting of REE, Sc, Y, Th, Zr, Hf, Ti, Nb, Ta and P are more immobile. The concentration of LILE is chiefly controlled by the behaviour of the fluid present. Since, these elements are concentrated in the crust they can be used as indicators for many crustal related processes. Most of the trace elements are normally controlled by the accessory phases present in the rocks, e.g., Zr by zircon, Sr by plagioclase, Nb and Ta by ilmenite or sphene. Moreover, negative Nb anomalies can be used as an indicator of subduction related environment.

4.3 RARE EARTH ELEMENTS (REE)

The REE comprises a series of 15 Lanthanide elements from La (57) to Lu (71) in the periodic table (La, Ce, Pr, Nd, Pm, Sm, Eu, Gd, Tb, Dy, Ho, Er, Tm, Yb and Lu). Within the series the atomic number increases with corresponding decrease in their atomic size (La=1.160 to Lu=0.977Å). This group can be divided into two subgroups as Light Rare Earth Elements (LREE) from La to Gd and Heavy Rare Earth Elements (HREE) ranging from Tb to Lu. In most of the cases the Eu lies out off the trend that is why it is not included in either of these two sub-groups. However, elements between Sm to Ho are sometimes grouped as Middle REE (MREE). Since their size varies within a small range the fractionation in geological environment are relative to each other. The REEs generally occur in +3 oxidation state, however Eu can occur in reducing environment at +2 state while Ce can also occur in +4 state. In the REE diagram the concentration values of the REEs in the samples are normalized with chondrite values and plotted against the atomic numbers to eliminate Oddo-Harkin effect, and characterizing REE pattern of the rock or mineral types. Chondrites are used because they represent the primitive solar material which is the source of the Earth's bulk composition. The chondritic normalized plot indicates (a) initial concentration of the source material, (b) degree of partial melting and (c) subsequent fractional crystallization. Eu anomaly is also an important criterion to characterize the rocks. If the Eu lies above the normal trend it is called as positive anomaly and below the trend then negative anomaly. This anomaly can be quantified by Eu/Eu* values where, $Eu^*=\sqrt{(Sm_N/Gd_N)}$ (Taylor and McLennan, 1985). The values above 1 are assigned as positive anomaly while below 1 as negative anomaly.

4.4 ANALYTICAL PROCEDURE

For the bulk chemical analysis of the different metamorphic rock units of the area covering form Helang to Badrinath and Malari (Fig. 4.1), 46 samples including metasediment, migmatite, migmatite-leucosome and *insitu* melt (tourmaline bearing leucogranite) were processed. All the samples were fresh and unweathered and collected from undisturbed *insitu* occurrences. Each samples weighing about 3-5 kg were thoroughly washed with reverse osmosis (RO) water under pressure to remove dust and other impurities. The dried samples were then broken and reduced to smaller chips of about 1 to 2 cm sized and crushed in jaw crusher (FRICH model) and reduced to less than 5 mm diameter in five steps. All the fractions were mixed thoroughly followed by coning and quartering for systematic reduction of the sample quantity. A representative fraction (finer than 60 mesh size of BSM) of ~250 gm were put into ball mill grinder (RETSCH CENTRIFUGAL BALL MILL S100) for about 30 minutes at 450 rpm and the process were repeated till the 250 mesh size were obtained. The considered fraction was then crushed manually with mortar and pestle to acquire fine powder. Rock powders were then taken in teflon beakers and dissolved with 3 ml of purified HF (48%) and 1ml of conc. HNO_3 acid followed by 2 ml of HNO_3 and 2 ml of purified 6N HCl to obtained complete dissolution. After evaporation to dryness 1 ml of conc. HNO_3 was added to the sample (standard) with clear solution made up a volume of 100 ml in a clean volumetric flask. In case of standard samples, the solution was made in similar manner. All the solutions were transferred and preserved in a PFE bottle for analysis. For internal standard 1 ml of 1 ppm ^{103}Rh was added to the 100 ml of each sample to make an internal reference value of

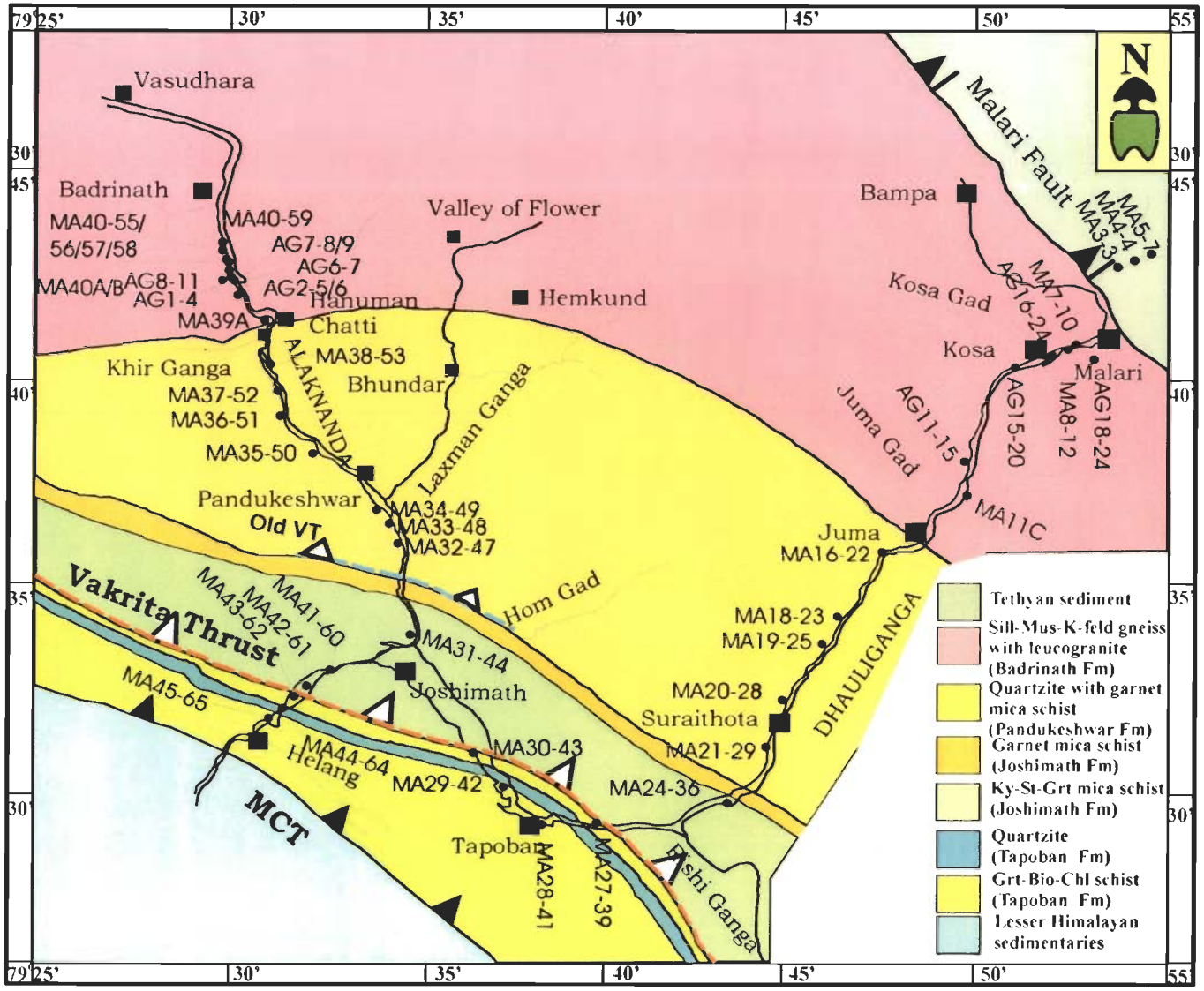

Figure 4.1: Sample location map along Alaknanda and Dhauliganga valley for geochemical analysis

10 ppb. This internal standard allowed to make drift correction so that each mass spectral region were distinct. Couple of procedural blanks were also prepared. The blank, calibration standards and samples were run in a sequence along with two minute wash of the nebulizer-spay chamber with 5% HNO_3 in between 10 samples. Data acquisition and reduction were done under software control.

For trace and REEs all the samples were analyzed in Perkin Elmer Sciex Elan DRC-e (Axial Field Technology) controlled by an associated computer software Elan Instrument Control Version 3.0 which is installed at the Institute Instrumentation Centre, IIT Roorkee. For calibration of the elements during the analysis, reference standards of QLO-1, AGV-2 and BCR-2 were used. The standards were also prepared before the analysis with 20 mg of the reference samples in similar manner as of rock samples.

4.5 RESULTS AND DISCUSSSION

4.5.1 TRACE ELEMENT GEOCHEMISTRY

For the trace elemental geochemistry 17 elements including 8 REE were selected and their absolute abundances are listed in Table 4.1. The concentrations of compatible-incompatible elements were normalized with the Primordial Mantle (Sun and McDonough, 1989) and plotted on multi-elemental variation diagram (spider diagram; Figure 4.2). The line joining Rb and Ba is flatter in the metasediment and migmatite than leucosome and leucogranite indicating presence of mica in the rock. From this spider diagram it is also evident that the metasediment and the migmatite show a very similar pattern with negative anomalies of Ba, Nb, Sr, Zr and Ti, in addition to this Th and Y show a slight positive character. Negative Nb anomalies can be attributed to volcanic or plutonic

rocks above subduction zone and negative Sr and Zr anomalies may reflect the crystallization of plagioclase and zircon from the magma from where the source rocks to sediment formed, rather than as a product of the sedimentary processes. However, the leucosome shows a little change in anomaly pattern. In the metasediment Th is high as compared to U but almost same in migmatite, whereas, leucosome have higher U concentration as compared to Th. The positive anomaly of Th and Y in the metasediment indicates the presence of accessory phases like monazite, xenotime and apatite most of which retain in the restite during partial melting, therefore, shielding the elements from the melt and hence producing negative anomaly in the leucosome and leucogranite. Though the xenotime carries highest Y concentration ranging form 40 to 46 wt % Y_2O_3 it gets over early in the metamorphic stage with the growth of garnet. Though it can reappear with the breakdown of garnet (Pyle and Spear, 1999) seems to have lesser role in the bulk Y budget in the present rocks since Th is depleted with increase in U. The most important Y bearing mineral in general is the garnet which acts like sink for Y. However, garnet is present in most of the samples of metasediment, migmatite and leucogranite, however, it does not seem to be a controlling factor because absence or presence of it do not alter the pattern. Therefore, minerals for controlling Y anomaly appear to be xenotime and other accessory phase like monazite, apatite etc. The positive anomaly of U and lesser negative anomaly of Zr in the leucosome can be attributed to the presence of zircon in the assemblage which is also evident from the thin section studies where

Table 4.1: Absolute abundance of Trace elements in samples from Alaknanda and Dhauliganga valley

	Metasediment												
	AG1-4	AG2-5	AG2-6	AG6-7	AG7-9	AG11-15	AG15-20	AG16-24	MA16-22	MA20-28	MA21-29	MA24-36	MA27-39
Rb	150.14	102.84	98.00	195.85	105.06	152.46	127.88	168.29	87.51	255.33	170.86	116.80	312.37
Ba	465.93	402.18	480.84	385.24	640.77	1000.63	528.77	879.91	423.13	1088.55	663.74	736.36	507.46
Th	13.47	12.15	7.08	11.45	15.44	18.04	15.51	7.29	18.36	16.48	13.37	29.60	14.89
U	2.25	1.98	0.95	1.71	2.67	3.00	1.13	1.22	2.20	1.74	1.22	3.39	4.67
Nb	2.61	9.61	2.65	9.95	2.73	12.23	11.61	8.06	1.28	10.65	1.86	10.17	6.96
La	35.46	26.62	15.13	25.55	16.15	49.12	41.78	21.56	23.83	38.03	29.17	63.85	48.14
Ce	68.19	51.90	31.02	55.05	32.06	88.14	75.98	48.04	43.96	68.09	43.42	116.29	85.63
Sr	98.82	78.60	58.93	62.35	94.41	48.48	59.20	142.42	110.38	87.26	85.39	46.84	67.30
Pr	NA	NA	NA	NA	NA	10.23	9.04	NA	5.29	8.14	4.98	13.56	10.25
Nd	28.47	24.53	11.97	23.68	15.02	25.02	31.97	19.01	13.55	29.18	17.93	54.65	38.75
Sm	5.84	5.04	2.84	4.98	3.73	4.80	6.12	3.52	3.15	6.69	4.42	9.85	5.41
Zr	24.52	21.36	8.01	34.19	2.81	2.65	2.82	4.83	2.36	4.95	4.65	8.62	2.68
Eu	1.43	1.36	0.92	1.42	0.83	1.21	1.81	0.78	0.83	1.87	1.49	2.97	1.74
Ti	1.90	1.51	NA	1.48	NA	1242.06	1003.51	NA	900.87	1203.50	668.99	1023.82	705.02
Ho	0.47	0.43	NA	0.34	NA	0.24	0.47	NA	0.33	0.38	0.49	0.66	0.35
Y	NA	NA	5.22	NA	9.32	6.33	11.84	4.80	11.05	15.73	13.28	17.36	5.47
Yb	0.89	0.91	0.37	0.40	0.61	0.39	0.95	0.34	0.43	0.72	0.82	1.21	0.46

.....*continued*

	Metasediment												
	MA28-41	MA29-42	MA30-43	MA31-44	MA32-47	MA33-48	MA34-49	MA35-50	MA36-51	MA37-52	MA38-53	MA39-54	MA39A
Rb	218.91	136.70	51.39	101.56	100.18	108.11	64.28	60.66	47.41	91.79	172.70	203.28	176.66
Ba	935.90	506.44	558.54	972.63	589.59	577.78	445.97	608.44	616.66	557.57	525.20	541.92	727.78
Th	21.82	17.43	10.39	19.22	17.69	16.50	6.31	5.15	4.95	7.22	11.22	17.30	31.10
U	3.76	3.64	0.75	2.15	2.88	3.27	0.79	1.28	1.21	0.84	1.90	2.02	5.15
Nb	20.67	4.43	2.64	7.17	10.53	6.44	1.75	2.35	5.89	1.87	6.12	15.39	10.14
La	48.15	36.46	19.74	47.78	52.06	50.95	15.59	21.31	24.43	23.10	43.73	53.99	81.31
Ce	98.68	64.78	35.41	71.35	101.81	100.99	29.09	39.19	40.79	42.29	79.36	96.06	146.27
Sr	132.84	130.41	43.60	83.36	47.13	55.11	18.79	151.95	112.83	142.13	119.66	50.75	93.35
Pr	14.17	7.32	4.17	7.95	12.40	11.16	3.35	4.58	4.76	4.84	9.32	11.30	17.76
Nd	38.20	25.03	14.75	28.46	45.11	40.58	12.17	16.18	17.06	17.11	32.66	26.08	61.32
Sm	8.60	4.42	4.24	5.23	7.01	5.87	2.28	2.30	2.96	3.22	5.12	4.24	10.96
Zr	16.23	5.80	22.49	5.68	4.46	3.13	4.44	2.12	2.69	2.37	5.71	15.85	4.99
Eu	2.54	1.67	1.36	1.94	2.30	1.78	0.81	0.77	0.81	1.10	1.70	1.14	3.24
Ti	1684.46	598.43	723.85	893.95	1294.38	725.10	644.02	965.35	735.28	1231.63	1443.83	894.77	1359.52
Ho	0.74	0.32	0.39	0.38	0.34	0.22	0.31	0.31	0.25	0.28	0.40	0.59	0.79
Y	29.40	8.76	13.23	10.11	9.28	5.66	8.06	7.85	4.77	6.98	10.24	15.70	24.27
Yb	1.34	0.46	0.86	0.86	0.56	0.43	0.63	0.56	0.46	0.58	0.74	0.99	1.32

.....continued

	Metasediment						Migmatite			Leucogranite
	MA41-60	MA42-61	MA43-63	MA44-64	MA45-65	AG8-11-M	MA8-12	MA11C	MA40-59	AG18-28
Rb	98.81	260.97	236.05	413.60	57.53	105.24	171.72	265.79	145.48	379.79
Ba	861.72	715.91	807.58	736.85	319.38	203.34	512.85	413.56	802.67	181.63
Th	33.02	36.02	21.58	35.20	3.28	5.46	18.08	7.83	15.85	1.74
U	3.71	5.01	5.12	4.97	0.32	0.87	1.62	2.97	4.26	11.69
Nb	7.03	19.70	4.59	17.96	3.13	1.85	14.13	9.01	11.99	23.29
La	75.67	67.80	74.00	52.07	22.66	15.32	41.97	15.06	39.65	3.42
Ce	135.11	117.88	146.00	92.86	40.24	28.17	75.16	28.20	71.73	6.91
Sr	87.27	134.36	45.02	28.19	78.00	133.27	72.05	63.59	72.01	52.85
Pr	16.37	14.35	18.76	10.85	4.67	NA	9.01	3.37	8.52	NA
Nd	56.10	71.94	48.10	42.01	16.57	10.20	32.41	10.52	27.44	3.05
Sm	10.37	11.36	7.89	8.81	2.00	2.30	6.96	2.60	5.98	0.79
Zr	27.32	36.74	14.07	8.27	3.01	23.16	4.06	4.44	11.21	6.28
Eu	3.10	3.12	2.37	2.26	0.49	0.74	2.32	0.88	1.76	0.10
Ti	1464.39	947.70	1166.46	944.29	696.85	1.39	1377.52	826.85	916.69	NA
Ho	0.79	0.99	0.63	0.96	0.18	0.20	0.64	0.22	0.56	NA
Y	20.22	34.68	19.78	30.96	5.24	NA	15.38	7.65	15.06	3.44
Yb	1.22	1.63	1.34	1.63	0.34	0.30	1.13	0.51	1.00	0.19

.....continued

	Leucosome									
	AG7-8	AG8-11GT	AG8-11-L	MA7-10	MA40A	MA40B	MA40-55	MA40-56	MA40-57	MA40-58
Rb	149.66	164.30	127.47	123.02	144.30	141.65	71.44	106.79	77.40	83.67
Ba	209.52	276.79	71.61	591.04	162.51	103.10	160.22	286.19	170.64	102.18
Th	2.23	5.24	0.39	5.32	3.51	0.98	0.82	2.03	0.99	0.56
U	2.35	4.86	0.54	4.32	6.63	1.02	0.64	1.68	0.57	0.40
Nb	0.48	1.90	0.55	2.24	1.39	1.49	0.25	0.21	0.45	0.44
La	4.94	22.96	1.32	20.80	12.48	13.76	3.04	6.31	3.04	1.84
Ce	10.36	41.11	2.65	48.05	22.62	18.76	6.10	12.68	5.99	3.66
Sr	57.47	250.18	119.15	48.89	113.96	60.21	148.90	155.16	96.13	113.49
Pr	NA	4.92	NA	5.48	2.65	1.89	NA	NA	NA	NA
Nd	5.04	17.93	1.15	19.20	6.12	2.33	2.66	6.07	3.10	1.48
Sm	1.33	3.10	0.25	3.26	1.21	0.80	1.87	0.44	5.40	0.28
Zr	2.66	1.79	1.53	4.87	3.52	2.89	1.45	2.78	2.37	1.54
Eu	0.67	1.31	0.84	1.30	1.00	0.77	0.79	0.36	1.01	0.74
Ti	NA	235.12	NA	829.22	506.03	580.68	NA	NA	NA	NA
Ho	NA	0.81	NA	0.27	0.26	0.16	NA	NA	NA	NA
Y	6.18	18.05	2.05	5.81	6.53	3.60	4.91	8.14	1.21	1.13
Yb	0.45	2.50	0.28	0.66	1.04	0.32	0.81	0.73	0.12	0.10

* NA=Not Analyzed

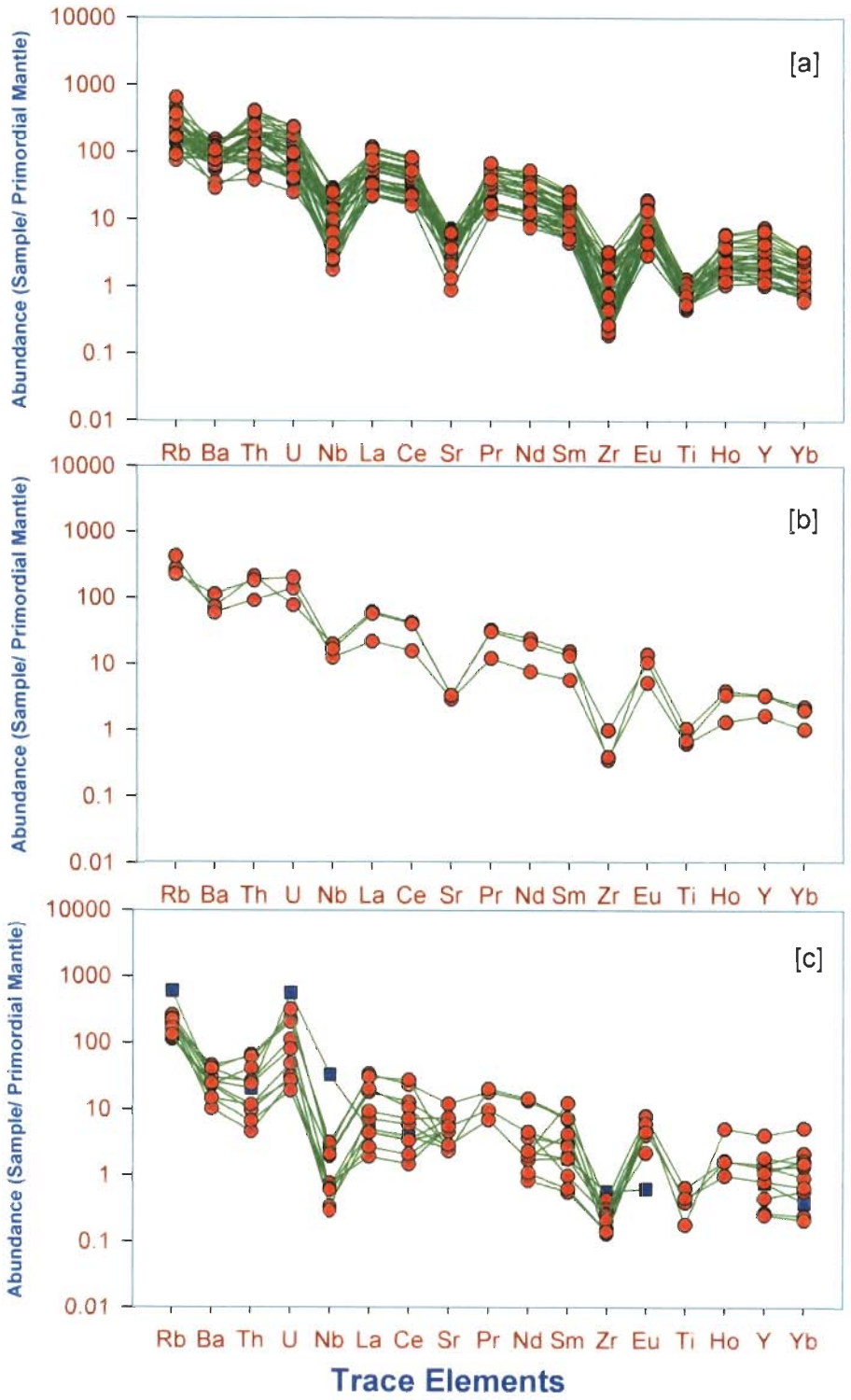

Figure 4.2: Spider diagram for different rocks of Alaknanda and Dhauliganga valley (a) metasediment (b) migmatite (c) leucosome and tourmaline leucogranite (filled Squares)
most of the zircons are

segregated into the leucosome-melanosome part. Negative anomalies of Nb and Ti are more pronounced in the leucosome which can be attributed to concentration of sphene and rutile, however, the presence of ilmenite does not have controlling effect on the pattern. The presence of positive Sr and Eu anomalies reveal an enrichment of feldspar cumulate in leucosome (Fig. 4.2c).

4.5.2 REE GEOCHEMISTRY

The absolute abundances of REEs are given in the Table-4.2. The data were normalized with C1-chondrite values (Sun and McDonough, 1989) and plotted in common logarithmic scale against their elements (Figure 4.3). The REE-normalized diagram clearly show a similar pattern in metasediments and migmatite samples with less fractionation in both LREE and HREE which is smooth and somewhat flat pattern with slight positive Gd and Tm anomaly along with feeble negative anomaly in Eu and Er (Figure 4.3a, b). Sm, Nd and other LREE pattern indicate that they reside predominantly in the accessory phases like apatite and monazite in most of the metasediments. In case of leucosome, the fractionation of HREE is prominent along with pronounced Eu positive anomaly (Figure 4.3; 4.4c, 4.4d). In overall picture the REE pattern in leucosome is distinct with enriched pattern of HREE giving a slightly concave upward curve (Figure 4.3c). C1-chondrite normalized pattern indicate feeble Ce anomaly which can be attributed to the presence of monazite in the rock and the positive Eu anomaly attributed to feldspar cumulates within the leucosome. This positive Eu anomaly can also be explained by the process of melt extraction and shielding of accessory phases by restite biotite and garnet or these could be due to removal of REE having 3+ which is hosted in the ferromagnesium and accessory phases stored

away during melting processes. These patterns also indicate that leucosome does not contain significant amount of restite material and they represent, the initial liquids, which have not been fractionally crystallized or underwent crystal accumulation. However, the heterogeneity in the REE pattern in leucosome specially Sm and Nd are the clear indication of the disequilibrium melting or segregation. The enriched pattern of HREE can be attributed to the garnet segregates in the leucosome. In the similar view, the Himalayan leucogranite indicate concentration of LREE which is controlled by monazite dissolution and 10% contributed by apatite along with 50% contribution of MREE and >90% of HREE (Ayres and Harris 1997). Considering these points and the present pattern the negative anomaly in Sm and Nd are likely to be controlled by monazite which remains arrested in the melanosome part in few samples. The strong positive anomaly of Eu indicates the accumulation of plagioclase in the leucosome which is one of the dominant mineral in few leucosome samples. The values of Eu anomaly are also given in the Table 4.2 defined by Eu/Eu^{*}, which is distinctly less than 1 in case of metasediment and more than 1 in case of leucosome.

Table 4.2: Absolute abundance of REE in samples from Alaknanda and Dhauliganga valley

	Metasediment												
	AG1-4	AG2-5	AG2-6	AG6-7	AG7-9	AG11-15	AG15-20	AG16-24	MA16-22	MA20-28	MA21-29	MA24-36	MA27-39
La	35.46	26.62	15.13	25.55	16.15	49.12	41.78	21.56	23.83	38.03	29.17	63.85	48.14
Ce	68.19	51.90	31.02	55.05	32.06	88.14	75.98	48.04	43.96	68.09	43.42	116.29	85.63
Pr	NA	NA	NA	NA	NA	10.23	9.04	NA	5.29	8.14	4.98	13.56	10.25
Nd	28.47	24.53	11.97	23.68	15.02	25.02	31.97	19.01	13.55	29.18	17.93	54.65	38.75
Sm	5.84	5.04	2.84	4.98	3.73	4.80	6.12	3.52	3.15	6.69	4.42	9.85	5.41
Eu	1.43	1.36	0.92	1.42	0.83	1.21	1.81	0.78	0.83	1.87	1.49	2.97	1.74
Gd	6.29	5.16	NA	5.08	NA	6.12	7.69	NA	3.09	7.01	5.19	10.14	5.93
Tb	0.48	0.73	0.28	0.54	0.42	0.60	0.80	0.34	0.32	0.82	0.58	1.21	0.48
Dy	2.65	2.53	1.03	2.01	1.47	2.70	3.04	1.20	1.72	3.01	2.26	4.31	2.64
Ho	0.47	0.43	NA	0.34	NA	0.24	0.47	NA	0.33	0.38	0.49	0.66	0.35
Er	1.21	1.10	0.48	0.60	0.77	0.43	1.03	0.49	0.87	0.81	0.97	1.43	0.69
Tm	0.19	0.16	0.08	0.11	0.12	0.08	0.17	0.10	0.13	0.19	0.18	0.23	0.10
Yb	0.89	0.91	0.37	0.40	0.61	0.39	0.95	0.34	0.53	0.72	0.82	1.21	0.46
Lu	NA	NA	0.03	NA	0.05	0.03	0.07	0.02	0.05	0.07	0.08	0.09	0.04
ΣREE	151.57	120.47	64.15	119.76	71.24	189.11	180.92	95.39	97.65	165.01	111.98	280.44	200.62
$\Sigma LREE_{(La-Gd)}$	145.68	114.61	61.88	115.76	67.79	184.63	174.39	92.90	93.70	159.01	106.59	271.30	195.86
La_N/Yb_N	28.58	20.98	29.33	45.82	18.88	***89.59***	31.46	45.48	32.25	37.88	25.52	37.99	75.07
La_N/Sm_N	3.92	3.41	3.44	3.31	2.80	6.60	4.41	3.96	4.88	3.67	4.26	4.19	5.74
Eu/Eu*	0.72	0.82	NA	0.86	NA	0.68	0.81	NA	0.81	0.83	0.95	0.91	0.94

.....*continued*

	Metasediment												
	MA28-41	MA29-42	MA30-43	MA31-44	MA32-47	MA33-48	MA34-49	MA35-50	MA36-51	MA37-52	MA38-53	MA39-54	MA39A
La	48.15	36.46	19.74	47.78	52.06	50.95	15.59	21.31	24.43	23.10	43.73	53.99	81.31
Ce	98.68	64.78	35.41	71.35	101.81	100.99	29.09	39.19	40.79	42.29	79.36	96.06	146.27
Pr	14.17	7.32	4.17	7.95	12.40	11.16	3.35	4.58	4.76	4.84	9.32	11.30	17.76
Nd	38.20	25.03	14.75	28.46	45.11	40.58	12.17	16.18	17.06	17.11	32.66	26.08	61.32
Sm	8.60	4.42	4.24	5.23	7.01	5.87	2.28	2.30	2.96	3.22	5.12	4.24	10.96
Eu	2.54	1.67	1.36	1.94	2.30	1.78	0.81	0.77	0.81	1.10	1.70	1.14	3.24
Gd	9.28	5.48	4.78	6.94	7.88	6.93	2.96	2.78	3.01	4.18	6.19	5.02	11.52
Tb	1.14	0.55	0.55	0.65	0.93	0.78	0.31	0.31	0.39	0.41	0.65	0.60	1.34
Dy	4.94	2.29	1.93	2.70	3.75	2.98	1.67	1.73	1.71	1.69	3.19	3.28	4.76
Ho	0.74	0.32	0.39	0.38	0.34	0.22	0.31	0.31	0.25	0.28	0.40	0.59	0.79
Er	1.78	0.77	0.88	0.96	0.82	0.52	0.80	0.86	0.65	0.68	1.02	1.49	1.98
Tm	0.27	0.11	0.13	0.13	0.12	0.08	0.11	0.12	0.10	0.10	0.14	0.22	0.31
Yb	1.34	0.46	0.86	0.86	0.56	0.59	0.68	0.56	0.46	0.58	0.74	0.99	1.32
Lu	0.11	0.03	0.10	0.07	0.06	0.06	0.07	0.06	0.04	0.07	0.10	0.10	0.11
ΣREE	229.94	149.69	89.27	175.40	235.14	223.48	70.21	91.06	97.41	99.65	184.33	205.09	342.99
$\Sigma LREE_{(La-Gd)}$	219.62	145.16	84.43	169.65	228.57	218.26	66.25	87.11	93.81	95.84	178.09	197.82	*332.38*
La_N/Yb_N	25.77	56.85	***16.46***	39.95	66.83	61.78	16.46	27.06	38.09	28.59	42.12	38.99	44.12
La_N/Sm_N	5.32	3.01	5.89	4.80	5.61	4.41	5.98	5.33	4.63	5.51	8.23	4.79	3.61
Eu/Eu*	1.04	0.92	0.98	0.95	0.85	0.95	0.93	0.83	0.92	0.92	0.76	0.88	0.87

.....continued

	Metasediment						Migmatite			Leucogranite
	MA41-60	MA42-61	MA43-63	MA44-64	MA45-65	AG8-11-M	MA8-12	MA11C	MA40-59	AG18-28
La	75.67	67.80	74.00	52.07	22.66	15.32	41.97	15.06	39.65	3.42
Ce	135.11	117.88	146.00	92.86	40.24	28.17	75.16	28.20	71.73	6.91
Pr	16.37	14.35	18.76	10.85	4.67	NA	9.01	3.37	8.52	NA
Nd	56.10	71.94	48.10	42.01	16.57	10.20	32.41	10.52	27.44	3.05
Sm	10.37	11.36	7.89	8.81	2.00	2.30	6.96	2.60	5.98	0.79
Eu	3.10	3.12	2.37	2.26	0.49	0.74	2.32	0.88	1.76	0.10
Gd	12.98	13.24	8.46	11.01	1.84	2.65	8.51	2.67	6.73	NA
Tb	1.48	1.47	1.01	1.22	0.21	0.29	0.90	0.36	0.82	0.12
Dy	5.13	6.46	4.76	5.84	1.12	1.43	3.45	2.11	4.35	0.49
Ho	0.79	0.99	0.63	0.96	0.18	0.20	0.64	0.22	0.56	NA
Er	1.91	2.35	1.76	2.12	0.46	0.53	1.62	0.59	1.25	0.23
Tm	0.28	0.38	0.26	0.36	0.07	0.08	0.25	0.08	0.21	0.04
Yb	1.22	1.63	1.34	1.63	0.34	0.30	1.13	0.51	1.00	0.19
Lu	0.12	0.14	0.11	0.14	0.02	NA	0.15	0.03	0.19	0.01
ΣREE	320.62	313.11	315.45	232.14	90.87	62.21	184.47	67.22	170.18	15.36
$\Sigma LREE_{(La-Gd)}$	309.70	299.70	305.58	219.87	88.47	***59.38***	176.34	63.31	161.80	14.28
La_N/Yb_N	44.64	29.84	39.61	22.91	47.33	36.63	**26.76**	21.10	**28.57**	-------
La_N/Sm_N	4.71	3.85	6.05	3.82	7.32	4.30	3.90	3.74	4.28	2.79
Eu/Eu*	0.78	0.89	0.70	0.78	0.92	0.82	0.92	1.02	0.85	NA

.....*continued*

	Leucosome									
	AG7-8	AG8-11GT	AG8-11-L	MA7-10	MA40A	MA40B	MA40-55	MA40-56	MA40-57	MA40-58
La	4.94	22.96	1.32	20.80	12.48	13.76	3.04	6.31	3.04	1.84
Ce	10.36	41.11	2.65	48.05	22.62	18.76	6.10	12.68	5.99	3.66
Pr	NA	4.92	NA	5.48	2.65	2.60	NA	NA	NA	NA
Nd	5.04	17.93	1.15	19.20	6.12	2.33	2.66	6.07	3.10	1.48
Sm	1.33	3.10	0.25	3.26	1.21	0.80	1.87	0.44	5.40	0.28
Eu	0.67	1.31	0.84	1.30	1.00	0.77	0.79	0.36	1.01	0.74
Gd	NA	3.65	NA	4.37	1.52	1.14	NA	NA	NA	NA
Tb	0.17	0.46	0.03	0.39	0.20	0.16	0.08	0.23	0.06	0.04
Dy	0.90	4.23	0.32	1.31	1.39	0.73	0.77	1.33	0.14	0.09
Ho	NA	0.81	NA	0.27	0.26	0.16	NA	NA	NA	NA
Er	0.56	2.36	0.25	0.60	0.66	0.39	0.63	0.78	0.07	0.04
Tm	0.09	0.34	0.05	0.09	0.11	0.07	0.11	0.13	0.01	0.01
Yb	0.45	2.50	0.28	0.66	1.04	0.32	0.81	0.73	0.08	0.10
Lu	0.03	0.56	0.06	0.02	0.15	0.02	0.18	0.09	0.02	0.02
ΣREE	24.53	106.26	7.21	105.80	51.40	42.01	17.03	29.16	18.92	8.30
$\Sigma LREE_{(La-Gd)}$	22.34	95.00	6.21	102.46	47.59	40.16	14.46	25.86	18.54	8.00
La_N/Yb_N	7.86	6.58	***3.34***	22.59	8.65	***30.88***	2.69	6.21	27.33	13.01
La_N/Sm_N	2.40	4.78	3.34	4.12	6.64	11.12	1.05	9.30	0.36	4.27
Eu/Eu*	NA	1.19	NA	1.05	2.24	2.46	NA	NA	NA	NA

* NA=Not Analyzed

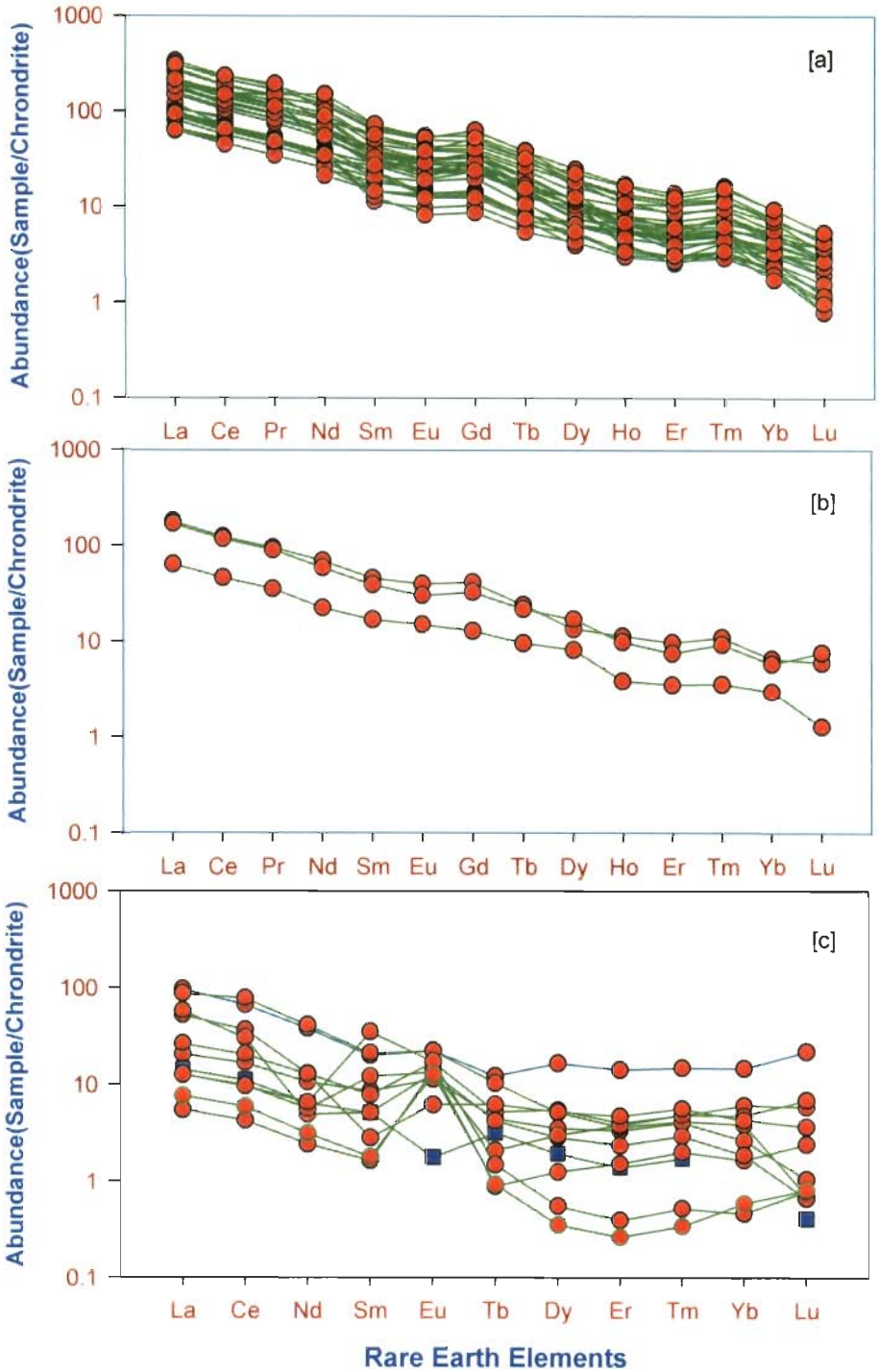

Figure 4.3: REE diagram for different rocks of Alaknanda and Dhauliganga valley (a) metasediment (b) migmatite (c) leucosome and tourmaline leucogranite (filled squares).

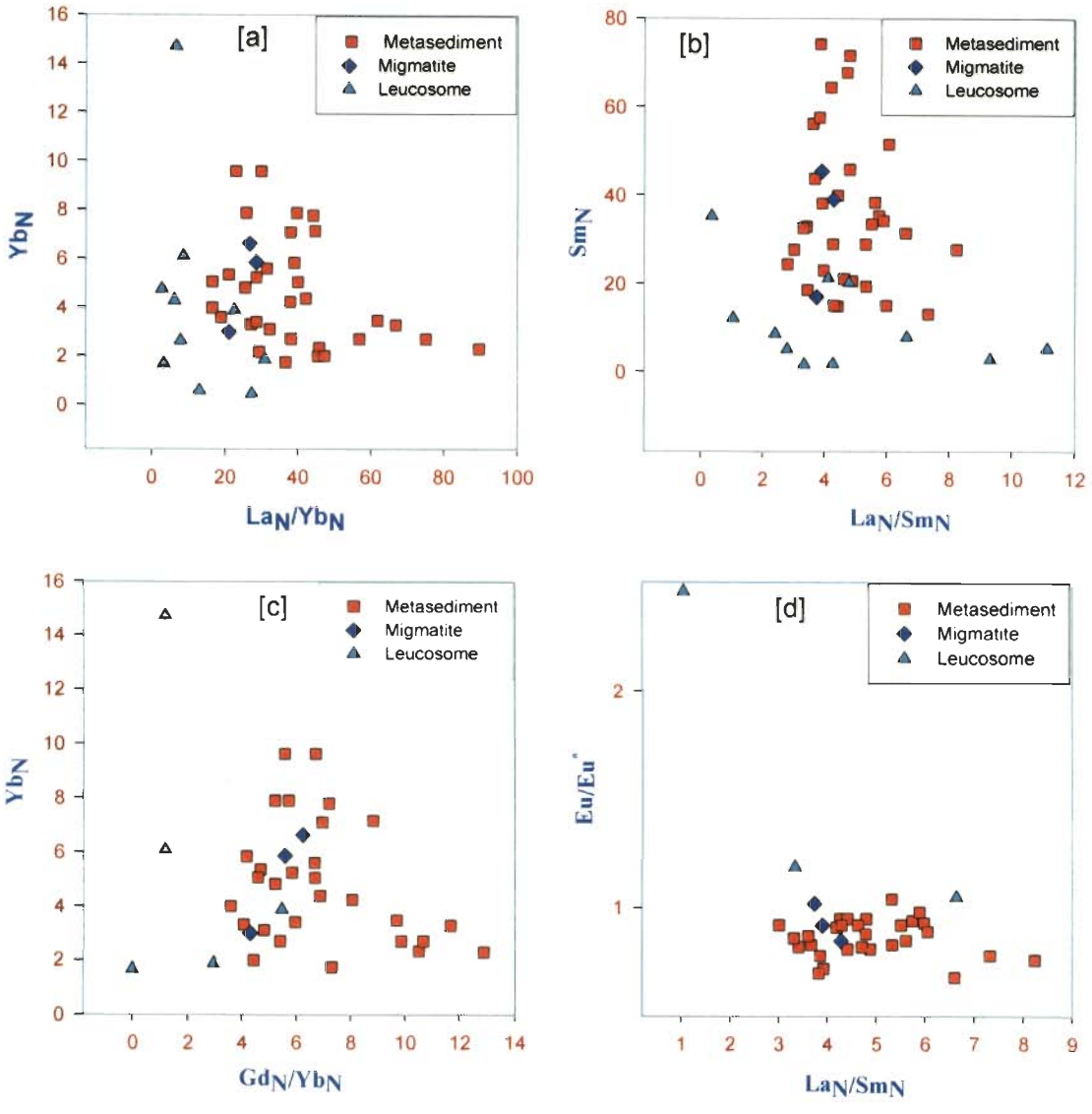

Figure 4.4: Fractionation diagram for metasediments, migmatites, leucosome and leucogranite (a) fraction for all REE (b) fractionation for light REE (c) fractionation for heavy REE and (d) europium fractionation diagram.

CHAPTER - 5

GEOCHRONOLOGY

5.1. INTRODUCTION

Last three decades have seen radiogenic studies of rocks and minerals which have been used profoundly for quantifying the time space of the geological events and to unravel the geologic history of difficult and complex tectonic region. During earlier dates radiogenic isotopes were used for determining age of the rocks and minerals, however, with the advent of sophisticated instrumentation and better techniques for pre-concentration of elements, isotopic studies have been increasingly used in petrologic studies to identify geological processes and also source rock evaluation. Despite the fact that, different radio-isotopic systems are available for geologic investigations number of advantages and disadvantages exists over one another. Rb-Sr system is one of the most widely used radio isotopic methods in the field of geology. The occurrence of Rb and Sr in most of the rocks are usually varied, in acidic and intermediate it is more and in basic rocks it is less. However, in minerals like feldspar, mica and other silicate minerals it is abundant. During metamorphic events redistribution or re-homogenization of Rb-Sr take place between minerals and rock. The bulk chemistry of rock does not change e.g., the expelled Sr from biotite usually does not leave the rock if the system is closed and it is preferentially incorporated in Ca-rich minerals such as apatite or plagioclase (Jager, 1979). Moreover, Sr in apatite can preserve the initial $^{87}Sr/^{86}Sr$ and this tool has been successfully applied to granitic rocks to constrain the initial $^{87}Sr/^{86}Sr$ (Motohiro and Kazuhiro, 2003; Motohiro, 2005). The Rb-Sr systematic is widely

applied in determination of mineral crystallization/cooling age and evaluation of cooling or exhumation history as they record last geothermal event. However, the determination of metamorphic age greatly depends upon the degree of metamorphism e.g., in low grade metamorphism the age of a mineral having particular blocking temperature will give the metamorphic maximum while in high grade metamorphism the timing of peak metamorphism is normally inferred from total resetting of the Rb-Sr minerals within whole rock system. The partial Sr-exchange can occur at low temperatures between adjacent minerals causing partial resetting age. Under higher pressure metamorphic condition phengite component in white mica increases therefore the fractionation of $(Rb/Sr)_{Biotite}/(Rb/Sr)_{Phengite}$ increases from about 0.05 to more than 100. Further, if some active fluids are present in the system a complete homogenization of Sr isotope or complete Sr-exchange between the different minerals of a rock does not necessarily require a molten state. Under conditions of amphibolite facies metamorphism, usually complete Sr-homogenization takes place among different minerals. However, muscovite commonly resists rejuvenation and Sr-exchange especially in the coarse grained pegmatites (Jager, 1979). In most of the earth surface processes and geologic activities like alteration, fluid mechanism, metasomatism and weathering, Rb and Sr sustain mobility. On the contrary, Sm and Nd belong to light REE and remain relatively immobile during the processes of weathering, erosion, fluid activity and hydrothermal metasomatism. However, Sm-Nd system carries disadvantages due to the relative longer half life making the system not suitable for dating younger rocks but can be used to characterize the rock body.

The rocks of the present study area are mostly schist and gneiss, which gives us an ample opportunity for systematic study of Rb-Sr whole rock-mineral (biotite and muscovite) pair for constraining the cooling ages of the terrain. These two minerals give different closing temperatures (300C±50^{0}C for biotite and 500C±50^{0}C for muscovite) and therefore, provide a good evaluation of rate of exhumation or cooling history of the HHC. Sm-Nd isotopic measurement has also been carried out to evaluate the source rock characterization. Further, the combined application of the Sr and Nd isotopic diagram has been used for the source rock characterization. The concentrations of both the elements increase with increasing degree of fractionation or differentiation making these isotopes as unique character even in the mixed rocks of different sources. Sr is relatively immobile under hydrothermal activities while Rb, is one of the most abundant trace elements in the crust, is very susceptible to mobility under hydrothermal activity. During sedimentation, metamorphism and melting, Sr retained mostly in plagioclase during crystallization gets partitioned among the associated minerals but the whole rock chemistry during metamorphism remains unchanged. Therefore, Sr fairly reflects the original composition of a suit of rocks. In case of Sm-Nd systematic, both the elements are immobile under hydrothermal conditions and so their isotopic compositions reflect the actual proportions of the rock. By combining both the Sr and Nd isotopic compositions different metamorphic rocks in a terrane can be discriminated and hence their petrogenesis can be evaluated.

5.2 Rb-Sr SYSTEMATIC

Both Rb and Sr are occurring widely in most of the igneous, metamorphic and sedimentary rocks preferably in acidic to intermediate and even to a lesser extend in

basic rocks. Both the elements occur in trace quantity in the earth and the presence of these two elements in rocks and minerals is governed by the chemistry of the minerals present in the rock. Chemically, Rb is an alkali Group IA monovalent element which has ionic radius of 1.48 Å. It has two naturally occurring isotopes, ^{85}Rb and ^{87}Rb with isotopic abundance of 72.2% and 27.8% respectively and only ^{85}Rb is radiogenic which decays to ^{87}Sr with a decay constant of 1.42×10^{-11} yr^{-1} with corresponding half-life of 4.88×10^{9} years (Steiger and Jaeger, 1977). The natural isotopic ratios $^{85}Rb/^{87}Rb$ is equal to 2.59265. Rb is most incompatible element during the crystallization due to its large ionic size and susceptibility to mobility in the earth surface processes because of its solubility in water and hydrous fluids like other alkali elements. The ratio of Rb/Sr tends to increases as the crystallization advances e.g., pegmatite possibly has the highest value of Rb/Sr ratio around 10, while biotite and phengite have the highest ratio followed by muscovite, chlorite and K-feldspar among all rock forming minerals. Due to the similar valency and very close similarity in the ionic size between Rb and potassium, Rb can substitute easily K (K=1.33 Å radius), therefore, Rb normally found in most of the the K-bearing minerals such as mica and K-feldspar (Dickins, 1995).

Sr is an alkali earth Group IIA bivalent element having ionic radius 1.13 Å and has four stable naturally occurring isotopes ^{84}Sr, ^{86}Sr, ^{87}Sr and ^{88}Sr with isotopic abundance of 0.56%, 9.87%, 7.04% and 82.53% respectively and has recommended isotopic ratios of $^{86}Sr/^{88}Sr$ and $^{84}Sr/^{86}Sr$ are 0.1194 and 0.056584 respectively. Out of these four ^{87}Sr is a radiogenic daughter isotope produced by radioactive decay of ^{87}Rb. This, ^{87}Sr within the rocks can be incorporated from two sources: (i) primordial ^{87}Sr formed during nucleo-synthesis at the time of earth's

formation and its early dates and known as initial Sr and (ii) radiogenic decay of ^{87}Rb as daughter product. The ionic radius of Sr^{+2} is similar to that of Ca^{+2}(0.99 Å), therefore, Sr can replace Ca in most of the minerals such as plagioclase, apatite, fluorite, epidote, garnet, K-feldspar and other. However, the ability of Sr^{+2} to replace Ca^{+2} is somewhat control by the fact that Sr^{+2} favours eight fold co-ordinated site, while, Ca^{+2} being of smaller size accommodate in both six and eight fold co-ordination site. Sr^{+2} ions can be captured in the place of K^{+1} which in turn is adjusted by the $Si^{+4} \leftrightarrow Al^{+3}$ replacements to maintain electrical neutrality (Dickins, 1995).

The decay of ^{87}Rb to ^{87}Sr takes place with an emission of negatively charged beta particle, antinutrio and energy and can be depicted as:

$$^{87}Rb \rightarrow {}^{87}Sr + \beta^{-} + \bar{\upsilon} + Q \qquad \text{----------5.1}$$

Where, $\bar{\upsilon}$ is the antineutrino and Q is the decay energy equivalent to 0.275 MeV.

If the system is closed and we put these isotopes in the basic equation then the expression becomes

$$^{87}Sr = {}^{87}Sr_i + {}^{87}Rb\,(e^{\lambda t} - 1) \qquad \text{----------5.2}$$

Where, ^{87}Sr of the right hand side of the equation is the total number of ^{87}Sr atoms present in the system at present day, $^{87}Sr_i$ is the number of ^{87}Sr present at the time when system got closed, ^{87}Rb is the number of atoms today and λ is the decay constant. Since mass spectrometer can measure accurately only the ratios, the isotopes in the equation 5.2 has to be expressed in the form of isotopic ratios, which can be done by normalizing all the isotopes by ^{86}Sr. Since ^{86}Sr is non-radiogenic it does not affect the principle of the equation. Therefore, the equation 5.2 will become

$$^{87}Sr/^{86}Sr = (^{87}Sr/^{86}Sr)_i + {}^{87}Rb/^{87}Sr\,(e^{\lambda t} - 1) \qquad \text{----------5.3}$$

Where, $^{87}Sr/^{86}Sr$ is the present day isotopic ratio in the rock or mineral which is measured by a mass spectrometer,

$(^{87}Sr/^{86}Sr)_i$ is the isotopic ratio present at the time of formation of the rock or mineral (unknown) and

$^{87}Rb/^{87}Sr$ is the present time isotopic ratio present in the rock or mineral can be measured by a mass spectrometer.

The $^{87}Sr/^{86}Sr$ ratio in the rock or mineral is measured by a suitable mass spectrometer while the concentrations of Rb and Sr are usually determined either by XRF or by isotopic dilution method followed by $^{87}Rb/^{87}Sr$ calculation. This equation 5.3 represents a straight line equation of y=c+mx, where, the intercept with y-axis give the ratio $(^{87}Sr/^{86}Sr)_i$ and the slope of line $m = (e^{\lambda t} - 1)$ will provide the age of the rock. The slope -age relation is given as:

$$m = (e^{\lambda t} - 1)$$

$$t = 1/\lambda \ln(m + 1)$$

$$t = 1/\lambda \ln\left[\frac{\frac{^{87}Sr}{^{86}Sr} - \left(\frac{^{87}Sr}{^{86}Sr}\right)_i}{\frac{^{87}Rb}{^{86}Sr}} + 1\right] \qquad \text{----------5.4}$$

Using this equation and initial Sr ratio from the evolutionary plot between $^{87}Sr/^{87}Sr$ vs. $^{87}Rb/^{87}Sr$, the age of the rocks or minerals can be calculated (Faure, 1986; Dickins, 1995).

In order to find out the initial concentration of the ratio $(^{87}Sr/^{86}Sr)_i$ present in the samples as defined in the equation 5.3 & 5.4, a graphical evolutionary plot $^{87}Sr/^{86}Sr$ vs $^{87}Rb/^{86}Sr$ can be made which will give this straight line. When two or more co-genetic samples or different minerals of a sample along with the whole rock

values are plotted and the best fit/regression line gives a perfectly straight line it is called as isochron. The slope of this line gives the age of the mineral or rock as defined in the equation 5.4. In an isochron the data points are deviate from the line only within a certain tolerance limit and if the data point scatters around the straight line and the deviation of which falls outside the tolerance limit the line is called an errorchron. For construction of isochron numerous regression methods are available for best line fitting (McIntyre et al., 1966; York, 1966, 1969; Brooks et al., 1972).

To express the relation between the geological error and the analytical errors which create the scattering of the data points, York (1969) and Brook et al. (1968, 1972) introduced the concept of Mean Squared Weighted Deviates (MSWD). If the scattering of the data points are exactly equivalent to predicted from the analytical errors, then the calculation will give MSWD=1. By excess scattering of data points yield MSWD >1, while, less scattered data points will give MSWD<1. The distinction between the isochron and errorchron can beobserved by applying "rule of thumb" (Brook et al. 1972) according to which MSWD < 2.5 will define an isochron fit within the limits of analytical error otherwise the line will be an errorchron, for which the scattering of data points are explained mainly due to geological error. Normally, in most of the cases, it is considered that for samples to be defining a high degree confidence isochron the MSWD of the data points must be unity or very close to it.

The slope of the isochron varies with the age of the samples. Therefore, in Sr-evolution diagram at t=0(crystallization or formation of the rock), the slope of the isochron is parallel to the abscissa. It increases to the higher gradients as the Rb starts decaying to Sr with time in a closed system.During metamorphism complete re-homogenization of the Sr isotopes may happen, which, in turn, will give a new

smaller slope of straight line in Sr-evolution diagram defined by the minerals present in the rock (Dickins, 1995).

At elevated temperature near to crystallization, the daughter nuclide diffuses out as fast as it is produced by radioactive decay. As the system cools down the diffusion decreases and at ambient temperature, the loss of daughter nuclides through diffusion becomes negligible or absent and the daughter products accumulate without any further loss. This minimum temperature at which the loss of daughter product in the minerals through diffusion gets blocked is called "blocking temperature" or most preferably "closure temperature" (Dodson, 1979). It is noteworthy, that closure temperatures of minerals do not represent a fixed temperature rather it gives a small range of temperature. Different minerals have different closure temperature in different isotopic system. Therefore, the metamorphic mineral ages from orogenic belt generally record their cooling history rather than their primary crystallization age. In slow cooling metamorphic terranes, continuous transition of high temperature provides intracrystalline volume diffusion of ^{87}Sr preferably along the cleavages as fast as it is formed by decay of Rb until low temperature is achieved. Closure temperatures of biotite and muscovite are $300\pm50^{0}C$ and $500\pm50^{0}C$ respectively (Jager, 1979). Therefore, depending upon the closure temperature and the mineral cooling age it is possible to calculate the rate of cooling or exhumation of the terrain.

5.3 Sm-Nd SYSTEMATIC

Samarium (Sm) and Neodymium (Nd) are trivalent light rare earth elements (LREE) which are widely distributed in many rock forming silicates, phosphates and carbonate minerals. The ionic radii of Sm and Nd are 1.04Å and 1.08 Å respectively.

In the universe Nd is 3.2 times more abundant than Sm and their concentrations in common minerals and rocks are normally less than 10 ppm (except for phosphate minerals like allanite, apatite, etc. and alkaline igneous rocks which have higher concentrations). The ratio of Sm/Nd in minerals ranges from 0.14 (k-feldspar) to 0.54 (garnet). Both Nd and Sm have seven naturally occurring isotopes (excluding ^{146}Sm). The isotopes of Nd are ^{142}Nd, ^{143}Nd, ^{144}Nd, ^{145}Nd, ^{146}Nd, ^{148}Nd and ^{150}Nd and out of these ^{143}Nd and ^{142}Nd are the radioactive alpha decay product of ^{147}Sm and ^{146}Sm (extinct nuclide) respectively. The seven isotopes of Sm are ^{144}Sm, ^{147}Sm, ^{148}Sm, ^{149}Sm, ^{150}Sm, ^{152}Sm and ^{154}Sm and out of these ^{147}Sm, ^{148}Sm and ^{149}Sm are radioactive capable of producing ^{143}Nd, ^{144}Nd and ^{145}Nd respectively. Out of these three ^{143}Nd and ^{145}Nd have long half-lives (ca. 10^{16} yr) because of that they are not capable of producing measurable variations in the daughter isotopes even during the whole life of the earth. The half-life of ^{147}Sm (106 Ga) is sufficiently short to produce small but measurable differences in ^{143}Nd abundance over periods of several million years and therefore they are being used for age determination (Dickins, 1995).

The concentrations of both the elements increase with the increase in degree of differentiation in the line of Bowen's reaction series but their Sm/Nd ratios decrease. Because the ionic size of Nd^{+3} is larger than the Sm^{+3} which give larger ionic potential (charge/size) providing more concentration of the former in the liquid which also forms a weaker ionic bond that are more easily broken than those of Sm^{+3}.

Like Rb-Sr systematic the age determination of rocks can be worked out from bivariant diagram of $^{143}Nd/^{144}Nd$ vs $^{147}Sm/^{144}Nd$ using isochron method having following equation

$^{143}Nd/^{144}Nd = (^{143}Nd/^{144}Nd)_i + {}^{147}Sm/^{144}Nd\ (e^{\lambda t}-1)$ ----------5.5

Where, $\lambda = 6.54 \times 10^{-12}\ yr^{-1}$ (Steiger and Jaeger, 1977).

The ages of the Sm-Nd system are normally expressed in the forms of model ages i.e., the measure of the length of time that the sample has been separated from the mantle, from where it was originally derived. The two frequently quoted models for the mantle reservoir are the Chondritic Uniform Reservoir (CHUR) and Depleted Mantle (DM).

T-CHUR model ages are calculated based on the assumption that the earth's primitive mantle at the formation of the earth had the same isotopic composition of Nd as the average chondritic meteorite. Therefore, the primitive or initial ratio of Nd is synonymous with the Nd composition of the bulk earth. It is evident that model ages are sensitive to difference in the Sm/Nd ratio between the sample and the CHUR and only the fractionated samples having different Sm/Nd ratio can yield precise ages. T-CHUR model is calculated using the following equation.

$$T_{CHUR}^{Nd} = \frac{1}{\lambda} \ln \left[\frac{\left(\frac{^{143}Nd}{^{144}Nd}\right)_{sample,today} - \left(\frac{^{143}Nd}{^{144}Nd}\right)_{CHUR,today}}{\left(\frac{^{147}Sm}{^{144}Nd}\right)_{sample,today} - \left(\frac{^{147}Sm}{^{144}Nd}\right)_{CHUR,today}} + 1 \right] \quad \text{----------5.6}$$

Depleted Mantle (DM) model age has proposed on the basis of observed initial $^{143}Nd/^{144}Nd$ ratio in Precambrian rocks where the Sm/Nd ratio yields higher value than the CHUR, which leads to the suggestion that the mantle which supplied the continental crust has evolved since earliest times. The depletion of the light REE from the chondritic reservoir took place between 2.5 to 3.0 Ga that is the time of major episode of crust generation and the depletion continues to present day in a linear path (Liew and McCulloch, 1985). Due to partial melting of CHUR the magma

gives lower Sm/Nd ratio than that of the CHUR because with increase in degree of fractionation the concentration of both Sm and Nd increases but their ratio decreases. The residual solids which are depleted in LILE that left behind after withdrawal of the magma give higher Sm/Nd ratios than the chondritic reservoir.

Table 5.1: Different isotopic ratios for normalization of Nd isotope and calculation of model age and epsilon parameter (Rollinson, 1993)

Normalizing factors		
$^{146}Nd/^{142Nd}$ = 0.636151 (1) = 0.63613 (3) = 0.63223 (4)	$^{150}Nd/^{142Nd}$ = 0.2096 (1) = 0.209627(2)	$^{146}Nd/^{144Nd}$ = 0.7219 (5)
Chondritic Uniform Reservoir (CHUR)		
$(^{143}Nd/^{144}Nd)_{CHUR, 4.6Ga}$	0.505829 (1)	0.50677±10 (7) 0.50663 (8), preferred value
$(^{143}Nd/^{144}Nd)_{CHUR, today}$	0.511847 (2) 0.511836 (10)	0.51262 (8) 0.512638 (9), preferred value
$(^{147}Sm/^{144}Nd)_{CHUR, today}$	0.1936 (now superposed) (7) 0.1967 (1)	0.1966 (9) 0.1967 (12) 0.19637-0.1968 (16)
Depleted Mantle (DM)		
$(^{143}Nd/^{144}Nd)_{DM, today}$	0.51235 (10) 0.512245 (11)	0.51315 (12) 0.51316 (9) 0.531114 (15) 0.51317-0.51330 (16)
$(^{147}Sm/^{144}Nd)_{DM, today}$	0.214 (10) 0.217 (13) 0.225 (14) 0.230 (11)	0.2137 (12) 0.222 (15) 0.233-0.251(16)

1) Jacobsen and Wasserburg (1980); 2) Wasserburg et al., (1981); 3) DePaolo (1981); 4),5) O'Nions et al., (1977); 6) O'Nions et al., (1979); 7) Lugmair et al.,(1975); 8) Hawkesworth and van Calstere (1984); 9) Goldstein et al., (1984); 10) McCulloch and Black (1984); 11) McCulloch and Chappell (1982); 12) Peucat et al. (1988); 13) Taylor and McLennan (1985; 14) McCulloch et al., (1983) 15) Michard et al., (1985); 16) Allegre et al., (1983)

Therefore, most rocks of the continental crust are expressed with reference to the DM reservoir rather than CHUR which can be calculated by substituting the proper values of DM in $(^{143}Nd/^{144}Nd)_{CHUR}$ and $(^{147}Sm/^{144}Nd)_{CHUR}$ in the equation 5.6. From the model ages as described above it is evident that the initial ratio of $(^{143}Nd/^{144}Nd)$

in the rock of either igneous or metamorphic origin is normally compared with the corresponding ($^{143}Nd/^{144}Nd$) of CHUR. However, the differences in the ratios are normally very low due to the long half-life. This ifficulty can overcome by considering "epsilon parameter' as introduced by DePaolo and Wasserberg (1976) which is expressed as:

$$\varepsilon_{CHUR}^{t,today} = \left[\frac{\left(\frac{^{143}Nd}{^{144}Nd} \right)_{i(sample)}}{\left(\frac{^{143}Nd}{^{144}Nd} \right)_{CHUR,t,today}} - 1 \right] \times 10^4 \qquad \text{----------5.7}$$

For convenience to deal with the different problem, the epsilon values can be expressed in three different ways as (i) ε_{Nd} values with respect to isochron (equation 5.8) (ii) ε_{Nd} values for an individual rocks at their time of formation (equation 5.9) and (iii) ε_{Nd} values for individual rocks at present (equation 5.10). These equations are as follows:

$$\varepsilon_{Nd}^{isochron,t} = \left[\frac{\left(\frac{^{143}Nd}{^{144}Nd} \right)_{i(sample)}}{\left(\frac{^{143}Nd}{^{144}Nd} \right)_{CHUR,t}} - 1 \right] \times 10^4 \qquad \text{----------5.8}$$

$$\varepsilon_{Nd}^{t} = \left[\frac{\left(\frac{^{143}Nd}{^{144}Nd} \right)_{sample,t}}{\left(\frac{^{143}Nd}{^{144}Nd} \right)_{CHUR,t}} - 1 \right] \times 10^4 \qquad \text{----------5.9}$$

$$\varepsilon_{Nd}^{today} = \left[\frac{\left(\frac{^{143}Nd}{^{144}Nd} \right)_{sample,today}}{\left(\frac{^{143}Nd}{^{144}Nd} \right)_{CHUR,today}} - 1 \right] \times 10^4 \qquad \text{----------5.10}$$

The isotopic ratios of CHUR and DM at different time are given in the Table 5.1 while the other ratios will come from the rocks. The epsilon parameters of rocks are sometimes also expressed with respect to the ratios of DM instead of CHUR in the equations 5.8 and 5.10.

The epsilon values may be either positive or negative for any sample. The positive values indicate that the rocks were derived from residual solids (depleted source) which are depleted in the large ion lithophile elements (LILE) due to the preferential partitioning of the LILE into the liquid phase during partial melting. The negative values on the other hand indicate that the rocks were derived from the sources (enriched LILE) which have lower Sm/Nd ratio than the chondritic or primordial reservoir. If epsilon value is zero it may indicate that the rock could have been derived directly from the primordial reservoir.

5.4 SAMPLPLE PREPARATION

5.4.1 MECHANICAL PREPARATION

For geochronologic purpose, fresh and unweathered samples were collected during the field work. The location map of the samples is given in Figure 5.1. To minimize the unnecessary carriage of the sample weight, the outer surface of the samples was chopped in the field itself. The selected samples of about 3-5 kg size were thoroughly brushed with fine copper brush in the sample preparation laboratory and washed with reverse osmosis (RO) water under pressure. The samples were then allowed to dry under regulated low ampere infra red lamp. The dried samples

were then broken with cleaned steel hammer over clean steel table which was kept over white paper spreading around it to collect the splitted sample chips. After reducing the sample size to about cubic inch all the fractions were then put into steel jaw crusher (Fig. 5.2a, FRICH model), where the samples were reduced to less than 5 mm diameter in a step by step manner. In each step the samples were sieved with 1 mm sieve size to remove the smaller fractions and finer dust particles. After finishing the processes of one sample the whole assembly, the jaws and the collecting baskets were cleaned with acetone and blown out with compressed high pressure air.

All the fractions including the smaller and finer fraction separated by sieving during crushing and the remainder fractions were taken into clean paper and mixed thoroughly for homogenization of the sample with sunmica plates and steel scoop which were then coned and quartered for systematic reduction of the sample quantity. The process was repeated till the representative samples stand for purposeful quantity. Two fractions were taken out from the rocks one for whole rock geochronology and/or geochemistry and the other for mineral separation. During the process repeated sieving was performed with 60 mesh size (BSM) sieve to separate out the finer fractions and the grinding continued till the entire sample pass through 60 mesh sizes. The fractions between 60 and 170 mesh size (BSM) were used for mineral separation.

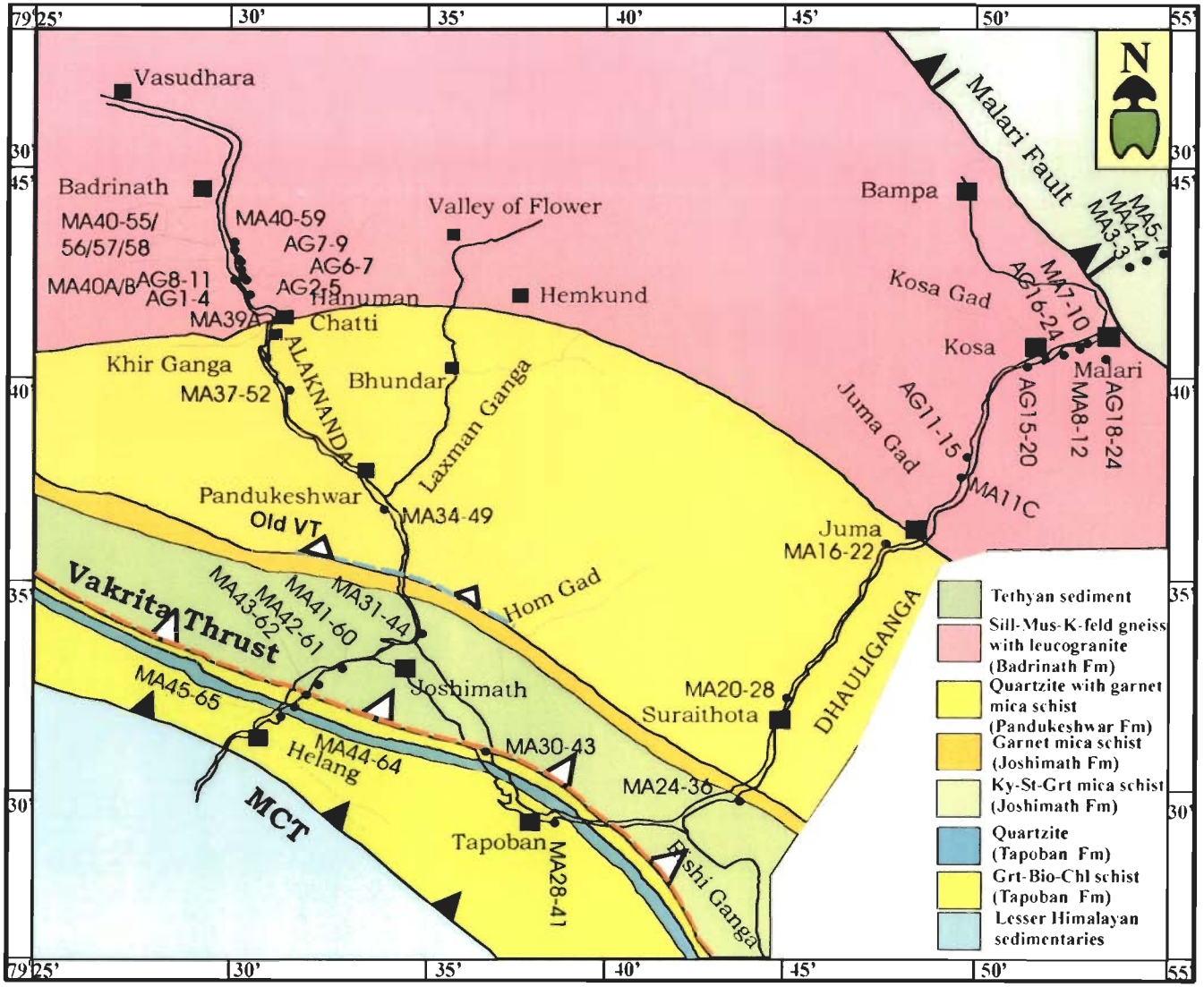

Figure 5.1: Sample location map along Alaknada and Dhauliganga valley forgeochronoly

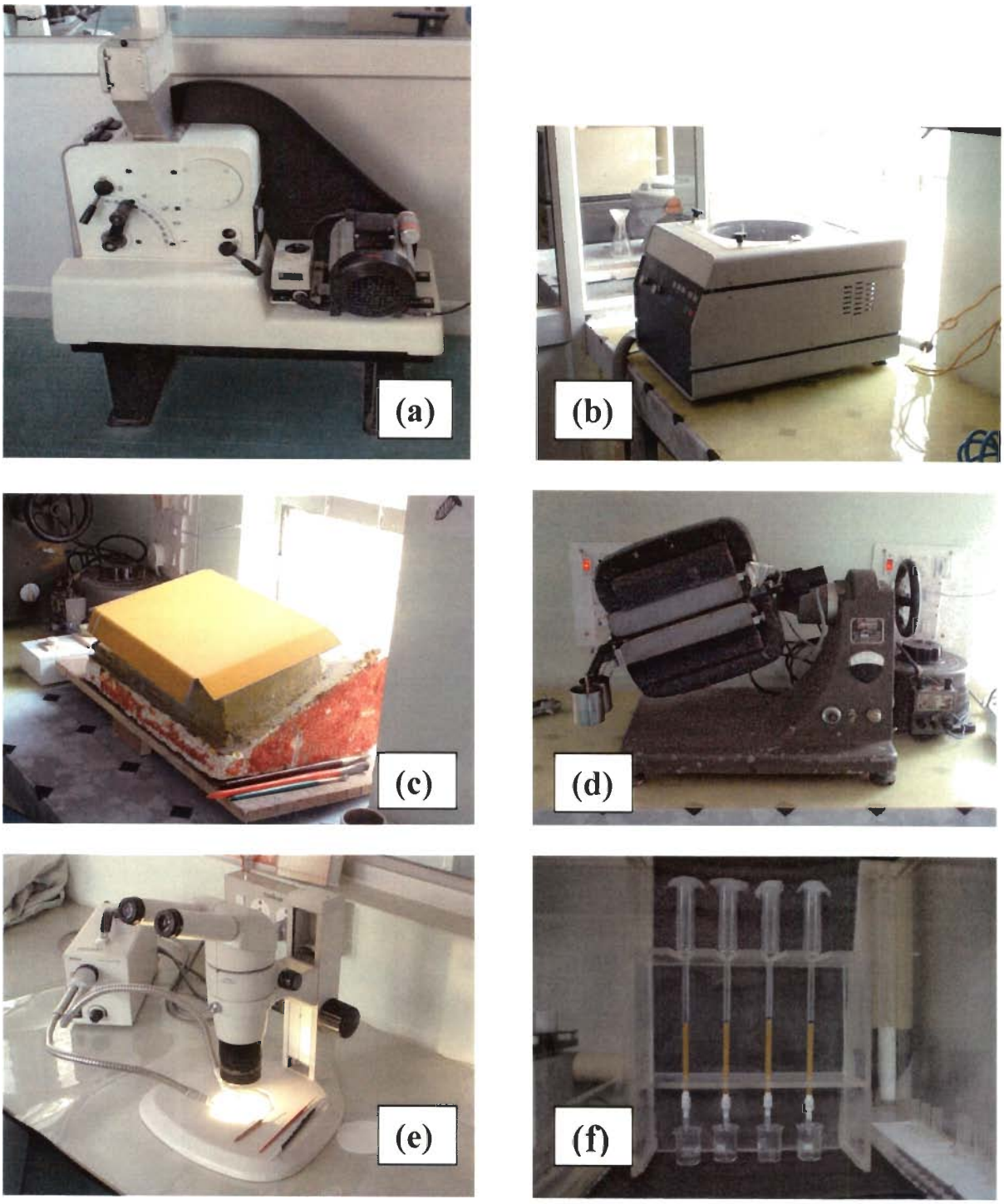

Figure 5.2: Different instruments used during sample preparation at geochronolological sample preparation laboratory, Earth Sciences, IIT Roorkee (a) Jaw Crusher (b) Ball mill (c) Mica vibrator (d) Magnetic Isodynamic separator (e) binocular microscope and (f) ion exchange column (TIMS, lab IIC, IIT Roorkee)

The sample fraction for geochronology and/or geochemistry were put into ball mill grinder (Fig. 5.2b, RETSCH CENTRIFUGAL BALL MILL S100) in which two tungsten carbide cylindrical cups along with 10 balls of same material in each cup. The samples were put to fill one third of each cup or just to immerse the balls in the samples then run for about 30 minutes at 450 rpm. After first run the samples were agitated with clean steel spoon to mix the samples and again run for 30 minutes. The samples were checked if the desired fineness was achieved by soiling and rubbing into two fingers. The same processes were repeated if required fineness has not been achieved. Further, they were grinded in agate mortar taking a very small quantity at a time for double assurance to its fineness.

The sample fractions between 60 and 170 mesh sizes (BSM) for mineral separation were washed in an agate mortar by rubbing gently under isopropyl alcohol or RO water. The finer fractions and dusts were removed fully with repeated washing with isopropyl alcohol or RO water. The samples were then dried under regulated low ampere infra red lamp and sieved through 170 mesh size (BSM). The clean samples (60 to 70 mesh size) were then run over the regulated electromagnetic vibrating table (Fig. 5.2c) to differentiate the flaky tabular minerals e.g., mica and amphiboles from the more granular and spherical fractions like feldspars and quartz. This was the followed by running in isodynamic separator (Fig. 5.2d, FRANTZ) to separate magnetic and non magnetic fractions depending upon the susceptibility to magnetism. In between different samples the whole assembly and the sample flowing copper plate were cleaned by wiping out with acetone and blowing out with compressed high pressure air.

The purified fractions were again washed in isopropyl alcohol and dried under regulated low ampere infra red lamp. Further, samples were hand picked under binocular microscope (Fig 5.2e, NIKON) by spreading over a glass slide. About 100 mg of each sample were hand picked for isotopic analysis. During picking of minerals utmost cares had been taken to remove those grains having visible inclusion and compounded margin by other minerals for that white and black background and different angle of the light beam were employed to make a clear contrast.

5.4.2 CHEMICAL PREPARATION

For chemical treatment of the samples highly purified acids were used. The acids were prepared in the lab with first distillation in a quartz-glass distillation unit under sub-boiling condition for two times and followed by distillation in double bottle distillation unit of teflon. About 100 mg of the fine powdered rock samples and 35-50 mg of mineral separates were dissolved in 3 ml of HF (48%) and 1 ml of concentrated HNO_3 in a tightly capped 15 ml PFA teflon vials (savillex). The samples were first allowed to dissolve at room temperature for at least 36 hrs and then checked whether the samples were digested completely or not. If the solution is not clear and undigested particles were seen then vials were tightly capped and kept over hot plate at about 150^0C for at least 24 hrs. After cooling completely the caps were opened carefully and all the small droplets moistening the walls of the vial were collected to the sample by tapping and shaking slowly. The sample solutions were evaporated to dryness into jelly form at about 80^0C and then redissolved and evaporated two times each in 2 ml of concentrated HNO3 and in 2 ml of 6N HCl. The dried samples looking brown mud cake

were then bring into solutions with 2 ml 2N HCl which give complete clear solution. After this the solution samples, in tightly capped vials, were kept in weighing chamber for at least 12 hrs to bring an equilibrium condition with the chamber condition and spiked with required isotopes.

Spike is a known quantity of a particular isotope. The technique for calculation of unknown isotopes of the samples with the help of spike is known as isotopic dilution. For whole rock and minerals, the spikes were prepared separately for Rb and in all the case the spikes were prepared in such a manner that 50 mg of spike give optimum proportion with respect to the Rb in the sample. For Rb and Sr the spikes were prepared with ^{87}Rb and ^{84}Sr respectively. The exact composition and concentration of the isotope in the spikes were verified separately by calibration using standard solution.

Spiking of the samples was done in the weighing chamber by adding accurately measured quantity of ^{87}Rb and ^{84}Sr spikes to the samples and keeping them overnight for homogenization followed by evaporation to dryness of the samples over the hot plate in low temperature condition. The dried samples were then brought into solution of 1.1 ml of 2N HCl and allowed complete dissolution followed by transferring into 1.5 or 2 ml centrifuge tube to run in centrifuge device for about 7 minutes to separate out the precipitates, if there were any. After this step, the solution was ready for the ion exchange column for pre-concentration of Rb and Sr.

A set of four columns made of quartz-glass which were properly cleaned in hot acid for sufficiently long time and washed in hot distilled water for at least 12 hours. The columns were fitted with freshly cut frit of accurate size and then fitted with frit stopper.

The ratio between the column diameter to length of the resin bed (column) was kept at 1:25 (generally 1:10) for better separation. The columns were kept in vertical position in a bench and the half of each column was filled with MQ water. Calculated amount of cation resin of Bio Rad AG 50W-X8, 200-400 mesh in chloride form was first washed in purified 6N HCl for three times and poured down into the columns with the help of syringe and pipe. While packing the resin the columns were dipped in beakers filled with MQ water to protect from the air bubble formation in the column that might enter in the resin bed of the columns (Fig. 5.2f). The columns were allowed eluting at least 100 ml of 6N HCl and followed by 50 ml of 2N HCl for conditioning. The columns were calibrated by loading synthetic and standard samples of about 5 ppm each for Rb and Sr in the prescribed eluent and collected every 1 ml in centrifuge tubes and then analyzed in ICP for knowing the exact position of the elements from the column. According to these data run sheet was formulated (Table 5.1). After completion of elution the columns were locked keeping at least 5 ml of eluent in each column so that they never get dried. From time to time the procedural blank, acid blank and water blank and the column blank were performed in the lab.

Since the REEs normally reside in the accessory minerals special attention was given if any particles were left undissolved. During the spiking of Rb and Sr the spikes of ^{149}Sm and ^{150}Nd were also added. The REEs were collected during regeneration process of the primary column operated for separation of Rb and Sr (see Table 5.1). The collected REE elute was dried at about 80^0C and dissolved in 2 ml of 0.05N HNO_3

for extraction chromatography which was done in Ln SPEC pre-packed columns (Eichrom).

Table 5.1: Run chart of Rb-Sr Separation (Primary Column, used in the National Facility on Geochronology and Isotope Geology at IIC, IITR)

Name: Date:
Sample Type: Address:
Sample Location:
Purpose: Sample No:

Column No./Steps	A	B	C	D
Load 1ml sample in 2N HCl and collect the volume in a beaker and discard	□	□	□	□
Load 1ml 2N HCl, discard	□	□	□	□
Load 1ml 2N HCl, discard	□	□	□	□
Load 1ml 2N HCl, discard	□	□	□	□
Load 1ml 2N HCl, discard	□	□	□	□
Load 8ml 2N HCl, discard	□	□	□	□
Load 6ml 2N HCl, collect in savillax vial for Rb	■	■	■	■
Load 13ml 2N HCl, discard	□	□	□	□
Load 10ml 2N HCl, collect in savillax vial for Sr	■	■	■	■
Load 8ml 2N HCl, discard				
Collection of REE during regeneration of the column				
Load 5ml 6N HCl, discard	□	□	□	□
Load 10ml 6N HCl, collect in savillax vial for REE	■	■	■	■
Load 20ml 6N HCl, discard	□	□	□	□
Load 30ml 6N HCl, discard	□	□	□	□
Conditioning the column for next separation for Rb-Sr				
Load 30ml 2N HCl, collect and discard	□	□	□	□
Load 30ml 2N HCl, collect and discard	□	□	□	□

Note:

- *Every steps of the operation should properly be marked in this table.*
- *After separation, the column should be regenerated and conditioned.*

In Ln Spec column, di(2-ethylhexyl) orthophosphoric acid (HDEHP) is used as an extractant in the resin (Ln resin). Using this column radium, neodymium, promethium and samarium can be extracted successfully and also many more analytical applications are possible. Sequential separation of Sm, Nd, Th and U in silicate rocks

can be done using Eichrom's TRU Resin in series with Ln Resin (Pin et al. 1996). However, we have adopted the cation exchange chromatography for separation of REE together in a group followed by elution in the Ln Spec pre-packed column for separation of Sm and Nd from the REE group (Table 5.2).

Table 5.2: Run chart for separation of Sm and Nd (Ln Spec Column used in the National Facilities of Geochronology, Isotope Geology at IIC, IITR.

Date:
User Name:

Sample ID				
Sample Weight				
Spike Weight				
Sample Type				

	Sample ID	Sample ID	Sample ID	Sample ID
Column Cleaning **5 ml 1N HCl**	□	□	□	□
Conditioning 5 ml **0.25N HCl**	□	□	□	□
Add 2 ml Sample dissolved in **0.05N HNO_3**	□	□	□	□
Wash and Discard 1+1 ml **0.25N HCl**	□	□	□	□
Wash and Discard 1.5+1.5 ml **0.25N HCl**	□	□	□	□
Wash and Discard 3 ml **0.25N HCl**	□	□	□	□
Collect Nd (6 ml) 3+3 ml **0.25N HCl**	■	■	■	■
Wash and Discard 1.5 ml **0.75N HCl**	□	□	□	□
Collect Sm 1.5 ml **0.75N HCl**	■	■	■	■
Column Cleaning 5 ml **0.25N HCl**	□	□	□	□
Column Conditioning 4 ml **0.25N HCl**	□	□	□	□
Close the Column	□	□	□	□
Evaporation procedure for Sm and Nd fractions				
Evaporate below 100^0C	■	■	■	■
Add a little MQ water + 5 drop of conc. HNO_3	■	■	■	■
Add 1 ml 6N HCl and dry	■	■	■	■
Dry at 150^0C (about 20 minutes)	■	■	■	■

Filaments were prepared by welding the cut pieces of 0.001" thick, 0.03" wide and 0.7" long in the poles of the filament assembly with the help of spot welder. These filaments were put into the filament degassing device which was set in particular

ampere (e.g., 5 ampere for W and Re and 2.5 ampere for Ta) with particular slopes for individual filament metal for removing all the gases present in the filament so that they do not interfere the ionization process. There are two banks of receptacles each of which 15 slots are provided to hold the filaments. However, only one bank was used at a time for the safety of the device. The pressure of the degassing device was maintained at better than $5x10^{-7}$bar. For loading, batches of five samples were put in the degassed filaments positioned in the slots provided in the sample evaporation unit (Fig. 5.4a) which were loaded with 1µL of TaF_5 solution (1% Ta) to activate the sample during ionization and dried them at less than 0.5 ampere current. The samples of Rb in fluoride form was added with 3 µL of 0.05N HCl and allowed to dissolve by stirring with micro-tip fitted in the pipette. In case of Sr, degassed W filament and TaF5 as an activator for Nd and Sm degassed Ta filament and H_3PO_4 as an activator were used. Over the spot of partially dried TaF_5 about 2 µL of the sample (normally ~500 ng for Sr and ~200 for Rb) was loaded and evaporated in 0.8 ampere current till the samples became like white cake after this the current was increased slowly upto 4.3 ampere to bring the filaments to dull red and keep for about five seconds. During this process TaF_5 was completely evaporated in the form of fumes. The current was then quickly brought to zero position. For Nd and Sm about 1µL of 0.5N H_3PO_4 was loaded at the center of the filament and dried at about 0.5 ampere. Over the spit 2 µL of sample (2-200 ng) diluted in 2µL MQ water was loaded and evaporated at about 1 ampere. The current was rose slowly upto 2.2 ampere where the filament turns dull red and the H_3PO_4 was

completely evaporated out. The sample loaded filaments were inserted into the turret, which can house 21 filaments posts.

For Sm and Nd, two double filament assembly were used one for evaporation i.e., the sample loading filament (Ta filament) and another for ionization (Re filament). During ionization process in the ion source REEs always tend to evaporate as a molecule, typically as an oxide rather than as a metal. To overcome this problem sample were allowed to evaporate at low temperature (evaporation filament) and the neutral atom or molecules that were emerging out were decomposed and ionized by the ionization filament kept at high temperature. The resistance of each filament holder was checked at the time of loading them in the turret, the gap between the two filaments was confirmed by eye as well as non-flowing of current between them with the help of an electronic meter.

All the samples including the whole rock and mineral separates were analyzed in the Thermo Finnigan TRITON T1 Thermal Ionization Mass Spectrometer (TIMS, 5.4b) installed at the Institute Instrumentation Centre, IIT Roorkee, India. The instrument has nine faraday cup configuration with Retarding Potential Quadrupole lenses (RPQ), which is an electrostatic filter that can improve the abundance sensitivity, e.g., in $^{238}U\pm1$ sensitivity can improves from 2 ppm to 20 ppb, causing determination of isotopic ratios with the highest accuracy.

To check the efficiency and validation of the instrument, standard samples of NIST SRM 987 and JNdi were run in a periodic manner and the ratio of $^{87}Sr/^{86}Sr$ and $^{143}Nd/^{144}Nd$ was cross checked with the referred value (0.710240, Choudhury et al.,

2004) of the standard. Out of 21 slots in the turret normally 20 were used for samples and one for standard. The procedure blank for Sr and Nd were regularly checked. The internal precision for Sr and Nd was checked by using the static and dynamic multi-collection data acquisition modes which were normally found indistinguishable. External precision of the instrument was also checked by considering the $^{87}Sr/^{86}S$ ratio of standard (NIST SRM 987) run periodically over the year while for Nd standard sample of BCR-2 was used in each batch of the samples besides the periodic blank measurements. The tracer of ^{87}Sr and ^{87}Rb calibration has been done by analyzing about 30 mg of BCR-2 (USGS rock standard). The concentration obtained after offline double spike correction reveal very good agreement with the referred values lying within the error limit as the concentration of Rb and Sr are 46 and 343 ppm respectively against the quoted values of 48±2 and 346±14 for BCR-2. Though the analytical precision of the data are superior, as shown by the measurements on international standards, the error ascribed to $^{87}Sr/^{86}Sr$ is 0.05% and that to the $^{86}Rb/^{86}Sr$ measurements is 0.05% for isochron plotting.

5.4 RB-SR RESULTS

Out of the 27 rock samples considered for the isotopic calculation; 16 samples belong to Alaknanda valley and 20 to Dhauliganga valley. In total 81 samples were analyzed which included 27 wholerock, 24 biotite and 21 muscovite separates. The results from the two valleys are given in the Table 5.4 & 5.5 showing very consistent

and significant variation in mineral cooling age mineral cooling ages for the Vaikrita Group in both the sections and also for the Munsiari Formation. From the data it is evident that the muscovite age of the Vaikrita for both the valley ranges between 14 00 to 20.20 Ma and biotite varies between 7.24 Ma and 13.67 Ma. However, most of the muscovite gives ages between 20 to 17 Ma and biotite falls within 13 to 10 Ma (see the frequency of the age group in Fig. 5.4 a, b). The average muscovite age of the Vaikrita Group is 17.63 Ma (n=18) and for biotite 11.17 Ma (n=15), which excludes the migmatite samples and samples close to the VT. Migmatite samples yield biotite age between 8.4 to 9.42 Ma while the pelite near the VT yield 7.24 Ma of biotite age. The relatively lower cooling age of biotite in migmatite indicates the higher cooling rate. In the mineral cooling age vs. distance plot for the Vaikrita Group show lowering of age at the central position of the thrust sheet (Fig. 5.5 and 5.6) due to the lower ages yield by the samples of the central part of the thrust sheet (Figure 5.3 and 5.4). The lower ages are yielded by the pelitic sample sandwiched between the quartzite bands of Pandukeshwar Formation, migmatites and the samples adjacent to the Vaikrita Thrust (VT). Interestingly, the muscovite ages of the samples adjacent to the VT do not vary from those of the migmatite zone and show almost flat pattern

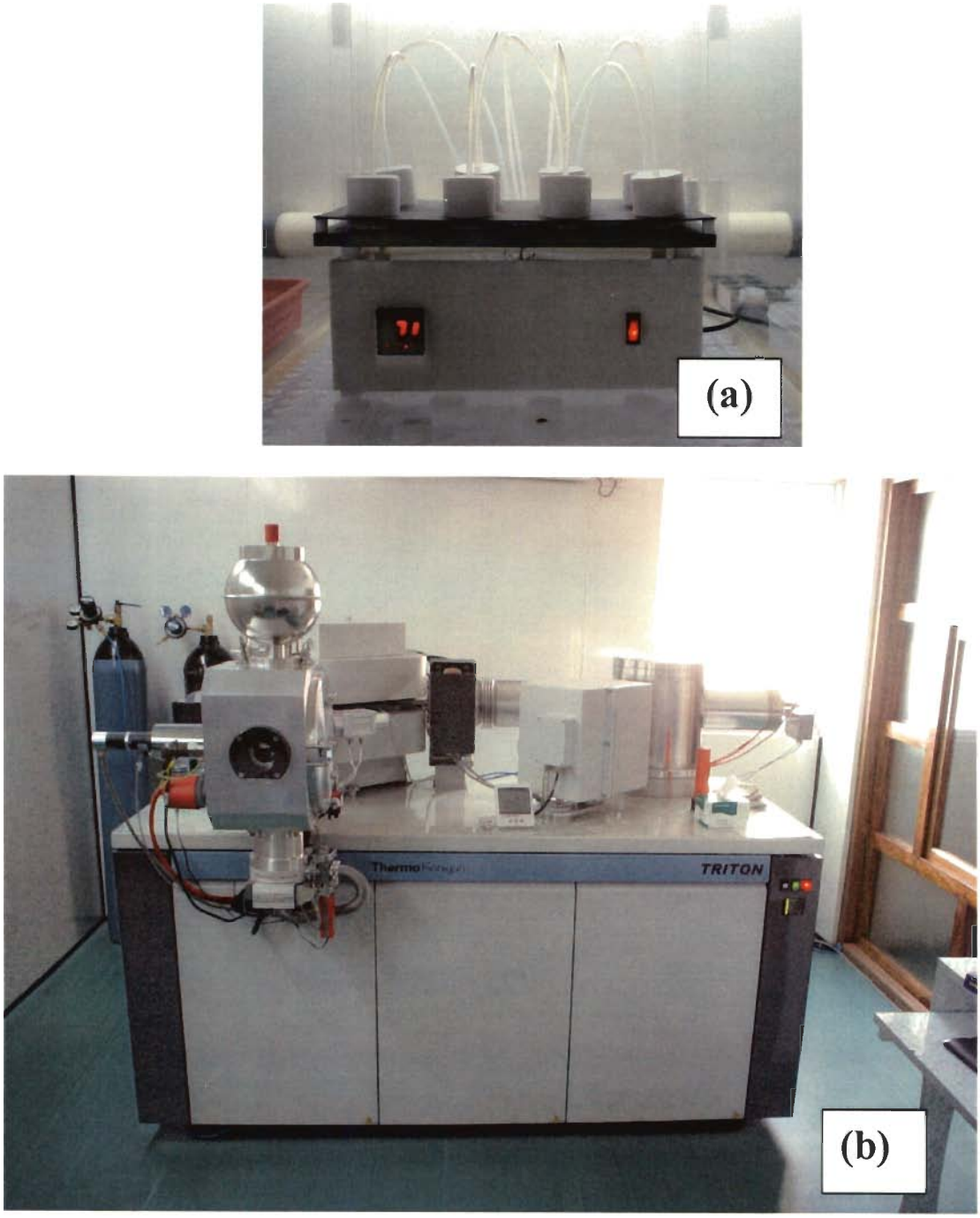

Figure 5.3: (a) Sample evaporation unit and (b) Thermal Ionization Mass Spectrometer (TIMS, Thermo Finigann, Triton T1) housed at the National Facility Geochronology/ Isotope Geology laboratory, Institute Instumentation Center, IITR.

Table 5.4: Rb and Sr analytical data of whole rock and mineral separates from Alaknanda Valley.

Sl. No	Sample No.	Rb (ppm)	Sr (ppm)	$^{87}Rb/^{86}Sr$* (atomic)	$^{87}Sr/^{86}Sr$ $\pm 2\sigma$ ** (atomic)	Age (Ma) (WR – minerals)
1	**MA 31-44**					
	Whole Rock	101	85	3.433	0.745744 ± 0.000014	
	Biotite	133	2	494.222	0.829709 ± 0.000016	12.05 ± 0.08
	Muscovite	321	20	35.908	0.755120 ± 0.000017	20.30 ± 1.10
2	**MA 34-49**					
	Whole Rock	62	18	10.099	0.858462 ± 0.000102	
	Biotite	645	4	465.094	0.896657 ± 0.000018	5.91 ± 0.09
	Muscovite	366	61	49.107	0.867309 ± 0.000017	15.97 ± 0.22
3	**MA37-52**					
	Whole Rock	83	146	1.646	0.734852 ± 0.000016	
	Biotite	779	5	480.045	0.803289 ± 0.000022	10.07 ± 0.08
	Muscovite	372	33	32.432	0.740936 ± 0.000014	13.90 ± 1.20
4	**AG 1-4**					
	Whole Rock	149	99	4.400	0.758314 ± 0.000008	
	Biotite	519	3	500.358	0.844366 ± 0.000004	12.22 ± 0.10
	Muscovite	250	56	13.015	0.760755 ± 0.000014	20.40 ± 4.30
5	**MA39A**					
	Whole Rock	176	92	1.516	0.689228 ± 0.000021	
	Biotite	220	5	751.3	0.819259 ± 0.000028	12.21 ± 0.01
6	**AG 2-5**					
	Whole Rock	102	83	3.587	0.749394 ± 0.000014	
	Biotite	330	3	329.657	0.808555 ± 0.000057	12.78 ± 0.13
	Muscovite	185	31	17.157	0.752467 ± 0.000012	15.90 ± 2.70
7	**AG 6-7**					
	Whole Rock	198	62	9.327	0.850644 ± 0.000010	
	Biotite	339	4	272.135	0.888828 ± 0.000058	10.23 ± 0.17

8	**AG 7-9**					
	Whole Rock	106	96	2.653	0.750521 ± 0.000006	
	Biotite	721	1	2490.675	1.143516 ± 0.000102	11.12 ± 0.06
	Muscovite	233	7	560.2	0.888761 ± 0.000063	17.46 ± 0.11
9	**AG 8-11**					
	Whole Rock	108	136	2.319	0.784794 ± 0.000013	
	Biotite	372	2	562.558	0.851655 ± 0.000039	8.40 ± 0.08
	Muscovite	298	20	42.83	0.794653 ± 0.000019	17.14 ± 0.96
10	**MA 40-55**					
	Whole Rock	72	150	1.401	0.789810 ± 0.000039	
	Muscovite	335	21	47.918	0.794064 ± 0.000017	6.44 ± 0.83
11	**MA 40-59**					
	Whole Rock	142	75	5.485	0.767141 ± 0.000027	
	Biotite	219	1	1294.000	1.017296 ± 0.000033	13.67 ± 0.04
	Muscovite	253	14	37.959	0.775608 ± 0.000026	18.40 ± 1.20

* error ±0.05 %

** 2 standard deviation of mean

Table 5.5: Rb and Sr analytical data of whole rock and mineral separates from Dhauliganga Valley.

Sl. No	Sample No.	Rb (ppm)	Sr (ppm)	$^{87}Rb/^{86}Sr$* (atomic)	$^{87}Sr/^{86}Sr$ ±2σ ** (atomic)	Age (Ma) (WR – mineral)
1	**MA 45-65**					
	Whole Rock	59	78.7	2.194	0.816579 ± 0.000031	
	Biotite	569	1	3779.100	0.927468 ± 0.000038	2.07 ± 0.01
2	**MA 44-64**					
	Whole Rock	418	29	43.677	0.993977 ± 0.000009	
	Biotite	793	1	1950.900	1.049468 ± 0.000056	2.05 ± 0.03

3	**MA 43-62**					
	Whole Rock	234	52	13.274	0.977803 ± 0.000008	
	Biotite	732	2	1074.845	0.999288 ± 0.000037	1.43 ± 0.01
4	**MA 42-61**					
	Whole Rock	255	136	5.511	0.864783 ± 0.000016	
	Biotite	1083	2	1657.455	0.953129 ± 0.000022	3.77 ± 0.01
	Muscovite	587	10	167.018	0.884533 ± 0.000016	8.61 ± 0.05
5	**MA 41-60**					
	Whole Rock	93	92	3.595	0.751688 ± 0.000072	
	Biotite	400	1	936.383	0.888531 ± 0.000067	10.33 ± 0.04
	Muscovite	174	62	45.214	0.761898 ± 0.000018	17.27 ± 0.89
6	**MA 30-43**					
	Whole Rock	49	44	3.279	0.746939 ± 0.000012	
	Muscovite	321	20	46.897	0.755120 ± 0.000017	13.21 ± 0.84
7	**MA 28-41**					
	Whole Rock	217	136	4.656	0.797807 ± 0.000070	
	Biotite	467	3	579.975	0.838356 ± 0.000038	4.96 ± 0.07
8	**MA 24-36**					
	Whole Rock	117	49	6.919	0.750407 ± 0.000165	
	Biotite	332	1	1933.850	0.847871 ± 0.000016	3.56 ± 0.04
	Muscovite	123	79	158.276	0.789066 ± 0.000595	17.99 ± 0.05
9	**MA 20-28**					
	Whole Rock	254	90	4.239	0.779137 ± 0.000091	
	Biotite	489	2	579.975	0.838356 ± 0.000027	7.24 ± 0.07
	Muscovite	235	112	76.736	0.799195 ± 0.000016	19.48 ± 0.53
10	**MA 16-22**					
	Whole Rock	89	112	2.302	0.764887 ± 0.000021	
	Biotite	633	3	620.119	0.860605 ± 0.000018	10.91 ± 0.07
	Muscovite	321	28	33.689	0.771108 ± 0.000019	14.00 ± 1.20

11	**MA 11C**					
	Whole Rock	265	60	12.898	0.846606 ± 0.000081	
	Biotite	1777	1	5293.000	1.552690 ± 0.000032	9.42 ± 0.01
	Muscovite	872	5	476.845	0.947052 ± 0.000049	15.25 ± 0.02
12	**AG 11-15**					
	Whole Rock	150	46	9.584	0.782336 ± 0.000008	
	Biotite	464	3	521.587	0.860909 ± 0.000018	10.81 ± 0.10
	Muscovite	123	21	36.651	0.789228 ± 0.000015	17.90 ± 1.40
13	**AG 15-20**					
	Whole Rock	127	59	6.266	0.789295 ± 0.000007	
	Biotite	429	2	799.867	0.926521 ± 0.000081	12.18 ± 0.08
	Muscovite	225	16	31.583	0.796187 ± 0.000208	19.20 ± 1.50
14	**AG 16-24**					
	Whole Rock	171	143	3.487	0.758623 ± 0.000021	
	Biotite	918	3	1142.410	0.952973 ± 0.000057	12.02 ± 0.07
	Muscovite	336	10	42.470	0.768653 ± 0.000019	18.12 ± 0.96
15	**MA 8-12**					
	Whole Rock	189	74	7.451	0.777376 ± 0.000015	
	Biotite	819	4	458.716	0.857360 ± 0.000039	12.48 ± 0.09
	Muscovite	256	35	21.287	0.781016 ± 0.000019	18.50 ± 2.70
16	**AG 18-28**					
	Whole Rock	382	53	21.064	0.761710 ± 0.000088	
	Muscovite	424	3	452.777	0.885156 ± 0.000196	20.13 ± 1.10

* error ± 0.05 % ** 2 standard deviation of mean

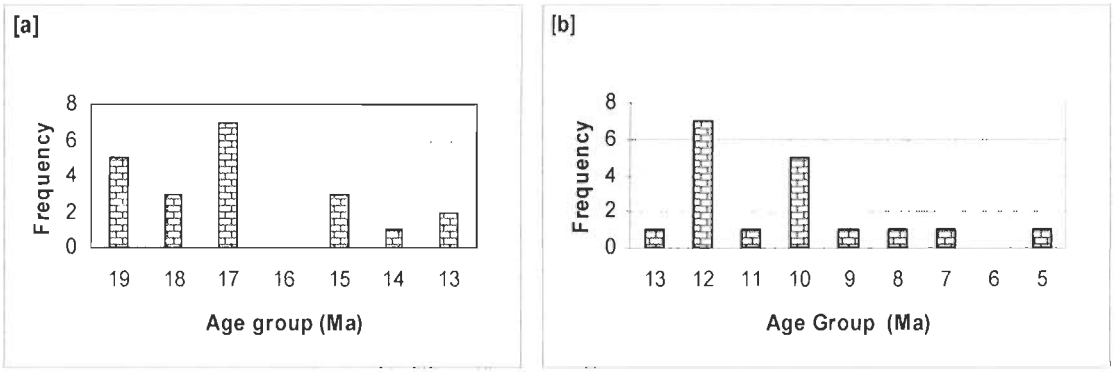

Figure 5.4: Frequency graph of the age group of the Alaknanda and Dhauliganga valley (a) muscovite age (b) biotite age of the Vaikrita Group respectively.

The muscovite and biotite ages indicate that exhumation in central portion started after the closure temperature of muscovite (500±50^{0}C). On the hand, Munsiari Formation yields biotite ages 2.07-2.05 Ma and MCT zone samples yield muscovite age 8.61 Ma and biotite as low as 1.43 ± 0.01. The overall pattern of the ages in biotite and muscovite show a sharp break in age across the VT. This pattern is clear indication that the metamorphism of M_2 episode in the Vaikrita Group took at an early age (~20 to ~17), based on muscovite ages near the VT zone giving about 8.61 Ma indicating probability of reactivation of the VT zone around that time to a temperature of 500^{0}C. The package of the HHC (Munsiari Formation) probably indicates that they have undergone a different cooling or exhumation pattern, which is faster in nature as indicated by younger age (Fig. 5.5).

5.5 COOLING AND EXHUMATION HISTORY

The rate of cooling and exhumation of the HHC of Alaknanda and Dhauliganga valley muscovite-biotite co-genetic pair age data by Rb-Sr wholerock-mica ages having

closure temperature 500±50^{0}C (muscovite) and 300±50^{0}C (biotite) have been used. There are two methods of calculating cooling and exhumation rate as described by Mancktelow and Grasemann (1997). For any calculation geothermal gradient plays a crucial role, which is influenced by the topography of terrane including height, lateral heat loss across the deep vertical cliff, rate of erosion and other lithospheric properties such as thermal diffusivity, thermal diffusivity, heat and also by heat generated during shearing. However, in any isotopic system with closure temperature >200^{0}C the estimation of cooling rate is shearing. Advection of heat during rapid exhumation rate is an important factor in the cooling rate calculations. However, in any isotopic system having closure temperature >200^{0}C the estimation of cooling rate is not much influenced by topography (Mancktelow and Grasemann, 1997). Therefore, if we consider all these factors the calculation of cooling and exhumation rate is not straightforward and only numerical modeling can give more precise evolution path. To the contrary, numerical modeling have shown that small changes in the input parameters such as 2D fault geometry, slip rate, lower boundary condition can produce large variations in the predicted thermal history (Ruppel and Hodges, 1994). Therefore, in this present study a simplified method is considered in one dimensional frame with the assumption that 30 ± 10^{0}C/km steady-state geothermal gradient persists over the calculated age (Table 5.4 & 5.5).I. The calculated data are listed in Table 5.6 and the values are plotted with the corresponding distance from the MCT (Fig. 5.6), which shows very similar pattern for both the cooling rate and exhumation rate. This indicates that the cooling of the rocks is controlled by the rate of exhumation. The rate of cooling

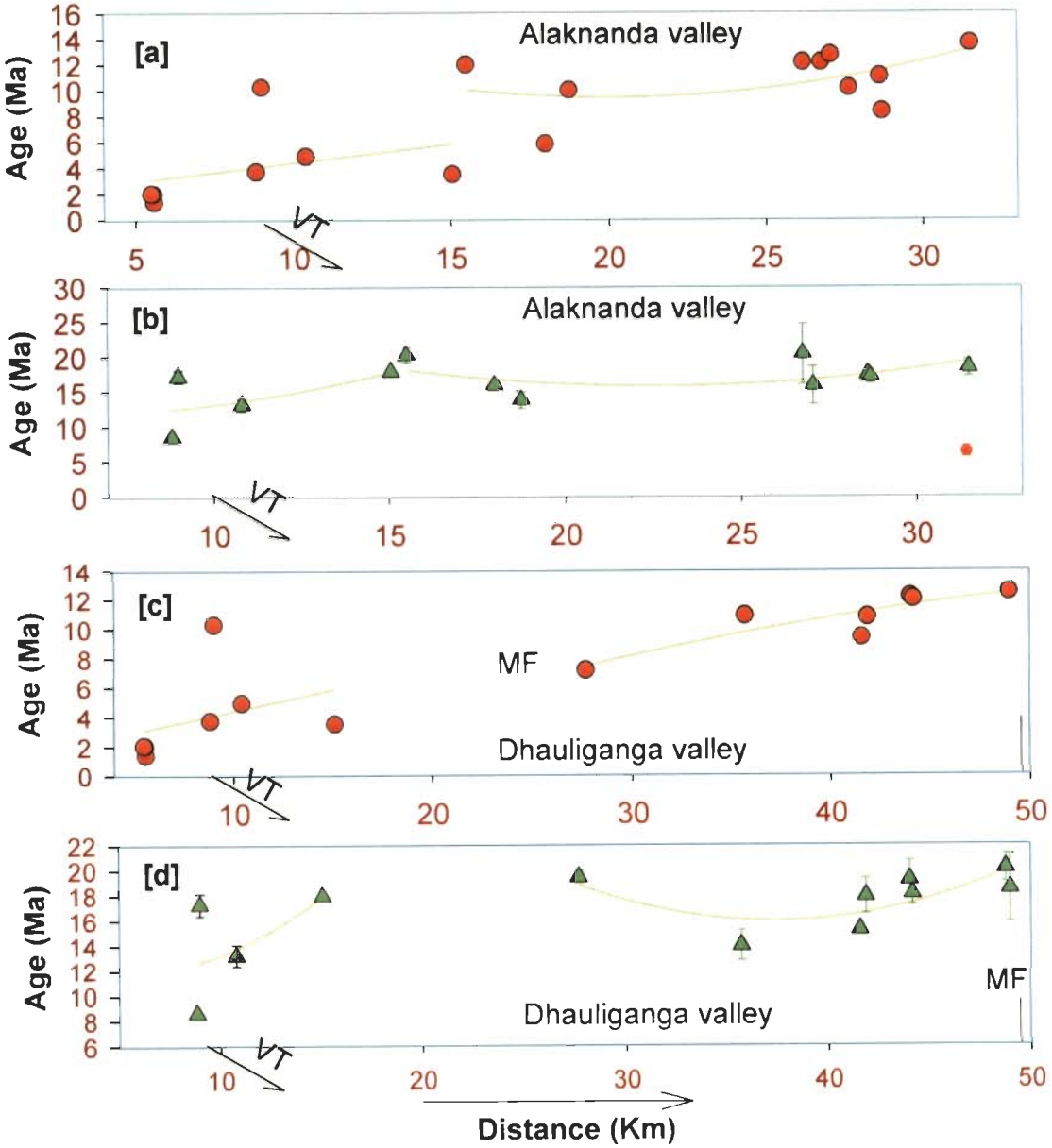

Figure 5.5: The distance versus age variation diagram for Alaknanda valley (a) biotite and (b) muscovite cooling ages and (c) biotite age vs distance & (d) muscovite cooling age plot against distance from MCT for Dhauliganga valley

Table5.4: Cooling and exhumation rate of Alaknanda and Dhauliganga valley calculated

Sample	Age (Ma)		Cooling Rate (^{0}C/Ma)	*Exhumation Rate(mm/yr)
	Muscovite	Biotite	Calculated rate	Calculated rate
MA 40-59	18.4±1.2	13.67±0.04	42.28±0.44	1.41±0.47
MA 8-12	18.5±2.7	12.48±0.09	33.22±0.57	1.11±0.37
AG 16-24	18.12±0.96	12.02±0.07	32.79±0.39	1.09±0.36
AG 15-20	19.2±1.5	12.18±0.08	28.49±0.41	0.95±0.32
AG 8-11	17.14±0.96	8.4±0.08	22.88±0.37	0.76±0.25
AG 11-15	17.9±1.4	10.81±0.1	28.21±0.41	0.94±0.31
AG 7-9	17.46±0.11	11.12±0.06	31.55±0.35	1.05±0.35
on the basis of muscovite-biotite pair in Rb-Sr system				
MA 11C	15.25±0.02	9.42±0.01	34.31±0.35	1.14±0.38
AG 2-5	15.9±2.7	12.78±0.13	64.10±0.94	2.14±0.71
AG 1-4	20.4±4.3	12.22±0.1	24.45±0.63	0.81±0.27
MA37/52	13.9±1.2	10.07±0.08	52.22±0.47	1.74±0.58
MA 16-22	14±1.2	10.91±0.07	64.72±0.53	2.16±0.72
MA 34/49	15.97±0.22	5.91±0.09	19.88±0.35	0.66±0.22
MA 31-44	20.3±1.1	12.05±0.08	24.24±0.38	0.81±0.27
MA 41-60	17.27±0.89	10.33±0.04	28.82±0.38	0.96±0.32
MA 24-36	17.99±0.05	3.56±0.04	13.86±0.35	0.46±0.15
MA 42-61	8.61±0.05	3.77±0.01	41.32±0.35	1.38±0.46
MA 20-28	19.48±0.53	7.24±0.07	16.34±0.36	0.54±0.18
* Geothermal gradient assumed to be 30±10^{0}C/km				

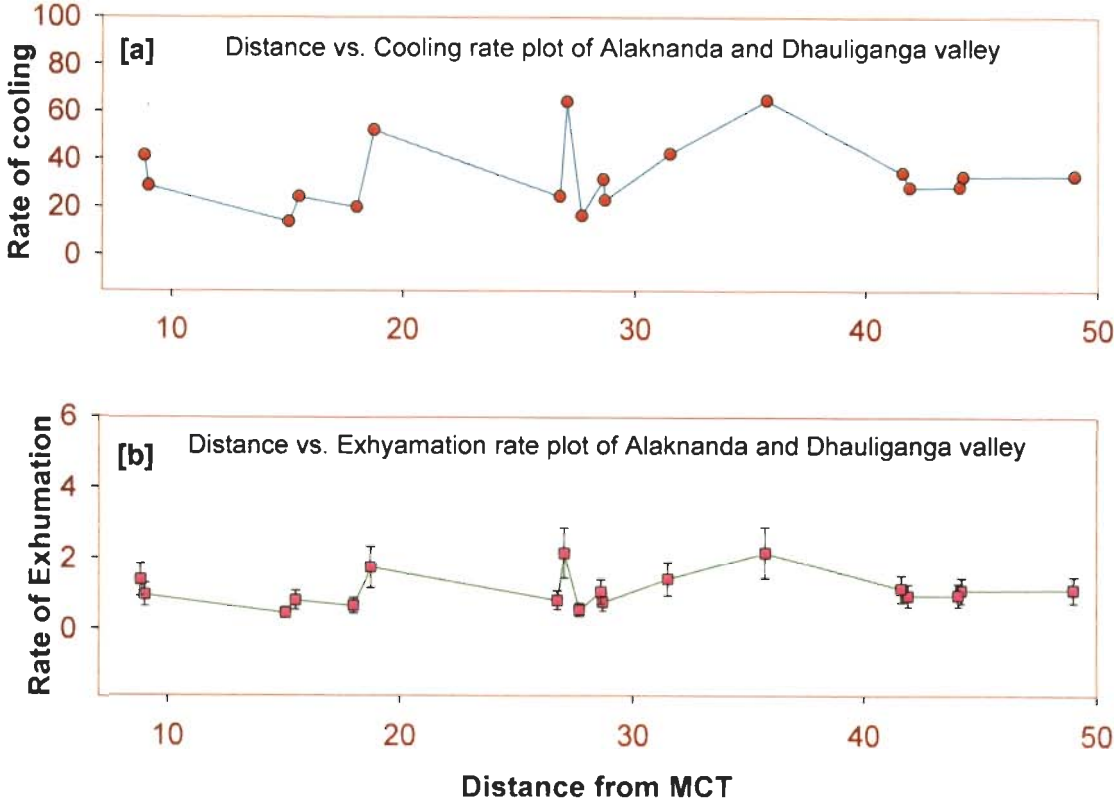

Figure 5.6: (a) Distance versus cooling rate of the rochs from Alaknanda and Dhauliganga valley & (b) distance vs. exhumation rate of the rocks from Alaknanda and Dhauliganga valley.

or exhumation is higher at central part of the thrust sheet indicating a concave upward geotherms. In the middle of this high exhumation zone as there is indication of reversal of isotherms as marked by depression in the curve indicating. Near Vaikrita Thrust mineral cooling ages gives high exhumation rate of about 1.36 mm/yr between 8.61 Ma and 2 Ma, which is followed by an exceedingly high rate between 2 Ma and present time within the Munsiari Formation. Considering the biotite cooling age the rate of cooling should be about100^{0}C/Ma or more since the last two million year. The high cooling rate is associated with shallow geothermal gradient. This is also supported by the

exceedingly high erosion rate observed in the dynamic and rugged terrain of Himalaya, e.g., the upper catchment area of Ganga river in the HHC of the NW Himalaya at Sutlej and Alaknanda valley show very high rate of erosion with a comparatively lower rate in the Lesser Himalayan Sequence as shown by the cosmogeneic nuclear isotopes (Vance, et al., 2003).

5.5 Sm-Nd RESULTS

A total of 27 samples including metasediments, migmatite and leucosomes of the HHC along with Tethyan sediments were analyzed for Sm-Nd isotopic calculations. The ratios are recalculated in the form of ε_{Nd} at present time along with their T_{DM} ages are listed in Table 5.7 to 5.12 along with the corresponding values of $^{87}Sr/^{86}Sr$. The ratios have been recalculated at 46 Ma, keeping the SHRIMP U-Pb age (Singh et al., 2003) from Bhagirathi valley for re-homogenization age and listed in Table 5.9 and 5.10. The 500 Ma has also been considered by other workers as the time of re-homogenization (Ahmed et al., 2000; Richards et al., 2005). The average values of $\varepsilon_{Nd}(0)$ and present day $^{87}Sr/^{86}Sr$ for Vaikrita Group gives ~ -16 (ranging between -7.0 to -21.4) and 0.787588 (ranging between 0.751521 to 0.864788) respectively while for Munsiari Formation the values are ~-25 (-24.0 to -25.8) and 0.905278 (ranging between 0.993977 to 0.816579). Some samples mainly of leucosome yield anomalous values of ε_{Nd} probably due to high Sm/Nd ratio in the rock and $^{87}Sr/^{86}Sr$ gives very high values indicating a disequilibrium melting of the crustal rocks. The present day values of ε_{Nd} and $^{87}Sr/^{86}Sr$ are plotted in the Nd-Sr diagram showing scattering data (Fig. 5.8a). In the

diagram leucosome samples fall away from the other samples which are clearly seen even though they do not concentrate in an area in the plot. The metasediments of the Vaikrita Group give ε_{Nd} values between -21.1 to -10. 5 while $^{87}Sr/^{86}Sr$ values ranges between 0.699228 and 0.977803 while most of the samples yield inconsistent T_{DM} ages. The migmatite samples yields similar values of ε_{Nd} and $^{87}Sr/^{86}Sr$ to that of the migmatite. Two samples of Munsiari metasediments gives a relatively higher ε_{Nd} and $^{87}Sr/^{86}Sr$ values while T_{DM} ages are also high (Table 5.7 to 5.12). Therefore, the source of the Munsiari seems to be different from that of the Vaikrita Group. On the other hand, the plot would give better distinction between the Munsiari and the Vaikrita if we remove the leucosome and leucogranite samples. The calculated ε_{Nd} and $^{87}Sr/^{86}Sr$ at 46 Ma yield lesser values. For Vaikrita average values are ~-14 (ranging between ~-6 to~-20) and ~0.770155 (ranging between 0.743501 and 0.861178) while for Munsiari Formation the values are ~-23 (-22.8 and 24.7) and ~ 0.890292 (0.815145 and 0.965438). The values at 500 Ma most of the sample resulted into positive indicating (Table 5.9 and 5.12) the last re-homogenization of the rocks took place at much later date than 500 Ma.

Table 5.7: The isotopic data of Sm and Nd calculated at t=0 for the samples from Alaknanda valley ratio.

Alakhnanda Valley		T=0										
Sample	Nd (ppm)	Sm (ppm)	147/144	143/144 corr.	147 Sm [µm]	144 Nd [µm]	143/144 calc.	143/144 (i)	e Nd	T (DM, Ga)	144 Nd [ppm]	147 Sm [ppm]
Vaikrita												
Metasediments												
AG 1-4	28.0	5.8	0.124817	0.511766	0.0007	0.0055	0.511766	0.511766	-17.0	2.35	6.65	0.847824
MA 41-60	57.0	11.2	0.118623	0.511831	0.0011	0.0094	0.511831	0.511831	-15.7	2.09	13.53	1.638736
MA 42-61	73.9	12.8	0.104791	0.511708	0.0015	0.0141	0.511708	0.511708	-18.1	2.00	17.53	1.875671
MA 43-62	44.9	7.7	0.103031	0.511198	0.0008	0.0082	0.511198	0.511198	-28.1	2.66	10.66	1.121616
Migmatites												
MA 40-59	28.9	6.2	0.128934	0.511757	0.0007	0.0055	0.511757	0.511757	-17.2	2.47	6.87	0.904299
AG 8-11	9.6	2.0	0.125096	0.512281	0.0001	0.0011	0.512281	0.512281	-7.0	1.49	2.27	0.290280
Leucogranite												
MA 40A	5.7	1.2	0.132040	0.512256	0.0002	0.0011	0.512256	0.512256	-7.4	1.66	1.35	0.182561
MA 40B	2.4	0.7	0.168791	0.511669	0.0001	0.0005	0.511669	0.511669	-18.9	4.86	0.56	0.097106
MA 40-56	5.9	0.4	0.042141	0.511811	0.0001	0.0015	0.511811	0.511811	-16.1	1.19	1.40	0.060441
MA 40-57	2.4	7.0	1.808255	0.512190	0.0010	0.0006	0.512190	0.512190	-8.7	-0.09	0.56	1.031910
MA 40-58	1.5	0.3	0.113011	0.511499	0.0000	0.0004	0.511499	0.511499	-22.2	2.47	0.36	0.041273
Munsiari Metasediments												
MA 44-64	40.8	8.4	0.124360	0.511315	0.0010	0.0081	0.511315	0.511315	-25.8	3.08	9.68	1.228377
MA 45-65	9.4	1.7	0.110615	0.511409	0.0003	0.0023	0.511409	0.511409	-24.0	2.54	2.22	0.251223

Table 5.8: The isotopic data of Sm and Nd calculated at t= 46 Ma for the samples from Alaknanda valley.

Alakhnanda Valley	**T=46 Ma**											
Sample	Nd (ppm)	Sm (ppm)	147/144	143/144 corr.	147 Sm [µm]	144 Nd [µm]	143/144 calc.	143/144 (i)	e Nd	T (DM, Ga)	144 Nd [ppm]	147 Sm [ppm]
Vaikrita Metasediments												
AG 1-4	28.0	5.8	0.124817	0.511766	0.0007	0.0055	0.511766	0.511728	-15.9	2.35	6.65	0.85
MA 41-60	57.0	11.2	0.118623	0.511831	0.0011	0.0094	0.511831	0.511795	-14.6	2.09	13.53	1.64
MA 42-61	73.9	12.8	0.104791	0.511708	0.0015	0.0141	0.511708	0.511676	-17.0	2.00	17.53	1.88
MA 43-62	44.9	7.7	0.103031	0.511198	0.0008	0.0082	0.511198	0.511167	-26.9	2.66	10.66	1.12
Migmatites												
MA 40-59	28.9	6.2	0.128934	0.511757	0.0007	0.0055	0.511757	0.511718	-16.0	2.47	6.87	0.90
AG 8-11	9.6	2.0	0.125096	0.512281	0.0001	0.0011	0.512281	0.512243	-5.8	1.49	2.27	0.29
Leucogranites												
MA 40A	5.7	1.2	0.132040	0.512256	0.0002	0.0011	0.512256	0.512217	-6.3	1.66	1.35	0.18
MA 40B	2.4	0.7	0.168791	0.511669	0.0001	0.0005	0.511669	0.511618	-17.8	4.86	0.56	0.10
MA 40-56	5.9	0.4	0.042141	0.511811	0.0001	0.0015	0.511811	0.511799	-15.0	1.19	1.40	0.06
MA 40-57	2.4	7.0	1.808255	0.512190	0.0010	0.0006	0.512190	0.511646	-7.6	-0.09	0.56	1.03
MA 40-58	1.5	0.3	0.113011	0.511499	0.0000	0.0004	0.511499	0.511465	-21.1	2.47	0.36	0.04
Munsiari Metasediments												
MA 44-64	40.8	8.4	0.124360	0.511315	0.0010	0.0081	0.511315	0.511277	-24.7	3.08	9.68	1.23
MA 45-65	9.4	1.7	0.110615	0.511409	0.0003	0.0023	0.511409	0.511376	-22.8	2.54	2.22	0.25

Table 5.9: The isotopic data of Sm and Nd calculated at t=500 Ma for the samples from Alaknanda valley.

Alakhnanda Valley	**T=500 Ma**											
Sample	Nd (ppm)	Sm (ppm)	147/144	143/144 corr.	147 Sm [µm]	144 Nd [µm]	143/144 calc.	143/144 (i)	e Nd	T (DM, Ga)	144 Nd [ppm]	147 Sm [ppm]
Viakrita Metasediments												
AG 1-4	28.0	5.8	0.124817	0.511766	0.0007	0.0055	0.511766	0.511357	-4.5	2.35	6.65	0.85
MA 41-60	57.0	11.2	0.118623	0.511831	0.0011	0.0094	0.511831	0.511442	-3.2	2.09	13.53	1.64
MA 42-61	73.9	12.8	0.104791	0.511708	0.0015	0.0141	0.511708	0.511364	-5.6	2.00	17.53	1.88
MA 43-62	44.9	7.7	0.103031	0.511198	0.0008	0.0082	0.511198	0.510861	-15.5	2.66	10.66	1.12
Migmatites												
MA 40-59	28.9	6.2	0.128934	0.511757	0.0007	0.0055	0.511757	0.511335	-4.6	2.47	6.87	0.90
AG 8-11	9.6	2.0	0.125096	0.512281	0.0001	0.0011	0.512281	0.511871	5.6	1.49	2.27	0.29
Leucogranites												
MA 40A	5.7	1.2	0.132040	0.512256	0.0002	0.0011	0.512256	0.511824	5.1	1.66	1.35	0.18
MA 40B	2.4	0.7	0.168791	0.511669	0.0001	0.0005	0.511669	0.511116	-6.3	4.86	0.56	0.10
MA 40-56	5.9	0.4	0.042141	0.511811	0.0001	0.0015	0.511811	0.511673	-3.6	1.19	1.40	0.06
MA 40-57	2.4	7.0	1.808255	0.512190	0.0010	0.0006	0.512190	0.506267	3.8	-0.09	0.56	1.03
MA 40-58	1.5	0.3	0.113011	0.511499	0.0000	0.0004	0.511499	0.511129	-9.7	2.47	0.36	0.04
Munsiari Metasediments												
MA 44-64	40.8	8.4	0.124360	0.511315	0.0010	0.0081	0.511315	0.510908	-13.3	3.08	9.68	1.23
MA 45-65	9.4	1.7	0.110615	0.511409	0.0003	0.0023	0.511409	0.511047	-11.4	2.54	2.22	0.25

Table 5.10: The isotopic data of Sm and Nd calculated at t=0 for the samples from Dhauliganga valley.

Dhauliganga Valley		T=0										
Sample	Nd (ppm)	Sm (ppm)	147/144	143/144 corr.	147 Sm [µm]	144 Nd [µm]	143/144 calc.	143/144 (i)	e Nd	T (DM, Ga)	144 Nd [ppm]	147 Sm [ppm]
Vaikrita												
Metasediments												
AG 11-15	97.1	4.8	0.029958	0.511542	0.0004	0.0119	0.511542	0.511542	-21.4	1.33	23.04	0.70
AG 16-24	18.7	3.0	0.097645	0.511600	0.0002	0.0023	0.511600	0.511600	-20.3	2.02	4.44	0.44
MA 16-22	13.4	3.2	0.144014	0.511663	0.0003	0.0022	0.511663	0.511663	-19.0	3.19	3.18	0.47
AG 15-20	31.0	6.2	0.121592	0.511694	0.0007	0.0061	0.511694	0.511694	-18.4	2.38	7.37	0.91
MA 28-41	37.9	8.6	0.137784	0.511945	0.0009	0.0063	0.511945	0.511945	-13.5	2.39	9.01	1.27
MA 24-36	55.6	10.5	0.114273	0.511995	0.0012	0.0102	0.511995	0.511995	-12.5	1.76	13.19	1.54
MA 31-44	29.9	5.3	0.107762	0.511881	0.0006	0.0056	0.511881	0.511881	-14.8	1.81	7.10	0.78
Migmatites												
MA 8-12	31.8	6.9	0.131881	0.511964	0.0007	0.0052	0.511964	0.511964	-13.2	2.19	7.55	1.02
MA 11C	9.6	2.6	0.160846	0.512098	0.0003	0.0019	0.512098	0.512098	-10.5	2.97	2.28	0.37
Leucogranite												
AG 18-28	3.0	0.9	0.173816	0.511787	0.0001	0.0007	0.511787	0.511787	-16.6	5.01	0.70	0.12
Leucosome												
MA 7-10	19.5	3.6	0.110477	0.511593	0.0004	0.0039	0.511593	0.511593	-20.4	2.28	4.63	0.52
Tethyan Sediments												
MA 4-4	30.8	5.9	0.115137	0.511779	0.0007	0.0061	0.511779	0.511779	-16.8	2.10	7.30	0.86
MA 5-7	26.6	5.0	0.113444	0.512182	0.0006	0.0052	0.512182	0.512182	-8.9	1.47	6.31	0.73

Table 5.11: The isotopic data of Sm and Nd calculated at t= 46 Ma for the samples from Dhauliganga valley.

Dhauliganga Valley	**T=46 Ma**											
Sample	Nd (ppm)	Sm (ppm)	147/144	143/144 corr.	147 Sm [µm]	144 Nd [µm]	143/144 calc.	143/144 (i)	e Nd	T (DM, Ga)	144 Nd [ppm]	147 Sm [ppm]
Vaikrita Metasediments												
AG 11-15	97.1	4.8	0.029958	0.511542	0.0004	0.0119	0.511542	0.511533	-20.2	1.33	23.04	0.70
AG 16-24	18.7	3.0	0.097645	0.511600	0.0002	0.0023	0.511600	0.511570	-19.1	2.02	4.44	0.44
MA 16-22	13.4	3.2	0.144014	0.511663	0.0003	0.0022	0.511663	0.511619	-17.9	3.19	3.18	0.47
AG 15-20	31.0	6.2	0.121592	0.511694	0.0007	0.0061	0.511694	0.511658	-17.3	2.38	7.37	0.91
MA 28-41	37.9	8.6	0.137784	0.511945	0.0009	0.0063	0.511945	0.511904	-12.4	2.39	9.01	1.27
MA 24-36	55.6	10.5	0.114273	0.511995	0.0012	0.0102	0.511995	0.511960	-11.4	1.76	13.19	1.54
MA 31-44	29.9	5.3	0.107762	0.511881	0.0006	0.0056	0.511881	0.511848	-13.6	1.81	7.10	0.78
Migmatites												
MA 8-12	31.8	6.9	0.131881	0.511964	0.0007	0.0052	0.511964	0.511924	-12.0	2.19	7.55	1.02
MA 11C	9.6	2.6	0.160846	0.512098	0.0003	0.0019	0.512098	0.512049	-9.4	2.97	2.28	0.37
Leucogranite												
AG 18-28	3.0	0.9	0.173816	0.511787	0.0001	0.0007	0.511787	0.511735	-15.4	5.01	0.70	0.12
Leucosome												
MA 7-10	19.5	3.6	0.110477	0.511593	0.0004	0.0039	0.511593	0.511560	-19.2	2.28	4.63	0.52
Thetyan Sediments												
MA 4-4	30.8	5.9	0.115137	0.511779	0.0007	0.0061	0.511779	0.511744	-15.6	2.10	7.30	0.86
MA 5-7	26.6	5.0	0.113444	0.512182	0.0006	0.0052	0.512182	0.512148	-7.7	1.47	6.31	0.73

Table 5.12: The isotopic data of Sm and Nd calculated at t=500 Ma for the samples from Dhauliganga valley.

Dhauliganga Valley		**T=500 Ma**										
Sample	Nd (ppm)	Sm (ppm)	147/144	143/144 corr.	147 Sm [μm]	144 Nd [μm]	143/144 calc.	143/144 (i)	e Nd	T (DM, Ga)	144 Nd [ppm]	147 Sm [ppm]
Vaikrita												
Metasediments												
AG 11-15	97.1	4.8	0.029958	0.511542	0.0004	0.0119	0.511542	0.511444	-8.8	1.33	23.04	0.70
AG 16-24	18.7	3.0	0.097645	0.511600	0.0002	0.0023	0.511600	0.511280	-7.7	2.02	4.44	0.44
MA 16-22	13.4	3.2	0.144014	0.511663	0.0003	0.0022	0.511663	0.511191	-6.5	3.19	3.18	0.47
AG 15-20	31.0	6.2	0.121592	0.511694	0.0007	0.0061	0.511694	0.511296	-5.8	2.38	7.37	0.91
MA 28-41	37.9	8.6	0.137784	0.511945	0.0009	0.0063	0.511945	0.511494	-0.9	2.39	9.01	1.27
MA 24-36	55.6	10.5	0.114273	0.511995	0.0012	0.0102	0.511995	0.511620	0.0	1.76	13.19	1.54
MA 31-44	29.9	5.3	0.107762	0.511881	0.0006	0.0056	0.511881	0.511528	-2.2	1.81	7.10	0.78
Migmatite												
MA 8-12	31.8	6.9	0.131881	0.511964	0.0007	0.0052	0.511964	0.511532	-0.6	2.19	7.55	1.02
MA 11C	9.6	2.6	0.160846	0.512098	0.0003	0.0019	0.512098	0.511571	2.0	2.97	2.28	0.37
Leucogranite												
AG 18-28	3.0	0.9	0.173816	0.511787	0.0001	0.0007	0.511787	0.511218	-4.0	5.01	0.70	0.12
Leucosome												
MA 7-10	19.5	3.6	0.110477	0.511593	0.0004	0.0039	0.511593	0.511231	-7.8	2.28	4.63	0.52
Thetyan Sediments												
MA 4-4	30.8	5.9	0.115137	0.511779	0.0007	0.0061	0.511779	0.511401	-4.2	2.10	7.30	0.86
MA 5-7	26.6	5.0	0.113444	0.512182	0.0006	0.0052	0.512182	0.511810	3.7	1.47	6.31	0.73

Table 5.13: The isotopic ratios of $^{87}Sr/^{86}Sr$ for samples from Alaknanda and Dhauliganga valley.

	T=0	T=46	T-500	Sample No	T=0	T=46	T-500
Alakhnanda Valley				Dhauliganga Valley			
AG 1-4	0.758314	0.748787	0.731618	AG 11-15	0.782336	0.776074	0.714047
MA 41-60	0.751688	0.749339	0.726073	AG 16-24	0.758623	0.756345	0.733777
MA 42-61	0.864788	0.861187	0.825521	MA 16-22	0.764887	0.763383	0.748485
MA 43-62	0.977803	0.96913	0.883222	AG 15-20	0.789295	0.785201	0.744648
MA 40-59	0.767141	0.763557	0.728059	MA 28-41	0.797807	0.794765	0.764632
AG 8-11	0.784979	0.783464	0.768456	MA 24-36	0.750407	0.745886	0.701107
MA 40A	1.240162	1.239848	1.236735	MA 31-44	0.745744	0.743501	0.721283
MA 40B	1.436272	1.435649	1.429474	MA 8-12	0.777376	0.772507	0.724286
MA 40-56	1.228459	1.228173	1.225345	MA 11C	0.746606	0.738178	0.654704
MA 40-57	1.11232	1.11199	1.108722	AG 18-28	0.76171	0.747947	0.611623
MA 40-58	1.112643	1.112333	1.109258	MA 7-10	1.243819	1.243676	1.242259
MA 44-64	0.993977	0.965438	0.682767	MA 4-4	1.1968	1.196536	1.193921
MA 45-65	0.816579	0.815145	0.800946	MA 5-7	0.726999	0.716136	0.608541

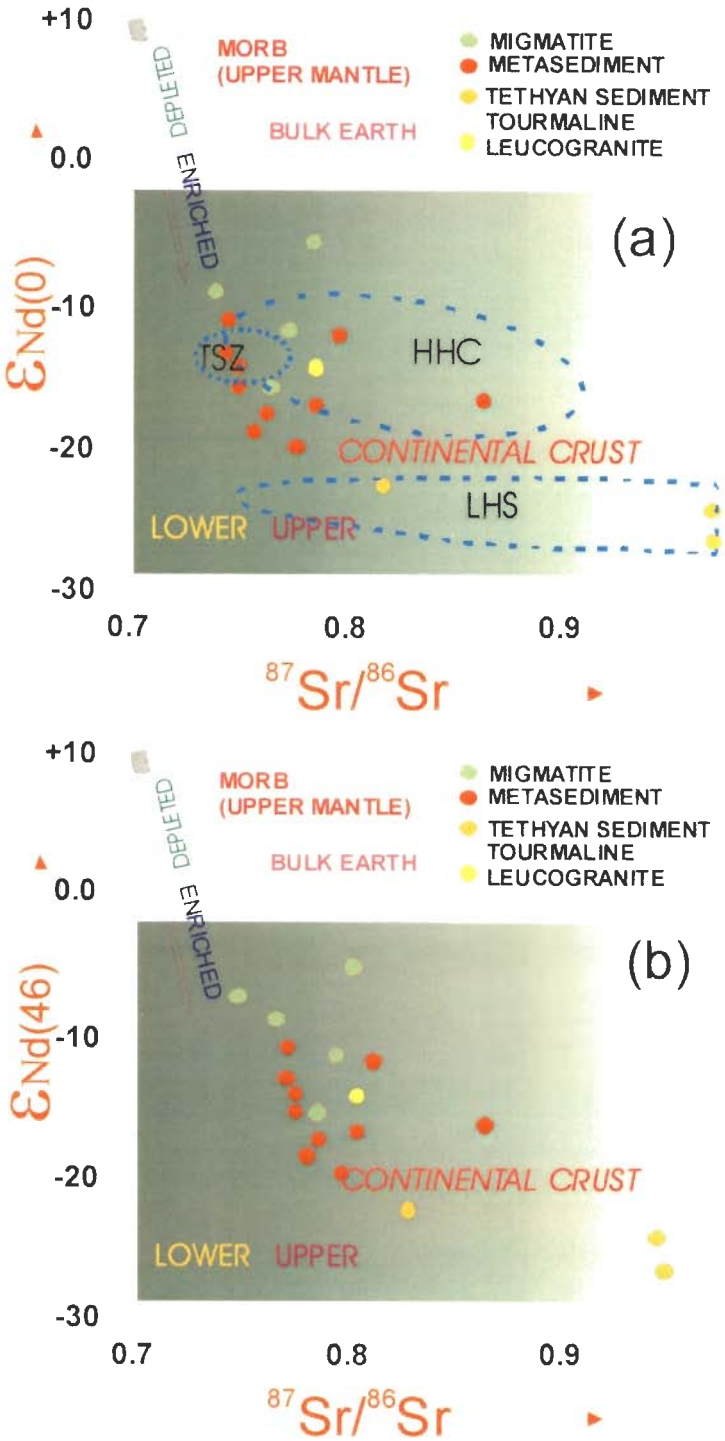

Figure 5.8: Nd-Sr source rock discrimination diagram for Tethyan, Vaikrita Group and Munsiari Formation of HHC along Alaknanda and Dhauliganga valley (a).the values of X and Y axis are calculated at t=0, the fields marked by blue dotted lines are from Ahmed et al., 2000 and(b) calculated values at t= 46 Ma.

CHAPTER - 6

DISCSSIONS AND CONCLUSION

The Himalaya is a classical and unique example of the continent-continent collison tectonics. After initial collision underthrusting of the northerly-moving Indian Plate with the Eurasian Plate has extensively remobilised the Proterozoic basement and cover sediments within a major intracontinental ductile shear zone during Cenozoic (Bouchez and Pecher, 1981; Brunel, 1986; Jain and Anand, 1988; Le Fort, 1988). The Higher Himalayan Metamorphic (HMB) belt comprising of the Higher Himalayan Crystallines (HHC) and metasedimentary part of Lesser Himalaya Sequence (LHS) is a linear belt occurring all along the Himalaya exhibit polyphase Barrovian metamorphism throughout the orogenic belt (Windley, 1983; Sandhu, 1985; Das, 1987; Pecher, 1989; Staubli, 1989). The middle and upper part of the sequence is mainly occupied by migmatite, *insitu* melt (tourmaline bearing leucogranite) with Tertiary Leucogranite, known as the Higher Himalayan Leucogranite (HHL) Belt, along the northern margin within Indian sector (Searle and Fryer, 1986, Searle, 1992; Harris et al., 1993, 1994; Guillot and Le Fort 1995), Nepal sector (Le Fort, 1981., Deniel, et. al., 1987, France-Lanord, et. al., 1988, England, et. al., 1992, Catlos, et. al., 2004; Harris et al., 2004) and Bhutan sector (Deitrich and Gansser, 1981). In the NW-Himalaya within the Indian sector, migmatite and *in situ* melt are occurring in a narrow zone at the middle or upper part of the HHC. However, the HHL represents either: (i) crustal anatectic melting due to fluid migration during intracontinental thrusting along the Main Central Thrust (MCT) (Le Fort, 1975, 1981, 1986; Searle and Fryer, 1986; Le Fort et al.,

1987; France-Lanord and Le Fort, 1988; England et al., 1992), (ii) decompressional-controlled dehydration melting due to slip along the South Tibetan Detachement Zone (STDZ) along which the leucogranite plutons occur (Harris et al., 1993; Inger and Harris, 1993; Harris and Massey, 1994; Guillot and Le Fort, 1995; Searle at al., 1992) or (iii) vapour-absent muscovite dehydration melting of metamorphic rocks due to shear heating along a continuous active decollement (Harrison et al., 1997, 1999). Nevertheless, the leucogranite belt has been emplaced in a very short time span between 24 and 19 Ma from the western sector in Zanskar to Nepal and Bhutan (Davidson et al., 1997; Searle et al., 1997, 1999). Their crystallization ages are much younger than the peak Himalayan metamorphism at Zanskar (37-28 Ma – Vance and Harris, 1999; Walker et al., 1999), Garhwal (44-26 Ma – Prince et al., 2000, 2001; Foster et al., 2000), Annapurna in Nepal (36 Ma – Hodges et al., 1996), the Everest region in Nepal (32-23 Ma – Simpson et al., 2000) and Bhutan (36-34 Ma – Edward and Harrison, 1997). The migmatite zone is associated with sillimanite-muscovite or sillimanite-k-feldspar grade of metamorphism along Parbati, Sutlej and Baspa Valleys (all in Himachal Pradesh), and the Bhagirathi, Alaknanda and Dhauliganga Valleys (all in Uttarakhand). These migmatite occurrences are often related to local mesoscopic differentiation during anatexis (Singh, et. al., 2004). The HHC is having best exposure to study the relationship among the metamorphic sequence, migmatite and leucogranite like Seigneurs Massif, Pyrenees, France (Wickham, 1987), St Malo, France (Brown, 1979), Black Hill, South Dakota (Nabelek et al., 1992), Quetico-Nemiscav Superprovince, Canada (Sawyer, 1998), South Mountain Batholith, Nova Scotia, Canada (Clarke et al., 1993). Typically, the

migmatite represents the highest metamorphic grade in regional metamorphic terrains.

These migmatite occurrences are often related to local mesoscopic differentiation during anatexis and thought to be representing fossilized partially molten source region of granites and may have remained hot over tens of millions of years. The melting generally occurs/collects in low pressure sites, synchronously with deformation. The migmatite may result into granite generation from anatexis of crustal rocks along with segregation, aggregation, ascent and emplacement of resultant magma (Brown, 1994). These bodies have also been attributed to the crustal dehydration melting reactions, which involves hydrous reactant giving rise to anhydrous melanosome and hydrous silicate melt as leucosome. Migmatite may represent an arrested stage of granite development in which leucosomes did not coalesce to form large scale bodies (Obata et al., 1994). Alternatively, migmatite and granite may not be genetically related with each other (White and Chappel, 1990).

The HHC of Alaknanda and Dhauliganga valley is tectonically bounded by Main Central Thrust (MCT) in the south and Malari Fault in the north. In between these two tectonic boundaries the Vaikrita Thrust (VT) is present within the HHC. The rocks occurring above the VT is classified as Vaikrita Group, a thick sequence of medium grade amphibolite facies schist and gneiss along with migmatite and leucogranite in the middle and upper part. The rocks of HHC show increase in metamorphic grade with increase in structural level indicating presence of inverted metamorphism as indicated by other sections within northwest Himalaya, Nepal and Sikkim (Pilgrim and west, 1928; Auden, 1935; Le

Fort, 1975; Thakur, 1977; Sinha-Roy, 1982; Arita, 1983; Brunel and Kienast, 1986; Hodges and Silverberg, 1988; Mohan *et al.,* 1989; Searle and Rex, 1989; Staubli, 1989; Pecher, 1989; Pognante *et al.,* 1990; Treloar *et al.,* 1990). This phenomenon reveals the presence of lower grade rocks near the base of the MCT-hangingwall at lower structural levels and higher grade rocks towards higher structural levels. The inverted metamorphism has been explained by different models either independently or in combination e.g. recumbent folding and thrust imbrication, frictional shear heating along the MCT, downward transfer of heat from the hot HHC or granitic bodies to the cold Lesser Himalaya (Loczy, 1907; Pilgrim and West, 1928; Le Fort, 1975; Sinha-Roy, 1982; Frank *et al.,* 1977; Brunel and Kienast, 1986; Treloar *et al.,* 1990; for reviews see Windley, 1983, Hodges *et al.,* 1988).

In the field no structural or metamorphic break in grades have been observed, in both the sections between basal Munsiari Formation and the overlying Vaikrita Group. The grade of metamorphism increases from chlorite to staurolite zone within the basal Munsiari Formation followed by kyanite, and sillimanite zone schists and gneisses with migmatite and leucogranite in the north near Badrinath and Malari along Alaknanda and Dhauliganga valley respectively. The boundaries of migmatite zone in both the valleys transform gradually into psammitic gneiss on both side, and are more prominent in the Dhauliganga valley. The melt present in the migmatites in both the valleys ranging between ~ 10% to around 40% with the lesser production of *in situ* melt in the Dhauliganga valley, probably due to presence of calc-silicate rocks. *In situ* melts got accumulated in the form of small elongated pods or lenses occurring along the foliation of the

migmatite indicating the fossilized stage of melting in the rock while in the upper part small veins, dykes and sills of tourmaline bearing leucogranite and also quartzo-feldspathic melts are found indicating a possible link between *insitu* melt and main Higher Himalayan Leucogranites (HHL) bodies. At places, *insitu* melt are occurring along extensional planes which are occurring as conjugate set indicating that these planes acted as conduit for melt extraction and transportation. Thin layers of leucosome rich in sillimanite are very prominent feature of the Dhauliganga migmatite which is devoid of tourmaline and garnet. On the contrary, leucosome of the Alaknanda valley containing thin segregated layers consists of garnet and tourmaline in the plagioclase rich groundmass. The appearance and composition is very similar to that of tourmaline bearing leucogranite from the Higher Himalayan Leucogranite (HHL). The presence of leucosome in the Alaknanda valley, migmatite segregated into leucosome bands which reaching upto about 40cm thick while such feature is absent in the Dhauliganga valley. Melanosome and leucosome bands of the lower part show mafic salvages and deformation in disharmonic manner. The difference in melt volume in the two valleys seems to be due to their nature of the host rocks. The Alaknanda migmatite have more pelitic rocks while The Dhauliganga migmatite seems to have more of metagraywackes along with calc-silicate bands.

The rock types along the Alakhananda and Dhauliganga Valleys indicate different metamorphic zones and typical mineral assemblages indicating different reactions. In the chlorite-biotite zone mineral assemblage is Biotite- Muscovite-Chlorite± Epidote± Calcite- Quartz. Here biotites are occurring as patches along the periphery of the phengite and chlorite with subordinate muscovite. The textural

relationship and mineral assemblages clearly suggest reaction for the biotite formation as

Phengite + Chlorite → Biotite + Phengite-poor muscovite + Quartz + H_2O,

while the garnet formation reaction can be deduced from the assemblages of the garnet schist in the Munsiari Formation and can be written as

Muscovite+ Chlorite → Garnet+ Biotite+ Quartz+ H_2O.

The staurolite forming reaction can be written as follows because small ideoblastic staurolite grains are occurring as small post tectonic garnets along with large syntectonic garnet where the grains are wrapped by thin layers of chlorite, muscovite and quartz.

Garnet + Muscovite + Chlorite → Staurolite + Biotite + Quartz + H_2O,

While, the probable reaction for kyanite formation appears to be

Staurolite + Muscovite + Quartz → Kyanite + Biotite + H_2O

and the nucleation of sillimanite at the fringe of kyanite and plagioclase indicate a polymorphic transformation reaction of the Al_2SiO_5. Generation of melt has also been observed along the grain boundaries, the formation of fibrolite and melt suggest from leucosome to be

Muscovite + Biotite + Quartz + H_2O → Sillimanite (fibrolite) + melt.

Form the textural relationship between porphyroblast and matrix at least three stages of garnet have been identified from the rocks of the HHC. The earliest Gt_1 is the large porphyroblasts showing spiral inclusion and early stage Gt_{2a} has small inclusion free garnets occurring with staurolite. In the later stage of growth, large porphyroblastic garnet show internal foliation having elongated staurolite occurring parallel to the external foliation. Again, staurolites are found in

the matrix with inclusions of ilmenite occurring parallel to the main foliation indicating a syntectonic staurolite growth and the garnet porphyroblast containing the staurolite and is classified as Gt_{2b}. The second generation garnets with haphazard inclusions are overgrown by another garnet Gt_3 of third generation which is devoid of inclusion. These three garnet types indicate at least three stages of growth and in turn three stages of metamorphism.

The rim temperature of garnet occurring in upper most portion of the basal Munsiari Formation gives 520±90^{0}C and pressure 6.8±2.0 Kbar, whereas, after crossing the Vaikrita Thrust there is jump in pressure and temperature data. Garnet from lower part of the overlying Vaikrita Group rock gives rim temperature of 698±90^{0}C with pressure 10.3±1.1 kbar, whereas, the core gives temperature of about 589^{0}C at pressure of 8.5 Kbar. After this moving upward in structural level rim temperature is 708±41^{0}C with pressure 11.9±1.4 Kbar for kyanite gneiss (MA 23-36) near Suraithota. The core of the same sample gives temperature of about 610^{0}C at pressure of 7.5 Kbar. The P-T data indicate an increase of about 100^{0}C in temperature and about 4.5 Kbar pressure increase from core to rim. The uppermost part of the Joshimath Formation lying just below the Pandukeshwar quartzite giving rim temperature of 675±43^{0}C, and pressure of about 11.5±1.3 and witness almost same pressure-temperature condition as evident from the sample which is within the error limit of the last sample. The core (inclusion) and rim thermobarometry of the samples AG 14-18 and AG15-21of Badrinath Formation indicates slight increase in temperature of about 30-50^{0}C and reduction in pressure of about 2 kbar. However, rim data from samples of Badrinath and Pandukeshwar Formations reveal almost constant temperature at about

650±50^{0}C with decrease in pressure from 7.3±2.1 Kbar to 5±1.6Kbar towards the northern part in migmatite zone. However, the total reduction in pressure from the samples nearby Vaikrita Thrust to migmatite zone is about 5-6 kbar.

The garnet profiles also indicate the similar pattern with outer rim post retrogression indicating post tectonic nature. The syntetonic garnet Gt_1, give the earlier part of the pressure temperature path by monitoring the increase in X_{Ca} and Fe/Fe+Mg pattern in the profile. In the profile X_{Mn} shows bell-shape pattern which is typical of normal zoning with increase in temperature. The smallest garnet Gt_2 (Fig. 3.18b) show flat pattern because of its smaller size get homogenized with the change in pressure and temperature during post tectonic growth. The pressure-temperature versus distance plot (Fig. 3.14) also indicate a somewhat decrease in both pressure and temperature away from VT towards north for both the sections followed by an almost stable temperature in the centre and again followed by a slight increase in rim temperature with subsequent reduction in rim pressure. This thermobarometric information suggests the decompression of the overloading crustal slabs due to the surface erosion or extensional tectonic operating near the northern boundary of the HHC. Whereas, the reduction in pressure of about 5-6 kbar from Vaikrita Thrust to Migmatite zone indicate near-isothermal decompression. However at the central portion of the Vaikrita Group there is a slight reduction in temperature and pressure.

Form the estimated pressure and temperature for core (inclusion) and rim (matrix) of the different samples all across the HHC and their zoning profile reveals that the rocks have undergone two path of evolutionin P-T diagram; (i) path-I and (ii) path-II (Fig. 6.1). Path-I is characterized by gradual increase in both

pressure and temperature from about ~600^{0}C to 700^{0}C to about ~7 to ~12 kbar in pressure. This path has been defined and confined to the kyanite (±sillimanite) zone rocks near Vaikrita Thrust, i.e., in the lower part of the Vaikrita Group. The other path for pressure and temperature, P-T path-II is characterized by decompression of pressure of about 2-3 Kbar with a slight increase of temperature of about 30-50^{0}C from core to rim. This type of path is confined to the sillimanite and migmatite zone in both the sections of HHC.

The trace and REE geochemical characteristics of metasediment, migmatite and leucosome reveal almost similar pattern with lower concentration of trace and REE within the leucosome fractions. The pattern of trace and REE can be attributed to different models for the formation of migmatite are (a) metamorphic differentiation at subsolidus temperatures by chemical and/or mechanical process, (b) metasomatism at subsolidus or hypersolidus conditions, (c) injection of foreign magma along foliation planes, (d) artial melting (anatexis) with or without segregation of initial melts and (e) layer by layer transformation. Even combination of two or more of these models can explain the geochemical pattern which is controlled by the mineral phases that enters in the melt (Hammouda et al., 1996; Tommasini and Davies, 1997; Kresel and Davidson, 1999, 2002).

If we look at the metamorphic segregation model which differentiates minerals under subsolidus condition can produce similar pattern with different concentration level of the elements. Such differentiation has also been evident from the thin layers of garnet in the upper part of leucosome, even though the garnets having high specific gravity than the surrounding silicic melt remain afloat. This probably

indicates low temperature melting (i.e. melting temperature has just reached the liquidus), in this condition, the viscosity of the melt would be high which probably can support the garnets in the melt. At the same time, the enriched pattern of HREE can be attributed to the high concentration in the garnet present within the melt. The garnet layers can also be due to comparatively earlier melting of more micaseous layer and late stage melting of the garnet rich layer. The large number of small pods of leucosome occurring within the migmatite zone also indicates similar mechanism/ model of partial melting (anatexis). During partial melting (anatexis) small scale segregation have also taken place and it appears as if the leucosomes (melt) were derived from the adjacent melanosome and mesosome due to their low solubility in the felsic melt at around 700-800^{0}C. Since REE are quite immobile during hydrothermal alteration and metasomatism, the observed REE pattern of different rock types along the Alakhnanda and Dhauliganga cannot be attributed to this model. Similarly, injection of magma model has also been ruled out because that cannot produce the pattern as has been observed. In case of injection of magma, the pattern would have been of different elemental concentration, which mainly depend upon the source rocks, mechanism of partial melting (batch or fractional melting) and also percentage of melting and would have given different pattern.

Experimental results indicating two important systems for melting; (a) dehydration-melting of hydrous mineral of the metasediment (dry system) and (b) H_2O saturated (wet) system. However, experiment on melting indicated that water-fluxed melting produces plagioclase and quartz (trondjemitic) below 750^{0}C

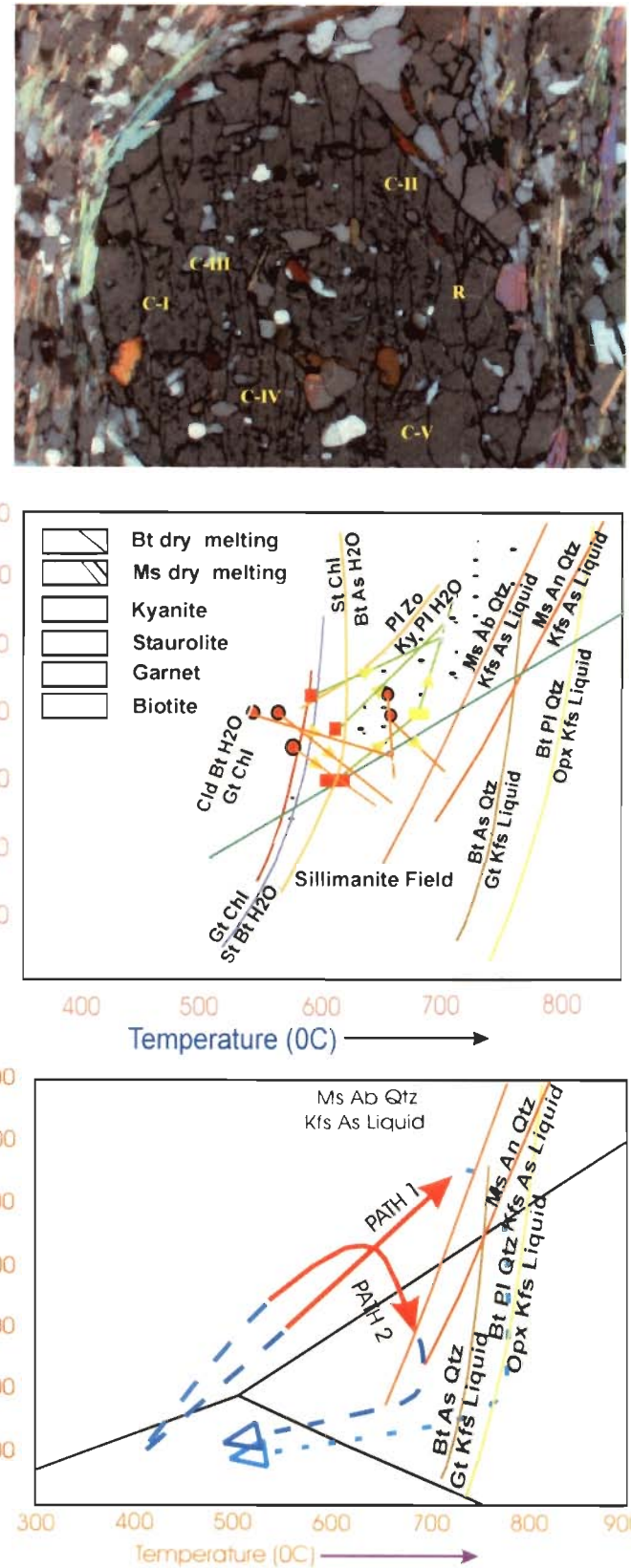

Figure 6.1 (a) Photomicrographs showing the locations within garnet which have been considerer for extracting P-T path(b) the plot of the core rim values of pressure andtemperature (c) the constructed P-T pathe of the HHC of Alaknanda and Dhauliganga valley

(Patino-Douce and Harris, 1997). The leucosome of the migmatite shows presence of dominant plagioclase (albite) suggesting H_2O saturated condition for melting rather than dehydration melting. Initial melting has probably yielded with small patches of unseggregated melt and residuum (melanosome). The melt generation in muscovite-dehydration melting reaction, gives typically low melt producibility (Harris et al., 1995). Thin section studies of the leucosome indicate plagioclase-quartz domain suggesting presence of pre-melting dominant plagioclase in both melanosome and leucosome of the migmatite. If the leucosome (plagioclase+quartz) represents a pure melt containing plagioclase which is present in pods indicating that initial melt produced melt as per the equation

Plagioclase+ K-feldspar+ Quartz ± Sillimanite +H_2O↔Melt.

After this melting, cooling magma would typically produce biotite first and after prolonged fractionation, the boron (B) content of the melt could increase to sufficient value for the tourmaline saturation. The source of boron could be muscovite of sedimentary rocks, which can have upto 1340 ppm of boron (Henry and Dutrow, 1996; Sperlich, et al., 1996). Further, partial melting involving the breakdown of biotite producing garnet, present in some of the leucosome is due to the reaction

Biotite+Plagioclase+Sillimanite +H_2O↔Garnet + K-feldspar + Melt.

However, on the basis of petrography i.e., the textural relationships in leucosome and migmatite, the melt producing reaction involving muscovite, plagioclase and quartz (Thompson and Tracy 1979) could be:

Muscovite+Plagioclase+ Quartz+H_2O↔Melt+Sillimanite+Biotite

and

Muscovite+Plagioclase+ Quartz +↔Melt+Sillimanite+ K-feldspar+Biotite

The above reaction can also help in explaining the presence of positive Eu anomaly in the REE pattern of leucosome.

Cooling age for wholerock-muscovite and wholerock-biotite pair has also been applied to the rocks of the Alakhananda and Dhauliganga Valleys to evaluate cooling and exhumation history of the terrain. The muscovite ages from the Vaikrita group of both the valleys range between 20 and 14 Ma while biotite ages varying between 13 and 7 Ma indicating that terrain were at around 500^0C isotherm between 20 and 14 Ma that brought down to 300^0C isotherm between 13 and 7 Ma. Since the calculation of cooling and exhumation rate is not straightforward which carries a number of controlling factors and again the problems associated with the 2-D modeling. Here, considering the point that topography of the terrain do not affect the rate of cooling and exhumation for higher closure temperature mineral pairs (Mancktelow and Grasemann, 1997). Therefore, in this study rate of cooing and exhumation is calculated using muscovite (500 ± 50^0C) and biotite (300 ± 50^0C) pair in a simple one-dimensional frame with assumption that 30 ± 10^0C/km steady-state geothermal gradient persists over the calculated age that is the time when the diffusion of radiogentic isotope freezes within the mineral.

Interestingly, the muscovite ages of the samples adjacent to the VT do not vary from those of the migmatite zone, while the biotite ages change largely, justifying the remobilization of the LILE due the ductile deformation at MCT zone. MCT zone samples yield muscovite age of 8.61 Ma while biotite ages are as low

as 1.43 ± 0.01 Ma. Similarly, the Munsiari Formation yields biotite ages between 2.07-2.05 Ma. The age pattern, across the HHC also show a sharp break in the ages across the VT, i.e., between the Vaikrita and the Munsiari Formation. The calculated cooling and exhumation in the central portion of the Vaikrita Group, the basal Munsiari Formation indicates very fast exhumation. Considering the average cooling age of muscovite and biotite from the Vaikrita Group and the Munsiari Formation, cooling path has been constructed (Fig. 6.2), which clearly indicate two distinct patterns. The samples of the Vaikrita Group give a gentle path indicating moderate exhumation rate between ~17 to ~11 Ma. Whereas, basal Munsiari Formation indicating a very fast cooling and exhumation rate.

ε_{Nd} and $^{87}Sr/^{86}Sr$ values for source rock characterization calculated at present day values, at 46 Ma value considering SHRIMP U-Pb age (Singh et al., 2003) from Bhagirathi valley for re-homogenization age and at 500 Ma which has been considered by other workers as the time of re-homogenization (Ahmed et al., 2000; Richards et al., 2005) indicate that there is similarity in data as published earlier by many workers in NW Himalaya and Nepal Himalaya. The data clearly indicate that the calculated values at t=o and t=46 Ma, are more comparable with the range of the published data while the values calculated at t=500 Ma for most of the samples resulted into positive values and their $^{87}Sr/^{86}Sr$ ratios are giving lesser values than the BABI (Basaltic Achondrite Best Initial). Therefore, for the Vaikrita Group of rocks the re-homogenization is post-dating 500 Ma, which has been widely used for the Himalayan rocks. It also appears that the rocks of the HHC were re-homogenized comparatively in recent time. The average values of present day ε_{Nd} and $^{87}Sr/^{86}Sr$ for the Vaikrita Group of rocks give about -16 and

0.901836 respectively while for Tethyan it is about -17 and 1.002341 and for Munsiari Formation the values are about -24 and 0.905278. The average values of ε_{Nd} and $^{87}Sr/^{86}Sr$ at t=46 Ma gives, ~16 and 0.790327 for metasediment, ~-10 and 0.764427 for migmatite, ~-14 and 1.2286 for leucogranite and leucosome, ~-12 and 0.997426 for tethyan sediment and ~-23 and 0.890229 for metasediment of the Munsiari Formation. The values of $\varepsilon_{Nd}(46)$ and $^{87}Sr/^{86}Sr$ calculated at t=46 Ma gives clear separation of migmatite from mestasediment while the values at t=0 do not discriminate migmatite from metasediments. Leucosome samples yield anomalous values of $\varepsilon_{Nd}(0)$ due to high Sm/Nd ratio and present day $^{87}Sr/^{86}Sr$ ratio gives very high values indicating a disequilibrium melting of the crustal rocks.

Mineral assemblages, geochemical data and exhumation and/or cooling age history in addition to field character do indicate that migmatite leucosome and small volume of *insitu* tourmaline bearing leucogranite indicate cummulation rock from water-saturated melting of pelitic metasedimentary rocks. The formation of migmatite happened at around 46 Ma corresponding to peak metamorphic event due to collision tectonics of the Himalayan orogeny. At this time Sr-Nd isotopic ratio also got re-homogenized. The presence of feeder dykes for main tourmaline-bearing leucogranite indicate that the source for the main body could be migmatite which is also being supported by similarity in REE pattern of the main body could *insitu* tourmaline bearing leucogranite. The dyking occurred due to buoyancy or injection mechanism within the upper part of the HHC. After leucogranite formation, terrain exhumed separately with different exhumation rate, lower package being exhumed faster with overlying package as much slower rate. Within the upper package the central portion has exhumed at lesser rate as

compared to the two flanks bounded by the Vaikrita Thrust in the south and the Malari Fault in the north.

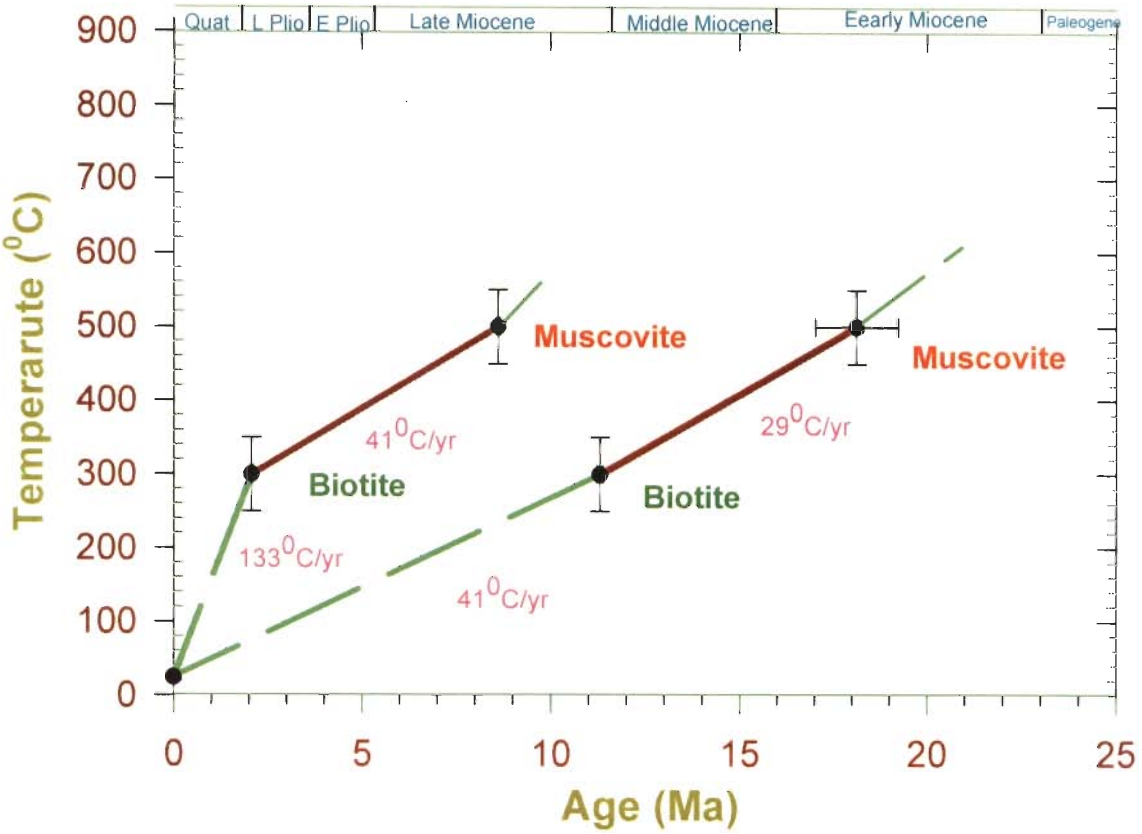

Figure 6.2: The cooling path of the HHC along Alaknanda and Dhauliganga valley using muscovite and biotite cooling age

REFERENCES

Achache, J., Courtillot, V. and Zhou, Y. X., 1984. Paleaogeographic and tectonic evolution of Southern Tibet since Middle Cretaceous times: New paleomagnetic data and synthesis, J. Geophys. Res., V-89, pp. 10,311–10,339.

Ahmad, T., Harris, N., Bickle, M., Chapman, H., Bunbury, J., Prince, C., 2000. Isotopic constraints on the structural relationships between the Lesser Himalayan Series and the High Himalayan Crystalline Series, Garhwal Himalaya. Geol. Soc. Am. Bull., V-112, pp. 467–477.

Arita, K. 1983. Origin of the inverted metamorpism of the Lower Himalayas, Central Nepal. Tectonophysics. V-95, pp. 43-63.

Auden, J. B., 1934. The geology of the krol belt. Records of Geol. Surv. India,. V-66, pp. 357– 454.

Auden, J.B., 1935. Traverses in the Himalaya. Rec. Geol. Surv. India, V-69, pp. 123-167.

Auden, J. B., 1937. The structure of the HimaLayas in Garhwal, Rec. Geol. Surv. India. V- 71, pp.407-433.

Auden, J.B., 1948. Some new limestone and dolomite occurrences in Northern India. Indian Minerl., v. 2, pp. 77-91.

Auden, J.B., 1949. General report of G.S.I. for 1939. Rec. Geol. Surv. India, V-78, pp. 74-78.

Ayres, M., and Harris, N., 1997,–REE fractionation and Nd-isotope disequilibrium during crustal anatexis: Constraints from Himalayan leucogranites: Chemical Geology, V-139, pp. 249–269.

Beck, R. A., Burbank, D. W. Sercombe, W. J. Khan, A. M. and Lawrence, R. D., 1996. Late Cretaceous ophiolite obduction and Paleocene India-Asia collision in the westernmost Himalaya, Geodin. Acta, V-9, pp. 114–144.

Berman RG, 1988. Internally-consistent thermodynamic data for minerals in the system Na_2O-K_2O-CaO-MgO-FeO-Fe_2O_3-$A1_2O_3$-SiO_2-TiO_2-H_2O-CO_2. Jour. Petrol., V-29, pp. 445-522.

Berthe, D., Choukroune, P. And Jegouzo, P., 1979. Orthogneiss, mylonite and non coaxial deformation of granites: the example of the South Armorican Shear Zone. Journal of Structural Geology V-1, pp. 3142.

Berthelsen, A., 1951. A geological section through the Himalaya. Medd. Dansk Geol. Foren., V-12, pp. 102-104.

Besse, J., V. Courtillot, J. P. Pozzi, M. Westphal, and Y. X. Zhou, 1984. Paleomagnetic estimates of crustal shortening in the Himalayan thrusts and Zangbo suture, Nature, V-311, pp. 621–626

Bhargava, O. N., 1960. The tectonic windows of the Lesser Himalaya. Him. Geol, V-10, pp. 135-155.

Bhargava, O. N., 1980. Outline of the stratigmphy of Eastern Himachal Pradesh,with special reference to the Jutogh Group. In K.S.Valdiya and S.B.Dhatia eds: Straiigraphy and Correlations of the Lesser-Himalayan Formations, Hindustan Publ. Corp., New Delhi, pp. 117-125.

Bhatia, S. B., 1982. Facies, fauna, and flora of the Tertiary of NW Himalaya: A synthsis, J. Palaeont. Soc. India, Spl. Pub., V-1, pp 8-20.

Bordet, P., 1973. On the position of the Himalayan Main Central Thrust within Nepal Himalaya. Proc. Semin. Geodynamics Himalayan Region, NGRI, Hyderabad. pp. 148-155.

Bouchez, J.L. and Pêcher, A., 1981. The Himalayan Main Central Thrust pile and its quartz-rich tectonites in central Népal. Tectonophysics, V-78, pp. 23–50.

Brooks, C., Hart, S.r., Wendt, I. 1972. Realistic use of two-error regression treatment as applied to rubidium-strontium data. Rev. Geophys. Space Phys., V-10, pp. 551.

Brown, M. 1994. The generation, segregation, ascent and emplacement of granite magma: the migmatite-to-crustally-derived granite connection in thickened orogens. Earth Sci. Rev., V-36, pp. 83-130.

Brunel, M., 1986. Ductile thrusting in the Himalaya: shear sense criteria and stretching lineation. Tectonics, V-5, pp. 247-265.

Brunel, M., and Kienast, J.R., 1986, Etude petro-structurale des chevauchements ductiles himalayans sur la transversale de l'Everest-Makalu (Nepal oriental): Candian Journal of Earth Sciences, V-23, pp. 1117-1137.

Burbank, D. W., R. A. Beck, and T. Mulder, The Himalayan foreland basin, in: Yin, A. and Harrision, T. M. (eds) The Tectonic Evolution of Asia, Cambridge Univ. Press, Cambridge, pp. 149-188.

Burchfiel, B. C., Zhiliang, C., Hodges, K.V, Yuping, L., Royden, L.H., Deng C., and Xue, J., 1992. The South Tibetan detachment system, Himalayan orogen: Extension contemporaneous with and parallel to shortening in a collisional mountain belt, Geol. Soc. Amer. Spec. Paper 269, pp. 41.

Burchfiel, B.C., Royden, L.H., 1985. North–south extension within the convergent Himalayan region. Geology 13, 679– 682.

Burg J. P.; Davy P.; Nievergelt P.; Oberli F.; Seward D.; Zhizhong D. and Meier M., 1997. Exhumation during crustal folding in the Namche-Barwa syntaxis. Terra Nova, V-9, Issue 2, pp. 53-56.

Burg, J. P. M., Guiraud, G. M., Chen, Li, G.C., 1984. Himalayan metamorphism and deformations in the northern Himalayan belt (Southern Tibet China). Earth Planet. Sci. Lett. V-69, pp. 391– 400.

Carosi, R., Lombardo, B., Molli, G., Musumeci, G., Pertusati, P. C., 1998. The South Tibetan detachment system in the Rongbuk valley, Everest region. Deformation features and geological implications. J. Asian Earth Sc., V-16, pp 299–311.

Catlos, E.J., Dubey, C.S., Harrison, T.M. and Edwards, M.A., 2004. Late Miocene Movement within the Himalayan Main Central Thrust Shear Zone, Sikkim, NE India. Jour. Meta. Geol., V-22, pp. 207-226.

Catlos, E.J., Dubey, C.S., Marston, R.A. and Harrison, T.M., 2003. Moving mountains; reactivation of the Himalayan Main Central Thrust at 4 Ma, Bhagirathi River, NW India. Geological Society of America Meeting Abstract, V-35(6), pp. 96.

Cerveny, P. F., Naeser, N. D., Zeitler, P. K., Naeser, C. W., Johnson, N. M., 1988. History of uplift and relief of the Himalaya during the past 18 million years; evidence from sandstones of the Siwalik Group. In: Kleinspehn, K.L., Paola, C. (Eds.), New Perspectives in Basin Analysis. Springer-Verlag, New York, pp. 43–61.

Clarke, D. B., McDonald, M.A., Reynolds, P.H. and Longstaff, F.J., 1993. Leucogranite from the eastern part of the South Mountain Batholith, Nova Scotia. Jour. Petrol., V-34, pp. 653-679.

Clift P. D. and Blusztajn, J., 2005. Reorganization of the Western Himalayan river system after five million years ago, Nature, V-438, pp. 1001-1003.

Coleman, M.E., 1996. Orogen-parallel and orogen-perpendicular extension in the central Nepalese Himalayas. Geol. Soc. America Bull. V-298, 553– 571.

Copeland, P., Harrison, T.M., 1990. Episodic rapid uplift in the Himalaya revealed by 40Ar/39Ar analysis of detrital K-feldspar and muscovite, Bengal fan. Geology, V-18, 54– 357.

Courtillot, V., Besse, J., Vandamme D., Montigny, R., J.Jaeger, J., and Capetta, H. Deccan flood basalts at the Cretaceaous/Tertiary boundary?, Earth Planet. Sci. Lett, V-80, 361–374, 1986.

Coward, M. P., Jan, M. Q., Rex, D., Tarney, J., Thirlwall, M. and Windley, B. F., 1982. Geotectonic framework of the Himalaya of North Pakistan. J Geol. Soc. London, V-139, pp. 299-308.

Critelli, S., and Garzanti, E. 1994. Provenance of the Lower Tertiary Murree redbeds (Hazara-Kashmir syntaxis, Pakistan) and initial rising of the Himalayas, Sediment. Geology, V-89, 265–284.

Daniel, C. G., Hollister, L. S., Parrish, R. R. and Grujic, D., 2003. Exhumation of the Main Central Thrust from Lower Crustal Depths, Eastern Bhutan Himalaya Jour. Meta. Geol., V- 21 (4), pp. 317–334.

Davidson, C., Grujic, D.E., Hollister, L.S. and Schmid, S.M. 1997. Metamorphic reactions related to decompression and synkinematic intrusion of leucogranite, High Himalayan Crystallines, Bhutan. J. Metam. Geol., V-15, pp. 593–612.

de Sigoyer, J., Chavagnac, V., Blichert-Toft, J., Villa, I. M., Luais, B., Guillot, S., Cosca, M., Mascle, G., 2000. Dating the Indian continental subduction and collisional thickening in the northwest Himalaya: multichronology of the Tso Morari eclogites. Geology. V-28,pp. 487–490.

DeCelles, P. G., Gehrels, G. E., Quade, J. and Ojha, T. P., 1998. Eocene-early Miocene foreland basin development and the history of Himalayan thrusting, western and central Nepal. Tectonics, V-17, pp. 741-765.

DeCelles, P. G., Robinson, D. M., Quade, J., Ojha, T. P., Garzione, C. N., Copeland, P. and Upreti, B. N., 2001. Stratigraphy, structure, and tectonic evolution of the Himalayan fold-thrust belt in western Nepal. Tectonics, V-20, pp. 487-509.

DeCelles, P. G., Robinson, D. M. and Zandt, G., 2002. Implications of shortening in the Himalayan fold-thrust belt for uplift of the Tibetan Plateau, Tectonics, V-21(6), 1062, doi:10.1029/ 2001TC001322.

Deniel C., Vidal P., Fernandez A., Le Fort P., and Peucat J.J., 1987. Isotopic study of the Manaslu granite (Himalaya, Nepal): inference on the age and source of Himalayan leucogranites: Contrib. Mineral.Petrol., v. 96, p. 78-92.

DePaolo, D.J., 1981a. Trace element and isotopic effects of combined wallrock assimilation and fractional crystallization: Earth Planet. Sci. Lett. V-53, pp.189-202

DePaolo, D.J., 1981b. Nd isotopes in the the Colorado Front Range and crust-mantle evolution in the Proterozoic. Nature, V-291, pp. 193-196.

DePaolo, D.J., 1981c. Nd isotopic studies: Some new perspectives on earth structure and evolution: EOS 62, pp. 137-140.

DePaolo, D.J., 1981d. A neodymium and strontium isotopic study of the Mesozoic calc-alkaline granitic batholiths of the Sierra Nevada and Peninsular Ranges, California. J. Geophys. Res. V-86, pp. 10470-10488.

Desio, A., 1977. On the geology of Deosai plateau, Kashmir. Mem. Accad.Naz. Lincei, V-15, pp. 1-19.

Dewey, J. F., Shakelton, R. M., Chang, C. and Sun, Y., 1988. The tectonic evolution of the Tibetan Plateau, Phil. Trans. Royal Soc. London., V-327(A), pp. 379-413.

Dickin, A. P., 1995. Radiogenic Isotope Geology, Cambridge University Press.

Dietrich V., and Gansser A., 1981. The leucogranites of the Bhutan Himalaya (crustal anatexis versus mantle melting): Schweiz. Mineral. Petrogr. Mitt., V-61 (2-3), pp. 177-202.

Dodson, M. H., 1979. Theory of cooling ages. In: Jagert, E. and Hunziker, J.C. (eds). Lectures in Isotope Geology, p. 194.

Edward M.A., and Harrison, T.M., 1997. When did the roof collapse? Late Miocene north–south extension in the high Himalaya revealed by Th-Pb monazite dating of the Khula Kangri granite. Geology, V-25, pp. 543–546.

England, P., LeFort, P., Molnar, P. and Pécher, A. 1992. Heat sources for tertiary metamorphism and anatexis in the Annapurna-Manaslu region, central Nepal. J. Geophys. Res., V-97, pp. 2107–2128.

Epard J.L., Steck A., Vannay J.C., Hunziker J., 1995. Tertiary himalayan structures and metamorphism in the kulu valley (mandi-khoksar transect of the western himalaya) - shikar beh nappe and crystalline nappe: *Schweiz Mineral Petrogr Mitt*, V-75 (1), pp. 59-84.

Faure, G. 1989, Principles of Isotope Geology (2nd Eds), John Wiley, pp.589.

Florence, F.P. and Spear, F.S., 1991. Effects of diffusional modification of garnet growth zoning on P-T path calculations. Contributions to Mineralogy and Petrology, V-107, pp. 487-500.

Foster, G., Kinny, P., Prince, C., Vance, D. and Harris, N., 2000. The significance of monazite U–Th–Pb age data in metamorphic assemblages; a combined study

of monazite and garnet chronometry. Earth Planet. Sci. Lett., V-181, pp. 327–340.
France-Lanord, C. and LeFort, P. 1988. Crustal melting and granite genesis during the Himalayan collision orogenesis. Trans. R. Soc. Edinb., V-99, pp. 183–195.
France-Lanord, C., Derry, L., Michard, A., 1993. Evolution of the Himalaya since Miocene time: isotopic and sedimentological evidence from the Bengal fan. In: Treloar, P.J., Searle, P.M. (Eds.), Himalayan Tectonics. The Geol. Soc. Special Publication, V-74, pp. 603– 621.
Frank, W., Thoni, M and Purtscheller, F., 1977. Geology and petrography of Kulu-South Lahul area. Colloq. Int. Cent. Nat. Res. Sci., V-33, pp. 147-172.
Gairola, V. K., 1975. On the petrology and structure of the Central Crystallines of the Garhwal Himalayas,Uttar Pradesh. Him. Geol,V- 5, pp. 455-368.
Galy and Lenord, F., 2001. Higher erosion rates in the Himalaya: geochemical constrains in riverine fluxes. Geology, V-29, pp. 23-26.
Galy, A., Lanord, F. C., Derry, L. A., 1996. The late Oligocene–early Miocene Himalayan belt: constraints deduced from isotopic compositions of early Miocene turbidites in the Bengal fan. Tectonophysics . V-260, 109– 118.
Gansser, A., 1964. Geology of the Himalayas, Wiley, New York, NY, pp. 289.
Ghosh, P; Padia, J. T and Mohindra, R., 2004. Stable isotope studies of paleosol sediments from Upper Siwalik of Himachal Himalaya evidence from high monsoonal intensity during Miocene? Paleog, Paleocl, Paleoe, V-206, pp. 103-114.
Guillot, S., 1999. An overview of the metamorphic evolution in Central Nepal, J. Asian Earth Sci, V-17, pp. 713-725.
Guillot, S. and Le Fort, P. 1995. Geochemical constraints on the bimodal origin of High Himalayan leucogranites. Lithos, V-35, pp. 221–234.
Guillot, S. and. Allemand, P., 2002. Two-dimentional thermal modeling of the early tectonometamorphic evolution in central Himalaya, J. Geodyn., V-34, pp. 77-98.
Guillot, S., Cosca, M., Allemand, P., LeFort, P., 1999. Contrasting metamorphic and geochronologic evolution along the Himalayan belt. In: Macfarlane, A., Sorkhabi, R.B., Quade, J. (Eds.), Himalaya and Tibet: Mountain Roots to Mountain Tops. Geol. Soc. America Spl. Papers, V-328, pp. 117– 128.
Guillot, S., Garzanti, E., Baratoux, D., Baratoux, D., Marquer, D., Maheo, G. and de Sigoyer, J., 2003. Reconstructing the total shortening history of the NW Himalaya, Geoch. Geoph. Geosy. G3, V-4(7), 1064, doi:10.1029/2002GC000484.
Gupta. L.N., 1976. A Contribution to the geology of Lansdowne area Garhwal I limatsyas. India. Jour. Geol. Soc. India, V-17. pp. 449-460.
Gupta., K. R. and Sharma, K. K., 1978. Some observations on the geology of the Indus and Shyok valleys between Leh and Panamik, district Ladakh, Jammu and Kaslimir, India. Recent Researches in Geology, V-7, pp. 133-143.

Hammouda T., Pichavant M., and Chaussidon M., 1996. Isotopic equilibration during partial melting: An experimental test of the behavior of Sr. Earth Planet. Sci. Lett., V-144, pp. 109–121.

Harris, N., 1995. Significance of weathering Himalayan metasedimentary rocks and leucogranites for the Sr isotopic evolution of sea water during the early Miocene, Geology, V-23(9), pp. 795-798.

Harris, N., Inger, S. and Massey, J. 1993. The role of fluids in the formation of High Himalayan leucogranites. in: P.J. Treloar and M.P. Searle (Eds), Himalayan Tectonics, Geol. Soc. London Spec. Publ. 74, pp. 391–400.

Harris, N. and Massey, J., 1994. Decompression and anatexis of Himalayan metapelites. Tectonics, V-13, pp. 1537–1546.

Harris, N. B. W., Caddick, M., Kosler, J., Goswami, S., Vance, D. and Tindle, A. G., 2004. The pressure-temperature-time path of migmatites from the Sikkim Himalaya. Jour. Meta. Geol., V-22 (3), pp. 249–264.

Harris, N., Ayres, M. & Massey, J., 1995. Geochemistry of granitic melts produced during the incongruent melting of muscovite : Implications for the extraction of Himalayan leucogranite magmas. Jour. Geophy. Res., V-B100, pp. 15767-15777.

Harrison, T. M., Ryerson, F. J., LeFort, P., Yin, A., Lovera, O. M., Catlos, E. J., 1997. A Late Miocene–Pliocene origin for the Central Himalayan inverted metamorphism. Earth Planet. Sc. Lett., V-146, E1– E8.

Harrison, T.M., Grove, M., Lovera, O.M., Catlos, E.J. and D'Andrea, J. 1999. The origin of Himalayan anatexis and inverted metamorphism: Models and constraints. J. Asian Earth Sci., V-17, pp. 755–772.

Hashimoto, H., Ohta, Y. and Akiba C., (eds.) 1973. Geology of the Nepal Himalaya. Hokkaido Univ., Sapporo, Japan. pp. 281.

Henry, D.J. and Dutrow, B.L., 1996. Metamorphic tourmaline and its petrological application. In: Boron – Mineralogy, Petrology and Geochemistry, Grew, E.S. and Anovitz, L.M., (eds), Mineral. Soc. Am., pp. 503-557.

Herren, E., 1987. Zanskar shear zone: northeast–southwest extension within the Higher Himalaya. Geology, V-15, pp. 409– 413.

Hodges, K. V., 2000. Tectonics of the Himalaya and southern Tibet from two decades perspectives. Geol. Soc. Amer. Bull., V-112, pp. 324-350.

Hodges, K. V. and Silverberg, D. S., 1988. Thermal evolution of the greater Himalaya, Garhwal, India. Tectonics, V 7, pp. 583-600.

Hodges, K. V., Parrish, R. R., Searle, M. P., 1996. Tectonic evolution of the central Annapurna Range, Nepalese Himalayas. Tectonics, V-15, 1264– 1291.

Holland TJB, 1989. Dependence of entropy on volume for silicates and oxide minerals, a review and a predictive model. Am Mineral., V-74, pp. 5-13.

Holland, J.B. and Powell, R., 1998. THERMOCALC programme.

Holland, J.B. and Powell, R., 2005. THERMOCALC programme V. 3.25.

Honegger, K., Dietrich, V., Frank, W., Gansser, A., Thoni, M., and Trommsdorf, V., 1982. Magmatism and metamorphism in the Ladakh Himalayas (the Indus-Tsangpo suture zone), Earth. Planet. Sci. Lett., V-60, pp. 253–292.

Hubbard, M. S., 1996. Ductile shear as a cause of inverted metamorphism: example from the Nepal Himalaya. Journal of Geology, V-104, pp. 493-499.

Hubbard, M., 1989. Thermobarometric constraints on the thermal history of the Main Central thrust zone and Tibetan slab, eastern Nepal Himalaya. J. Metam. Geol., V- 7, pp. 19-30.

Hubbard, M. S., Harrison, T. M., 1989. 40Ar/39Ar age constraints on deformation and metamorphism in the MCT Zone and Tibetan Slab, eastern Nepal Himalaya, Tectonics. V-8, pp. 865–880.

Huyghe, P., Galy, A., Mugnier, J.L., France-Lanord, C., 2001. Propagation of the thrust system and erosion in the Lesser Himalaya: geochemical and sedimentological evidence. Geology, V-29, 1007– 1010.

Inger, S., and Harris, N. B. W., 1992, Tectonothermal evolution of the High Himalayan crystalline sequence, Langtang Valley, northern Nepal: Journal of Metamorphic Geology, v. 10, p. 439–452.

Inger, S. and Harris, N. 1993. Geochemical constraints on leucogranite magmatism in the Lantang valley, Nepal Himalaya. J. Petrol., V-34, pp. 345–368.

Jacobsen, S. B. & Wasserburg, G. J., 1980. Sm-Nd isotopic evolution of chondrites. Earth Planet. Sci. Lett. V-50, pp. 139-155.

Jaeger, J. J., Courtillot, V.and Tapponnier, P., 1989. Paleontological view of the ages of the Deccan Traps, the CretaceousrTertiary boundary, and the India–Asia collision, Geology, V-17, pp. 316–319,

Jager, E., 1979. The Rb-Sr Method, Lectures in Isotope Geology in Jager, E. and HunZiker, J. C. (eds,) Spinger, pp. 13-26.

Jain, A.K. and Anand, A., 1988. Deformational and strain patterns of an intracontinental collision ductile shear zone – an example from the Higher Garhwal Himalaya. Jour. Struct. Geol., V-10 (7), pp. 717-734.

Jain, A.K. and Manickavasagam, R.M. 1993. Inverted metamorphism in the intracontinental ductile shear zone during Himalayan collision tectonics. Geology, V-21, pp. 407-410.

Jain, AK. and Patel, R.C. 1999. Structure of the Higher Himalayan crystalline along the Suru-Doda valleys (Zanskar), NW Himalaya. In: Jain, A.K. and Manickavasagam, R.M. (Eds.) Geodynamics of the NW Himalaya. Gond. Res. Group Mem. No. 6, pp. 91-110.

Jain, A.K., Manickavasagam, R.M., and Singh S., 1999. Collision tectonics in the NW Himalaya: deformation, metamorphism, emplacement of leucogranite along Valleys, Himachal Pradesh. In: Jain, A.K., Manickavasagam, R.M. (Eds.) Geodynamics of the Himalaya, Gond. Res. Group Mem. No. 6, pp. 3-37.

Jain, A. K., Kumar, D., Singh, S., Kumar, A. and Lal, N., 2000. Timing, quantification and tectonic modelling of Pliocene-Quaternary movements in the NW Himalaya: evidence from fission track dating, Earth Planet. Sci. Lett., V-179, pp. 437-451.

Jain, A. K., Singh. S., and Manickavasagam, R. M., 2002. Himalayan Collision Tectonics. Gondwana Research Group Memoir V-7, 114 p.

Klootwijk, C. T., Gee, J. S., Peirce, J. W., Smith, G. M., and L.McFadden, P., 1992. An early India-Asia contact: Paleomagnetic constraints from Ninetyeast Ridge, ODP Leg 121, Geology, V-20, pp. 395–398,

Knesel, K. M. and Davidson, J. P., 1999. Sr isotope systematics during melt generation by intrusion of basalt into continental crust. Contrib. Mineral Petrol., V-136, pp. 285–295.

Knesel, K. M. and Davidson, J. P., 2002. Insight into collisional magmatism from isotopic fingerprints of melting reactions. Science, V-296, pp. 2206-2208

Kohn, M. J. Elizabeth, F. J. R. and Harrision, T. M., 2001. Pressure-temperature-time path discontinuity in the Main Central Thrust Zone, central Nepal, Geology,V-29(7), pp. 571-574.

Kretz, R., 1983. Symbols for rock forming minerals.Am. Mineral., **68**, 277-279.

Kumar, G., 1997. Geology of Arunachal Pradesh. Geol. Surv. India, Banglore. Spear, S. F., 1993. Metamorphis Phase equilibrium and Pressure –Temperature – Time Paths, Min. Soc. America, Monograph, 1-799.

Kumar, G., Mehndi, S. H. and Prakash, G., !972. A review of stratigraphyof parts of Uttar Pradesh Tethys Himalaya. I. Paleont. Soc. India, V-15, pp 86-98.

Le Fort, P., 1975. Himalaya. the collided range: present knowledge of the continental arc. Am. J. Sci., V- 275(A), pp. 1-44.

Le Fort, P., 1981. Manaslu leucogranite: A collision signature of the Himalaya. A model for its genesis and emplacement. J. Geophys. Res., V-86, pp. 10545-10568.

Le Fort, P., 1986, Metamorphism and migmatism during Himalayan collision: In Coward, M.P. and Ries A.C., eds., Collision Tectonics: Geological Society Special Publication, V-19, pp. 159-172.

Le Fort, P., Cuney, M., Deniel, C., Lanords, C.F., Sheppard, N.F., Upreti, B. N. and Vidal , P., 1987. Crustal generation of the Himalayan leucogranite. Tectonophysics, V-134, pp. 39-57.

Le Pichon, X., Fournier, M. and Jolivet, L. 1992. Kinematics, topography and extrusion in the India-Eurasia collision, Tectonics, V-11, pp. 1085–1098.

Leech, M. L., Singh, S., Jain, A. K., Klemperer, S. L., and Manickavasagam, R. M., 2005. The onset of India-Asia continental collision: early, steep subduction required by the timing of UHP metamorphism in the western Himalaya, Earth. Planet. Sci. Lett., V-234, pp. 83-97.

Leech, M.L., Singh, S., Jain, A.K., Klemperer, S.L. and Manickavasagam, R.M., 2006. Reply to comment by P.J. O'Brien on: "The onset of India-Asia continental collision: Early, steep subduction required by the timing of UHP metamorphism in the western Himalaya" by Mary L. Leech, S. Singh, A.K. Jain, Simon L. Klemperer and RM. Manickavasagam, Earth Planetary Science Letters 234 (2005) 83-97. Earth Planetary Science Letters, V-245, pp. 817-820.

Leech, M.L., Singh, S. and Jain, A.K., 2007. Zircon reveals complex history in the UHP Tso Morari Complex, western Himalaya. International Geological Review, V-49, pp. 313-328.

Liew, T.C. and McCulloch, M.T. Genesis of granitoid batholiths of Peninsular Malaysia and implications for models of crustal evolution: evidence from a Nd-Sr isotopic and U-Pb zircon study. Geochim. Cosmochim. Acta., V-**49, pp.** 587-600.

Loczy, L.,1907: Beobacbtungen im ostfichen Himalaya. Foktr. Kozlem., V-35 (9), pp. 1-24.

Macfarlane, A. M., Hodges, K. V. and Lux, D., 1992. A structural analysis of the Main Central Thrust zone, Langtang National Park, central Nepal Himalaya. GSA Bulletin, V-104(11), p. 1389-1402.

Mancktelow N.S. and Grasemann B., 1997. Time-dependent effects of heat advection and topography on cooling histories during erosion. Tectonophysics, V-270, pp. 167-195.

Manickavasagam, R.M., Jain, A.K., Singh, S. and Asokan, A., 1999. Metamorphic evolution of the northwest Himalaya, India: Pressure-temperature data, inverted metamorphism, and exhumation in the Kashmir, Himachal, and Garhwal Himalayas. in: A. Macfarlane, R.B. Sorkhabai and J. Quade (Eds.), Himalaya and Tibet: Mountain Roots to Mountain Tops, Geol. Soc. Am. Spec. Pap. 328, pp. 179–198.

Mattauer, M., 1986. Intracontinental subduction, crust-mantle decollement and crustal-stacking wedge in the Himalaya and other collision belts. In: Coward, M.P and Ries, A. (Eds.) Collision Tectonics. Spec. Publ. Geol. Soc. London No. 10, pp. 37-50.

Matte, P., Mattauer, M., Jolivet, J. M. and Griot, D. A., 1997. Continental subductions beneath Tibet and the Himalayan orogeny: A review, Terra Nova, V-9, pp. 264–270,.

McCulloch M.T. and Chapp;ll B.W., 1982, Nd isotopic characteristics of S and I-type granites. Earth Planet. Sci. Lett., V-58, pp.51-64.

McCulloch, M.,T., Jaques, A.,L, Nelson, D.,R. and Lewis, J.,D., 1983, Nd and Sr isotopes in kimberlites and lamproites from western Australia: an enriched mantle origin. Nature, V-302, pp. 400-403.

McCulloch, M.T. and Black L.P., 1984, Sm—Nd isotopic systematics of Enderby Land granulites and evidence for the redistribution of Sm and Nd during metamorphism. Earth Planet. Sci Lett., V-71, pp. 46-58.

McElroy. R., Cater, I., Roberts, J., Prgkham, A. and Bond, M. 1990. The structure and stratigraphy of SE Zanskar, Ladakh Himalaya. Jour. Geol. Soc. London, V-147, pp. 989-997.

McIntyre, G. A., Brooks, C.,Compston, W. and Turek, A., 1966. The statistical assessment of Rb-Sr isochrons. Jour.Geophys. Res., V. 71, pp. 54-59.

Medlicott, H. B., 1864. On the geological structure and relationship of the southern portion of the Himalayan ranges between the rivers Ganges and Ravee. Mem. Geol. Surv. India, V-3, pp. 212.

Meigs, A. J., Burbank, D. W., Beck, R. A., 1995. Middle–late Miocene (N10 Ma) formation of the Main Boundary Thrust in the western Himalaya. Geology, V-23, pp. 423– 426.

Metcalfe, R.P., 1993, Pressure, temperature and timew constaints on metamorphism across the Main Central Thrust zone and High Himalayan Slab in the Garhwal Himalaya, *in* Treloar, P.J., and Searle, M.P., eds., Himalayan Tectonics: Geological Society of London Special Publication no. 74, pp. 485-510.

Michard A., Gurriet P., Soudant M. and Albarede F., 1985. Nd isotopes French phanerozoic shales: external vs internal aspects of crustal evolution. Georkim. Cosmoc on. Aria, V-49, pp. 601-610.

Middlemiss, C. S., 1887, Physical geology of West British Garhwal with notes on the route traverses through Jaunsar-Bawar and Tehri Garhwal. Rec. GeoL. Sur. India, V-29, pp. 26-40.

Miller, C., Klotzli, U., Frank, W., Thoni, M., Grasemann, B., 2000. Proterozoic crustal evolution in the NW Himalaya (India) as recorded by circa 1.80 Ga mafic and 1.84 Ga granitic magmatism. Precam. Res., V-103 (3–4), pp. 191– 206.

Mohan, A., Windley, B. E and Searle, M. P., 1989. Geothermometry and development of inverted metamorphism in the Darjeeling-Sikkim region of the eastern Himalaya. J. Meta. Geol., V-7, pp. 95-110.

Molnar, P., and Tapponnier, P., ,1975. Cenozoic tectonics of Asia: Effects of a continental collision, Science, V-189, pp. 419–426.

Molnar, P., Pardo-Casas, F., and Stock, J., 1988. The Cenozoic and Late Cretaceous evolution of the Indian Ocean Basin: Uncertainties in the reconstructed positions of the Indian, African and Antarctic plates, Basin Res., V-1, pp. 23–40.

Motohiro, T. and Kazuhiro, S., 2003. Heterogeneity of initial ^{87}Sr / ^{86}Sr ratios within a single pluton: evidence from apatite strontium isotopic study. Chem. Geol., V-199, pp. 89– 197.

Motohiro, T., 2005. The use of apatite as a record of initial ^{87}Sr / ^{86}Sr ratios and indicator of magma processes in the Inagawa pluton, Ryoke belt, Japan. Chem. Geol., V-221, pp. 157– 169

Murphy, M. A., Yin, A., 2003. Structural evolution and sequence of thrusting in the Tethyan fold-thrust belt and Indus-Yalu suture zone, southwest Tibet. Geol. Soc. Am. Bull. V-115, pp 21–34.

Myrow, P. M., Hughes, N. C., Paulsen, T. S., Williams, I. S., Parcha, S. K., Thompson, K. R., Browring, S. A., Peng, S. C. and. Ahluwalia, A. D., 2003. Intregated tectonostratigraphic analysis of the Himalaya and implications for its tectonic reconstruction, Earth Planet. Sci. Lett., V-212, pp. 433-441.

Nablek, P.I., Russ-Nableck, C. And Haeussler, G.T., 1992. Stable isotope evidences for the petrogenesis and fluid evolution in the proterozoic Harney Peak leucogranite, Black Hill, South Dakota. Geochim. Cosmochim. Acta, V-56, pp. 403-417.

Najman, Y., 2006. The detrital record of orogenesis, A review of approaches and techniques used in the Himalayan sedimentary basins, Earth Sci. Rev. V-74 ,pp. 1 –72.

Najman, Y., and Garzanti, E., 2000. An integrated approach to provenance studies: Reconstructing early Himalayan palaeogeography and tectonic evolution from

Tertiary foredeep sediments, Northern India, Geol. Soc. Am. Bull., V-112, pp. 435–449.

Najman, Y., Bickle, M. and Chapman, H., 2000. Early Himalayan exhumation: isotopic constraints from the Indian foreland basin, Terra Nova, V-12, pp. 28-34.

Najman, Y., Pringle, M. R., M. S. and Godin, L., 2001. Ar-Ar dating of the oldest Himalayan sediments indicates erosion >15 My later than previously believed, Nature, V-410, pp-194–197,

Nakata, T., 1972: Geomorphic history and crustal movements of the foothills of the Himalayas. Tohoku Univ. Sci. Rep. Ser. 7 (Geogr), V-22, pp. 39-34.

O'Nionn R.K., Hamilton P. J. and Evensen N. M., 1977, Variations in 143Nd/144 Nd and 87Sr/86Sr in oceanic basalts. Earth Planet. Sci. Lett., V-34, pp. 13-22.

O'Nions R.K., Hamilton P J. and Hooker P.J., 1983, A Nd isotope investigation of sediments related to crustal development in the British Isles. Earth Planet. Sci, Lett., V-63, pp. 229-240.

Obata, M., Yoshimura, Y., Nagakawa, K., Odawara, S. And Osani, Y., 1994. Crustal anatexis and melt migration in the Higo metamorphic terrane, west-central Kyushu, Kumamoto, Japan, Lithos, V-32, pp. 135-147.

Parrish, R. R. and Hodges, K. V., 1996. Isotopic constraints on the age and provenance of the Lesser and Greater Himalayan sequences, Nepalese Himalaya, Geol. Soc. Am. Bull., V-108(7), pp. 904-911.

Patel, R.C., Sandeep Singh., Asokan A., Manickavasagam, R.M., and Jain, A.K., 1993, Extensional tectonics in the Himalayan orogen Zanskar, NW India, *in* Treloar, P.J., and Searle, M.P., eds., Himalayan Tectonics: Geological Society of London Special Publication 74, pp. 445-459.

Patiño Douce A.E., and Harris N., (1998): Experimental constraints on Himalayan Anatexis: *Journal of Petrology*, V-39(4), pp. 689-710.

Patriat, P., and Achache J., 1984. India–Asia collision chronology has implications for crustal shortening and driving mechanism of plates, Nature, V-311, pp. 615–621,

Patzelt, A., Li, H., Wang, J. and E. Appel, 1996. Pleomagnetism of Cretaceous to Tertiary sediments from southern Tibet: Evidence for the extent of the northern margin of India prior to the collision with Eurasia, Tectonophysics, V-259, pp. 259–284.

Pecher, A. 1978. Deformations et metamorphisms associes a une zone de Cisaillement. Exemple du grand chevar Chement Central Himalayan (M.C.T.), transversale des Annapurnas et du Manas lu, Nepall. These d'sat. univ. sci. Med. Grenoble, France, p.354.

Pecher, A. and Le Fort, P., 1986. The metamorphism in the Central Himalaya, its relations with the thrust tectonics. In: Le Fort, P, Coichen, M. and Montenat, C. (Eds.) Sci. de la Terre, mem. 47, pp. 285-309.

Pecher, A., 1989. The metamorphism in the central Himalaya. Jour. Meta. Geol., V-7, pp-31-41.

Peucat J.J., Vidal P., Bernard Griffiths, J. and Condie, K. C., 1988, Sr, Nd and Pb isotopic systemetics in the Archaean low to high-grade transition zone of southern India: syn accretion vs. post-accretion granulites. 3. Geology, V-97, pp. 537—550.

Pilgrim, G. E. and West, W. D., 1928. The structure and correlation of the Simla rocks. Mem. Geol. Surv. India, V-53, pp. 1-140.

Pognante U. and Benna P., 1993. Metamorphic zonation, migmatization and leucogranites along the Everest transect of Eastern Nepal and Tibet: record of an exhumation history. In: Himalayan Tectonics. Treloar P.J. & Searle M.P. (eds). Geological Society Special Publication, V-74, pp. 323-340.

Pognante, U., Castelli, D., Benna, P., Genovese, G., Obreli, F., Meier, M. and Tonarini, S., 1990. The crystalline units of the High Himalayas in the Lahul-Zanskar region (northwest India): metamorphic-tectonic history and geochronology of the collided and imbricated Indian plate. Geol. Mag., V-127, pp. 101-116.

Powell, C. M., Roots, S. R. and Veevers, J. J., 1988. Pre-breakup continental extension in East Gondwanaland and the early opening of the eastern Indian Ocean, Tectonophysics, V-155, pp. 261–283.

Prince, C. I., Harris, N. and Vance, D., 2001. Fluid-enhanced melting during prograde metamorphism. J. Geol. Soc. London V-158, pp. 233-241

Prince, C. I., Kosler, J., Vance, D. and Gunther, D., 2000. Comparison of Laser ablation ICP-MS and isotope dilution REE analyses – implications for Sm-Nd garnet geochronology. Chem. Geol. V-168, pp. 255-274.

Pyle, J. M. and Spear, F. S., 1999. Yttrium zoning in garnet: Coupling of major and accessory phases during metamorphic reactions. Geol. Mins. Res.,V-1, pp. 1-49.

Rage, J.C., Cappetta, H., Hartenberger, J.L., Jaeger, J.J., Sudre, J., Vianeyliaud, M., Kumar, K., Prasad, G.V.R. and Sahni, A., 1995, Collision age, Nature, V-375, pp. 286,.

Ramsay, J.G., 1967. Folding and fracturing of rocks. New York, McGraw-Hill, 568 p.

Ratschbacher, L., Frisch, W., Liu, G., Chen, C., 1994. Distributed deformation in southern and western Tibet during and after the India–Asia collision. J. Geophys. Res., V-99, 19817– 19945.

Replumaz, A., and Tapponnier, P. 2003. Reconstruction of the deformed collision zone Between India and Asia by backward motion of lithospheric blocks, J. Geophys. Res., 108(B6), 2285, doi:10.1029/2001JB000661,

Richards, A., Argles, T, Harris, N., Parrish, R., Ahmed, T., Darbyshire, F. and Draganits, E., 2005. Himalyan architecture constrained by isotopic tracers from clastic sediments, Earth Planet. Sci. Lett., V-236, pp. 773-796.

Robinson, D.M., DeCelles, P.G., Patchett, P.J., Garzione, C.N., 2001. The kinematic evolution of the Nepalese Himalaya interpreted from Nd isotopes. Earth and Planet. Sci. Lett. V-192, pp. 507– 521.

Rollinson, H., 1993. Using geochemical data: evaluation, presentation, interpretation, Longman Scientific & Technical, pp. 1-352.

Rowley, D. B., 1996. Age of initiation of collision between India and Asia: A review of Stratigraphic data, Earth Planet. Sci. Lett., V-145, pp. 1-13.

Roy, A.B. and Valdiya, K.S., 1988. Tectonometamorphic evolution of the great Himalayan Thrust Sheets in Grahwal Region, Kumaun Himalaya. Jour. Geol. Soc. India, v-32, pp. 106-124.

Ruppel, C. and Hodges, K.V., 1994. Pressure-temperature-time paths from two-dimensional thermal models; prograde, retrograde, and inverted metamorphism, Tectonics, v. 13, 17-44.

Sawyer, E.W., 1998. Formation and evolution of granitic magma during crustal reworking: the significance of diatextites. Jour. Petr., V-39, pp. 1147-1167.

Scharer, U., Copeland, P., Harisson, T., M. and Searle, M., P., 1990. Age cooling history and origin of post collisional leucogranites in the Karakoram batholith: A melt system isotope study of north Pakistan, J. Geology, V-29, pp. 233-251.f

Schelling, D. and Arita, K., 1991. Thrust tectonics, crustal shortening and the structures of the far eastern Nepal Himalaya. Tectonics, V-10, pp. 851-862.

Schelling, D., 1992. The tectonostratigraphy and structure of the eastern Nepal Himalaya, Tectonics. V-11, pp. 925– 943.

Schelling, D., Arita, K., 1991. Thrust tectonics, crustal shortening, and the structure of the far-eastern Nepal, Himalaya, Tectonics. V-10, pp. 851–862.

Searle, M. P. and Fryer, B. J., 1986. Garnet, tourmaline and muscovite bearing leucogranites, gneisses and migmatites of the Higher Himalaya from Zanskar, Kulu, Lahoul and Kashmir, In. Coward, M. P. and Ries, A. C. (Eds) Collision tectonics. Geol. Soc. Spl. Publ. No 19, pp. 185-201.

Searle, M. P. and Fryer, B. J.,1986. Garnet, tourmaline and muscovite- bearing leucogranites, gneisses and migmatites from the Higher Himalaya of Zanskar, Lahoul, Kulu and Kashmir. in: M.P. Coward and A. C. Ries (Eds.) Collision Tectonics, Geol. Soc. London Spec. Publ. 19, pp. 185-201.

Searle, M. P., 1983. Stratigraphy, structure and evolution of the Tibetan-Tethys zone in Zanskar and the Indus suture zone in the Ladakh Himalaya., Trans. R. Soc. Edinburgh Earth Sci.,V-73, pp. 205–219,.

Searle, M. P., Parrish, R. R., Hodges, K. V., Hurford, A., Ayres, M. W. and Whitehouse, M. J., 1997, Shishma Pangma Leucogranite, South Tibetan Himalaya: field relations, geochemistry; age, origin and emplacement, J. Geol., V-105, pp. 295-317.

Searle, M. P., Windley, B. F., Coward, M. P., Cooper, D. J. W., Rex, D.,Tingdong, L., Xuchang, X., Jan, V. C., Thakur, V. C., and Kumar, S., 1987. The closing of Tethys and the tectonics of the Himalaya, Geol. Soc. Am. Bull., V-98m, pp. 678–701.

Searle, M.P. and Rex, A.J., 1989. Thermal model of the Zanskar Himalaya. Jour. Metam. Geol., V-7, pp. 124-134.

Searle, M.P., 1986. Structural evolution and sequence of thrusting in the High Himalayan, Tibetan Tethyan and Indus suture zones of Zanskar and Ladakh, western Himalaya. J. Str. Geol. V-8, pp. 923–936.

Searle, M.P., 1991. The Geology and Tectonics of the Karakoram Mountains . John Wiley and sons, Chichester 358 pp.

Searle, M.P., Metcalfe, R.P., Rex, A.J. & Norry, M.J., 1993. Field relations, petrogenesis and emplacement of the Bhagirathi leucogranite, Garhwal Himalaya. In: Treloar, P.J. & Searle, M.P. (eds) Himalayan Tectonics. Geol.I Soc. London, Spl. Pub., V-74, pp. 429–444.

Searle, M.P., Noble, S.R., Hurford, A.J. and Rex, D.C. 1999. Age of crustal melting, emplacement and exhumation history of the Shivling leucogranite, Garhwal Himalaya. Geol. Mag, V-136 (5), pp. 513-525.

Searle, M.P., Parrish, R.R., Hodges, K.V., Hurford, A., Ayres, M.W. and Whitehouse, M.J. 1997 Shishma Pangma Leucogranite, South Tibetan Himalaya: field relations, geochemistry, age, origin and emplacement. Jour. Geol., V-105, pp. 295-317.

Searle, M.P., Waters, D.J., Rex, D.C. and Wilson, R.N. 1992. Pressure, temperature and time constraints on Himalayan metamorphism from eastern Kashmir and western Zanskar. J. Geol. Soc. London, V-149, pp. 753-773.

Shah, S. K. and Sinha, A. K., 1974. Stratigraphy and tectonics of the "Tethyan" zone in apart of Western Kumaun Himalaya, Him. Geol., V-3, pp. 72-82.

Shah, S. K. and Sinha, A. K., 1974. The first record of algal bioherms in the Palaeozoic sequence of the Tethyan zone of the Kumaun Himalaya. Curr. Sci., V-43. p. 131.

Sharma, K. K Choubey, V. M. and Chatti, H. R., 1991. Geological setting of the ophiolites and magmatic arc of Lohit Himalaya (Arunachal Pradesh) India with special refernce ti their petrochemistry. In: Sharma, K .K. (Eds.) Geology and Geodynamic evolution of the Himalyan Collision Zone, Pt.-2, Phys. Chem. Earth, V-18, pp. 221-236.

Sharma, K. K., 1987. Crustal growth and two-stage India-Eurasia collision in Ladakh, Tectonophysics, V-143, pp. 17-28.

Sharma. K. K., 1977. A contribution to the geology of Satluj Valley, Kinnaur, Himachal Pradesh, India. Sci. de la Terre., V-268, pp. 369-378.

Simpson, R.L., Parrish, R.R., Searle, M.P. and Waters, D.J., 2000. Two episodes of monazite crystallisation during metamorphism and crustal melting in the Everest region of the Nepalese Himalaya. Geology, V-28, pp. 403–406.

Singh I. B., 1999. Tectonic control on sedimentation in Ganga Plain Foreland Basin constraints on Siwalik sedimentation models. In: Jain, A.K. and Manickavasagam, R.M. (Eds.) Geodynamics of the NW-Himalaya, Gond. Res. Group Mem. 6, pp. 247-262.

Singh S., 1993, Collision Tectonics: Metamorphics and geochronological constraints from parts of Himachal Pradesh, NW-Himalaya [Ph.D. thesis]: University of Roorkee, Roorkee, 289p.

Singh, S. and Jain, A. K., 2003. Himalayan Granitoids. In: Singh, S. (ed.) Granitoids of the Himalayan Collisional Belt, Journal of the Virtual Explorer, 11, 1-20.

Singh, S., 2001. Status of geochronological studies in Himalaya: a review. Jour. Indian Geophys. Union., V-5 (1), pp 57-72.

Singh, S., Barley, M. E. and Jain, A.K. 2003 Episodic influx of Magma during the Himalayan orogeny: evidence from SHRIMP U-Pb zircon ages of metapelites and granitic bodies from Bhagirathi Valley, NW Himalaya, India. The origin of granites and related rocks (Arima, M., Nakajima, T. and Ishihara, S. – eds.). Geol. Surv. Japan, Intrim Report, V-29, pp. 140.

Singh, S., Jain, A.K., Choudhary, A.K., Singha, Th. N.B. and Arya, A.K., 2004. Himalayan Migmatite and its relation with leucogranite generation. Workshop on Indian Geotransects, Wadia Institute of Himalayan Geology, Dehradun, 18-23.

Spear, F.S., 1988. Metamorphic fractional crystallization and internal metasomatism by diffusional homogenization of zoned garnets. Contributions to Mineralogy and Petrology, V-99, pp. 507-517.

Spear, F.S., 1993. Metamorphic Phase Equilibria and Pressure-Temperature-Time Paths. Mineralogical Society of America, Washington, D. C., 799 p.

Spear, F.S., Peacock, S.M., Kohn, M.J., Florence, F.P. and Menard, T., 1991. Computer programs for petrologic P-T-t path calculations. American Mineralogist, V-76, pp. 2009-2012.

Sperlich, R., Giere, R. and Frey, M., 1996. Evolution of compositional polarity and zoning in tourmaline during prograde metamorphism of sedimentary rocks in the Swiss central Alps. Am. Mineral., V-81, pp. 1222-1236.

Srivastava, P., Mitra, G., 1994. Thrust geometries and deep structure of the outer and Lesser Himalaya, Jumoan and Garhwal (India): implications for evolution of the Himalayan fold and thrust belt, Tectonics, V-13, pp. 89–109.

Staubli, A., 1989. Polyphase metamorphism and the development of the Main Central Thrust. Jour. Metamorph. Geol., V-7, pp. 73-93.

Steck, A., 2003. Geology of the NW Indian Himalaya. Eclogae Geologicae Ivetiae, pp. 147– 213.

Steiger, R. And Jaeger, E, 1977. Subcommission on geochronology: Convention on the use of decay constants in geo and cosmo-chronology. Earth Planet. Sci. Letters, V- 36, pp. 359.

Stephenson, B. ., Waters, D. J., Searle, M. P., 2000. Inverted metamorphism and the Main Central Thrust: field relations and thermobarometric constraints from the Kishtwar Window, NW Indian Himalaya,. J. Met. Geol. V-18, pp. 571– 590.

Stocklin, J., 1980. Geology of Nepal and its regional frame. J. Geol. Soc. V-137, pp. 1–34.

Tandon, S.K., 1991. The Himalayan foreland: focus on Siwalik basin. In: Tandon, S.K., Pant, C.C. and Casshyap, S.M. (Eds.) Sedimentary Basins of India, Gyanodaya Prakashk. pp. 171- 201.

Taylor S.R. and McLennan SM., 1985, The continental crust: its composition and evolution. Blackwell, Oxford

Thakur, V C, Rawat, B. S, and Islam, R., 1990. Zanskar Crystalline some observations on its lithostatigraphy, deformation, metamorphism and regional framework, J. Him. Geol., V-1, pp. 11-25.

Thakur, V. C., 1993. Geology of the Western Himalaya. Phy. Chem. Earth, V-19, pt. I-IV, pp. 113-116.

Thakur, V.C., 1977. Divergent isograds of metamorphism in some parts of Higher Himalayan Zone. Sci. de la Terra, V-268, pp. 433-441.

Thakur, V.C., 1980. Tectonics of the Central Crystallines of Western Himalaya. Tectonophysics., V-62, pp. 141-154.

Thomas, M. W.,1998. Phase Equilibria in Metamorphic Rocks: Backgroung and Petrological Applications, Springer, 1-309.

Thompson, A.B. and Tracy, R.J., 1979. Model systems for anatexis of pelitic rocks: I. Theory of melting reactions in the system $CaO–KAlO_2–NaAlO_2–Al_2O_3–SiO_2–H_2O$. Contrib. Mineral. Petrol., V-70, pp. 429–438.

Tommasini S. and Davies G. R. (1997) Isotope disequilibrium during anatexis: A case study of contact melting, Sierra Nevada, California. Earth Planet. Sci. Lett., V-148, pp. 273-285

Tracy, R.J., 1982, Compositional zoning and inclusions in minerals, *in* Ferry, J.M. eds., Characterization of metamorphism through mineral equilibria: Mineralogical Society of America: Reviews in Mineralogy, V-10, pp. 355-397.

Treloar, P. J., and. Coward, M. P., 1991. Indian plate motion and shape: Constraints on the geometry of the Himalaya orogen, Tectonophysics, V-191, pp. 189–198.

Treloar, P. J.; Carney, J. N.; Crow, M. J.; Evans, J. A.; and Barton, C. N. 1990. Pressure-temperature-time paths of granulite metamorphism and uplift, Zambesi belt, N.E. Zimbabwe. *In* Vielzeuf, D., and Vidal, P., eds. Granulites and crustal evolution. NATO ASI Ser. Ser. C Math. Phys. Sci. V-311, pp. 223-241

Treloar, P.J., Broughten, R.D., Williams, M.P., Coward, M.P. and Windley, B.F., 1989. Deformation, metamorphism, and imbrication of Indian plate, south of the Main mantle thrust, north Pakistan. J. Metam. Geol., V-7, pp. 111-125.

Trzcienski, W.E., Jr., 1977. Garnet zoning: Product of continuous reaction. Canadian Mineralogist, V-15, pp. 250-256.

Valdiya, K. S. and Gupta, V. D., 1972. A contribution to the geology of northestern Kumaon, with special reference to the Hercinian gap in Tethys Himalaya, Him. Geol., V-2, pp1-33.

Valdiya, K. S., 1977. Structural set up of the Kumaun Lesser Himalaya. In: Ecologie et geologie de l', Himalaya, C.N.R.S., Paris, Coll. Int., V-268, pp. 449-462.

Valdiya, K. S., 1988. Tectonics and evolution of the central sector of the Himalaya. Phil. Trans. R. Soc. London, A326, pp. 151-175.

Valdiya, K. S., 1989. Trans-Himadri intracrustal fault and basement upwarps south of Indus-Tsangpo Suture Zone. In. Tectonics of the western Himalaya (eds.) Malinconico, L. L. and Lillie, R. J., Geol. Soc. Amer. Spl. Paper, V-232, pp.153-168.

Valdiya, K. S., 1995. Proterozoic sedimentation and Pan-African geodynamic development in the Himalaya. Prec. Res. V-74, pp. 35-55.

Vance, D. and Harris, N.B.W., 1999. Timing of prograde metamorphism in the Zanskar Himalaya. Geology, V-27, pp. 395-398.

Vance, D., Muller, W., Villa, I. M., 2003. Geochronolog: linking the isotopic record with petrology and textures- an introduction.

Vannay, J. C. and Grasemann, B., 1998, Inverted metamorphism in the High Himalaya of Himachal Pradesh (NW India): Phase equilibria versus thermobarometry, Schweitz. Miner. Petrol. Mitt., V-78, pp. 107-132.

Vannay, J. C. and Hodges, K. V., 1996. Tectonometamorphic evolution of the Himalayan metamorphic core between Annapurna and Dhaulagiri, Central Nepal. J. Meta. Geol., V-14, pp. 635-656.

Wadia, D. N., 1931, The syntaxis of the Northwest Himalaya: its rocks, tectonics and orogeny, Rec. Geol Surv. India, V-65, pp. 189-134.

Wadia, D. N., 1937. The Crtaceous volcanic series of Astor-Deosai, Kashmir and its intrusions, Rec. Geol. Surv. India, V-72, pp. 123-146.

Walker, J. D., Martin, M. W., Bowering, S. A., Searle, M. P., Water, D. J. and Hodges, K. V., 1999. Metamorphism, melting and extension: age constraints from the High Himalayan Slab of southeast Zanskar and Northwest Lahaul. Jour. Geol., V-107, pp. 473-495.

Wasserburg Gj., Jacobsen S. B., DePaolo, D. J., McCulloch M. T. and Wen J., 1981, Precise determinations of Sm/Nd ratios, Sm and Nd isotopic abundances in standard solutions. Geochim. Cosmochim. Acta. V-45, pp. 2311—2323.

White, A.J.R. and Chappel, B.W., 1990. Per magma ad magma down-under. Geol. Jour., V-25, pp. 221-225.

White, N. M., Pringle, M., Garzanti, E., Bickle, M., Najman, Y., Chapman, H., Friend, P., 2002. Constraints on the exhumation and erosion of the High Himalayan Slab, NW India, from foreland basin deposits, Earth and Planet Sci. Lett., V-195, pp. 29–44.

Whittington, A. G., Foster, G. L., Harris, N. B. W., Vance, D., and Ayres, M. W., 1999. Lithostratigraphic correlations in the western Himalaya-An isotopic approach, Geology, V-27, pp. 585-588.

Whittington, A., Foster, G., Harris, N., Vance, D., Ayres, M., 1999. Lithostratigraphic correlations in the western Himalaya—an isotopic approach, Geology,V-27, pp. 585– 588.

Wickham, S.M., 1987. Crustal anatexis and granite petrogenesis during low-pressure regional metamorphism: the Trois Seigneurs Massif, Pyrenees, France. Jour. Petrol., V-28, pp. 127-169.

Windley, B. F., 1988. Tectonic framework of the Himalaya, Karakoram and Tibet, and problems of their evolution, Phil. Trans. Roy. Soc. London, Series A, Math. and Phys. Sci., V-326(1589), Tectonic Evolution of the Himalayas and Tibet, pp. 3-16.

Windley, B.F., 1983. Metamorphism and tectonics of the Himalaya, Geol. Soc. London Journ. V-140, pp. 849– 865.

Worley B, Powell R., 2000. High-precision relative thermobarometry: theory and example. J Metamorph Geol, V-18, pp. 91-101

Wyss M., Hermann J. & Steck A. (1999): Structural and metamorphic evolution of the northern Himachal Himalaya, NW India. Eclogae Geologicae Helvetiae, V- 92, 3-44.

Yin, A. and Harrison, T. M., 1996. Cambridge Univ. Press, New York, pp. 149–188

Yin, An, 2006. Cenozoic tectonic evolution of the Himalayan orogen as constrained by along-strike Variation of structural geometry, exhumation history, and foreland sedimentation, Earth Sci. Rev., V-76, pp.1–131.

York, D., 1966. Least Square fitting of a straight line. Canad. Jour. Phys. V-44, pp. 1079.

York, D., 1969. Least square fitting of a straight line with correlated errors. Earth Planet. Sci. Lett., V. 5, pp. 320.

Zhao, W., Nelson, K.D., Team, P. I., 1993. Deep seismic reflection evidence for continental underthrusting beneath south Tibet, Nature, V-366, pp. 557-559.

APPENDIX-I

MICROPROBE ANALYSIS OF GARNET OF ALAKNANDA AND DHAULIGANGA VALLEYS

OXIDES/ CATIONS	DL25-44-C1		DL22-40-C3		AG1-4-C2	DL36-63-C4	DL16-28-C2				DL2-4-C2	
	GARNET		GARNET		GARNET	GARNET	GARNET				GARNET	
	RIM		RIM		RIM	RIM	RIM				RIM	
	WEIGHT%											
SiO2	**37.765**	**37.540**	**37.321**	**37.736**	**37.958**	**37.583**	**36.885**	**37.504**	**37.295**	**37.402**	**37.073**	**37.291**	**37.169**	**37.727**
Al2O3	21.261	21.044	21.117	21.054	20.959	20.135	20.568	19.513	19.215	21.053	20.823	20.888	19.539	19.934
FeO	24.976	25.178	25.179	31.450	31.639	37.982	37.664	39.295	39.181	31.504	31.767	31.799	35.644	36.318
MgO	2.738	2.744	2.655	2.983	2.944	1.556	1.495	02.312	02.289	3.993	3.999	4.072	1.613	1.712
MnO	0.945	0.906	1.048	2.870	3.086	3.202	3.102	01.333	01.375	1.754	1.475	1.623	1.547	1.542
CaO	11.250	11.241	11.198	3.644	3.641	0.897	0.962	00.460	00.448	3.030	2.987	2.989	2.576	2.519
K2O	–	–	–	–	–	–	–	–	–	–	–	–	–	–
Na2O	–	–	–	–	–	–	–	–	–	–	–	–	–	–
TiO2	–	–	–	–	–	–	–	–	–	–	–	–	–	–
Total	98.935	98.651	98.518	99.737	100.226	101.356	100.675	100.417	99.804	98.735	98.123	98.661	98.088	99.752
	CATIONS (BASED ON 12 OXYGEN)													
Si	**3.002**	**2.998**	**2.988**	**3.023**	**3.030**	**3.037**	**3.000**	**3.052**	**3.057**	**3.011**	**3.007**	**3.008**	**3.073**	**3.067**
Al	1.992	1.981	1.993	1.988	1.972	1.918	1.972	1.872	1.857	1.998	1.991	1.986	1.904	1.910
Fe	1.661	1.682	1.686	2.107	2.112	2.567	2.562	2.675	2.686	2.121	2.155	2.145	2.464	2.469
Mg	0.325	0.327	0.317	0.356	0.350	0.187	0.181	0.281	0.280	0.479	0.484	0.490	0.199	0.207
Mn	0.064	0.061	0.071	0.195	0.209	0.219	0.214	0.090	0.096	0.200	0.101	0.111	0.108	0.106
Ca	0.958	0.962	0.961	0.313	0.311	0.078	0.084	0.040	0.039	0.261	0.261	0.258	0.228	0.219
K	–	–	–	–	–	–	–	–	–	–	–	–	–	–
Na	–	–	–	–	–	–	–	–	–	–	–	–	–	–
Ti	–	–	–	–	–	–	–	–	–	–	–	–	–	–
Total	8.002	8.011	8.016	7.983	7.984	8.005	8.014	8.012	8.015	7.990	7.997	7.999	7.976	7.978

MICROPROBE ANALYSIS OF GARNET OF ALAKNANDA AND DHAULIGANGA VALLEYS

OXIDES/ CATIONS	AG11-14-C2	AG14-18-C4	AG14-18-C4	AG15-21-C4	AG15-21-C4	AG17-25						
	GARNET	GARNET	GARNET	GARNET	GARNET	GARNET						
	RIM	RIM	CORE	RIM	CORE	RIM						
	WEIGHT%											
SiO2	**35.235**	**35.317**	**36.343**	**37.165**	**36.655**	**36.527**	**37.670**	**37.667**	**37.865**	**37.276**	**37.296**	**37.193**	**36.739**
Al2O3	20.697	20.480	20.516	20.891	20.531	20.755	20.002	19.134	20.512	20.623	19.575	20.450	20.159
FeO	35.597	36.060	32.979	33.450	33.388	32.291	33.407	33.840	33.619	33.896	33.268	34.701	34.302
MgO	2.205	1.985	1.933	1.933	2.226	2.249	1.773	1.757	1.806	1.701	1.529	1.830	1.748
MnO	5.461	5.823	5.910	5.875	5.566	5.960	4.909	4.144	5.372	5.713	5.927	6.602	5.539
CaO	0.745	0.516	0.843	0.806	1.038	1.009	2.707	2.799	2.340	2.029	0.665	0.609	0.553
K2O	–	–	–	–	–	–	–	–	–	–	–	–	–
Na2O	–	–	–	–	–	–	–	–	–	–	–	–	–
TiO2	–	–	–	–	–	–	–	–	–	–	–	–	–
Total	99.940	100.181	98.524	100.120	99.405	99.792	100.469	99.341	101.514	101.239	98.259	101.385	99.039
	CATIONS (BASED ON 12 OXYGEN)												
Si	**2.905**	**2.914**	**3.001**	**3.014**	**2.999**	**2.997**	**3.047**	**3.083**	**3.026**	**3.032**	**3.086**	**3.005**	**3.026**
Al	2.011	1.992	1.997	1.997	1.980	2.008	1.907	1.846	1.931	1.936	1.910	1.947	1.957
Fe	2.455	2.488	2.277	2.269	2.284	2.216	2.260	2.317	2.295	2.251	2.302	2.345	2.363
Mg	0.271	0.244	0.238	0.234	0.272	0.275	0.214	0.214	0.192	0.216	0.189	0.220	0.215
Mn	0.381	0.407	0.413	0.404	0.386	0.414	0.336	0.287	0.402	0.364	0.415	0.452	0.387
Ca	0.066	0.046	0.075	0.070	0.091	0.089	0.235	0.246	0.163	0.201	0.059	0.053	0.149
K	–	–	–	–	–	–	–	–	–	–	–	–	–
Na	–	–	–	–	–	–	–	–	–	–	–	–	–
Ti	–	–	–	–	–	–	–	–	–	–	–	–	–
Total	8.089	8.090	8.001	7.987	8.011	7.999	7.999	7.99	8.008	8.000	7.960	8.022	7.996

MICROPROBE ANALYSIS OF GARNET OF ALAKNANDA AND DHAULIGANGA VALLEYS

OXIDES/ ELEMENTS	DL18-31-C1			DL36-63-C4			DL41-71-C1				DL32-56	
	GARNET			GARNET			GARNET				GT 1	GT 2
	RIM			RIM			RIM			CORE	RIM	
	WEIGHT%											
SiO2	**37.800**	**37.896**	**38.116**	**37.504**	**37.235**	**37.295**	**38.794**	**38.872**	**38.967**	**39.211**	**37.903**	**36.671**	**37.573**
Al2O3	21.442	21.352	21.505	19.513	19.659	19.215	20.770	21.078	21.088	21.166	20.872	20.628	20.876
FeO	32.288	31.889	31.838	39.295	39.518	39.181	24.447	24.389	24.055	25.181	24.796	29.695	30.263
MgO	5.877	6.338	6.189	2.312	2.040	2.289	2.698	2.540	2.567	3.233	3.129	1.178	1.283
MnO	1.298	1.065	1.043	1.333	1.449	1.376	2.025	2.168	2.057	1.454	1.312	5.899	4.519
CaO	0.831	0.852	0.855	0.460	0.468	0.448	11.689	11.744	11.901	11.671	11.468	5.022	5.336
K2O	–	–	–	–	–	–	–	–	–	–	–	–	–
Na2O	–	–	–	–	–	–	–	–	–	–	–	–	–
TiO2	–	–	–	–	–	–	–	–	–	–	–	–	–
Total	99.536	99.390	99.545	100.417	100.804	99.804	100.422	100.792	100.634	101.916	99.480	99.093	99.849
	CATIONS (BASED ON 12 OXYGEN)												
Si	**2.999**	**3.002**	**3.011**	**3.052**	**3.038**	**3.057**	**3.042**	**3.037**	**3.043**	**3.027**	**3.002**	**2.9979**	**3.029**
Al	2.005	1.994	2.002	1.872	1.891	1.857	1.920	1.941	1.941	1.926	1.948	1.988	1.984
Fe	2.142	2.113	2.0103	2.675	2.697	2.686	1.603	1.593	1.571	1.625	1.642	2.030	2.041
Mg	0.695	0.748	0.729	0.280	0.248	0.279	0.315	0.296	0.299	0.372	0.369	0.143	0.154
Mn	0.087	0.071	0.069	0.092	0.100	0.095	0.134	0.143	0.136	0.095	0.088	0.408	0.309
Ca	0.071	0.072	0.072	0.040	0.041	0.039	0.982	0.983	0.996	0.965	0.973	0.440	0.461
K	–	–	–	–	–	–	–	–	–	–	–	–	–
Na	–	–	–	–	–	–	–	–	–	–	–	–	–
Ti	–	–	–	–	–	–	–	–	–	–	–	–	–
Total	7.999	8.001	7.988	8.012	8.016	8.014	7.997	7.993	7.986	8.010	8.024	8.008	7.978

MICROPROBE ANALYSIS OF GARNET OF ALAKNANDA AND DHAULIGANGA VALLEYS

OXIDES/ ELEMENTS	AL5-11		AL6-16		MA23-35							
	GARNET 1	GARNET 2	GARNET 1	GARNET 2	GARNET 1			GARNET 2			GARNET 2/1	
	RIM		RIM		RIM			RIM			RIM	
	WEIGHT%											
SiO2	37.233	**37.153**	37.244	**36.673**	**39.026**	**38.911**	**38.682**	**39.138**	**38.797**	**39.289**	**37.867**	**39.406**
Al2O3	21.044	21.105	20.821	20.494	21.228	21.366	21.360	21.516	21.807	21.554	21.991	21.686
FeO	34.890	34.771	30.616	29.232	31.922	31.479	31.557	31.838	31.329	31.438	31.405	31.608
MgO	2.074	1.857	4.359	3.126	6.794	7.313	6.079	7.246	7.308	7.593	5.557	5.797
MnO	4.653	3.789	3.217	6.102	0.729	0.664	1.439	0.817	0.731	0.765	3.341	3.137
CaO	1.260	1.979	2.947	2.127	1.449	1.594	1.773	1.504	1.515	1.395	1.566	1.716
K2O	–	–	–	–	–	–	–	–	–	–	–	–
Na2O	–	–	–	–	–	–	–	–	–	–	–	–
TiO2	–	–	–	–	–	–	–	–	–	–	–	–
Total	101.152	100.654	99.205	97.756	101.147	101.326	100.890	102.058	101.487	102.034	101.727	103.350
	CATIONS (BASED ON 12 OXYGEN)											
Si	2.994	**2.996**	2.994	**3.011**	**3.029**	**3.011**	**3.020**	**3.009**	**2.994**	**3.014**	**2.957**	**3.017**
Al	1.995	2.006	1.973	1.984	1.942	1.948	1.966	1.950	1.984	1.949	2.024	1.957
Fe	2.346	2.345	2.058	2.007	2.072	2.037	2.060	2.048	2.022	2.017	2.051	2.024
Mg	0.248	0.223	0.522	0.383	0.786	0.843	0.708	0.831	0.841	0.868	0.647	0.662
Mn	0.317	0.259	0.219	0.424	0.048	0.043	0.095	0.053	0.048	0.049	0.221	0.203
Ca	0.108	0.171	0.254	0.187	0.121	0.132	0.148	0.124	0.125	0.115	0.131	0.141
K	–	–	–	–	–	–	–	–	–	–	–	–
Na	–	–	–	–	–	–	–	–	–	–	–	–
Ti	–	–	–	–	–	–	–	–	–	–	–	–
Total	8.009	8.001	8.019	7.997	7.999	8.015	7.997	8.015	8.014	8.012	8.031	8.004

MICROPROBE ANALYSIS OF GARNET OF ALAKNANDA AND DHAULIGANGA VALLEYS

OXIDES/ ELEMENTS	AG2-5			AG6-7			MA39A			DL53-95			
	GARNET			GARNET			GARNET			GT 1	GT 2	GT 3	
	RIM			RIM			RIM			RIM		RIM	CORE
	WEIGHT%												
SiO2	**37.887**	**37.686**	**38.018**	**37.848**	**38.384**	**37.631**	**39.232**	**38.489**	**38.455**	**37.875**	**38.083**	**37.995**	**37.499**
Al2O3	20.939	20.669	20.879	20.773	20.702	20.686	21.226	21.072	21.028	21.492	21.911	21.574	21.472
FeO	29.269	28.480	29.081	31.721	31.748	31.958	31.965	31.669	31.386	29.452	29.834	28.899	30.555
MgO	2.732	2.433	2.562	3.258	3.395	3.501	4.686	4.788	4.798	4.854	4.919	5.822	4.785
MnO	8.476	8.723	8.368	5.070	4.998	4.786	4.617	4.460	4.244	1.740	1.385	1.276	1.521
CaO	1.485	1.363	1.442	1.244	1.349	1.269	0.992	0.973	1.060	3.189	3.183	3.072	3.083
K2O	–	–	–	–	–	–	–	–	–	–	–	–	–
Na2O	–	–	–	–	–	–	–	–	–	–	–	–	–
TiO2	–	–	–	–	–	–	–	–	–	–	–	–	–
Total	100.787	99.355	100.350	99.915	100.576	99.831	102.719	101.451	100.971	98.602	99.314	98.639	98.915
	CATIONS (BASED ON 12 OXYGEN)												
Si	**3.029**	**3.051**	**3.047**	**3.039**	**3.057**	**3.027**	**3.043**	**3.025**	**3.032**	**3.020**	**3.011**	**3.012**	**2.995**
Al	1.973	1.972	1.972	1.966	1.944	1.961	1.941	1.952	1.954	2.020	2.042	2.016	2.021
Fe	1.957	1.928	1.949	2.130	2.115	2.149	2.074	2.082	2.069	1.964	1.973	1.916	2.041
Mg	0.326	0.294	0.306	0.390	0.403	0.419	0.542	0.561	0.564	0.577	0.579	0.688	0.569
Mn	0.574	0.598	0.568	0.345	0.337	0.326	0.303	0.297	0.283	0.117	0.093	0.086	0.103
Ca	0.127	0.118	0.124	0.107	0.115	0.109	0.082	0.082	0.089	0.272	0.269	0.261	0.264
K	–	–	–	–	–	–	–	–	–	–	–	–	–
Na	–	–	–	–	–	–	–	–	–	–	–	–	–
Ti	–	–	–	–	–	–	–	–	–	–	–	–	–
Total	7.985	7.962	7.967	7.978	7.971	7.993	7.986	7.999	7.991	7.970	7.978	7.979	7.994

MICROPROBE ANALYSIS OF GARNET OF ALAKNANDA AND DHAULIGANGA VALLEYS

OXIDES/ CATIONS	H-1									
	GARNET 1			GARNET 1/1	GARNET 2					
	RIM			RIM	RIM			CORE		
	WEIGHT%									
SiO2	**38.622**	**38.674**	**38.822**	**38.599**	**38.774**	**38.346**	**38.574**	**38.983**	**38.572**	**39.192**	**38.945**
Al2O3	20.915	20.898	21.111	20.896	20.927	20.732	20.710	20.954	20.981	21.084	20.754
FeO	28.184	28.132	29.076	29.010	29.601	29.416	29.240	29.422	29.148	29.365	29.248
MgO	3.758	3.767	3.972	3.772	3.852	3.202	3.292	3.949	4.160	4.184	4.186
MnO	1.246	1.167	1.088	1.890	1.647	3.094	2.094	1.295	1.222	1.262	1.287
CaO	7.355	7.338	6.963	5.834	5.886	4.959	5.889	5.636	6.163	6.142	6.206
K2O	–	–	–	–	–	–	–	–	–	–	–
Na2O	–	–	–	–	–	–	–	–	–	–	–
TiO2	–	–	–	–	–	–	–	–	–	–	–
Total	100.080	99.977	101.031	100.001	100.685	99.748	99.799	100.239	100.245	101.229	100.627
	CATIONS (BASED ON 12 OXYGEN)										
Si	**3.042**	**3.047**	**3.033**	**3.049**	**3.046**	**3.054**	**3.061**	**3.065**	**3.036**	**3.052**	**3.054**
Al	1.942	1.941	1.944	1.946	1.938	1.946	1.937	1.942	1.946	1.935	1.918
Fe	1.857	1.854	1.900	1.917	1.945	1.959	1.941	1.934	1.919	1.912	1.918
Mg	0.441	0.442	0.462	0.444	0.451	0.380	0.389	0.463	0.488	0.486	0.489
Mn	0.083	0.078	0.072	0.126	0.109	0.209	0.141	0.086	0.081	0.083	0.085
Ca	0.621	0.620	0.583	0.494	0.495	0.423	0.501	0.475	0.519	0.512	0.521
K	–	–	–	–	–	–	–	–	–	–	–
Na	–	–	–	–	–	–	–	–	–	–	–
Ti	–	–	–	–	–	–	–	–	–	–	–
Total	7.986	7.982	7.995	7.977	7.985	7.972	7.970	7.964	7.991	7.981	7.987

MICROPROBE ANALYSIS OF GARNET OF ALAKNANDA AND DHAULIGANGA VALLEYS

OXIDES/ CATIONS	DL50-90						DL18-30A		
	GARNET 1			GARNET 2			GARNET		
	RIM			RIM			RIM		
	WEIGHT%								
SiO2	**37.768**	**37..148**	**37.182**	**37.942**	**36.745**	**37.117**	**37.896**	**38.013**	**37.552**
Al2O3	20.439	20.332	20.386	20.339	19.987	20.004	21.337	21.062	21.032
FeO	35.079	36.270	36.081	35.695	35.836	35.729	22.851	22.537	22.363
MgO	3.093	2.945	2.971	2.827	2.752	2.625	1.652	1.888	1.912
MnO	0.486	0.751	0.787	0.128	0.143	0.273	0.931	0.800	0.848
CaO	2.082	2.221	2.173	2.952	2.932	3.057	14.962	14.916	14.794
K2O	–	–	–	–	–	–	–	–	–
Na2O	–	–	–	–	–	–	–	–	–
TiO2	–	–	–	–	–	–	–	–	–
Total	98.946	99.667	99.581	99.884	98.395	98.806	99.629	99.217	98.502
	CATIONS (BASED ON 12 OXYGEN)								
Si	**3.057**	**3.012**	**3.015**	**3.052**	**3.017**	**3.032**	**2.993**	**3.009**	**2.996**
Al	1.950	1.943	1.948	1.928	1.934	1.926	1.987	1.965	1.978
Fe	2.374	2.459	2.447	2.401	2.460	2.441	1. 510	1.492	1.492
Mg	0.373	0.356	0.359	0.339	0.337	0.319	0.194	0.223	0.227
Mn	0.033	0.052	0.054	0.009	0.010	0.019	0.062	0.054	0.057
Ca	0.180	0.193	0.189	0.254	0.258	0.267	1.266	1.265	1.265
K	–	–	–	–	–	–	–	–	–
Na	–	–	–	–	–	–	–	–	–
Ti	–	–	–	–	–	–	–	–	–
Total	7.968	8.016	8.011	7.984	8.016	8.005	8.013	8.008	8.015

MICROPROBE ANALYSIS OF GARNET OF ALAKNANDA AND DHAULIGANGA VALLEYS

OXIDES/ CATIONS	AG2-1										
	GARNET 1					GARNET 2		GARNET 3			
	RIM										
	WEIGHT%										
SiO2	**38.684**	38.996	37.946	36.807	38.505	38.474	**37.593**	**39.041**	**37.176**	**38.162**	**37.785**
Al2O3	20.091	20.239	20.162	20.665	20.183	20.620	20.495	20.177	20.493	20.717	19.934
FeO	30.189	30.754	30.948	30.554	30.418	31.779	29.775	31.461	28.967	29.345	29.244
MgO	1.924	2.014	1.929	2.112	2.180	2.323	2.342	2.208	1.474	1.584	1.453
MnO	1.061	1.741	2.073	1.733	1.536	1.553	1.488	1.537	2.658	2.647	2.821
CaO	8.648	8.250	7.471	8.075	8.697	7.395	7.729	7.260	9.651	9.767	9.523
K2O	–	–	–	–	–	–	–	–	–	–	–
Na2O	–	–	–	–	–	–	–	–	–	–	–
TIO2	–	–	–	–	–	–	–	–	–	–	–
Total	101.142	101.993	100.530	99.946	101.519	102	99.424	101.684	100.418	102.223	100.760
	CATIONS (BASED ON 12 OXYGEN)										
Si	**3.061**	3.062	**3.034**	**2.965**	**3.040**	**3.024**	**3.020**	**3.073**	**2.982**	**3.002**	**3.022**
Al	1.874	1.873	1.900	1.962	1.878	1.910	1.941	1.872	1.937	1.921	1.879
Fe	1.998	2.019	2.070	2.058	2.008	2.089	2.000	2.071	1.943	1.930	1.956
Mg	0.227	0.236	0.230	0.254	0.257	0.272	0.280	0.259	0.176	0.186	0.173
Mn	0.108	0.116	0.140	0.118	0.103	0.103	0.101	0.103	0.181	0.176	0.191
Ca	0.733	0.694	0.640	0.697	0.736	0.623	0.665	0.612	0.829	0.823	0.816
K	–	–	–	–	–	–	–	–	–	–	–
Na	–	–	–	–	–	–	–	–	–	–	–
Ti	–	–	–	–	–	–	–	–	–	–	–
Total	8.001	8.001	8.015	8.054	8.021	8.021	8.010	7.991	8.049	8.038	8.038

APPENDIX-II

MICROPROBE ANALYSIS OF BIOTITE OF ALAKNANDA AND DHAULIGANGA VALLEYS

OXIDES/ CATIONS	DL25-44-C1	DL22-40-C3	AG1-4-C2	DL36-63-C4	DL16-28-C2	DL2-4-C2
	BITITE	BIOTITE	BIOTIE	BIOTITE	BIOTITE	BIOTITE
	RIM	RIM	RIM	RIM	RIM	RIM

WEIGHT%

SiO2	**36.045**	**36.553**	**36.183**	**37.458**	**36.709**	**34.091**	**34.474**	**36.269**	**36.062**	**35.915**	**36.217**	**35.868**	**34.267**	**33.817**
Al2O3	17.775	17.821	17.639	17.605	17.633	17.226	16.359	18.032	18.127	18.431	18.729	18.561	16.403	16.639
FeO	16.695	16.857	16.725	18.476	19.055	24.810	24.700	23.806	23.585	16.603	16.979	16.782	22.546	22.533
MgO	11.394	11.084	11.233	10.147	9.797	5.173	5.145	07.463	07.719	11.126	10.835	11.053	5.271	5.345
MnO	0.144	0.157	0.138	0.089	0.082	0.052	0.092	00.051	00.048	0.027	0.055	0.073	0.039	0.050
CaO	0.094	0.046	0.064	_	0.044	0.098	0.061	00.032	00.032	0.008	0.046	0.009	0.014	0.019
K2O	9.028	8.0125	9.723	9.580	9.148	9.675	9.700	09.381	09.454	9.019	7.960	9.056	9.771	9.844
Na2O	0.219	0.178	0.258	0.249	0.312	0.048	0.314	00.091	00.116	0.246	0.273	0.265	0.388	0.000
TiO2	1.768	20.009	1.957	2.945	2.985	4.658	4.259	01.063	01.368	2.019	2.091	1.809	2.485	2.208
Total	93.163	92.831	93.920	96.550	95.764	95.830	95.102	96.729	96.511	93.393	93.185	93.476	91.186	90.456

CATIONS (BASED ON 22 OXYGEN)

Si	**5.533**	**5.592**	**5.533**	**5.588**	**5.536**	**5.339**	**5.447**	**5.541**	**5.522**	**5.489**	**5.515**	**5.484**	**5.599**	**5.572**
Al	3.216	3.214	3.179	3.096	3.134	3.180	3.047	3.247	3.272	3.320	3.361	3.345	3.159	3.231
Fe	2.143	2.157	2.139	2.305	2.403	3.250	3.264	3.041	3.020	2.122	2.162	2.146	3.081	3.105
Mg	2.607	2.528	2.561	2.257	2.203	1.208	1.212	1.700	1.762	2.535	2.459	2.519	1.284	1.313
Mn	0.019	0.020	0.018	0.011	0.011	0.007	0.012	0.007	0.006	0.004	0.007	0.009	0.005	0.007
Ca	0.016	0.008	0.010	_	0.007	0.017	0.010	0.005	0.005	0.001	0.008	0.002	0.003	0.003
K	1.768	1.586	1.897	1.823	1.760	1.933	1.955	1.828	1.847	1.758	1.546	1.767	2.037	2.069
Na	0.065	0.053	0.077	0.072	0.091	0.014	0.096	0.027	0.034	0.073	0.081	0.079	0.123	-------
Ti	0.204	0.231	0.225	0.330	0.339	0.549	0.506	0.184	0.158	0.232	0.240	0.208	0.305	0.274
Total	15.571	15.389	15.639	15.482	15.484	15.423	15.549	15.580	15.626	15.534	15.379	15.558	15.596	15.574

MICROPROBE ANALYSIS OF BIOTITE OF ALAKNANDA AND DHAULIGANGA VALLEYS

OXIDES/ CATIONS	AG11-14-C2 BIOTITE RIM	AG14-18-C4 BIOTITE RIM	AG14-18-C4 BIOTITE CORE	AG15-21-C4 BIOTITE RIM	AG15-21-C4 BIOTITE CORE	AG17-25 BIOTITE RIM					
WEIGHT%											
SiO2	**34.056**	**35.109**	**34.129**	**34.360**	**35.312**	**34.313**	**34.858**	**34.830**	**35.012**	**34.126**	**35.260**	**34.138**	**35.357**
Al2O3	17.775	18.784	18.349	18.465	18.751	18.263	18.807	17.812	18.408	17.592	18.309	18.704	18.103
FeO	20.502	21.590	22.389	22.543	21.067	21.298	22.441	22.840	21.560	23.534	23.954	23.432	23.523
MgO	6.967	7.313	6.389	6.487	7.891	7.833	6.232	5.772	5.598	5.528	5.425	5.310	5.253
MnO	0.175	0.250	6.347	0.182	0.102	0.131	0.245	0.224	0.154	0.162	0.176	0.166	0.190
CaO	0.021	0.037	0.147	0.026	0.014	_	_	0.024	0.018	0.001	0.007	0.017	0.015
K2O	11.307	11.880	0.086	9.707	9.738	9.815	12.544	12.336	12.317	11.961	9.999	9.884	9.820
Na2O	0.120	0.247	9.611	0.263	0.342	0.294	0.352	0.255	0.205	0.073	0.055	0.079	0.403
TiO2	1.662	1.903	0.298	3.478	3.143	3.207	2.153	2.331	3.704	3.374	4.005	3.730	3.910
Total	92.586	97.112	94.794	95.511	96.359	95.154	97.631	96.423	96.976	96.350	97.190	95.460	96.575
CATIONS (BASED ON 22 OXYGEN)													
Si	**5.466**	**5.389**	**5.337**	**5.333**	**5.375**	**5.321**	**5.370**	**5.446**	**5.397**	**5.355**	**5.401**	**5.326**	**5.442**
Al	3.363	3.399	3.382	3.379	3.364	3.338	3.415	3.283	3.345	3.254	3.306	3.440	3.284
Fe	2.752	2.772	2.928	2.926	2.682	2.762	2.891	2.987	2.779	3.089	3.069	3.057	3.028
Mg	1.667	1.673	1.480	1.501	1.791	1.811	1.431	1.345	1.286	1.293	1.239	1.235	1.025
Mn	0.024	0.033	0.019	0.024	0.013	0.017	0.032	0.030	0.020	0.022	0.023	0.022	0.025
Ca	0.004	0.006	0.014	0.004	0.002	_	_	0.004	0.003	0.000	0.001	0.003	0.003
K	2.315	2.327	1.917	1.922	1.891	1.942	2.465	2.461	2.422	2.395	1.954	1.967	1.928
Na	0.037	0.073	0.090	0.079	0.101	0.089	0.105	0.077	0.061	0.022	0.016	0.024	0.120
Ti	0.201	0.220	0.404	0.406	0.360	0.374	0.250	0.274	0.429	0.398	0.461	0.438	0.453
Total	15.828	15.892	15.572	15.573	15.579	15.652	15.961	15.907	15.743	15.828	15.470	15.512	15.488

MICROPROBE ANALYSIS OF BIOTITE OF ALAKNANDA AND DHAULIGANGA VALLEYS

OXIDES/ ELEMENTS	DL18-31-C1			DL36-63-C4			DL41-71-C1			DL32-56		AL5-11	
	BIOTITE			BIOTITE			BIOTITE			BT 1	BT 2	BT 1	BT 2
	RIM			RIM			RIM			RIM		RIM	
	WEIGHT%												
SiO2	**37.745**	**37.932**	**37.487**	**36.269**	**36.321**	**36.062**	**37.736**	**37.472**	**37.392**	**33.529**	**34.359**	**34.558**	**34.599**
Al2O3	18.809	18.504	18.236	18.032	17.806	18.127	18.204	18.218	18.115	16.539	17.928	18.819	19.326
FeO	12.840	13.024	12.674	23.806	23.281	23.585	18.475	18.148	18.553	25.751	26.191	21.391	20.502
MgO	14.738	14.833	14.461	7.463	7.806	7.719	10.412	10.037	10.527	5.203	5.554	6.596	6.508
MnO	0.033	0.022	0.023	0.051	0.068	0.048	0.191	0.219	0.168	0.378	0.305	0.098	0.112
CaO	0.055	0.041	0.086	0.032	0.007	0.032	0.053	0.077	0.053	0.076	0.135	0.015	0.092
K2O	8.340	7.550	7.944	9.381	9.411	9.454	9.215	9.412	9.519	9.044	9.068	9.268	9.153
Na2O	0.472	0.452	0.497	0.091	0.448	0.116	0.287	0.255	0.279	0.282	0.270	0.192	0.225
TiO2	1.152	1.146	1.181	1.603	1.541	1.368	1.869	1.909	1.856	4.343	2.681	4.825	4.666
Total	94.185	93.504	92.590	96.729	96.688	96.511	96.443	95.746	96.461	95.145	96.495	95.762	95.181
	CATIONS (BASED ON 22 OXYGEN)												
Si	**5.571**	**5.615**	**5.617**	**5.540**	**5.547**	**5.522**	**5.616**	**5.620**	**5.583**	**5.323**	**5.357**	**5.296**	**5.305**
Al	3.272	3.228	3.221	3.247	3.205	3.272	3.193	3.221	3.188	3.095	3.295	3.399	3.493
Fe	1.585	1.612	1.588	3.041	2.974	3.020	2.299	2.276	2.317	3.419	3.416	2.741	2.629
Mg	3.243	3.273	3.230	1.699	1.777	1.762	2.310	2.244	2.343	1.232	1.291	1.506	1.487
Mn	0.004	0.003	0.003	0.007	0.009	0.006	0.024	0.028	0.021	0.051	0.040	0.013	0.014
Ca	0.009	0.006	0.014	0.005	0.001	0.005	0.008	0.012	0.008	0.013	0.023	0.002	0.151
K	1.570	1.426	1.519	1.828	1.834	1.847	1.750	1.801	1.813	1.832	1.804	1.812	1.790
Na	0.135	0.129	0.144	0027	0.133	0.034	0.083	0.074	0.081	0.087	0.082	0.057	0.067
Ti	0.128	0.128	0.133	0.184	0.177	0.157	0.209	0.215	0.208	0.518	0.314	0.556	0.538
Total	15.518	15.421	15.470	15.579	15.656	15.625	15.494	15.492	15.562	15.570	15.623	15.383	15.339

MICROPROBE ANALYSIS OF BIOTITE OF ALAKNANDA AND DHAULIGANGA VALLEYS

OXIDES/ ELEMENTS	AL6-16		MA23-35							DL53-95			
	BT 1	BT 2	BIOTITE 1			BIOTITE 2			BIOTITE 1/1	BT 1	BT 2	BT 3	
	RIM	RIM	RIM			RIM			RIM	RIM	RIM	RIM	CORE
						WEIGHT%							
SiO2	34.185	**34.967**	35.0791	**30.430**	32.627	38.688	**37.412**	**38.400**	**33.498**	**32.954**	**37.392**	**37.102**	**37.129**	**37.092**
Al2O3	18.771	20.080	25.936	34.838	28.534	19.349	22.177	20.182	27.452	29.171	19.142	18.596	19.148	19.223
FeO	18.390	16.990	14.379	12.260	14.074	14.889	14.445	14.794	13.375	13.846	16.371	16.077	12.122	16.198
MgO	10.153	9.703	11.648	10.109	11.037	13.068	12.759	13.218	11.375	11.565	13.784	13.134	15.190	13.817
MnO	0.0183	0.196	0.042	0.068	0.061	0.094	0.056	0.083	0.049	0.067	0.072	0.037	0.032	0.133
CaO	0.015	0.025	0.154	0.237	0.196	0.025	0.185	0.038	0.275	0.207	0.027	0.045	0.106	0.019
K2O	9.104	9.534	7.034	6.541	7.464	7.632	7.571	7.964	6.679	5.806	8.938	8.908	8.355	8.869
Na2O	0.82	0.176	0.315	0.308	0.325	0.347	0.350	0.361	0.358	0.302	0.392	0.279	0.570	0.269
TiO2	2.392	2.739	1.554	0.924	1.380	1.255	1.325	1.300	1.434	1.364	2.268	2.727	2.427	1.953
Total	93.276	64.410	96.853	95.715	95.698	95.346	96.280	96.340	94.587	95.283	98.386	96.905	95.079	97.552
						CATIONS (BASED ON 22 OXYGEN)								
Si	5.307	**5.3171**	**5.108**	**4.348**	4.743	5.647	**5.396**	**5.556**	4.885	**4.750**	**5.396**	**5.433**	**5.425**	**5.394**
Al	3.434	3.599	4.363	5.868	4.889	3.329	3.770	3.442	4.719	4.956	3.256	3.209	3.298	3.294
Fe	2.388	2.161	1.716	1.465	1.711	1.817	1.742	1.790	1.643	1.669	1.976	1.969	1.481	1.970
Mg	2.349	2.199	2.478	2.153	2.392	2.844	2.743	2.851	2.473	2.485	2.965	2.867	3.308	2.995
Mn	0.024	0.025	0.005	0.008	0.007	0.012	0.007	0.010	0.006	0.008	0.009	0.004	0.004	0.014
Ca	0.002	0.004	0.024	0.036	0.030	0.004	0.028	0.006	0.043	0.032	0.004	0.007	0.017	0.003
K	1.803	1.085	1.281	1.192	1.384	1.421	1.393	1.470	1.273	1.068	1.645	1.664	1.558	1.645
Na	0.025	0.052	0.087	0.085	0.091	0.098	0.098	0.101	0.101	0.084	0.109	0.079	0.161	0.076
Ti	0.279	0.313	0.167	0.099	0.151	0.138	0.144	0.141	0.157	0.148	0.246	0.300	0.267	0.213
Total	15.611	15.521	15.228	15.257	15.399	15.310	15.321	15.367	15.270	15.200	15.607	15.534	15.519	15.606

MICROPROBE ANALYSIS OF BIOTITE OF ALAKNANDA AND DHAULIGANGA VALLEYS

OXIDES/ ELEMENTS	AG6-7			MA39A			DL50-90						AG2-5		
	BIOTITE			BIOTITE			BIOTITE 1			BIOTITE 2			BIOTITE		
	RIM			RIM			RIM			RIM			RIM		
	WEIGHT%														
SiO2	**36.664**	**39.079**	**36.849**	**36.713**	**36.872**	**37.438**	**36.747**	**37.652**	**36.484**	**37.261**	**37.404**	**37.825**	**36.019**	**37.220**	**37.593**
Al2O3	19.659	20.360	19.546	19.699	19.849	19.654	18.384	18.660	18.471	18.400	18.435	18.419	18.761	19.019	19.339
FeO	18.928	19.323	18.411	15.571	15.480	14.738	17.778	18.361	17.585	17.805	17.958	17.615	18.742	18.506	18.600
MgO	9.3434	9.454	9.390	12.266	12.206	12.174	11.192	11.280	11.177	10.757	11.028	11.264	9.452	9.590	9.717
MnO	0.136	0.151	0.109	0.079	0.111	0.081	0.008	0.005	0.025	0.008	0.021	0.056	0.289	0.239	0.171
CaO	0.044	0.054	_	0.032	0.021	0.044	0.023	0.066	0.022	0.020	0.033	0.051	0.032	0.025	0.018
K2O	9.628	2.3270	9.681	9.055	9.261	9.220	8.446	7.864	8.433	7.260	7.522	7.608	9.762	7.746	7.718
Na2O	0.008	_	0.016	0.548	0.497	0.477	0.362	0.506	0.455	0.403	0.423	0.451	0.282	0.271	0.232
TiO2	2.780	2.546	2.660	1.216	1.587	10.784	1.275	1.322	1.267	1.639	1.656	1.548	3.005	3.401	3.526
Total	97.283	93.294	96.662	95.178	95.885	95.610	94.216	95.714	93.919	93.554	94.481	94.837	96.344	96.018	96.914
	CATIONS (BASED ON 22 OXYGEN)														
Si	**5.433**	**5.735**	**5.479**	**5.465**	**5.449**	**5.519**	**5.566**	**5.596**	**5.544**		**5.613**	**5.643**	**5.417**	**5.518**	**5.512**
Al	3.34	3.522	3.426	3.456	3.457	3.415	3.282	3.268	3.309	3.279	3.261	3.239	3.326	3.323	3.342
Fe	2.346	2.372	2.289	1.938	1.913	1.817	2.252	2.282	2.235	2.512	2.254	2.198	2.357	2.295	2.281
Mg	2.084	2.068	2.082	2.722	2.689	2.675	2.527	2.499	2.532	2.425	2.467	2.505	2.119	2.119	2.124
Mn	0.017	0.019	0.014	0.010	0.014	0.010	0.001	0.001	0.003	0.001	0.003	0.007	0.037	0.030	0.021
Ca	0.007	0.008	_	0.005	0.003	0.007	0.004	0.010	0.004	0.003	0.005	0.008	0.005	0.004	0.002
K	1.820	0.436	1.837	1.719	1.746	1.734	1.632	1.491	1.635	1.400	1.440	1.448	1.873	1.465	1.444
Na	0.002	_	0.004	0.158	0.142	0.136	0.106	0.146	0.134	0.118	0.123	0.130	0.082	0.077	0.066
Ti	0.309	0.281	0.297	0.136	0.176	0.198	0.145	0.148	0.145	0.186	0.187	0.174	0.340	0.379	0.389
Total	15.452	14.441	15.430	15.609	15.590	15.511	15.517	15.441	15.541	15.299	15.352	15.353	15.557	15.212	15.182

MICROPROBE ANALYSIS OF BIOTITE OF ALAKNANDA AND DHAULIGANGA VALLEYS

OXIDES/ CATIONS	H-1										DL18-30A		
	BIOTITE 1		BIOTITE 1/1		BIOTITE 2						BIOTITE		
	RIM		RIM		RIM			CORE			RIM		
	WEIGHT%												
SiO2	**36.562**	**36.787**	**36.641**	**36.294**	**36.086**	36.209	36.948	36.884	**37.875**	**37.725**	**37.694**	**35.758**	**36.167**	**35.875**
Al2O3	17.804	17.691	17.828	16.889	16.987	17.800	18.254	18.114	17.332	17.280	17.387	17.146	17.017	17.105
FeO	17.097	17.234	16.706	17.472	16.933	16.700	16.896	17.065	13.923	13.792	13.823	20.192	20.093	19.982
MgO	10.659	10.542	10.530	10.430	10.536	10.700	11.063	10.858	12.878	12.767	12.682	9.208	9.230	9.161
MnO	0.120	0.101	0.119	0.137	0.159	0.134	0.092	0.090	_	0.014	0.033	0.269	0.227	0.262
CaO	0.032	0.044	0.029	0.133	0.131	0.043	0.040	0.059	0.062	0.071	0.052	0.020	0.014	0.024
K2O	9.188	9.584	9.642	9.384	9.373	9.593	9.613	9.700	9.106	9.088	9.049	10.287	10.293	10.167
Na2O	0.332	0.317	0.270	0.349	0.366	0.336	0.320	0.336	0.333	0.310	0.3320	0.148	0.123	0.168
TiO2	2.609	2.630	2.618	2.749	2.703	2.328	2.237	2.473	2.505	2.214	2.166	2.543	2.489	2.520
Total	94.403	94.929	94.384	93.835	93.272	63.572	95.463	95.573	94.014	93.261	93.388	95.570	95.653	95.262
	CATIONS (BASED ON 22 OXYGEN)													
Si	**5.546**	**5.563**	**5.561**	**5.571**	5.562	5.544	5.540	**5.534**	**5.661**	**5.681**	**5.668**	**5.493**	**5.540**	**5.517**
Al	3.183	3.153	3.189	3.055	3.086	3.212	3.226	3.204	3.053	3.067	3.082	3.104	3.072	3.101
Fe	2.369	2.179	2.120	2.243	2.182	2.103	2.119	2.141	1.740	1.737	1.739	2.594	2.574	2.570
Mg	2.410	2.376	2.382	2.386	2.420	2.442	2.473	2.429	2.869	2.866	2.883	2.108	2.108	2.100
Mn	0.015	0.013	0.015	0.018	0.021	0.017	0.012	0.011	_	0.002	0.004	0.035	0.029	0.034
Ca	0.005	0.007	0.005	0.022	0.022	0.007	0.006	0.009	0.010	0.011	0.008	0.003	0.002	0.004
K	1.778	1.849	1.867	1.837	1.840	1.874	1.839	1.857	1.736	1.746	1.736	2.016	2.011	1.995
Na	0.098	0.093	0.079	0.104	0.109	0.099	0.093	0.098	0.097	0.091	0.093	0.044	0.036	0.050
Ti	0.298	0.299	0.299	0.317	0.313	0.2681	0.252	0.279	0.281	0.251	0.245	0.294	0.287	0.291
Total	15.502	15.533	15.518	15.555	15.558	15.569	15.561	15.562	15.448	15.452	15.460	15.691	15.661	15.663

MICROPROBE ANALYSIS OF BIOTITE OF ALAKNANDA AND DHAULIGANGA VALLEYS

OXIDES/ CATIONS	AG2-1						
	BIOTITE 1			BIOTITE 2			
	RIM						
	WEIGHT%						
SiO2	**36.442**	35.192	**35.290**	**35.844**	**36.299**	**34.449**	**35.783**
Al2O3	16.025	15.789	16.313	15.098	14.913	15.902	16.380
FeO	25.895	25.240	25.055	25.033	24.089	25.138	23.701
MgO	5.932	6.516	6.053	7.047	7.135	7.001	7.276
MnO	0.147	0.165	0.139	0.054	0.067	0.105	0.075
CaO	0.012	0.008	0.003	0.022	0.018	0.53	0.052
K2O	9.783	9.992	9.576	9.494	9.498	9.662	9.328
Na2O	0.057	–	0.180	0.104	0.206	–	–
TIO2	2.727	2.603	2.673	2.636	2.524	2.425	2.913
Total	97.021	95.504	95.281	95.333	94.748	94.735	95.509
	CATIONS (BASED ON 22 OXYGEN)						
Si	**5.636**	5.548	**5.552**	**5.632**	**5.709**	**5.475**	**5.558**
Al	2.921	2.934	3.025	2.796	2.765	2.979	2.999
Fe	3.349	3.328	3.297	3.289	3.169	3.341	3.079
Mg	1.367	1.531	1.419	1.651	1.673	1.659	1.685
Mn	0.019	0.022	0.018	0.007	0.009	0.014	0.009
Ca	0.002	0.001	0.001	0.004	0.003	0.009	0.008
K	1.930	2.009	1.922	1.903	1.906	1.959	1.848
Na	0.017	–	0.055	0.032	0.063	–	–
Ti	0.317	0.308	0.316	0.311	0.298	0.290	0.340
Total	15.560	15.682	15.607	15.626	15.594	15.725	15.527

APPENDIX-III

MICROPROBE ANALYSIS OF MUSCOVITE OF ALAKNANDA AND DHAULIGANGA VALLEYS

OXIDES/ CATIONS	DL25-44-C1	DL22-40-C3	AG1-4-C2	DL36-63-C4	DL16-28-C2						DL2-4-C2	
	MUSCOVITE	MUSCOVITE	MUSCOVITE	MUSCOVITE	MUSCOVITE						MUSCOVITE	
	RIM	RIM	RIM	RIM	RIM						RIM	
	WEIGHT%											
SiO2	**49.649**	**47.817**	**51.032**	**52.050**	**51.765**	**48.089**	**50.102**	**47.787**	**47.029**	**48.666**	**48.371**	**50.145**	**48.929**	**44.015**
Al2O3	33.485	32.932	34.366	34.980	34.603	35.477	35.876	34.811	35.690	34.251	33.695	35.438	33.385	34.270
FeO	1.813	1.820	1.830	1.706	1.991	1.320	1.420	2.078	1.897	1.458	1.381	1.285	1.409	1.441
MgO	1.555	1.515	1.710	1.134	1.207	0.316	0.341	0.851	0.653	0.993	1.071	0.937	0.426	0.546
MnO	0.008	0.004	_	0.019	0.011	0.056	0.032	0.018	0.005	0.020	0.028	_	0.002	0.028
CaO	0.037	0.26	0.054	0.045	0.075	0.036	0.059	0.034	0.043	0.084	0.227	0.017	0.037	0.033
K2O	7.366	8.811	4.110	4.108	4.612	7.626	6.079	9.806	9.594	6.571	6.932	4.544	2.222	7.638
Na2O	0.403	0.410	0.265	0.495	0.459	_	0.073	0.210	0.315	0.827	0.806	0.709	0.050	_
TiO2	0.485	0.485	0.458	1.222	1.246	0.909	0.990	0.340	0.448	1.198	1.212	1.128	0.923	0.922
Total	94.799	93.820	93.826	95.760	95.968	93.829	94.972	95.935	95.675	94.067	93.724	94.204	87.383	88.892
	CATIONS (BASED ON 22 OXYGEN)													
Si	**6.494**	**6.398**	**6.584**	**6.579**	**6.563**	**6.343**	**6.451**	**6.290**	**6.200**	**6.392**	**6.397**	**6.462**	**6.661**	**6.169**
Al	5.162	5.194	5.226	5.211	5.171	5.516	5.445	5.401	5.546	5.303	5.252	5.383	5.357	5.662
Fe	0.198	0.204	0.198	0.180	0.211	0.146	0.153	0.229	0.209	0.160	0.153	0.139	0.160	0.169
Mg	0.303	0.302	0.329	0.214	0.228	0.062	0.065	0.167	0.128	0.194	0.211	0.180	0.087	0.114
Mn	0.001	0.000	_	0.002	0.001	0.006	0.004	0.002	0.001	0.002	0.003	_	0.001	0.003
Ca	0.005	0.004	0.007	0.006	0.010	0.005	0.008	0.005	0.006	0.012	0.032	0.002	0.006	0.005
K	1.229	1.504	0.676	0.663	0.746	1.283	0.999	1.647	1.614	1.101	1.171	0.747	0.385	1.366
Na	0.102	0.106	0.066	0.121	0.113	_	0.018	0.536	0.081	0.211	0.207	0.177	0.013	_
Ti	0.048	0.049	0.044	0.116	0.119	0.090	0.096	0.034	0.046	0.118	0.121	0.109	0.095	0.097
Total	13.543	13.761	13.130	13.092	13.162	13.451	13.239	13.827	13.829	13.494	13.545	13.199	12.765	13.585

MICROPROBE ANALYSIS OF MUSCOVITE OF ALAKNANDA AND DHAULIGANGA VALLEYS

OXIDES/ CATIONS	AG11-14-C2	AG14-18-C4	AG14-18-C4	AG15-21-C4	AG15-21-C4	AG17-25						
	MUSCOVITE	MUSCOVITE	MUSCOVITE	MUSCOVITE	MUSCOVITE	MUSCOVITE						
		RIM	CORE	RIM	CORE	RIM						
					WEIGHT%							
SiO2	**47.594**	**46.712**	**48.461**	**48.594**	**48.242**	**47.850**	**44.044**	**44.074**	**45.084**	**44.646**	**47.673**	**47.043**	**48.345**
Al2O3	35.272	35.727	35.481	35.826	35.976	35.559	35.463	35.805	35.173	36.217	34.299	34.139	35.560
FeO	0.968	1.107	1.428	1.468	1.325	1.329	1.836	1.286	1.508	1.561	1.381	1.377	1.404
MgO	0.380	0.720	0.583	0.591	0.639	0.681	0.411	0.470	0.351	0.327	0.496	0.392	0.508
MnO	0.051	0.014	0.036	0.019	0.035	0.012	0.044	0.012	0.037	0.057	0.019	0.014	0.021
CaO	0.006	0.015	0.016	0.020	0.025	0.001	0.034	0.020	0.007	0.003	0.020	0.027	0.015
K2O	10.890	10.450	9.225	8.958	8.330	8.128	11.902	12.208	12.578	12.550	9.273	9.352	9.285
Na2O	0.007	_	0.732	0.599	0.702	0.600	_	0.222	0.391	0.314	0.071	0.026	0.205
TiO2	0.441	0.523	0.803	0.784	0.921	1.040	0.390	0.523	0.871	0.861	1.062	1.072	1.093
Total	95.611	95.267	96.766	96.857	96.195	95.199	94.124	94.619	96.000	96.537	94.294	93.441	96.436
					CATIONS (BASED ON 22 OXYGEN)								
Si	**6.285**	**6.188**	**6.287**	**6.283**	**6.258**	**6.265**	**6.011**	**5.984**	**6.052**	**5.961**	**6.337**	**6.318**	**6.283**
Al	5.490	5.579	5.426	5.460	5.501	5.488	5.705	5.730	5.565	5.700	5.374	5.404	5.447
Fe	0.107	0.123	0.155	0.159	0.144	0.146	0.210	0.146	0.169	0.174	0.154	0.155	0.153
Mg	0.075	0.142	0.113	0.114	0.124	0.133	0.084	0.095	0.070	0.065	0.098	0.078	0.098
Mn	0.006	0.002	0.004	0.002	0.004	0.001	0.005	0.001	0.004	0.007	0.002	0.016	0.002
Ca	0.001	0.002	0.002	0.003	0.004	0.000	0.005	0.003	0.001	0.001	0.003	0.004	0.002
K	1.835	1.766	1.527	1.478	1.379	1.358	2.072	2.115	2.154	2.138	1.573	1.602	1.539
Na	0.002	_	0.184	0.150	0.177	0.152	_	0.059	0.102	0.081	0.018	0.007	0.052
Ti	0.044	0.052	0.078	0.076	0.090	0.102	0.040	0.053	0.088	0.086	0.106	0.108	0.107
Total	13.845	13.854	13.777	13.725	13.679	13.644	14.132	14.185	14.206	14.212	13.665	13.677	13.6827

MICROPROBE ANALYSIS OF MUSCOVITE OF ALAKNANDA AND DHAULIGANGA VALLEYS

OXIDES/ ELEMENTS	DL36-63-C4			DL41-71-C1			MA23-35					DL32-56	
	MUSCOVITE			MUSCOVITE			MUSCOVITE 1			MUSCOVITE 2		MS 1	MS 2
	RIM			RIM			RIM			RIM		RIM	
	WEIGHT%												
SiO2	**47.787**	**47.729**	**47.029**	**49.586**	**48.910**	**51.123**	**43.833**	**42.375**	45.738	**47.319**	**47.281**	**48.109**	**45.150**	**45.638**
Al2O3	34.811	34.739	35.690	33.091	32.631	34.032	35.847	37.380	37.353	35.164	34.810	37.001	33.795	32.795
FeO	2.078	2.735	1.897	1.714	1.605	1.723	1.121	1.224	1.055	0.774	0.865	0.724	2.163	2.536
MgO	0.851	0.762	0.653	1.462	1.462	1.514	0.675	0.734	0.759	0.620	0.725	0.685	0.634	0.812
MnO	0.018	0.023	0.005	0.009	_	0.042	0.025	0.039	0.016	0.030	0.009	0.002	0.043	0.30
CaO	0.034	0.043	0.043	0.060	0.068	0.092	0.104	0.220	0.124	0.032	0.042	0.080	0.064	0.039
K2O	9.806	9.599	9.594	8.502	8.999	6.481	8.954	8.658	8.478	8.431	8.482	7.497	10.718	10.427
Na2O	0.210	0.195	0.315	0.436	0.401	0.265	1.307	1.363	1.371	1.826	1.777	1.287	0.494	0.388
TiO2	0.340	0.449	0.448	0.327	0.337	0.411	0.230	0.379	0.453	0.534	0.653	0.482	0.552	0.422
Total	95.935	96.274	95.675	95.187	94.414	95.684	92.095	92.372	95.346	94.730	94.644	95.866	92.688	93.087
	CATIONS (BASED ON 22 OXYGEN)													
Si	**6.289**	**6.274**	**6.200**	**6.505**	**6.492**	**6.567**	**6.010**	5.803	6.022	**6.256**	**6.263**	**6.222**	**5.323**	**6.2628**
Al	5.401	5.383	5.546	5.117	5.105	5.153	5.794	6.034	5.797	5.480	5.435	5.640	3.095	5.304
Fe	0.229	0.301	0.209	0.188	0.178	0.185	0.129	0.140	0.116	0.086	0.096	0.078	3.419	0.291
Mg	0.167	0.149	0.128	0.286	0.289	0.290	0.138	0.149	0.149	0.1222	0.143	0.132	1.232	0.166
Mn	0.002	0.003	0.001	0.001	_	0.005	0.003	0.004	0.002	0.003	0.001	0.000	0.051	0.003
Ca	0.005	0.006	0.006	0.008	0.009	0.013	0.015	0.032	0.17	0.004	0.006	0.011	0.013	0.006
K	1.647	1.610	1.614	1.423	1.524	1.062	1.566	1.513	1.424	1.422	1.433	1.237	1.832	1.825
Na	0.054	0.049	0.081	0.111	0.103	0.066	0.348	0.362	0.350	0.468	0.456	0.323	0.087	0.103
Ti	0.034	0.044	0.044	0.032	0.034	0.039	0.024	0.039	0.045	0.053	0.065	0.047	0.519	0.043
Total	13.826	13.819	13.829	13.671	13.735	13.681	14.026	14.078	13.922	13.895	13.900	13.691	15.5702	14.006

MICROPROBE ANALYSIS OF MUSCOVITE OF ALAKNANDA AND DHAULIGANGA VALLEYS

OXIDES/ ELEMENTS	AL5-11		AL6-16		AG2-5	DL53-95		
	MS 1	MS 2	MS 1	MS 2	MUSCOVITE	MS 1	MS 2	MS 3
	RIM		RIM		RIM	RIM	RIM	RIM
	WEIGHT%							
SiO2	**45.206**	**45.826**	45.986	**45.219**	**50.562**	**50.581**	**5.620**	**48.569**	**46.232**	**45.797**
Al2O3	33.946	34.866	34.924	34.395	36.148	35.810	36.289	34.016	34.992	34.444
FeO	1.290	1.027	1.160	0.904	1.294	1.272	1.275	1.077	1.136	1.409
MgO	0.676	0.462	0.687	0.651	0.675	0.723	0.680	0.884	0.912	1.004
MnO	0.000	0.007	0.018	0.013	0.031	0.043	0.012	0.033	0.000	0.007
CaO	0.033	0.000	0.043	0.032	0.004	0.095	0.040	0.135	0.011	0.072
K2O	10.406	10.396	10.318	10.422	4.819	4.792	4.968	9.214	9.439	9.433
Na2O	0.645	0.655	0.631	0.597	0.300	0.385	0.344	1.115	1.124	1.013
TiO2	1.589	1.446	0.539	0.985	0.800	0.830	0.860	1.090	0.911	0.692
Total	93.790	94.686	94.304	93.220	94.634	94.531	95.058	96.133	94.756	93.872
	CATIONS (BASED ON 22 OXYGEN)									
Si	**6.131**	**6.136**	6.177	**6.151**	**6.478**	**6.491**	**6.464**	**6.349**	**6.159**	**6.170**
Al	5.427	5.503	5.529	5.515	5.459	5.417	5.462	5.243	5.495	5.469
Fe	0.146	0.115	0.130	0.103	0.139	0.136	0.136	0.118	0.127	0.158
Mg	0.137	0.092	0.137	0.132	0.129	0.138	0.129	0.0172	0.181	0.202
Mn	0.000	0.001	0.002	0.001	0.003	0.005	0.001	0.004	0.000	0.001
Ca	0.005	0.000	0.006	0.005	0.001	0.013	0.005	0.019	0001	0.010
K	1.801	1.776	1.768	1.809	0.788	0.784	0.809	1.537	1.604	1.621
Na	0.169	0.170	0.164	0.157	0.074	0.096	0.085	0.0285	0.290	0.265
Ti	0.162	0.145	0.054	0.101	0.077	0.080	0.079	0.107	0.091	0.070
Total	13.978	13.939	13.969	13.974	13.077	13.161	13.173	13.831	13.949	13.968

MICROPROBE ANALYSIS OF MUSCOVITE OF ALAKNANDA AND DHAULIGANGA VALLEYS

OXIDES/ ELEMENTS	H-1						DL18-30A			DL50-90					
	MUSCOVITE 1			MUSCOVITE 2			MUSCOVITE			MUSCOVITE 1			MUSCOVITE 2		
	RIM			RIM			RIM			RIM			RIM		
	WEIGHT%														
SiO2	**44.982**	**47.735**	48.123	48.714	49.081	**49.055**	**48.978**	**51.858**	**48.789**	**47.020**	**50.032**	**48.230**	**50.803**	**50.387**	**51.120**
Al2O3	28.970	31.980	33.223	31.591	32.781	32.301	32.698	34.606	31.654	33.294	36.091	36.504	37.258	36.843	37.848
FeO	5.429	1.636	1.734	1.628	1.494	1.624	1.867	1.931	1.940	4.710	2.209	1.004	0.816	1.051	0.843
MgO	3.420	0.991	0.959	1.256	1.116	1.180	1.352	1.456	1.496	2.397	1.293	0.427	0.481	0.786	0.484
MnO	0.030	–	–	–	0.022	0.012	–	0.013	0.047	–	–	0.027	0.002	–	0.025
CaO	0.050	0.026	0.015	0.014	0.025	0.063	0.042	0.016	0.098	0.053	0.061	0.093	0.019	0.004	0.046
K2O	9.610	9.630	9.481	9.657	9.552	9.462	10.006	6.313	9.982	6.191	5.443	7.295	4.726	4.410	4.336
Na2O	0.661	0.659	0.732	0.569	0.662	0.607	0.232	0.190	0.277	1.315	1.451	2.133	1.780	1.186	1.652
TiO2	1.333	0.739	0.735	0.943	0.881	0.817	0.661	0.700	0.937	0.557	0.323	0.0304	0.249	0.313	0.311
Total	94.486	93.398	95.002	94.371	95.613	95.122	95.836	97.083	95.220	95.536	96.902	96.017	96.133	94.980	96.665
	CATIONS (BASED ON 22 OXYGEN)														
Si	**6.197**	**6.451**	6.387	6.508	6.460	**6.491**	**6.452**	**6.557**	**6.482**	**6.211**	**6.359**	**6.249**	**6.423**	**6.429**	**6.408**
Al	4.705	5.094	5.198	4.975	5.086	5.038	5.078	5.158	4.957	5.184	5.407	5.575	5.552	5.542	5.593
Fe	0.625	0.185	0.193	0.182	0.164	0.178	0.206	0.204	0.216	0.520	0.235	0.109	0.086	0.112	0.088
Mg	0.702	0.199	0.189	0.250	0.219	0.233	0.266	0.274	0.296	0.472	0.245	0.082	0.091	0.149	0.090
Mn	0.003	–	–	–	0.002	0.001	–	0.001	0.005	–	–	0.003	0.000	–	0.003
Ca	0.007	0.004	0.002	0.002	0.003	0.009	0.006	0.002	0.014	0.007	0.008	0.013	0.002	0.001	0.006
K	1.689	1.660	1.605	1.646	1.604	1.597	1.682	1.018	1.692	1.043	0.883	1.206	0.762	0.718	0.694
Na	0.177	0.173	0.188	0.147	0.169	0.156	0.059	0.047	0.071	0.337	0.358	0.536	0.436	0.294	0.401
Ti	0.138	0.075	0.073	0.095	0.087	0.081	0.065	0.067	0.094	0.055	0.031	0.030	0.024	0.030	0.029
Total	14.245	13.843	13.837	13.806	13.756	13.786	13.814	13.329	13.827	13.831	13.526	13.804	13.377	13.275	13.313

APPENDIX-IV

MICROPROBE ANALYSIS OF PLAGIOCLASE OF ALAKNANDA AND DHAULIGANGA VALLEYS

OXIDES/ CATIONS	DL25-44-C1	DL22-40-C3	AG1-4-C2	DL36-63-C4	DL16-28-C2	DL2-4-C2
	PLAGIOCLASE	PLAGIOCLASE	PLAGIOCLASE	PLAGIOCLASE	PLAGIOCLASE	PLAGIOCLASE
	RIM	RIM	**RIM**	RIM	RIM	RIM

WEIGHT%

SiO2	**58.442**	**58.173**	**57.912**	**63.855**	**63.468**	**66.852**	**66.779**	**68.746**	**69.108**	**64.004**	**64.155**	**62.151**	**64.372**	**64.397**
Al2O3	26.550	26.669	26.222	23.812	23.188	21.746	21.119	19.058	18.829	23.040	62.151	22.433	21.921	21.338
FeO	–	–	–	–	–	–	–	–	–	–	–	–	–	0.012
MgO	–	–	–	–	–	–	–	–	–	–	–	–	–	–
MnO	–	–	–	–	–	–	–	–	–	–	–	–	–	–
CaO	8.271	8.462	8.559	4.063	3.901	3.177	3.181	0.426	0.353	3.968	4.019	3.882	4.263	4.046
K2O	0.132	0.159	0.134	0.126	0.220	0.117	0.074	0.070	0.079	0.106	0.132	0.104	0.098	0.108
Na2O	6.990	7.244	6.822	8.628	8.275	8.233	8.962	12.065	12.707	8.993	9.083	9.207	9.665	9.544
TiO2	–	–	–	–	–	–	–	–	–	–	–	–	–	–
Total	100.386	100.707	99.650	100.493	99.052	100.124	100.115	100.365	101.077	100.113	100.379	97.778	100.320	99.446

CATIONS (BASED ON 8 OXYGEN)

Si	**2.604**	**2.590**	**2.602**	**2.797**	**2.817**	**2.913**	**2.919**	**2.999**	**3.001**	**2.817**	**2.818**	**2.807**	**2.837**	**2.859**
Al	1.394	1.340	1.389	1.230	1.213	1.117	1.088	0.980	0.964	1.195	1.190	1.194	1.139	1.117
Fe	–	–	–	–	–	–	–	–	–	–	–	–	–	0.001
Mg	–	–	–	–	–	–	–	–	–	–	–	–	–	–
Mn	–	–	–	–	–	–	–	–	–	–	–	–	–	–
Ca	0.395	0.404	0.412	0.191	0.186	0.148	0.149	0.020	0.016	0.187	0.189	0.188	0.201	0.193
K	0.604	0.625	0.594	0.733	0.712	0.696	0.760	0.004	0.004	0.767	0.774	0.806	0.006	0.006
Na	0.008	0.009	0.008	0.008	0.013	0.007	0.004	1.021	1.070	0.006	0.007	0.006	0.826	0.822
Ti	–	–	–	–	–	–	–	–	–	–	–	–	–	–
Total	5.005	5.028	5.005	4.958	4.939	4.880	4.919	5.023	5.055	4.972	4.978	4.978	5.009	4.998

MICROPROBE ANALYSIS OF PLAGIOCLASE OF ALAKNANDA AND DHAULIGANGA VALLEYS

OXIDES/ CATIONS	AG11-14-C2	AG14-18-C4	AG14-18-C4	AG15-21-C1	AG15-21-C1	AG17-25
	PLAGIOCLASE	PLAGIOCLASE	PLAGIOCLASE	PLAGIOCLASE	PLAGIOCLASE	PLAGIOCLASE
	RIM	**RIM**	**CORE**	RIM	CORE	RIM

WEIGHT%

SiO2	**68.806**	**65.544**	**64.255**	**64.935**	**64.255**	**64.935**	**63.620**	**64.836**	**69.316**	**68.009**	**63.518**	**65.318**	**66.150**
Al2O3	19.833	20.566	23.112	23.770	23.112	23.770	22.598	23.462	20.745	20.944	20.926	20.864	21.707
FeO	–	–	–	–	–	–	–	–	–	–	–	–	–
MgO	–	–	–	–	–	–	–	–	–	–	–	–	–
MnO	–	–	–	–	–	–	–	–	–	–	–	–	–
CaO	2.110	2.094	4.164	4.029	4.164	4.029	5.053	5.254	2.239	2.776	3.149	3.049	3.142
K2O	0.199	0.167	0.172	0.210	0.172	0.210	0.257	0.191	0.193	0.242	0.281	0.232	0.232
Na2O	10.597	10.860	8.729	7.469	8.729	7.469	8.670	8.225	8.380	9.526	10.675	10.118	9.123
TiO2	–	–	–	–	–	–	–	–	–	–	–	–	–
Total	101.545	99.230	100.432	100.593	100.432	100.593	100.197	101.999	100.873	101.496	98.548	99.582	100.353

CATIONS (BASED ON 8 OXYGEN)

Si	**2.970**	**2.908**	**2.818**	**2.827**	**2.818**	**2.827**	**2.809**	**2.805**	**2.982**	**2.934**	**2.856**	**2.891**	**2.891**
Al	1.009	1.075	1.195	1.220	1.195	1.220	1.176	1.197	1.052	1.065	1.109	1.088	1.118
Fe	–	–	–	–	–	–	–	–	–	–	–	–	–
Mg	–	–	–	–	–	–	–	–	–	–	–	–	–
Mn	–	–	–	–	–	–	–	–	–	–	–	–	–
Ca	0.098	0.100	0.196	0.188	0.196	0.188	0.239	0.244	0.103	0.128	0.152	0.145	0.147
K	0.011	0.009	0.742	0.646	0.742	0.646	0.742	0.693	0.699	0.797	0.016	0.013	0.013
Na	0.887	0.934	0.010	0.012	0.010	0.012	0.015	0.011	0.011	0.013	0.931	0.868	0.773
Ti	–	–	–	–	–	–	–	–	–	–	–	–	–
Total	4.975	5.026	4.961	4.892	4.961	4.892	4.981	4.948	4.846	4.938	5.063	5.006	4.943

MICROPROBE ANALYSIS OF PLAGIOCLASE OF ALAKNANDA AND DHAULIGANGA VALLEYS

OXIDES/ ELEMENTS	DL18-31-C1	DL36-63-C4	DL41-71-C1	DL32-56		AL5-11	
	PLAGIOCLASE	PLAGIOCLASE	PLAGIOCLASE	PL 1	PL 2	PL 1	PL 2
	RIM	RIM	RIM	RIM		RIM	

WEIGHT%

SiO2	**67.996**	**67.344**	**67.343**	**68.746**	**68.434**	**69.108**	**61.491**	**61.519**	**61.788**	**61.484**	**61.601**	**60.350**	**63.247**
Al2O3	21.021	21.019	21.149	19.058	17.343	18.829	24.370	23.546	23.781	23.360	22.692	23.871	21.690
FeO	–	–	–	–	–	–	–	–	–	–	–	–	–
MgO	–	–	–	–	–	–	–	–	–	–	–	–	–
MnO	–	–	–	–	–	–	–	–	–	–	–	–	–
CaO	1.242	1.286	1.304	0.426	0.432	0.353	5.316	4.885	4.902	4.919	4.543	5.696	3.389
K2O	0.087	0.106	0.095	0.070	0.073	0.079	0.329	0.334	0.424	0.183	0.224	0.187	0.123
Na2O	10.847	10.859	10.903	12.065	11.935	12.707	8.586	8.718	8.802	8.577	9.025	8.524	9.750
TiO2	–	–	–	–	–	–	–	–	–	–	–	–	–
Total	101.193	100.613	100.793	100.365	98.823	101.077	100.092	99.003	99.707	98.523	98.084	98.628	98.199

CATIONS (BASED ON 8 OXYGEN)

Si	**2.939**	**2.931**	**2.926**	**2.999**	**3.030**	**3.000**	**2.728**	**2.756**	**2.751**	**2.764**	**2.783**	**2.722**	**2.842**
Al	1.071	1.078	1.083	0.980	0.937	0.964	1.274	1.243	1.248	1.238	1.208	1.269	1.499
Fe	–	–	–	–	–	–	–	–	–	–	–	–	–
Mg	–	–	–	–	–	–	–	–	–	–	–	–	–
Mn	–	–	–	–	–	–	–	–	–	–	–	–	–
Ca	0.057	0.060	0.061	0.020	0.020	0.016	0.253	0.234	0.234	0.237	0.219	0.275	0.163
K	0.005	0.006	0.005	0.004	0.004	0.004	0.018	0.019	0.024	0.010	0.013	0.011	0.007
Na	0.909	0.916	0.919	1.021	1.025	1.069	0.739	0.757	0.761	0.747	0.791	0.745	0.850
Ti	–	–	–	–	–	–	–	–	–	–	–	–	–
Total	4.982	4.991	4.994	5.023	5.016	5.055	5.013	5.010	5.017	4.999	5.015	5.022	5.011

MICROPROBE ANALYSIS OF PLAGIOCLASE OF ALAKNANDA AND DHAULIGANGA VALLEYS

OXIDES/ ELEMENTS	AL6-16		MA23-35		DL53-95		
	PL 1	PL 2	PLAGIOCLASE 1	PLAGIOCLASE 2	PL 1	PL 2	PL 3
	RIM		RIM	RIM	RIM	RIM	RIM
				WEIGHT%			
SiO2	91.287	**90.792**	65.884	**57.257**	**65.922**	**64.002**	**65.025**	**64.804**	**63.301**	**61.705**	**61.792**
Al2O3	23.325	23.647	21.939	29.881	21.569	21.474	21.752	21.735	22.105	22.229	22.939
FeO	–	–	–	–	–	–	–	–	–	–	–
MgO	–	–	–	–	–	–	–	–	–	–	–
MnO	–	–	–	–	–	–	–	–	–	–	–
CaO	5.186	5.186	3.397	3.193	3.292	3.540	3.648	3.609	3.492	4.205	4.612
K2O	0.212	0.206	0.095	0.113	0.095	0.070	0.082	0.061	0.081	0.082	0.070
Na2O	8.171	8.748	10.470	8.852	10.584	10.091	9.213	10.013	9.581	9.067	8.918
TiO2	–	–	–	–	–	–	–	–	–	–	–
Total	98.181	98.578	101.785	99.296	101.462	99.177	99.719	100.222	98.560	97.288	98.330
				CATIONS (BASED ON 8 OXYGEN)							
Si	2.763	**2.739**	2.858	**2.553**	**2.869**	**2.851**	**2.868**	**2.854**	**2.804**	**2.781**	**2.722**
Al	1.239	1.256	1.122	1.570	1.106	1.127	1.131	1.128	1.190	1.217	1.269
Fe	–	–	–	–	–	–	–	–	–	–	–
Mg	–	–	–	–	–	–	–	–	–	–	–
Mn	–	–	–	–	–	–	–	–	–	–	–
Ca	0.250	0.250	0.158	0.152	0.153	0.169	0.172	0.170	0.205	0.222	0.275
K	0.012	0.012	0.005	0.006	0.005	0.004	0.005	0.003	0.005	0.004	0.011
Na	0.714	0.764	0.881	0.765	0.893	0.872	0.788	0.855	0.799	0.778	0.745
Ti	–	–	–	–	–	–	–	–	–	–	–
Total	4.980	5.021	5.024	5.048	5.027	5.023	4.963	5.011	4.980	5.002	5.022

MICROPROBE ANALYSIS OF PLAGIOCLASE OF ALAKANDA AND BHAULIGANGA VALLEYS

OXIDES/ ELEMENTS	AG6-7			MA39A			AG2-5		
	PLAGIOCLASE			PLAGIOCLASE			PLAGIOCLASE		
	RIM			RIM			RIM		
	WEIGHT%								
SiO2	**62.165**	**61.785**	**62.501**	**67.323**	**67.705**	**68.052**	**61.874**	**61.258**	**61.198**
Al2O3	23.511	23.043	23.218	21.477	21.442	21.168	23.537	23.413	23.550
FeO	–	–	–	0.021	0.020	0.042	–	–	–
MgO	–	–	–	–	–	–	–	–	–
MnO	–	–	–	–	–	–	–	–	–
CaO	4.728	4.668	4.636	2.962	2.861	2.494	4.866	5.133	5.163
K2O	0.378	0.517	0.395	0.132	0.142	0.144	0.349	0.359	0.355
Na2O	8.941	8.720	9.089	10.804	10.683	10.975	8.491	8.464	8.344
TiO2	–	–	–	–	–	–	–	–	–
Total	99.723	98.733	100.395	102.719	102.854	102.877	99.117	98.628	98.610
	CATIONS (BASED ON 8 OXYGEN)								
Si	**2.765**	**2.775**	**2.776**	**2.889**	**2.899**	**2.912**	**2.765**	**2.755**	**2.752**
Al	1.232	1.220	1.216	1.087	1.082	1.067	1.239	1.241	1.248
Fe	–	–	–	0.001	0.001	0.001	–	–	–
Mg	–	–	–	–	–	–	–	–	–
Mn	–	–	–	–	–	–	–	–	–
Ca	0.225	0.225	0.221	0.136	0.131	0.114	0.233	0.247	0.249
K	0.021	0.029	0.022	0.007	0.008	0.008	0.019	0.021	0.020
Na	0.771	0.759	0.783	0.899	0.887	0.911	0.736	0.738	0.727
Ti	–	–	–	–	–	–	–	–	–
Total	5.015	5.009	5.018	5.020	5.007	5.014	4.993	5.003	4.997

MICROPROBE ANALYSIS OF PLAGIOCLASE OF ALAKNANDA AND DHAULIGANGA VALLEYS

OXIDES/ CATIONS	H-1				AG2-1			
	PLAGIOCLASE 1		PLAGIOCLASE 2		PLAGIOCLASE 1		PLAGIOCLASE 2	
	RIM		RIM		RIM		RIM	
WEIGHT%								
SiO2	**61.881**	**61.956**	**61.548**	**61.472**	**62.120**	61.636	**59.704**	**58.997**	**64.282**	**59.745**	**58.284**	**60.554**
Al2O3	22.007	22.541	22.494	23.063	22.894	22.538	24.500	25.429	22.760	26.434	25.077	25.903
FeO	–	–	–	–	–	–	–	–	–	–	–	–
MgO	–	–	–	–	–	–	–	–	–	–	–	–
MnO	–	–	–	–	–	–	–	–	–	–	–	–
CaO	4.916	5.184	5.335	5.885	5.435	5.303	8.198	8.827	5.726	9.167	8.767	9.120
K2O	0.105	0.128	0.133	0.104	0.115	0.125	0.093	0.089	0.129	0.139	0.111	0.101
Na2O	9.297	9.062	8.760	8.625	8.931	8.737	7.153	7.016	8.064	6.235	**6.805**	6.671
TiO2	–	–	–	–	–	–	–	–	–	–	–	–
Total	98.206	98.871	98.271	99.149	99.494	98.339	99.647	100.359	100.960	101.720	99.044	102.348
CATIONS (BASED ON 8 OXYGEN)												
Si	**2.797**	**2.782**	**2.779**	**2.756**	2.772	2.780	**2.676**	**2.633**	**2.813**	**2.624**	**2.635**	**2.644**
Al	1.172	1.193	1.197	1.219	1.204	1.198	1.294	1.338	1.174	1.368	1.336	1.333
Fe	–	–	–	–	–	–	–	–	–	–	–	–
Mg	–	–	–	–	–	–	–	–	–	–	–	–
Mn	–	–	–	–	–	–	–	–	–	–	–	–
Ca	0.238	0.249	0.258	0.283	0.259	0.256	0.394	0.422	0.269	0.431	0.425	0.427
K	0.006	0.007	0.007	0.006	0.007	0.007	0.005	0.005	0.007	0.008	0.006	0.006
Na	0.815	0.789	0.767	0.749	0.773	0.764	0.622	0.607	0.684	0.531	0.597	0.565
Ti	–	–	–	–	–	–	–	–	–	–	–	–
Total	5.028	5.020	5.009	5.013	5.015	5.006	4.991	5.005	4.946	4.962	4.999	4.974

APPENDIX-V

MICROPROBE ANALYSIS OF HORNBLENDE OF ALAKNANDA AND DHAULIGANGA VALLEYS

OXIDES/ CATIONS	AG2-1					
	HORNBLENDE 1			HORNBLENDE 2		
	RIM			RIM		
	WEIGHT%					
SiO2	**41.685**	**42.635**	**40.875**	**39.747**	**41.788**	**40.383**
Al2O3	13.908	14.142	14.012	18.127	13.806	16.114
FeO	21.351	21.389	21.097	21.775	23.529	21.744
MgO	6.009	5.994	5.834	4.025	4.581	4.786
MnO	0.183	0.173	0.190	0.176	0.197	0.210
CaO	10.950	10.969	11.079	11.244	10.992	11.036
K2O	0.463	0.470	0.454	0.530	0.247	0.553
Na2O	1.574	1.507	1.687	1.034	1.359	1.489
TIO2	0.542	0.564	0.462	0.231	0.263	0.475
Total	96.666	97.843	95.690	95.690	96.762	96.791
	CATIONS (BASED ON 23 OXYGEN)					
Si	**6.422**	**6.468**	**6.373**	**6.109**	**6.481**	**6.229**
Al	2.526	2.529	2.575	3.284	2.524	2.930
Fe	2.751	2.714	2.751	2.799	3.052	2.805
Mg	1.380	1.355	1.356	0.922	1.059	1.101
Mn	0.024	0.022	0.025	0.022	0.026	0.027
Ca	1.808	1.078	1.851	1.852	1.827	1.824
K	0.091	0.091	0.090	0.104	0.049	0.109
Na	0.470	0.443	0.510	0.308	0.409	0.445
Ti	0.063	0.064	0.054	0.027	0.031	0.055
Total	15.533	15.470	15.585	15.428	15.456	15.527

APPENDIX-VI

MICROPROBE ANALYSIS OF CHLORITE AND ILMENITE OF ALAKNANDA AND DHAULIGANGA VALLEYS

OXIDES/ CATIONS	AG2-1 CHLORITE RIM		DL50-90 ILMENTE		
			OXIDES/ CATIONS	RIM	
	WEIGHT%				
SiO2	**23.684**	**22.160**	**FeO**	**46.546**	**44.366**	**47.564**
Al2O3	20.710	20.497	TiO2	51.003	50.169	51.490
FeO	37.362	36.629	AL2O3	0.066	0.001	_
MgO	6.846	6.027	MgO	0.367	0.290	0.346
MnO	0.389	0.410	MnO	0.157	0.186	0.223
CaO	0.034	0.114	ZnO	0.116	0.120	0.062
K2O	_	_	Cr2O3	_	0.023	0.070
Na2O	0.198	0.899	V2O3	0.300	0.300	0.307
TIO2	0.074	0.078	SiO2	_	_	_
Total	89.297	86.814	Total	98.554	95.455	100.063
	CATIONS (BASED ON 6 OXYGEN)					
Si	**5.259**	**5.101**	**Fe**	**1.998**	**1.959**	**2.0153**
Al	5.420	5.561	Ti	1.969	1.992	1.962
Fe	6.938	7.052	Al	0.004	0.000	_
Mg	2.266	2.068	Mg	0.028	0.023	0.026
Mn	0.073	0.080	Mn	0.007	0.008	0.009
Ca	0.008	0.028	Zn	0.004	0.005	0.002
K	_	_	Cr	_	0.001	0.003
Na	0.085	0.401	V	0.012	0.013	0.012
Ti	0.012	0.013	Si	_	_	_
Total	20.061	20.305	Total	4.023	4.001	4.030